From STM To Nanomemory :

A transfer of technology feasibility study

A thesis presented to the
University of Warwick
in the year 1994 for the degree of
Doctor of Philosophy

by Jimmie Andrew Miller

ABSTRACT

Recent years have seen exponential increase in memory capacity for computer data storage. Increased bit density has been produced by decreasing feature sizes in microelectronic fabrication. As minimum microelectronic feature sizes are realized, new methods are being investigated to continue the increase in recording bit density.

This report examines features which are necessary to produce an electron-tunneling based memory which is postulated to increase the data density by a factor of 10^5-10^6 over current manufactured memories. A description is given for combining tunneling microscopy with memory technology to achieve this high density memory. Experiments using a tunneling tip to produce nanometer scale features on a surface are recounted. The repeatability and durability of the produced features are investigated with a summary of these aspects included for various materials reported in the literature. Some necessary mechanical and electrical design criteria for a tunneling memory are obtained. Observed and reported inconsistency in nanometer lithography are attributed to nonpredictable tunneling currents and resulting tip-sample separations. Experimental and theoretical work scrutinizing tunneling currents as a function of tip-sample displacement is included. Other factors affecting the practicality of a tunneling based memory are also incorporated.

LAYOUT OF THE THESIS

Chapter 1 describes the basic historical developments of information storage and the scanning tunneling microscope (STM). STM and memory technology are related in such a way as to describe the basis for a nanomemory.

Chapters 2-5 form a group relating to surface lithography experiments. Chapter 2 gives various techniques for using a tunneling probe to produce nanometer-sized surface modifications which could be readable as computer bits. Chapter 3 is a literature survey of concurrent and prior art dealing with altering a surface according to the techniques discussed in chapter 2 and is organized according to alteration methods. Since much of the work is concurrent and seldom builds upon previous experiments, it is alphabetically sequenced by author of the related work. Chapter 4 describes tunneling theory and uses it for the development of experiments to assess field induced alteration of surfaces on a nanometer scale. Chapter 5 summarizes the memory related properties of the promising materials and is based on the discussions of chapters 3 and 4. The chapter is organized alphabetically according to material studied. The chapter concludes the lithography series with a set of tables for quick reference on the relevant properties for each material.

Chapter 6 discusses the performance requirements of electrical and mechanical design with respect to field induced surface alteration and speed of a memory. The chapter concludes with a table of design criteria

for a tunneling based memory.

Chapters 7 and 8 form a group relating tunneling current versus tip-sample displacement experiments and theory. Chapter 7 describes experiments related to measuring and characterizing the tunneling current as a function of tip sample displacement. Described is a direct x-ray interferometer calibrated translation system for such measurements. Also, ambient effects on the tunneling characteristics were examined and discussed with respect to their influence on a tunneling memory. A more detailed theory is developed in chapter 8 to explain observation of the nonlinearity of the natural log of the tunneling current as a function of tip-sample displacement. Included is consideration of image forces along with a more accurate exponential equation to replace Simmons' (1961) approximation of the classical summation approach describing the image potential. Also investigated is the effect of lateral surface currents on the atomic images obtained by STM. Observation of recoverable electronic surface changes is reported. These are used to account for some "quirks" of measured tunneling currents.

Chapter 9 discusses various topics which, although related to atomic bit processing, do not readily fit into the other chapters. Such things as the changing of surfaces due to contamination and tip related effects are described and illustrated. Findings are related to their implications for a tunneling based nanomemory.

Chapter 10 summarizes the reported work and gives some general advice for methods and materials to be used for a practical nanomemory.

All STM images shown in this thesis are the authors work. The STM images are captioned as images instead of figures with a separate numbering system.

Any abbreviated author and date references can be looked up in the bibliography for full detail.

The thesis is written using the standardized spelling of American English.

ACKNOWLEDGEMENTS

I am indebted to many individuals for the completion of this thesis. This international cooperative program would not have been possible had it not been for the vision of **Dr. Keith Bowen** of the University of Warwick and **Dr. Robert Hocken** of the University of North Carolina at Charlotte. Thanks for handling the administrative red tape.

My Warwick advisor, **Dr. Stuart Smith**, is a creative man with the understanding to see projects to their expected end. He has allowed me to work independently while offering suggestions to maximize the benefits of the related work. Thanks for your patience and insight. You have demonstrated thoroughness and attentiveness to detail.

My UNC-C advisor and mentor, **Dr. Robert Hocken**, who envisioned the research project and obtained the necessary funding. Thanks for the support, encouragement, and freedom to investigate those areas which I deemed relevant and at the same time advising me of the direction you thought I should be heading. Also, thanks for asking many questions which challenged me to consider things in more detail. You have broadened my horizons in many areas not limited to the specific subject matter of this thesis, to this you have demonstrated your true value as a great educator.

There are also many fellow researchers which have contributed their advice. Thanks for listening.

Thanks to the technical staff at Warwick, **Frank, Rhod, Steve, David and others** which facilitated the completion of the residency project. Your hard work and dedication are much appreciated.

A special thanks to my **Parents** who have encouraged me throughout life to be as good as possible at whatever I put my hands toward accomplishing.

To **Joan Clarke** who housed me during my stay in Coventry. Your hospitality enabled me to concentrate on the work at the University. For this I am grateful.

I am also thankful to **God, the Creator**, for the mental abilities with which he has endowed me. Trusting in his plan has kept me from much anxiety which usually accompanies a project of this magnitude.

TABLE OF CONTENTS

INTRODUCTION

Manipulation of matter and energy has always been utilized to the benefit (or sometimes the detriment) of civilization. Energy contained in chunks of coal is released to raise the temperature of water. The water changes in form to steam, then increases in pressure resulting in a force being applied to a piece of iron, which moves, causing another piece of iron to rotate on a constrained iron rail. The result is that energy of heat is transformed into kinetic energy in tons of iron. Structures are constructed in such a way that a person can utilize the motion of the iron and travel from one place to another.

By knowing how to repeatably produce and control the release of energy from coal in such a way as to generate the motion of what we call a train, a technology is born. With the development and subsequent transfer of other technologies, i.e. chemical and electrical, the diesel train is developed which has no need of frequent stops to take on water and then the electric train which has no need of stopping for fuel either. However, it is still preferable to stop for the convenience of passengers and those loading and unloading freight.

This evolution and cultivation of applications is at least as old as recorded history, being revealed in the equity of law where a decision in one case is applied to another case. Similarly, the providential discovery of penicillin from mold led to a multitude of other antibiotics being produced from other molds. Archimedes is reported to have demonstrated the principle in warfare when he drew from the technology of optics to

make mirrors to focus light from the sun onto enemy ships setting them on fire.

1.1 The nanomemory concept

The purpose of this thesis is to examine a technology transfer from the field of scanning tunneling microscopy to the field of high density computer memory. The feasibility of manufacturing a computer memory with an areal bit density 10^5-10^6 times greater than present storage devices has been investigated. Quate[1] [1986] postulated that this high density memory, herein referred to as ***nanomemory***, could be manufactured utilizing the electromagnetic field between an atomically sharp tunneling probe and the conducting surface to alter the surface. Employing the same or similar tunneling probe to distinguish between an altered and an unaltered surface, provides the foundation for a computer bit memory structure (e.g. altered is a one, unaltered is a zero).

As Eric Drexler observed, "Our ability to arrange atoms lies at the foundation of technology"[2]. Whether the technology is on the level of a blacksmith who shapes metal into horseshoes or the chemist who has developed a recipe for manufacturing a particular polymer, in the final analysis it is atoms which are arranged to suit a particular need. Even though "we are still forced to handle atoms in unruly herds"[2], we should not always expect to be limited in this way. As Richard Feynman said, "The principles of physics... do not speak against the possibility of maneuvering things atom by atom. It is not an attempt to violate any

laws; it is something, in principle, which can be done."[3]

This investigation assesses those areas which would make this technology practical. These areas include: *1. alterability*, the ability to modify a surface on an atomic scale, i. e. write a bit, *2. reproducibility*, the ability of a set of applied physical parameters to repeatably produce the desired surface alteration, *3. durability*, the ability of the altered surface to remain in the same altered state for an indefinite period of time, and *4. readability*, the ability to distinguish between an altered and an unaltered area of the surface. During the various investigations of this thesis, discussion is focused primarily on these four criteria. However, other relevant areas relating to the development of such a memory will be included where appropriate.

By examining the similar details of operation of two seemingly distinctive technologies, a combination may be obtained which can develop a new generation technology. The following sections describe the history and principles of storage technology and scanning tunneling microscopy with emphasis on how the two may be integrated to produce a nanomemory.

1.2 A survey of information storage developments

Writing and drawing are some of the oldest forms of information storage. Whether the information is an idea or a beautiful location we desire to recall or relate, the marks on a piece of paper or other medium refresh our minds and inform others. Writing and drawing, however,

require a human intermediary to record the words or visual image. Other mechanical, optical or electro-magnetic information media have now been developed. These will be briefly reviewed below.

1.2.1 Visual developments

The first known device which enhanced drawing was the ***camera obscura*** (dark chamber). Developed in the 1500's, the device was a box large enough for a person to occupy and allowed no light except that which entered in through a small hole in one of its walls. The hole produced a faint inverted image on the opposite wall. This image was traced to give more accurate detail than freehand drawing. The addition of a lens in the 1600's made the image larger and produced greater contrast. In the early 1800's, the need for the human intermediary was eliminated by Joseph Niépce who exposed a metal plate that was chemically sensitive to light to capture an image. The exposure took 8 hours. A subsequent engraving process (etching) made the image permanent.[4]

1.2.2 Audio developments

The recording of sound came in 1877 with Thomas Edison's invention of the **phonograph**. The recording surface was a tin foil covered cylinder. As the cylinder was rotated, indentations were made in the tin by a stylus connected to a diaphragm that was voice modulated. When the stylus was allowed to retrace the indentions, it vibrated the diaphragm which reproduced the recorded sound. Inexpensive cylinders of cardboard covered with wax were used by the **graphophone** invented by Charles

Tainter and Chichester Bell in 1885. Emile Berliner's 1887 **gramophone** used a disc instead of a cylinder for recording.[4]

1.2.3 Electromagnetic developments

While cameras use a light induced electrochemical reaction to facilitate the storage of a visual image, the phonograph, graphophone, and gramophone use a mechanically induced material topography change to record and reproduce sound. However, the development of electromagnetism produced remarkable advances in sound recording. In 1888, Oberlin Smith disclosed the idea of magnetic recording using magnetic dust particles. In 1898, Valdemer Poulson demonstrated voice recording on a steel wire connected between two walls. A telephone voice coil was connected in series with a battery and electromagnet. The electromagnet was held by a moving carriage against the wire. As the carriage was moved, Poulson spoke into the voice coil. Connecting a telephone receiver in place of the battery and voice coil, and again moving the carriage across the wire, his words were reproduced. He also demonstrated that the recording was erasable by sliding a permanent magnet across the wire, preparing it for subsequent recording. The invention was called the **telegraphone**. One of the major applications was that of recording telephone messages. An early production design utilized a cylinder wound in wire for recording. He also investigated recording on tape, cylinders, and discs made of magnetic materials. Electrochemically deposited magnetic thin films were used for recording as early as 1906.[5] Although sound was the first application of magnetic recording, the

application to video and data recording also later became practical with similar technology. Recording advanced along with the development of materials processing, precision manufacturing, and more sophisticated techniques such as high frequency modulation.

1.2.4 Numerical storage and calculations

One of the earliest known numerical storage devices was the Chinese ***abacus***, used also by the ancient Romans and Greeks. Analogous to the contemporary shift register in an arithmetic processor, it stored one number at a time for future calculation. The Inca indians used a combination of colored strings and knots called a ***quipu*** (c. 1500) to store an accurate count.[4]

Blaise Pascal produced the first numerical mechanical wheel calculator in 1642. Gottfried Liebniz followed with the mechanical multiplier in 1673. These devices used mechanically stored numbers for their calculations. Joseph Jacquard used encoded punched cards as early as 1801 for controlling looms weaving elaborate fabric designs. This was one of the first precursors to computer numerically controlled machines. Punched card machines were also used by Herman Holerith for the census of 1890. A machine for four function arithmetic was first produced by Charles Xavier Thomas in 1820. Building on the key-set adding and printing machine developed by William Burroughs, the first commercial calculator with a mechanical keyboard was produced in 1911 by Jay Monroe.[6]

1.2.5 Three generations of computers

With the advent of the electronic vacuum tube, mechanical computation was eclipsed. John Vincent Atanasoff and Clifford Berry produced the first electronic computer in 1939 called the **ABC** (Atanasoff-Berry Computer). The ABC used capacitors for storage. Using Anatasoff's principles, John Mauchly and J. Presper Eckert built the **ENIAC** (Electronic Numerical Integrator And Calculator) in 1946.[6] The ENIAC utilized electronic vacuum tube based flip-flops for storage along with acoustic delay lines for registers.[7] Remington Rand Corporation's 1951 UNIVAC (UNIVersal Automatic Computer) included a magnetic drum capable of storing 16,000 characters[6] along with vacuum tube memory. Computers like the ABC, ENIAC, and UNIVAC using vacuum tubes are considered first generation computers.

The arrival of the second generation of computers in 1959 was precipitated by the development of the transistor in 1947 by John Bardeen and Walter Brattain[8]. The lower cost semiconductor based transistor replaced the unreliable and costly vacuum tube. The tube based memories were also replaced by less expensive core memories. Core memories are ferromagnetic donuts about the size of a grain of salt[6] and wound with wires for their magnetization and subsequent reading. The short-lived second generation was replaced by the third generation in 1964 using solid state technology and integrated circuits.

Current information storage is accomplished in one of two fundamental methods. Direct recording is used when exact analog

electronic waveforms are desired to be stored. Digital recording is used when the information is stored as a numerical binary code of electromagnetic pulses of the same magnitude. The binary code is comparable to Morse code where a unique series of two distinct sounds represent a specific symbol. The digital information may be directly generated by a computer or an analog to digital converter. State of the art computers use the binary code for calculations and decision making.

1.2.6 Storage technology

Memory media include integrated circuits, hard (rigid) and floppy (flexible) magnetic discs, magnetic tape or drums, punched paper tape, or laser read optical discs. The methods are not necessarily contemporary (punched paper cards were used by Jacquard in 1801 and by Holerith in the 1890's; magnetic discs, tape, and cylinders were examined by Poulson in the early 1900's). However, the processing technology for these methods involves improved materials and processing which make computer storage facilities substantially smaller, faster, and less expensive.

The purpose of the computer ultimately determines its size and composition. From fingernail sized single integrated circuit chips which monitor processes in an automobile to room sized supercomputers with parallel processing and large data handling networks, the computer uses media which satisfy its operating requirements. Information capacity, expense, size, and speed are among the things which are considered in the design of a computer.

There are two basic memory requirements for a computer. First there is the high speed random access memory (RAM) used by the command processor. The RAM temporarily stores the programs which the processor uses to determine the decisions the computer makes. Also, RAM is a working area for the processor to calculate, store, and manipulate information. The second kind of memory is long term storage of pre- or post-processed information, reference tables, or processing programs not currently in use.

Integrated circuits with access speeds near 70 ns are standard for RAM memory in order to reduce processing time. They are also used for preprogrammed dedicated use computers. For an access time of milliseconds, and large storage and retrieval capacity, hard magnetic discs are normally chosen. For personal use, and transferring smaller programs, soft disc use is routine. For machine program storage, paper tape is often used, but as personal computers become more available, more programming is loaded to the machines from operator programmable computers. For nonwritable high density information access, optical discs are growing in popularity. For backup of large programs and data, magnetic or paper tape is selected. Magnetic drum memories are no longer in common use due to large volume to surface area ratio, that is volume per bit is much smaller for discs or tape. So we see that most methods have their selective purposes.

1.2.7 Magnetic storage operation

The magnetic ring head of Figure 1 illustrates the basic principles

of conventional magnetic storage of information. The continuous relative motion between the flying head, the magnetizable medium, and the air between them produces a self-acting air bearing. This air bearing lifts the head above the medium giving it the appearance of *flying* and allowing it to float within 500[9] nm of the medium's surface. The aerodynamic floating of the head was serendipitously discovered while examining the crashing of the head into a drum. Willful attempts to produce a head crash during motion were more difficult than expected[9].

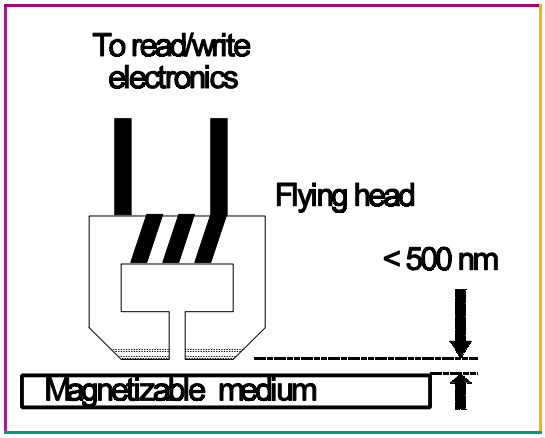

Figure 1:1 Basic design of a magnetic ring recording head.

The read/write electronics are capable of supplying a current to the coil around the highly permeable head. The fringing field at the gap in the head is used to change the magnetic field in the medium. These magnetic reversals are used to store information along a track. This magnetically written information is read back by retracing the same path that was used to record. The reversal in the magnetic field of the medium as it passes the head induces an electric current in the coil which is detected by the read electronics.[9] The address (location) of the data is determined by a unique prerecorded (i.e. by formatting) magnetic pattern in the tracks which are on either side of the stored information. The head follows these address tracks to the correct location and then reads or stores the information.

The magnetizable medium does not have to be a homogeneous material but usually consists of one or more layers of magnetizable thin films. "Head assemblies vary in width from 20 µm to 50 mm, while individual tracks range from some 10 µm to 6 mm. Up to 100 head elements have been built in a single stack using film fabrication technology."[10] These heads can produce an upper limit information density of around 100 kbit/mm^2 (>3 µm^2/bit).

Although the presented dual pole style of head is the most common in personal computers, heads exist based upon Faraday rotation (magneto-optic), magnetoresistance, and for Hall effect which "respond to magnetic flux rather than its rate of change"[10].

1.3 Scanning tunneling microscopy (STM) development and operation

The ability to measure the topography of surfaces lies at the heart of making precision parts and devices. In order to manufacture to a given specification, you must be able to measure the part to a greater accuracy to be assured that the piece is within tolerance.

1.3.1 Optical microscopes

Optical microscopes were first used to enhance observation of surface features. Reticles used for measuring feature dimensions have a resolution of a few micrometers. Using interferometric techniques, where two monochromatic rays of light are allowed to interfere, their limit in the lateral direction is about one-half the wavelength of the light used. Vertical resolution has been improved to less than one-half the

wavelength of light using multiple reflections between the optics and the sample. However, this decreases the lateral resolution due to misalignment of surface and optics. By using piezoelectric displacement of the optics and CCD cameras, vertical resolutions of 1 nm are obtained using computer fringe analysis. Other methods for obtaining high vertical resolution are ultra-beam microscopy (10-20 nm) and laser confocal microscopy (5 nm).[11]

1.3.2 Scanning electron microscopes

Optical microscopes allow the simultaneous viewing of many parts of the surface under inspection. However, it was with the development of electronic techniques which enabled an image to be constructed one spot at a time using scanning metrologies.

Scanning electron microscopes use magnetic fields to focus a beam of high energy electrons (1-50keV) down to nanometers in dimensions. This fine beam of electrons causes secondary electrons to be emitted from the surface. The number of emitted electrons is related to the angle of incidence and any sharp edges in the region. As the beam is also magnetically raster scanned across the surface, the change in emission for each point is shown in grey-scale on a cathode-ray tube (CRT) to produce an image of the surface. Lateral measurement ranges from nanometers to millimeters are possible. Although the lateral resolution can be nanometers, vertical information is difficult to obtain. Also the energetic electrons can cause heating of the sample and subsequent transformation. The vacuum can also be damaging.

1.3.3 Mechanically contacting stylus instruments[12,13]

Common engineering profile measurements are made with stylus instruments. Similar in operation to a phonograph pick-up, a diamond stylus is traced across a surface at speeds of around 10 μm/s to 1 mm/s, while a transducer registers the displacement of the stylus. Most transducers are one of three types, Linear Variable Differential Transformer or Inductor (LVDT or LVDI) or a capacitance probe. An x-y recorder is used to log multiple topographic traces of the surface. The vertical resolution is on the order of nanometers. The lateral resolution depends on the stylus tip radius. However, the stylus contact force is typically on the order of milli-Newtons causing deformation of the surface and leaving furrows.

*1.3.4 The **Topografiner***[14]

The topografiner was developed around 1971 as a noncontacting means of obtaining topographic information about a surface. A field emission[15] probe is positioned via three orthogonal piezoelectric ceramic elements (*piezos*). As two piezo rods scan the probe in the x and y directions, a servo circuit causes the z piezo to expand or contract to keep the voltage between the probe and sample approximately constant for a preset current. The voltages applied to the piezos are used to generate a 3-dimensional image of the surface. The probe hovers about 20 nm above the surface for field emission currents. Young *et al.*[14] reported a qualitative deviation of current characteristics from field emission theory as the tip-probe separation decreased below 2 nm. In this

range, the tunneling current follows the metal-vacuum-metal (MVM) theory of Simmons[16]. They were not able to operate in this range due to vibration. The lateral range was limited to 7.6 μm by the piezos. The lateral resolution was not determined, but the vertical resolution was limited to about 3 Å due to electronic noise and mechanical vibrations. It was originally thought that the prototype instrument needed to be expanded in range to 0.254 mm square area to be useful as a microtopography tool.

1.3.5 Scanning tunneling microscope: development

Going in the opposite direction that Young proposed for improving the Topografiner and unaware of Young's work[17], Binnig *et al.*[18] developed a similar instrument which demonstrated Angstrom resolution. By stabilizing the probe-tip separation to below 0.2 Å, and operating in the tunneling[19] regime instead of the field emission regime, atomic steps on surfaces were reported in 1982 and atomic resolution in 1983. These results, along with others, precipitated the awarding of Nobel Prizes to Binnig and Rohrer. The improved instrument became known as the Scanning Tunneling Microscope[20] (STM).

1.3.6 Scanning tunneling microscope: operation

In this instrument, atomically sharp conducting probes, made by etching, grinding, or cutting are *scanned* in a X-Y raster fashion over the surface whose topography is desired. The grinding and cutting processes do not necessarily produce symmetrically sharp tips, but do produce many microtips which are atomically sharp. Micrometer range scanning

displacements are usually accomplished by piezoelectric ceramics.

If there exists an externally applied electric potential between this tip and a conducting sample, and if the probe tip is brought to within Angstroms of the surface, a quantum mechanical *tunneling* current can be detected. Since the tip must be within Angstroms of the surface to tunnel, the microtip closest to the sample becomes the tunneling probe. This tunneling current is exponentially dependent[19] on the spacing between the probe and sample, such that, if the spacing decreases by 1 Å, the current increases, theoretically, to about 7-10 times the original current (see chapter 4 for greater detail). The tunneling current is typically on the order of nanoamps for a tip-sample spacing of a 1-10 Angstroms and 0.1-1 volt potential. This current is dependent on both the geometry and the electronic properties[21] of the surface layers of atoms and tip.

As the probe is scanned horizontally and servoed in the vertical direction to maintain a constant current, a two dimensional (vertical and lateral, or z versus x) trace of the surface can be obtained (as shown in

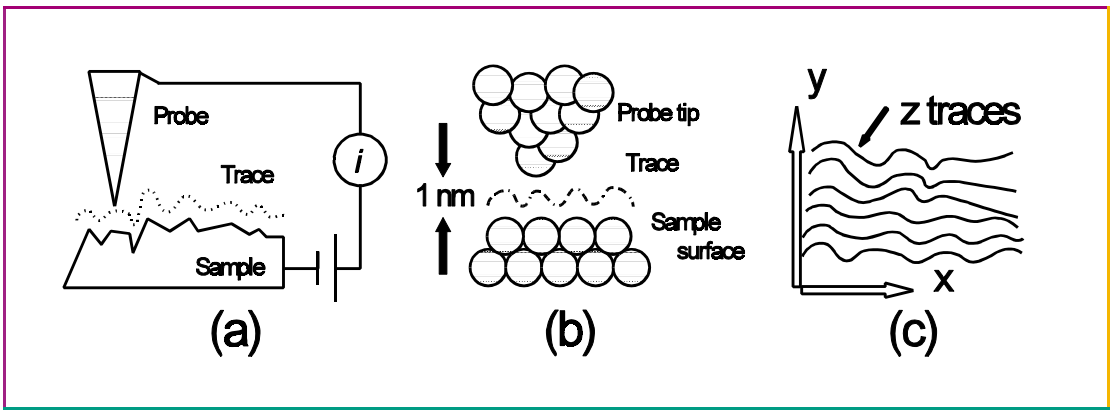

Figure 1:2. Illustrations of the principles of STM, showing (a) current flow between the tip and sample, (b) the nanometer separation of tip and sample, and (c) multiple trace formation of 3-D image.

Figure **1:2**(a). Since the current is dependent on geometry and electronic properties, the trace reflects both. Figure **1:2**(b) illustrates the possibility of obtaining atomic resolution if the tip is atomically sharp and the sample is sufficiently flat and homogeneous (The circular shapes represent the electronic orbitals of each atom). This trace is similar to that obtained by a contact surface profilometer with the exception that the STM probe does not, theoretically, come in contact with the surface.

Three dimensional topography can be established by making a z versus x trace, displacing the probe a nominal amount in the y direction and making another z versus x trace as shown in Figure **1:2**(c). If this process is repeated, a series of x,z traces can be used to created a three dimensional representation of the topography of the surface. The scanning is usually accomplished using computer control, and for each coordinate the height of the probe is also digitally recorded from the servoing feedback circuits. Since we now have the x,y,z data stored digitally, we can generate an *image* on a computer monitor which corresponds to the nanometer topography of the sample surface (hence it is *microscopy*). A typical STM topographical image revealing individual traces is shown in Image **1:2**(a). Image **1:2**(b) shows the same data as Image **1:2**(a) but in a greyscale form and as viewed from directly above the sample. A higher position of the surface is represented by a lighter region in the greyscale image.

Piezoelectric ceramics can expand or contract on the order of

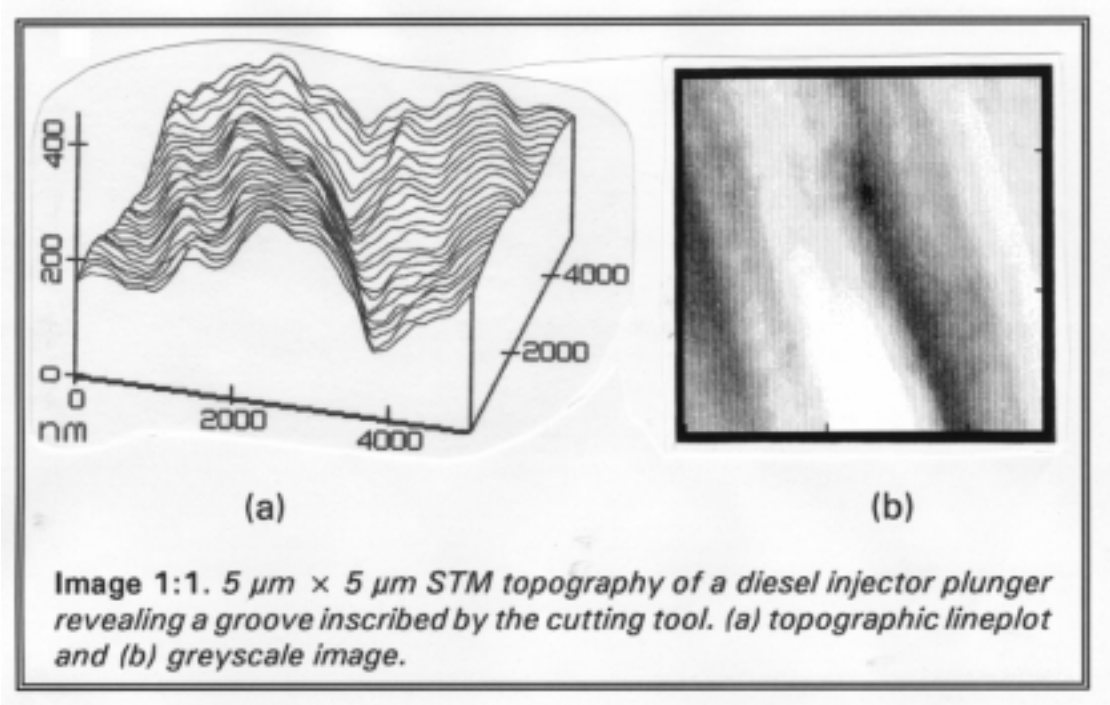

Image 1:1. *5 µm × 5 µm STM topography of a diesel injector plunger revealing a groove inscribed by the cutting tool. (a) topographic lineplot and (b) greyscale image.*

nanometers per volt applied. Since digital to analog (D/A) converters are capable of millivolt resolution, sub-Angstrom positioning becomes possible. Since D/A converters exist which are capable of resolution below one part per million and providing the subsequent electronics are capable of this extremely high precision, topography can be obtained with tens of micrometers of range and sub-Angstrom resolution. However, one usually does not obtain these detailed images over micrometer ranges because of the substantial amount of memory required to store the x,y,z data[22].

1.4 Technology comparison

Comparing similarities in operation between STM and magnetic memory technology will enable us to visualize a memory based on STM principles.

1.4.1 Non-contact nature

Notice first of all that, in principle, both are non-contact methods. The STM probe tip remains separated from the surface of the sample by dynamic feedback while the magnetic head is maintained in a flying position by aerodynamic forces between the head and medium.

1.4.2 Reading capabilities

Secondly, notice that both the STM probe and head are detecting (i.e.'reading') changes in material state. The STM reads the relative z position of the probe necessary to maintain a constant current between the tip and sample. More precisely, the STM probe detects the tunneling current which affects the feedback electronics which in turn can be 'read' to obtain height or current information. The magnetic memory head detects the flux reversals near the surface of the magnetic medium. Similarly, we 'read' the current induced by the magnetic reversals.

1.4.3 Size comparison

The most obvious difference is the size of what is detected. Magnetic memory detects micrometer sized magnetic reversals, while STM can detect sub-Angstrom scale differences in topography. If these differences in surface topography were intentionally generated to be memory 'bits', then we have a non-contact memory reading device. The bit reading scheme could involve any one of the following:

a. Change or rate of change of height of tip.

b. Current or rate of change of current between tip and sample, between consecutive tip positions (with digital

control).

c. The ac conductance between tip and sample.

If the bits were on the order of 3 nanometers in major dimension, the effective areal information density could be increased by a factor of one million over magnetic storage devices.

1.4.4 Positioning (or addressing) techniques

The position (address) for memory bits of a magnetic style memory rely on additional tracking heads which read other encoded magnetic bit patterns. The x,y position reading for an STM image is usually not read but assigned for each z data position. The assigned position is determined by the digital values of the D/A converters which control probe positioning. These assigned values may need to be software generated to give more accurate positioning if the piezoelectric ceramic displacements are known but not linear, but we will neglect this for the purpose of the present discussion. This is justified because the tip only needs to return to the same place each time and that place does not have to be known in an absolute sense. So, instead of reading the position of the probe, we effectively place (address) it where we desire it to be (repeatably, but not exactly), and use some method to retrieve the desired information at that point (address), whether topographical and/or memory bit.

1.5 Synthesis of an STM Memory

The basics principles of a memory device are addressing, reading, and writing. We have shown that an STM actually reads information and

is effectively addressed. Assume that we do have the capability to alter a surface by STM technology and that these alterations may be read as information. Let's assign a 1 to an altered position.

Figure **1:3** illustrates that we now have a stratagem for development of an STM based memory. The probe can be rastered in an x,y pattern to give us the addressing that we require. In the x direction, there is the need for more step positions per nanometer than reading (bit) positions so that comparison can be made for the determination of the state of the bit (altered or unaltered, i.e. 1 or 0). In Figure **1:3**, the probe is shown at the x_2,y_4 bit position. This bit would be read as altered and it's state determined as a 1.

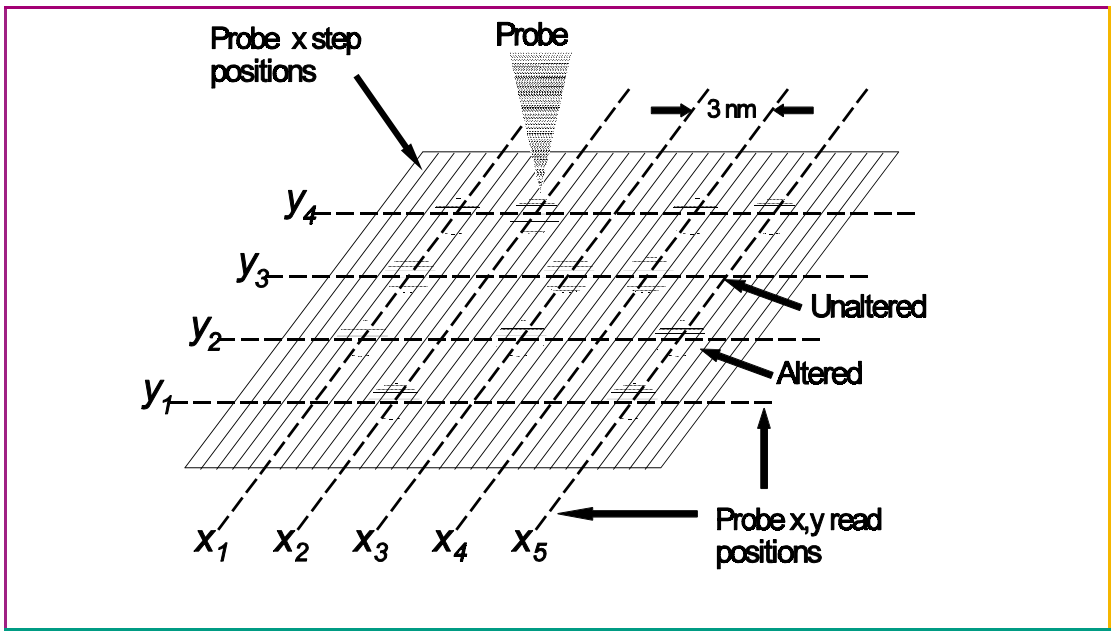

Figure **1:3** Synthesized STM based memory.

Similarly, if we read addresses (x_1-x_5,y_3) we determine the encoded information to be 10110.

The 3 nm spacing between read positions has been chosen to give

a 1 nm^2 bit area and 2 nm of non-altered spacing between bits for comparison. The more than 20 surface atoms in the 1 nm^2 area would need to be altered in some way to be recognized as an information bit. We will discuss this concern in the next few chapters.

[1] Quate, Calvin F., U. S. Patent #US4575822, Mar 11, 1986.

[2] Drexler, K. Eric, *Engines of Creation*, (Doubleday, New York, 1986).

[3] Feynman, Richard P., "There's plenty of room at the bottom" in *Miniaturization*, Horace D. Gilbert, ed., (Reinhold Publishing, New York, 1961).

[4] *World Book Encyclopedia*, (Field Enterprises Educational Corp., 1971).

[5] Camras, Marvin, *Magnetic Recording Handbook*, (Rienhold, New York, 1988).

[6] Awad, Elias M., *Business Data Processing*, (Prentice Hall, Englewood Cliffs, 1980).

[7] Huskey, Harry D., and Korn, Granino A., *Computer Handbook*, (McGraw Hill, New York, 1962).

[8] Sze, S. M., *Semiconductor Devices, physics and technology*, (Wiley & Sons, New York, 1985).

[9] Mee, C. Dennis, Daniel D., eds. *Magnetic Recording Volume I: Technology* (McGraw-Hill, New York, 1987).

[10] Reference 9, page 7.

[11] Bearden, Alan, O'Neill, Michael, P., Osborne, Leslie C., and Wong, Terrence L., "Imaging and vibrational analysis with laser feedback interferometry", Optics Letters **18(3),** 238-40 (1993).

[12] Young, Russell D., "Surface microtopography", Physics Today, **Nov** 43 (1971).

[13] Chetwynd, Derek G., and Smith, Stuart T., "High precision surface profilometry: from stylus to STM", in *From Instrumentation to Nanotechnology*, Gardner, J. W., and Hingle, H. T. eds. (Gordon and Breach, Philadelphia, 1991).

[14] Young, Russell, Ward, John, and Scire, Frederic, "The topografiner: An instrument for measuring surface microtopography", Rev. Sci. Instrum. **43**, 999 (1972).

[15] Fowler-Nordheim tunneling, see Wolf, E. L., *Principles of electron tunneling spectroscopy*, (Oxford University Press, New York, 1985), page 66.

[16] Simmons, John G., "Generalized Formula for the Electric Tunnel Effect between Similar Electrodes Separated by a Thin Insulating Film", J. Appl. Phys. **34**, 1793 (1963).

[17] Rev. Mod. Phys. **59 (3)** 615 (1987).

[18] Binnig, G., Rohrer, H., Gerber, Ch., and Weibel, E., "Surface studies by scanning tunneling microscopy", Phys. Rev. Lett. **49**, 57 (1982); Binnig, G., and Rorher, H., "Scanning tunneling microscopy, and atomic probe", Scanning Electron Microscopy/1983/III 1079 (1983);

[19] Described in full detail in Chapter 4.

[20] Binnig, G., and Rohrer, H., "Scanning tunneling microscopy", IBM J. Res. Dev. **30**, 355 (1986b); Hansma, Paul K., and Tersoff, Jerry T., "Scanning tunneling microscopy", J. Appl. Phys. **61**, R1 (1987).

[21] The tunneling current depends on the density of electrons at the surface and their Fermi energy. The density of electrons is substantially affected by any nearby charged regions and the tunneling material. The work-function between the tip and sample material produces a potential between them that affects the electron density. If the materials have been exposed to air, the surface may oxidize changing the surface material. A thin layer of water or other contaminates between the surface and probe can also affect the tunneling. See chapters 4 and 8 for more detailed theory of the tunneling equation along with relevant references.

[22] A data file containing only height information for 1 Å resolution over a 10 μm × 10 μm area would require 10^{10} bytes.

Chapter 2.

Scanning Tunneling Lithography: Techniques

Having described, in the previous chapter, a possible tunneling based nanomemory, the problem remains to utilize the STM probe to act as a means to lithographically 'write' information. Lithography here is used in the broader sense of marking a surface encompassing any technique. Quate[1] [1986] has obtained a general patent on the idea of using tunneling technology to produce memory bits. His patent suggests using an electromagnetic pulse between the tip and sample to produce a change (lithography) on the sample surface which can be detected.

Expanding on Quate's ideas, let us consider some possible tip-sample configurations which may be used to produce detectable changes in the sample surface. The following sections expound schema which may be able to produce the bits to be used in the memory and focuses on schema which work at room temperature and without the necessity of housing the probe and surface in vacuum. Discussion will involve both the basic pros and cons of the suggested memory schema with more detail given in subsequent relevant chapters.

2.1 Mechanical contact

We have mentioned in the previous chapter that the STM probe does not theoretically contact, but hovers within a nanometer of the surface to maintain a constant tunneling current. If the probe were forced

to momentarily contact the surface, the possible result would be an altered surface.[2] This is similar to machining with the probe acting as a cutting tool or as a mechanical indentor much like Edison's original phonograph.

Figure **2:1** illustrates this mechanical contact scheme. The tip is brought to within tunneling distance of a surface [Fig. **2:1**(a)]. Then, the tip is forced to indent the surface [Fig. **2:1**(b)], provided the tip is harder than the substrate[3]. This could be accomplished by removing the bias, causing the

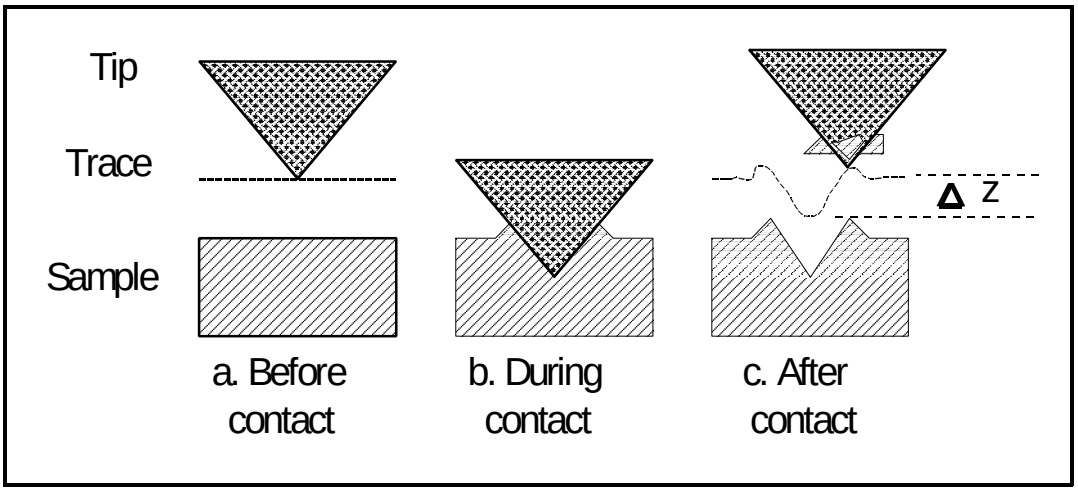

Figure 2:1. Mechanical contact method of altering surface, showing surface appearance and tip positions a) before, b) during, and c) after contact.

current to drop, effecting a servo response of the tip toward and into the surface. Another possible method would be to temporarily disable the servo feedback and mechanically or electrically displace the probe into the surface. The result would be an indentation in the surface as shown in Fig. **2:1**(c).

Using a microhardness indenter, Gane and Cox [1970a] tested annealed and cold-worked gold using a 200 nm radius spherical tungsten

probe. They found that as the indentations approached 200 nm, the hardness appeared to increase by a factor of 2-3. In a further study on Au, Al, Cu, Ni, Fe, and Zn, Gane [1970b] found that the apparent hardness increase was due to hydrocarbon contamination on the indenter or sample. The contamination allowed the surface to slip (during plastic deformation) with respect to the indenter, inducing lateral stress relief. Using a Berkovitch diamond[4], Pethica [1983] made indentations as shallow as 20 nm, which showed a piling up of material on the periphery.

This method has the advantage in that it is very simple to facilitate. However, since there is mechanical contact, material from the surface may deposit on the probe altering its geometry and tunneling properties. Also, since the spacing of bits we desire is on the order of nanometers, such a method would almost certainly cause the assumed position of the tip (addressing) to be corrupted after a series of indentions. This method also has the disadvantage that it could not be implemented "on the fly", that is, the tip must stop over a particular position, which would increase memory writing time.

2.2 Field evaporation of surface atoms

Pulses superimposed on the normal voltage between the tip and sample have been found to produce nanometer scale surface modification on graphite and metals.[5] This technique can be used to create a memory bit by the following procedure:

1. The tip is scanned close enough to the sample to induce

measurable tunneling [see Fig. **2:2**(a)].

2. A voltage pulse is superimposed on the normal bias causing "field evaporation" of atoms near the surface [see Fig. **2:2**(b)].

3. The resulting hole is read as a memory bit by once again scanning the surface and using the incremental change in height, delta Z, or current as a criterion for the existence of a memory bit [see Fig. **2:2**(c)].

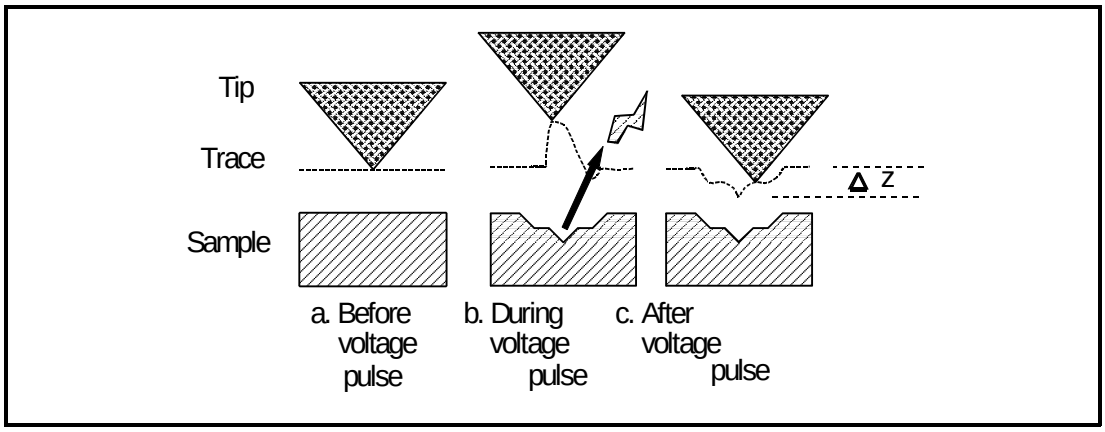

Figure 2:2. Simple surface alteration scheme for making nanometer scale memory bits.

Notice the change in position of the tip during the voltage pulse. This could result from the response of the servo feedback to induced currents. These induced currents could come from increased tip-sample current or from ac currents due to stray capacitances[6].

It is relatively easy to implement this scheme since the only materials necessary are the tip and conducting surface. The conducting surface needs to be free from any surface roughness comparable in size to the desired bit in order to be able to differentiate the bit from intrinsic surface structure. Conducting crystalline samples may be able to provide

the necessary surface smoothness, but they are expensive. The required flat surface may be produced by depositing a thin conducting film on polished glass or other flat surface which does not conduct as well. The field evaporation scheme for a thin film on a crystalline or smooth surface is shown in Figure **2:3**. Atoms in the thin film are field evaporated using the previous scheme to expose the substrate and leave a hole similar to the one in Figure **2:2**.

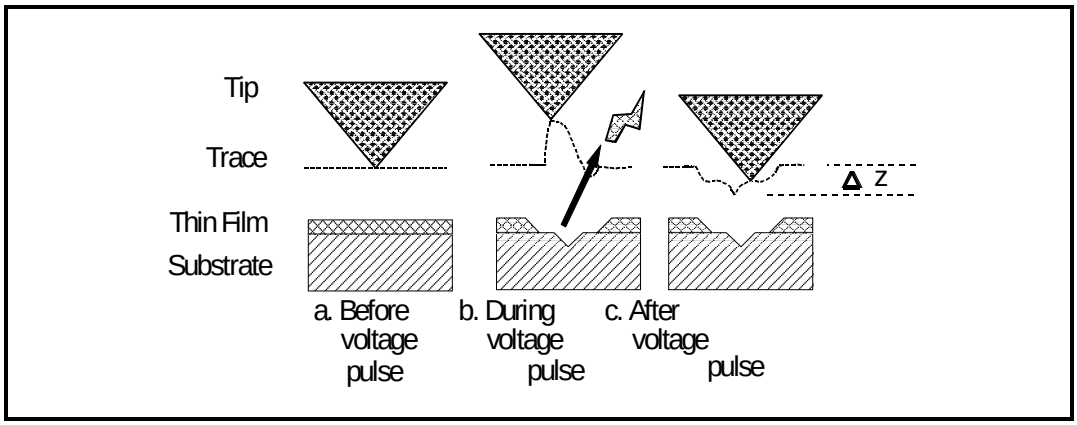

Figure 2:3. Simple thin film surface alteration scheme for making nanometer scale memory bits.

The material which has been field evaporated must end up somewhere else. If the material deposits on the tunneling tip or elsewhere in the memory area, the schemes of Figures **2:2** and **2:3** could be corrupted in the following four ways:

1. The material deposits on the tip changing the composition requiring a different voltage pulse to modify the substrate.
2. The material deposits on the tip changing the position of the point of the asperity closest to the sample. If, after making hundreds of thousands of bits, the effective position of the tip changes by the bit separation, tracking would be

destroyed.

3. The material from the tip could redeposit in a previously made bit (hole), filling it up, therefore reversing the information in that bit.

4. Voltage pulses applied between a tunneling tip and surface have been shown to cause diffusion of adsorbate atoms.[7] If the holes which have been created diffuse across the surface or reconstruct over a period of time, then the stored information can be lost, changed, or destroyed.

2.3 Field deposition onto substrate

It has been shown in the literature[8] that it is possible to deposit material onto a substrate from the tip, from organometallic gases, and from liquids. Figure **2:4** illustrates the simple case where the material comes from the tip.

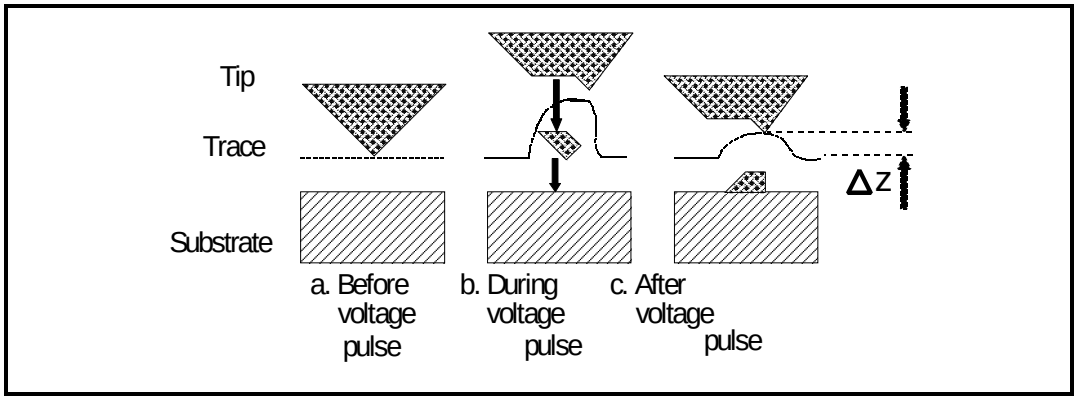

Figure 2:4. Tip deposition scheme for making nanometer scale memory bits.

Figure **2:5** illustrates the concept for a liquid or gas environment. The procedure is similar to that described for field evaporation, with the exception that the material comes from the tip or

ambient instead of the substrate. The material in the gas or liquid could be deposited either directly onto the sample or indirectly by contacting the tip first [see Fig. **2:5**(b)].

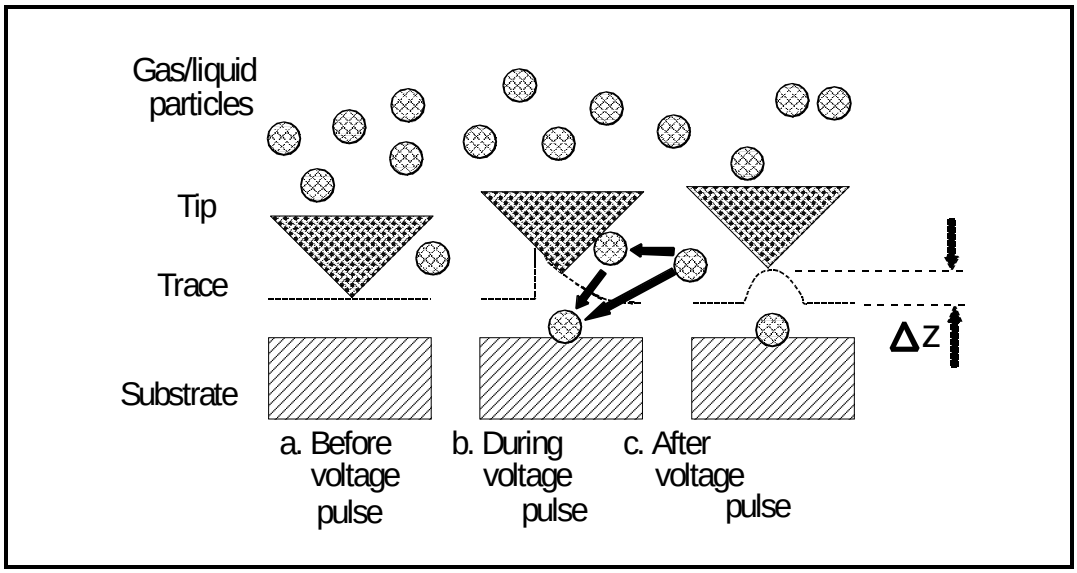

Figure 2:5. Gas/liquid environment alteration scheme for making nanometer scale memory bits.

When material leaves the tip [see Fig. **2:4**(b)], its shape is changed. Again, after many bits have been made, the position of the point on the tip would be changed enough to corrupt any tracking scheme. Material that is deposited from a gas or liquid would have to bond or react with the surface to prevent the material from being reabsorbed into the liquid or gas, and also prevent corruption of the bit by surface diffusion. If a liquid or gas scheme were incorporated into a manufactured memory, problems would arise with packaging the memory to prevent leakage of the ambient, while also adding additional expense.

2.4 Field induced chemical alteration of surface

This technique[9] utilizes an applied electric field to chemically modify a compound's structure. An applied voltage pulse between the STM tip and compound provides the energy necessary to break or induce bonding. This altered bonding changes the electrical properties and/or topography of the

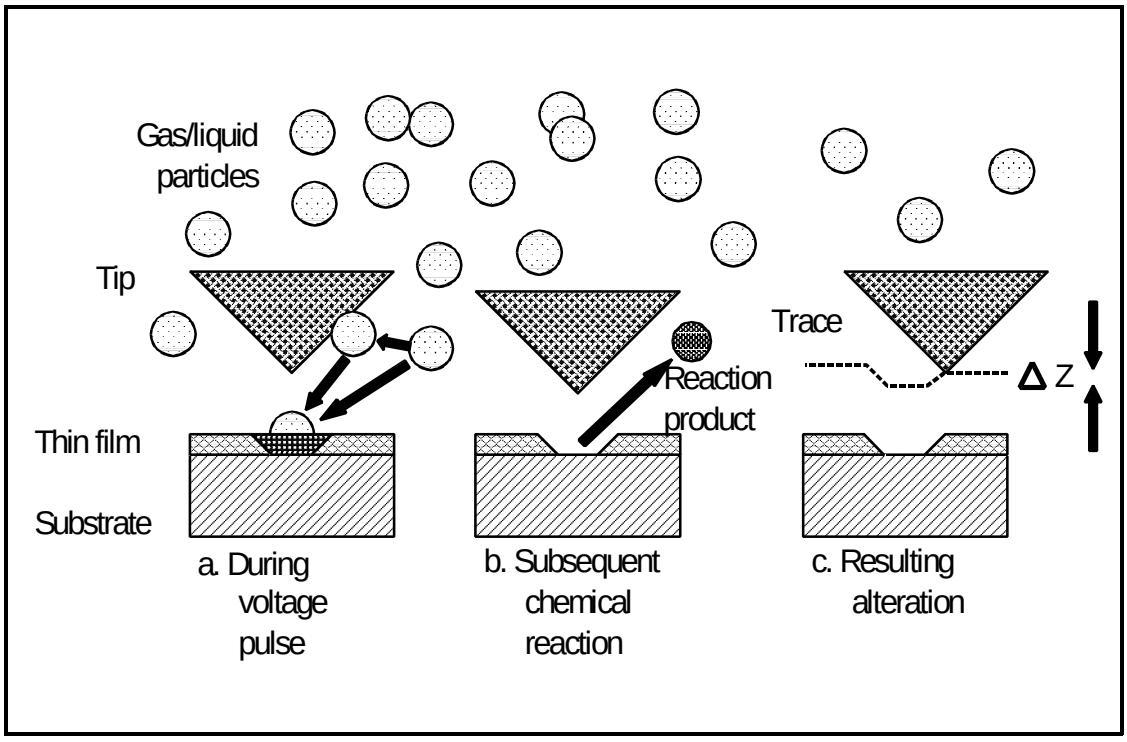

Figure 2:6. Field induced chemical and/or structural alteration scheme within a liquid or gaseous ambient.

surface. Such a scheme involving the presence of a liquid or gas is illustrated in Figure **2:6**. The voltage pulse invokes a change in the surface allowing material deposited from the ambient [Fig. **2:6**(a)] to react with the surface [Fig. **2:6**(b)] which produces a reaction product which is reabsorbed into the ambient. The resulting surface topography has been changed by the induced reaction [Fig. **2:6**(c)].

Figure **2:7** illustrates a similar process in which there is no

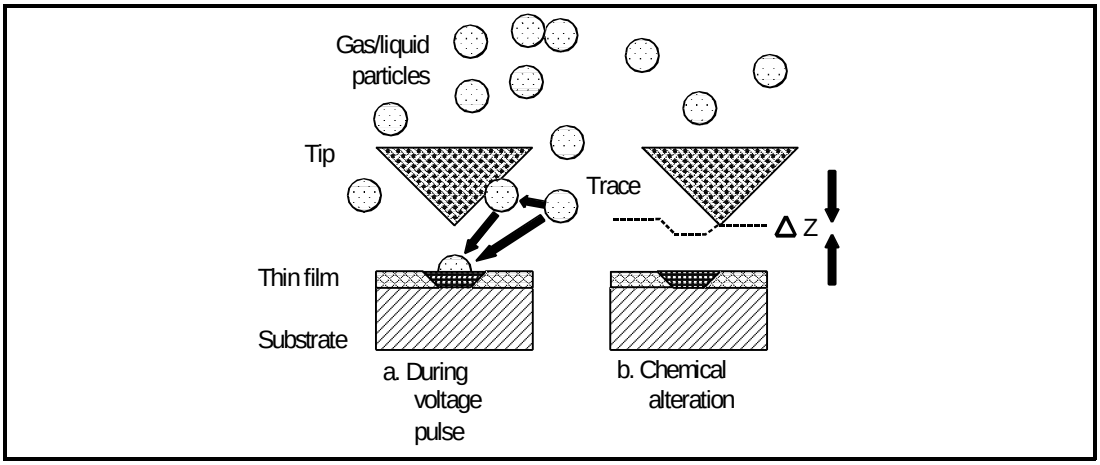

Figure 2:7. Chemical alteration due to an applied electric field with or without an ambient reaction.

discharged reaction product. The field induces a chemical change with or without a reactant from the ambient [Fig. **2:7**(a)]. Since tunneling depends on tip and sample chemical properties[10], the resulting surface may experience no actual topographical change [Fig. **2:7**(b)] and yet give the illusion of an apparent topography change. For small constant voltages, the predominant term affecting the current can be approximated[11] as e^{-ks}, where $k = 1.15\phi^{½}/[Å(eV)^{½}]$, ϕ is the average work functions (3-6 eV) of the tip and sample, and s is the tip-sample separation in Angstroms. If the work function decreases by half, the separation changes to about 1.4 of its initial value. For a normal tunneling current of 1 nA, the separation is less than a nanometer[12], which yields a height change on the order of a few Angstroms. Such a small height change may not be large enough to be detected above normal surface roughness. There could also be a simultaneous topography change which is detectable (Compare Fig. **2:5**c). Additionally, the presence of light[13] on the surface could be added into the chemical process to induce surface

chemical/topographical alteration. The effect of the light would only be observed over the tunneling region, if both photons and electric field were necessary for alteration of the surface.

2.5 Electrical charging of insulator interlayer

By using a sandwich structure consisting of a conducting substrate, a hole or electron trapping insulator, and a couple of monolayers of a

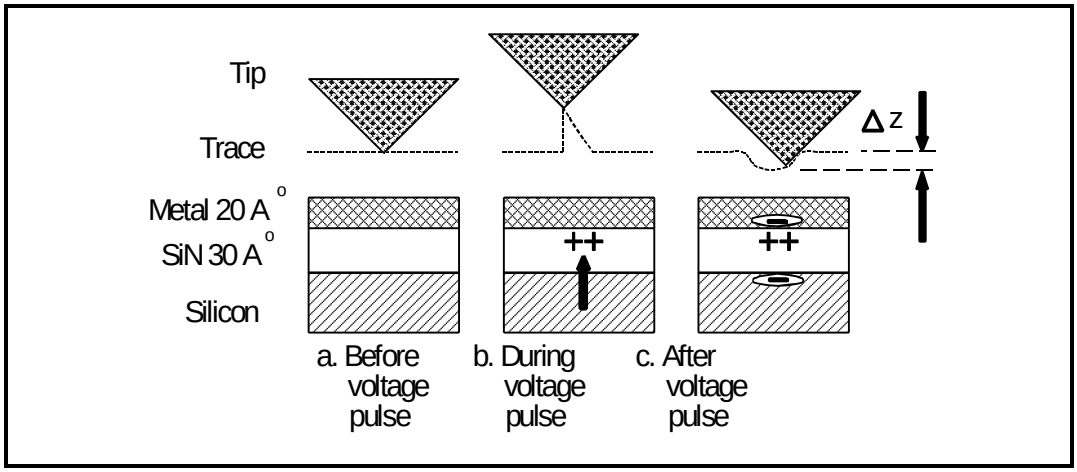

Figure 2:8. Si-Si_2N_3-Metal application of a substrate-insulator-metal scheme for making nanometer scale memory bits.

conducting thin film surface, it may be possible to create a memory using trapped charges[14] in the insulator to change the dc conductivity of the surface. This scheme is illustrated in Figure **2:8** using a Si-Si_2N_3-Metal (silicon-silicon nitride-metal) sandwich structure. The memory would work in the following manner:

1. The tip is scanned within tunneling distance of the sample [see Fig. **2:8**(a)],
2. A short duration (μS) voltage pulse superimposed on the bias causes charges to overcome the potential barrier

between the silicon and nitride, some of which get trapped in naturally occurring traps in the silicon nitride [see Fig **2:8**(b)].

3. The charges trapped in the nitride produce an image charge in the thin metal film on the nitride changing the films conductance, causing a change in the tip position as it scans over the newly manufactured bit [see Fig **2:8**(c)].

This method overcomes the problems associated with material particulates contaminating the memory surface or probe tip. However, a drawback to the substrate-insulator-metal method is that the charges may detrap over time if the surrounding potential barriers are not sufficiently large. Another problem would be manufacturing the surface film thin enough to be affected by the image charge. In the above particular example, getting a metal to adhere to the Si_2N_3 and forming a uniform 20 Å nanometrically flat film is by no means trivial. Using electrets as substrates would not work as well since their surrounding electric field degradation is higher than a monopolar charge.

2.6 Magnetizable interlayer

Another possible way of writing bits involves an insulating magnetic interlayer such as CrO_2 between a substrate and thin conducting film. The scheme is illustrated in Figure **2:9**. The bit writing procedure is as follows:

1. The tip is scanned within tunneling distance of the

sandwich structure surface [Fig. **2:9**(a)].

2. A magnetic field pulse is applied between the tip and magnetic interlayer changing the magnetic orientation of the interlayer [see Fig. **2:9**(b)].

3. The changed magnetic orientation of the interlayer affects the dc conductance of the surface film producing a height variation in the tip position as it scans. The bit is read by the rate of change of the tip height, delta Z, [Fig. **2:9**(c)].

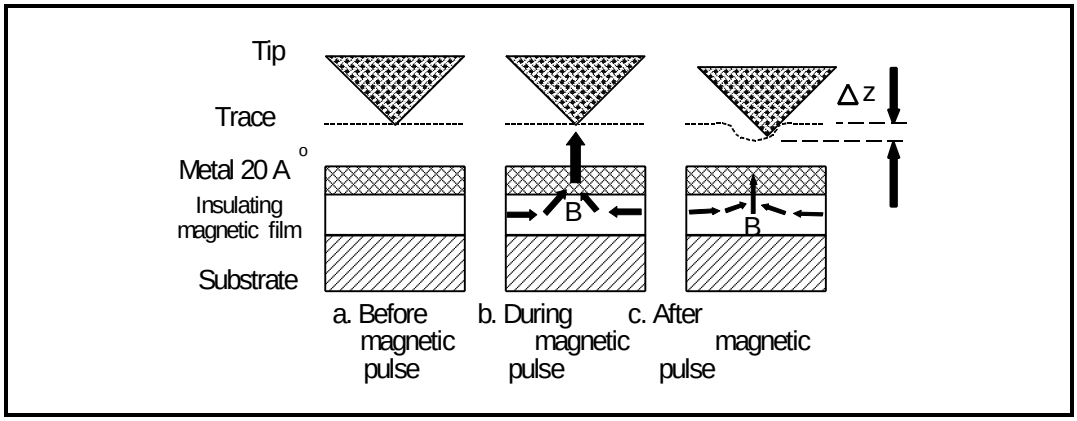

Figure 2:9. Magnetized interlayer scheme for making nanometer scale memory bits.

The minimum size for single domain magnetic particles is about 20 nm with smaller sizes becoming super paramagnetic.[15] This limits the bit size to 20 nm. However, the magnetized interlayer method conquers the problems of loose nanodust corruption and surface diffusion. However, any magnetic dust allowed in the vicinity may be attracted to the surface. Also, the question arises as to whether we will be able to sufficiently magnetize the interlayer and, if so, will the magnetization affect the

conductance a detectable amount: $\vec{F} = q\vec{v} \times \vec{B}$ away from magnetized area.

Another problem is changing the magnetic flux on such a small scale. Additionally, the application of a magnetic pulse will produce an attractive force between the tip and substrate. The tip should be constructed in such a way as to prevent mechanical contact during the presence of this force.

2.7 Alternate schema of reading the manufactured bits

This section gives a brief description of possible methods to produce a displacement in the height position of the z-axis to represent the existence of a bit. Since it is practically impossible to deposit thin films without some inherent nanometer scale topography, the manufactured bits must cause characteristic changes in height greater than that of the deposited films. Alternate methods of detecting (reading) the bits should be considered, if other techniques are found inadequate.

2.7.1 Bit reading via ac conductance

An ac signal could be superimposed on the tip to sample dc potential with a frequency much higher than the servo response of the probe. The ac conductance could be measured with lock-in-amplifier type circuits. This ac conductance may be sensitive enough to detect the type of changes the bit manufacturing schemes produce. The ac conductance would depend on the dc current, surface free electron density, work functions of the tip and sample, and the tip-sample geometry. Although

the required electronics are the same, this technique differs from capacitance[16] methods in that it detects electronically induced current changes (in phase with signal) rather than geometry induced charge displacements (out of phase).

Illustration of the expected ac bit detection measurements are shown in Figure **2:10**. The bits could be detected by changes in the ac conductance.

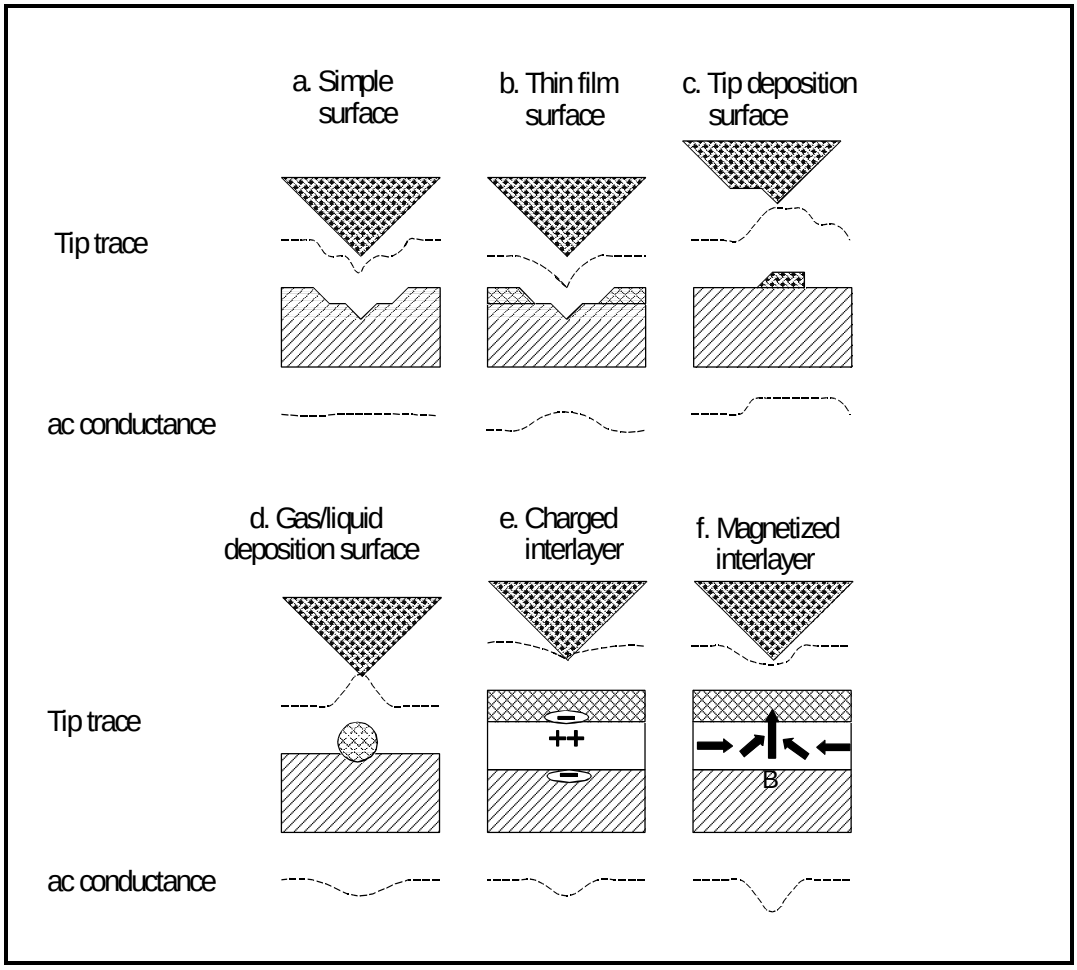

Figure 2:10. Conjectured ac conductances of the bit-making schemes of Figures **2:2**-**2:9**.

Figure **2:10**(a) shows that there should be very little change in the ac conductance because the substrate material the tip sees remains intrinsically the same. Although there is some topography, the tip remains

at a constant height above the substrate. If there is enough material removed from thin film to expose the substrate, as in Figure **2:10**(b) the ac conductance would be different for each of the two different surface materials. Similarly if material from the tip were deposited on the substrate as in Figure **2:10**(c), then the ac conductance should be higher between two like materials. Likewise, a particle deposited from a gas or liquid onto a surface would have a different conductance than that of the surrounding substrate as in Figure **2:10**(d). Although the surface material doesn't change in Fig **2:10**(e), the conductance is changed by the underlying static charge. Similarly, the underlying magnetization of the surface in Figure **2:10**(f) may have a sufficient effect on the surface to change the conductance. The hard part of implementing this scheme is getting the conductance detector close enough to the tip so that it is not affected by stray fields. Another problem will be getting enough ac amplification to detect the picoamp changes in current. This method could be particularly useful in overcoming problems associated with intrinsic sample topography.

2.8 Reported Experiments

Chapter 3, Scanning Tunneling Lithography: State of the Art, and Chapter 4, Scanning Tunneling Lithography: Experiments, give examples of research into modifying the surfaces of materials using a STM probe. The reported experiments will give further insight into the alterability, reproducibility, durability, and readability issues which must be

confronted. Chapter 5, Scanning Tunneling Lithography: Material Précis, gives a material oriented analysis for propensity as a memory basis.

2.9 Summary

We have described several possibilities for altering a surface in such a way as to be detectable as a memory bit. These include mechanical contact, field evaporation and deposition, field induced chemical alteration, and charging or magnetization of an interlayer under a thin film. Each method has its limitations and problems such as tip transformation resulting in corrupted addressing. The simplest methods are intentional tip-substrate contact and field evaporation/deposition of a surface. These methods require a minimum of processing procedures. Field methods are preferred over mechanical contact since it can be accomplished with the tip moving and thus reducing writing time. Evaporation is preferable to tip deposition since we desire the tip to maintain its addressing integrity. Our experiments, reported in Chapter 4, have been limited to field methods for their simplicity. Likewise we have relied on topography height changes for determination of alteration.

[1] Quate, Calvin F., "Method and means for data storage using tunnel current data readout", U. S. Patent # US4575822, Mar. 11, 1986.

[2] For a discussion of literature involving indenting with an STM tip, see Chapter 3, Section 3.1, Mechanical contact surface alteration.

[3] See Landman, Uzi, Luedtke, W. D., Burnham, Nancy J., and Colton, Richard J., "Atomistic Mechanisms and Dynamics of Adhesion, Nanoindentation, and Fracture", Science **248**, 454 (1990).

[4] The Berkovitch diamond indenter has a triangular base with the sides at an angle of 65.3 degrees to the vertical. Pethica reports that it has the same hardness relationship as a Vickers diamond.

[5] For a complete listing of references see Chapter 3, Section 3.2, Field induced material transport.

[6] For a theoretical discussion of the effect stray capacitance can have on the current to voltage converter of the STM see Chapter 6, Mechanical and Electrical Design Considerations.

[7] See Chapter 3, Section 3.3, Field induced diffusion of adsorbates, for detail and references.

[8] For detail and references see Chapter 3, Section 3.4, Field induced surface alteration within a gaseous ambient, and Section 3.5, Field induced deposition and etching within a liquid or transporting film.

[9] For references and detail see Chapter 3 , Section 3.6, Field and/or electron induced chemical modification.

[10] Such things as charged regions and the work function mentioned in Chapter 1.

[11] Simmons, John G., "Generalized Formula for the Electric Tunnel Effect between Similar Electrodes Separated by a Thin Insulating Film", J. Appl. Phys. **34**, 1793 (1963).

[12] See Chapter 4 for theoretical graphs of tunneling current versus tip-sample separation.

[13] For references and detail, see Chapter 3, Section 3.7, Illumination assisted field induced surface lithography.

[14] The charging of silicon nitride for the mechanism of a memory has been shown in Barrett, R. C., and Quate, C. F., "Charge storage in a nitride-oxide-silicon medium by scanning capacitance microscopy", J. Appl. Phys. **70,** 2725 (1991). For more detail and other references on thin film charging see Chapter 3, Section 3.8, Localized electrostatic charge implantation in films.

[15] Camras, Marvin, *Magnetic Recording Handbook*, (Rienhold, New York, 1988) page 94.

[16] Matey, J. R., and Blanc, J., "Scanning capacitance microscopy", J. Appl. Phys. **57** 1437 (1985); Bugg, C. D., and King, P. J., "Scanning capacitance microscopy", J. Phys. E: Sci. Instrum. **21** 147 (1988).

Chapter 3.

Scanning Tunneling Lithography: State of the Art

This chapter reviews the state of the art in surface alteration techniques using a scanning tunneling microscope. Application of this body of knowledge to the alterability, reproducibility, durability, and readability necessary for the development of a nanomemory will be discussed in separate sections in Chapter 5. The results of investigations for this thesis will be mentioned only briefly in this chapter with a more detailed description included in Chapter 4. The present body of knowledge is discussed including the variety of methods and parameters used for surface alteration and some postulated mechanisms. Discussion uses terminology of the previous chapter on proposed bit writing techniques. Unless otherwise noted, all work was carried out under ambient conditions. The works are classified according to the alteration method for easier comparison with Chapter 2 on techniques. Some papers are mentioned under more than one heading where there was more than one procedure reported. This chapter forms a detailed summary of the results as they are relevant to the fabrication of a nanomemory. Additionally, the results are classified and discussed by material in Chapter 5. This chapter along with Chapter 4 are important for the foundation of Chapter 5. However, for those interested in a summary of the experimental results, this chapter may be skipped and used as a detailed reference for Chapter 5. Since the works are summarized here, and in order to conserve space, the paper references are given at the

beginning of the discussion and do not appear at the end of the chapter, but are detailed in the bibliography at the end of the thesis. Other relevant references not the immediate subject of discussion are included as chapter endnotes. Tables summarizing each sections reports are included at the end of the chapter.

3.1 Mechanical contact surface alteration

Abraham *et al.* [1986] Surface alteration of Au in UHV with a W STM tip produced 10 nm sized features with an identifiable deformation region extending 50 nm away in major dimension. By reducing the tunneling resistance to 200 ohms, the feedback caused the probe to contact the surface. They also reported that the contact sometimes caused changes resulting in shifts and distortions of the tip, so that, they were no longer positioned over the same area of the surface.

Garfunkel *et al.* [1989] A crystalline surface of the low conductivity oxide $Rb_{0.3}MoO_3$ was altered by reducing the STM tunneling voltage to 10 mV forcing the tip to penetrate the surface layer to maintain the preset tunneling current. Features as small as 0.3 nm deep and 6 nm across were etched in the surface. Lines, 150 nm long by 8 nm wide by <1 nm deep, and a 100 nm square were formed by abrasively dragging the tip along the surface. The features produced were stable and did not degrade in time over a 4 hour period.

Gimzewski *et al.*[1987] For an iridium STM tip displacement of 3 nm towards the surface, a hillock 10 nm wide and 2 nm high was

formed on a silver film on silicon in UHV.They also produced indentations with a degraded tip, which could be diagnosed from changes in the current-voltage I(V) characteristic. They attributed the hillock formation to clean metal surfaces forming a cohesive bond which resulted in tensile necking as the tip was withdrawn. Cleanliness of the tip was determined by current vs tip-sample displacement I(S) characteristics. The indentations were thought to form when there was contamination present which prohibits cohesive bonding. Indentations <1 nm deep, disappeared before subsequent scans were completed.

Harmer *et al.* [1991] STM imaging of the high temperature superconductor, $YBa_2Cu_3O_{7-x}$ was found to alter the surface over time. The nucleation of holes was followed by growth and coalescence upon repeated rastering. Nucleation was presumed to occur at surface defects. The material was transformed using both, positive and negative, scan biases. They believe the transformation to be due to a mechanical tip-sample interaction. They propose that this interaction was due to adsorbate layers present in air. Rough surfaces were flattened, and squares and lines were formed while scanning with a bias of 1.51 V (insufficient for tunneling) and a current of 0.26 nA.

Jaklevic *et al.* [1988] A flat (111) terrace on a gold surface under UHV was touched by a tungsten STM tip producing monolayer deep craters. Some were only big enough to hold 3200 atoms (a 20 nm dia hole 1 nm deep). They suggest that the atoms from the crater may be forced into the bulk as interstitials. Sometimes tip contact caused a loss or gain

of asperity atoms resulting in a translation of the position. Over a period of 8 min, a hole big enough to hold 25 atoms was filled by what was thought to be surface migration. After 30 min, a hole missing 125 atoms became filled and after 120 min a 900 atom hole filled.

Marchon *et al.* [1988] Gently touching the surface of Re(0001) with a W tip produced clusters of 2-5 nm hills. Barrier height measurements suggest the clusters contained material electronically different from the bare Re surface.

McCord *et al.* [1987]. An insulating 20 nm film of calcium fluoride was machined by a tungsten STM tip. The tip was forced to penetrate the film in order to achieve tunneling. As the tip was laterally moved, 360 nm wide lines were machined out. The authors show evidence implying that particulates were left on the tip after machining.

Stroscio *et al.* [1991] The authors demonstrate a process for sliding CO and Pt along a Pt(111) surface and sliding Xe and Ni along a Ni(110) surface in UHV (at 4^{o}K). By adjusting the position of an STM tip with respect to an adsorbate, the electrostatic and van der Waals forces on an atom can be controlled to produce motion of the adsorbate. The authors demonstrate the ability to position atoms side by side to form lines or any desired planar structure.

van Loenen *et al.* [1990] By moving a tungsten STM tip 2 nm towards a silicon surface, circular holes were formed with "walls of atoms pushed away from their respective centers". The holes were 10 nm in diameter and were positioned side by side to form regular

arrays. By making hole spacing less than the hole diameter, continuous lines were formed. Experiments were done under UHV.

Virtanen *et al.* [1991] A Pt-Ir STM tip was used to mill a rough laser ablated $YBa_2Cu_3O_{7-x}$ thin film to nanometer scale flatness. By keeping the applied voltage low, the tip collided with the sample causing the surface to flatten. A sample with up to 600 nm surface structure was smoothed to one having 15 nm after milling. Square areas greater than 100 μm^2 were smoothed. Grooves were also milled having depths greater than 100 nm. Observing a fabricated line for 18 hr. revealed a continuous transformation of the region near the line which reached a steady state condition after about 1 hr.

Yokohata *et al.* [1990] Gold surfaces were indented with a Pt STM tip. Tip indentations from 30-300 nm were compared. For greater indentations, buckling of the tip was observed causing tip lateral displacements of up to 250 nm. Profile curves after indentation showed decreased resolution.

In a similar fashion, an atomic force microscopy[1] (AFM) probe has been used to mechanically contact and alter surfaces. Kim *et al.* [1991] produced wear regions on $NbSe_2$ and MoS_2 with widths ranging from 2-200 nm. Leung *et al.* [1992] show normal AFM scanning causing a time evolved roughening of a polystyrene surface. Weisenhorn *et al.* [1990] were able to nanometrically modify ammonium ions deposited onto a zeolite substrate.

The molecular dynamics work of Landman *et al.* [1990] for a Ni tip

coming into contact with a Au substrate show atoms leaving the tip to deposit on the sample and vice versa.

In STM work it is not uncommon for a tip to inadvertantly contact the sample. This type of mechanical contact often occurs during initial tip-sample engagement as the tip is positioned to within the tunneling region. If the sample surface cannot conduct the desired current or the electronic servo feedback responds too slow, the tip pushes into the surface. Image 3:1 shows and extreme example of collision damage in a silicon nitride thin film on silicon. The hole is 1.5 μm in diameter and at least 20 nm deep with damage extending over 5 μm.

Image 3:1. Tip engagement damage in a silicon nitride thin film. 10 μm × 10 μm.

3.2 Field-induced material transport

Literature concerned mainly with the induced transfer of material from one place to another using an increased electric field between the tip and sample is reported. The increased field in all examples is produced by an increase in potential between the tip and sample. This potential increase induces a corresponding increase in current and electrostatic force between the tip and sample, thus complicating determination of the

actual distortion mechanism. Most experiments were carried out in either an ultra-high vacuum (UHV) or in air without any other intentionally supplied gas or liquid between the tip and sample. Ambient air is present unless UHV is specifically mentioned.

Akari *et al.* [1991] The surface of WSe_2 was modified by superimposing a voltage pulse on the bias between the surface and a gold tunneling probe. Rectangular pulse shapes between 4 and 6 V, produced currents $\leq$ 200 nA and altered the surface. To produce structure, the pulse duration had to be altered between 10 and 400 ns depending on the sharpness of the tip. A cluster type feature was produced that was 5 nm in diameter and 1-2 nm deep. After 2 minutes the cluster had taken the shape of a triangle and grown slightly. The triangular structure continued to transform over time, increasing in size to 75 nm with the inner depth increasing to 12 nm after 20 min. Observing two triangles (produced by two pulses) over time, they eventually grew large enough to touch and fuse together. Imaging was performed with 0.6-0.9 V biases and a 0.5 nA current.

Albrecht *et al.* [1989]. Nanometer scale holes, 2-10 nm in diameter, were produced on the surface of HOPG. The holes were created with 3-8 V, 1-100 μs, pulses applied between the W tip and sample (sample positive). A typical hole, 0.7 nm deep and 4 nm across, revealed the perimeter of the hole to be higher than the surrounding surface. The threshold amplitude for hole formation was also tip dependent along with the size and shape of individual features. The holes

written toward the end of a series in a pattern were found to be as much as three times bigger than the initial holes. When a layer of graphite was unexpectedly removed by the tip, some holes in the pattern were still visible demonstrating that the features were in fact holes. 10 % of the tips that were experimented with did not produce any holes whatsoever. One tip produced holes on 496 out of 498 tries. Under ultrahigh vacuum, no holes were formed even with amplitudes as high as 10 V, nor were holes manufactured when the tip and sample were exposed to benzene, oxygen or 100 Langmires of water. The hole fabrication resumed upon venting to atmosphere. Voltage pulses under the water, however, resulted in the deposition of contaminants upon the surface. Examining the feedback response, indicated that the tip pulls away from the sample during pulsing. Intentionally extending the tip 100 nm towards the sample caused no surface features, possibly due to the elastic nature of the graphite. In view of their findings under controlled ambient environments, they suggest that a chemical reaction may be possible for the formation of holes.

Becker *et al.* [1987] A c-2×8 reconstructed (111) Ge surface was altered under UHV environment. The initial bias was -1.0 V and the W tip was servoed to 20 pA tunneling current. A bump that was 8 Å Full- width half-maximum (FWHM) was produced by raising the tip bias to -4 V and noticing a 1 Å rapid shift in the servoing response. Surface transformation was not always induced.

Casillas *et al.* [1991] In this work, a 50 nm Pt film was deposited onto mica. A 10 nm Ti film was then deposited onto to the Pt surface. The Ti film was thought to completely oxidize after coming into contact with air. The resulting TiO_2 was removed by linearly cycling a potential between ±2 V at a rate of 80 V s^{-1} between the film and a Pt-Ir STM tip. The initial tip to sample distance was set with a 0.3 V bias and a current of 0.5 nA, then held constant for alteration. After cycling the tip ±2 V for 0.25 s, a 5 nm radius disc shape was revealed. Voltage cycling as low as ±0.3 V produced what was thought to be TiO_2 removal. This small threshold value, they consider to be indicative of a physical process (e.g. dielectric breakdown) rather than a chemical reaction. They showed that the current-voltage characteristics were ohmic over the disc region and rectifying over the TiO_2 film. By changing peak voltages and/or initial tip-sample displacements, disc shaped regions with radii from 5-36 nm were produced.

Emch *et al.* [1989] Like Casillas, Emch used mica substrate but with a 100 nm Au film for studies. Tunneling currents near 1 nA and a tip bias of 100 mV were used for imaging. An irregular hole 10 nm wide was formed on the fly by applying a voltage pulse while the tip was scanning. Both hills and holes were formed. No polarity dependence was observed, but there appears to be a threshold voltage and minimum pulse width for formation. The flattest newest samples and fresh tips produced the minimum thresholds. Small, 5 nm wide, features were written with 3 V, 10 ns voltage pulses. Blunt or dirty tips required pulses of 5 V for surface

alteration, and were accompanied by massive tip change. In one experiment, three of four attempts to produce holes were successful. Diffusion was observed on the surface for naturally occurring and fabricated features. An irregular 10 nm hole was observed to disappear over time due to possible self-diffusion migration. Movement of gold steps was observed to be as much as 10 nm in 20 s. They report a private communication from G. Hadziioannou that hydrophilic Au surfaces become hydrophobic after a few moments exposure to air.

Heinzelmann *et al.* [1988] After raising the bias on a $HoBa_2Cu_3O_{7-x}$ sample to 4 V and the tunneling current to 10 nA for 5 s, a 75 nm edge triangular hole with a depth of 40 nm was produced. Ten minutes after the formation of the hole, the apparent depth had decreased to near 4 nm, even though the outer shape did not change. Repeating the process 80 times produced holes ranging in diameter from 10-80 nm. A threshold of 2.0 V was observed for modification to take place. Imaging with negative sample biases was not possible and imaging with positive sample biases below 1 V was only occasionally possible.

Hoffmann-Millack *et al.* [1990] A vacuum-annealed gold foil was altered with a 2 V stepped (1 V/step, 1 step/0.5 s) voltage pulse applied to the W tip. The rise time of the pulse was 60 ms. The feedback was operated with a time constant of 10 ms. The result was a 4.8-8.4 nm deep, 30×60 nm hole, corresponding to the movement of about 10^7 atoms. The hole began filling in without delay with the back wall slipping into the depression with diffusion velocities as high as 4.2 Å s^{-1}.

50 min later the hole had completely filled. The ability of a tip to endure the application of a pulse depended on its shape. The authors ruled out mechanical indentation because the feedback had plenty of time to respond, keeping the current constant. Since electrons tunnel to the tip, electron heating of the sample causing evaporation was dismissed as a mechanism. They conclude that there was ion arcing from the ambient which forced the removal of the atoms.

Li *et al.* [1989]. The surface of a 2 mm Au ball was altered. While the constant current feedback loop was operational (650 mV sample bias, 1 nA current), a voltage pulse was applied to the W tip producing craters ranging in diameter from 2-8 nm. The craters had protruding rim-like features. There was a 2.7 V threshold associated with formation. A large increase in tunneling current at the beginning of the pulse was attributed to the switching of the tip from normal STM emission to field emission like tunneling. They found no evidence for physical contact between the tip and sample. Imaging individual holes for over two hours showed no apparent diffusion degradation. For distinct sectors of the Au surface, they were not able to produce any discernable features using a 2.7 V pulse. Large mounds were sometimes formed and associated with much higher and longer duration currents. With a tip that was stable for days, they generated a 40×65 nm pattern resembling Plank's constant, $\hbar$, with minimum linewidths of 2 nm. Intense local heating due to a large input power density was associated with explosive evaporation of the

surface. Marella and Pease [1989] made some calculations on the suggested local heating mechanism. They found that heat conduction away from the source was dominant and a temperature rise less than 1^{o} K should be expected.

Lyo *et al.* [1991] Nanometer scale alterations were produced on a silicon (111) 7×7 reconstructed surface. A W tip was scanned (2 V, 200 pA) at an estimated 6 Å above the surface. The tip was moved toward the silicon (2-6 Å) and a 10 ms, 3 V pulse was applied to the sample. When the tip was moved 3 Å toward the sample a small mound about half the size of a 7×7 unit cell was deposited. For a 4 Å displacement a region with a 4 nm diameter was removed. A small mound inside a 5 nm hole (mound-moat) was observed when the tip was first moved 5 Å toward the surface with a 3 V pulse. The mound was thought to form when desorbing Si atoms pile up under the tip forming a bridge between the tip and sample. The removal of the mound in a mound-moat structure with a 3 V pulse and subsequent deposition of these atoms with a -3 V pulse at an adjacent position was demonstrated. Single atom desorption was obtained with a 5 Å displacement and a 1 V pulse, but was not as reproducible as the larger scale structures. Although not mentioned, it is assumed that the work was carried out in UHV chamber to prevent surface oxidation.

Mamin *et al.* [1991]. A gold STM tip was used as an emission source to deposit material on to surfaces in UHV and air. 15-20 nm wide and 2-3 nm high mounds were deposited when voltage pulses above

3.5-4.0 V were applied to the tip. Negative and positive biases produced mounds, but when positive tip biases were used, the mounds were larger. They found that the threshold voltage was dependent on tip-sample separation. The process was almost pulse duration independent with mounds produced for durations as small as 10 ns. When the bias was near threshold, the mounds increased in size to a 20-30 nm limit. Mounds were written in a methodical manner which produced letters and a facsimile of a world map. Depending on where the tip was positioned, material could be either deposited, removed to leave a hole, redeposited in the hole and then emptied. The authors suggest the deposition or removal process was dependent on the flat, convex, or concave shape of the surface near the tip. Au tips were also used to deposit on Pt and Si, and W on Au. The W typically produce holes in the Au. They also found that static discharges remote from the STM produced depositions over 100 nm areas. UHV work showed the process to be 50 % less reliable than in air. Larger (20-40 nm) mounds were created with -4.7 V × 20 ns pulses. The lithography was 90-100% reliable with most tips. Similar to Mamin *et al.* [1990]. Thousands of pulses were not found to degrade the tip's ability to write. However, the tip was occasionally observed to alter. They proposed that migration of atoms due to the high electric field was responsible for the tip's rugged self-healing endurance.

Marchon *et al.* [1988] The surface modification of Re(0001) covered with a half a monolayer of sulfur and completely immersed under silicone oil was reported. The sample bias was raised from the 500 mV

imaging potential to 3 V for 2 s. A hole 30×50 nm wide and 0.6 nm deep was produced. Currents exceeded 100 nA during pulsing. Similar attempts to form a hole in air were unfruitful. When the polarity was reversed (under oil), clusters were produced instead of holes. The clusters, varying in size from 1-10 nm, were scattered over an area greater than 100×100 nm. They have suggested local oxidation[2] as the mechanism producing the features. Whether the W tip or Re crystal oxidizes was dependent on the polarity of the applied voltage pulse. The role of the oil was not known. Even after the numerous processes, no significant change in tip position was detected.

McBride and Wetsel [1991]. Surface modification experiments were performed involving W and Au tips, and Au and Pt samples. The samples were prepared by advancing wires into a propane-oxygen torch flame. Using a rectangular voltage pulse between a W tip and Au sample produced craters in the Au about 15 nm in diameter and 4.5 nm deep. Local heating temperature estimations yielded values that were not considered adequate for thermal hole formation. Formation of mounds were observed when the high values of current due to the pulse continued after the voltage had been terminated. They conclude from this that the tip and sample were close enough for good electrical conduction. Mounds only were found to be formed when the tip to sample voltage was raised to -3.8 V for 150 μs. Both craters and mounds were reported for a -4 V × 250 μs pulse. Mounds were successfully formed on the Au using a Pt tip and a 150 μs pulse of ±3.8 V.

Using a Au tip and a Pt sample, no feature formation was found for a 150 μs pulse between 0 and -3.5 V. At -3.6 V a mound was produced about 2.5 nm high and 24 nm in diameter. For pulse values between -3.6 and -6 V surface modification was achieved. Varying the voltage duration between 150 μs and 2.5 ms produced no effect on mound formation. They found that a mound was created in every case in which the duration of the pulse current exceeded 200 μs. Observing the threshold of mound formation as a function of the log of the tunneling resistance revealed a linear relationship. Since, theoretically, the log of the tunneling resistance is proportional to the tip-sample spacing, this was direct evidence that the formation of the mound was related to a critical electric field. The electric field was determined to be 2.3 V nm^{-1}. Using a 3.8 V × 150 μs pulse and freshly prepared W tips and in different sample locations, a mound was formed four out of five times.

Miller and Hocken [1990] Holes and hills were produced on the surface of HOPG. While holding a Pt-Ir tunneling tip at ground, a voltage pulse to the sample produced features on the surface. Hole diameters varied from 0 nm for <2 V pulse to 20 nm for a 2.75 V pulse to 200 nm for a 8 V pulse. Increasing the setpoint tunneling current from 0.5 to 8 nA increased the damaged region from 20-30 nm to 60-80 nm respectively, for a 4 V square pulse. Pulse duration was found to have a role for times less than 10 μs and for square pulses. Structures as small as 1 nm were shown. A square pulse often produced two features and a triangular pulse sometimes generated triple features for 0.1 μs pulses.

Repeated sinusoidal fields were used to produce a 40 nm L-shaped structure. It was essential to continuously increase the voltage to maintain modification. Possible mechanisms discussed were impact ionization, and induced ac currents moving the tip and producing tip-sample contact. A more involved discussion of this work will be reported in Chapter 4, which reflects the work done by this author.

Mizutani *et al.* [1990] Modification of HOPG using a voltage pulse applied to a Pt tip was demonstrated. The HOPG had been in a box with a cup of water for 12 hours prior to use. Many +3.5 V, 350 μsec square pulses were applied to the tip during a scan at points around the circumference of a 10nm circle. The result was a monolayer 10 nm hole. They suggested the possible chemical reactions represented by equations (3,1) and (3,2). They were unable to estimate the amount of energy dissipated due to a saturation of the current to voltage converter. About 80% of the trials produced pits and 5% produced circles.

$$+ H_2O_{(liq.)} + 175.32 \frac{kJ}{mole} \Rightarrow CO_{(gas)} + \quad \textbf{(3,1)}$$

$$+ 2H_2O_{(liq.)} + 178.17 \frac{kJ}{mole} \Rightarrow CO_{2(gas)} + \quad \textbf{(3,2)}$$

Ohmori *et al.* [1991] Changes in surface features were reported for Pd and Pt sheets. A tip bias of 150 mV and a tunneling current of 2 nA were used for imaging. The changes occurred during imaging of the

samples. The Pd surface was imaged for 250 minutes. During this time, grooves and hills appeared to flatten out and the formation of a mound was noted. Changes to the surface of a Pt sample were not as noticeable, but the apparent growth of four pits was observed. A Pd sample annealed in a vacuum and imaged over time showed the surface morphology changing continuously. An analysis of the current was thought to show nothing that suggested contact between the tip and sample. It was argued that the formation of some mounds was evidence that the morphological changes were not due to tip changes. They proposed that the electrostatic image force was responsible for the changes. Using a 5 Å radius tip, 10 Å away from the surface, they calculated a pressure of 10^4-10^5 N m^{-2}. Although the theoretical pressure was reduced to 10^2-10^3 N m^{-2} by lowering the tip voltage to 10 mV (0.2 nA), smoothing of the Pd surface still occurred. X-ray photoemission spectroscopy (XPS) confirmed the existence of impurities on the sample.

Parkinson [1990] The etching of two-dimensional materials was observed as a result of imaging in an STM. The process began with hole nucleation on an flat surface and continued with the growth of the holes and culminated with the merging of the holes to form a flat surface. The process was allowed to repeat for deeper etching. Sharp edges and islands were found to etch more quickly than smooth edges. Square 500 nm regions 20 layers (12.3 nm) deep were formed over an 8 hr period. In some cases the nucleation rate exceeded the expansion rate and irregular surfaces were formed. The rates of hole expansion for

various materials were as follows: InSe > ZrS_2 > $TiSe_2$ > $SnSe_2$ > SnS_2 > $NbSe_2$ > TaS_2 > $MoSe_2$ > WSe_2 > MoS_2, WS_2 > PtS_2 > $ReSe_2$, WTe_2, $MoTe_2$. The W and Mo samples only etched slowly and only at biases > 1.0 V. Variation in etching rates was observed for different tips and identical results had been observed for Pt or W tips. Attempts to find a bias dependence showed no clear trend but showed that etching can occur for positive or negative voltages. They discussed four possible mechanisms for etching. The first was a field or current induced production of reactive species from organic impurities. These species diffuse and attack the most reactive sites. This was not thought to happen due to etching occurring at biases below 100 mV. The second involved thermal effects generated by the injected electrons with the heat produced evaporating surface atoms. Since there was no observed dependence on bias or current this was not confirmed. The third proposed process was field assisted evaporation due to induced polarization and image charge repulsion of ions. Dual bias polarity etching was hard to reconcile with this scheme. The fourth mechanism considered was abrasion (mechanical contact). They argued that this was not the case since current-displacement spectroscopy revealed exponential behavior. The images did not reveal any material built up at the edge of the etched regions. Momentary tip-sample contact was also suggested. The authors proposed the combination of any of the mentioned mechanisms. One may cause nucleation, while another may produce growth.

Rabe *et al.* [1991]. Silver thin films (200 nm) thermally evaporated on a green mica film produced 100 nm Ag(111) terraces that were flat within $\leq$1 nm. These terraces furnished an area for surface alteration studies. The imaging tunneling current was between 2 pA and 2 nA. While scanning along a line the sample bias was raised from 0.5 to 5 V four times using a 100 ns pulse. The result was a horizontal row of four holes about 10 nm in diameter. Using similar pulses, occasional hills were also produced. STM imaging after eleven attempted alterations revealed the formation of nine holes and two hills with one and possibly both of the hills being over a hole. They found that a steady state current and a 50 ns pulse were sufficient to produce holes. The current also did not significantly change over a time period greater than 20 μs, demonstrating that the mechanism was not a current effect. For negative sample biases, hillocks were produced with the observation that the current sometimes shoots up indicating a point contact. Limiting the current to 4 nA during hillock formation, prohibited current related thermal effects. They conclude that hole formation was caused by field evaporation of metal ions and the hillock formation due to tip instability after repeated silver transfer during hole formation.

Saulys *et al.* [1991] A conducting oxide, purple bronze ($Na_{0.9}Mo_6O_{17}$), was cleaved along the layers of sodium atoms. The height of a Pt-Ir STM tip was set with an 80 mV bias and a 2 nA tunneling current over an area with a topographical surface roughness less than 3 nm. A several second voltage pulse (< 1 μs rise time) was used for

surface alteration. They report voltage increases of 600-700 mV produced pits 5-10 nm in diameter and 2-8 nm in depth. More substantial alteration was found at higher biases (0.9-2.5 V). During subsequent scanning, the surface transformed in time to a crystal oriented faceted shape and then grew and coalesced with other holes to produce surface etching.

Schimmel *et al.* [1991] Alteration of the surface of WSe_2, having atomic smoothness and long range order, was demonstrated. The tunneling gap was produced with a 0.8 V bias and a 3-6 nA current while scanning in a constant height mode. Structures with 6 nm diameters were observed after the application of 5.8 V (20 ms) pulses to the tip. These structures were ring shaped and produced higher currents on the ring (constant height, current imaging). The diameters decreased monotonically with pulse amplitude. By decreasing the voltage pulse to between 2.5 and 3.5 V, structures 2-4 nm in diameter were produced. The smallest were circular but resembled mounds instead of rings. Using pulses between 2.3 and 2.7 V, structures with diameters less than 1 nm were observed. The images retained atomic order after structures were formed. Forming 100 similar features with the same tip produced no visible degradation in the imaging ability of that tip. They also found that alteration was possible under high vacuum (2×10^{-7} mbar). They conclude that these details demonstrate that the structures were not generated by chemical deposition or etching. They observed no difference in structures for tungsten or mechanically cut Pt-Ir tips. Observing a feature for two

days revealed no changes. No changes were detected when features were imaged with a 0.8V bias for several hours.

Schneir *et al.* [1988a]. A hole, 9 nm wide × 5 nm deep was formed in HOPG by raising the 0.4 tunneling bias to 4 V for 0.5 sec. By raising the bias to 3.2 V for 0.5 sec, a 1 nm hole was produced with apparent reconstruction of the surface extending out about 5 nm.

Schneir *et al.* [1988b]. An atomically flat surface region of a gold ball was modified. Under a fluorocarbon grease ambient, a 10 nm hole was formed by raising the sample bias from 0.1 V (for imaging) to 3 V, until the feedback electronics caused the tip to suddenly pull away from the sample. Mounds 5-10 nm were also formed for biases near 0.7 V. Holes and mounds were created for either polarity of sample voltage. Tips that were the most successful at producing mounds had previously been pushed into the gold surface. Determination beforehand of hole or mound formation was not possible. Some attempts at modification were not at all productive. Attempts in air were also unsuccessful. The features formed were all distorted by diffusion within about an hour.

Shedd *et al.* [1990] Series of holes were produced in a gold surface by raising the sample bias from 50 mV to 3-5 V and then reducing the bias back to 50mV. The holes made with 4 V bias appeared to be more consistent. The 3 V bias series of holes seemed to affect the integrity of the tip. Holes (20nm diameter) made in graphite with a 4 V bias seemed to be torn around the edges. Bias changes (50 mV to 3.5 V) to a graphite substrate produced holes about 20 nm in diameter and

depths ranging from 3-7 nm. Raising the bias to 3 V, bumps as small as 2 nm were deposited on the graphite surface.

Shen *et al.* [1991] Applying a voltage pulse (-30 to -180 V × 0.1-0.5 μs) to an HOPG sample after withdrawing the W STM tip 2.5-20 nm away from the surface produced localized 10 nm indentions surrounded by rings. The rings were produced by terracing of graphite layers. Small holes several atoms in diameter were sometimes observed. An increased amplitude pulse was needed to produce a second damaged area, possibly due to tip alteration. The experiments were done in a vacuum of about 0.04 Torr.

Sommerfeld *et al.* [1990] Au and Pt balls (3 mm) formed in the flame of an acetylene torch were used for STM surface modification experiments. Hills were produced with the feedback active and inactive. While the feedback was active, a 5 V × 20 ns pulse was applied to the sample. With the feedback inactive, a 5 V × 20 μs pulse was also applied. Both methods produced hill formation. In the situations where modification was achieved, a hill was always formed, never a hole. The polarity of the pulse was found to be inconsequential in feature formation, but the probability of hill formation depended on the magnitude of the bias. The tunneling tips were made of Pt-Rh. For the gold surface 22 of 23 attempts were successful, while 16 of 23 attempts produced hills on platinum. More hills were well-formed for the Au than the Pt surface. Pt exhibited a 4.3V threshold for hill formation, while the Au exhibited a threshold of 2.8 V. The effect of extended duration pulses

was also investigated. A 2 V bias with a current of 5 nA was maintained for 10 min without scanning. A surface alteration was invariably observed, sometimes the surface was altered past recognition (the tip may have altered), while other times a well formed mound was produced directly under the tip. The results were the same for Pt and Au surfaces. The mechanism they favored involves electrostatic attractive forces between the tip and sample. They estimated a capacitive force of 10^{-8}N. They theorize that forces in attraction could produce greater surface alteration than those in compression. They were not able to determine if the hill material came from the sample or the tip. Diffusion was observed with a 5.2 nm hill deteriorating to 1.5 nm with the surrounding region also changing. Spontaneous diffusion of steps in a terraced area was also observed.

Staufer *et al.* [1987]. The surface of an ion etched $Rh_{25}Zr_{75}$ glassy metal alloy with an rms surface roughness of 0.1 nm was modified in UHV. While tunneling (100 mV, 1 nA), the sample bias was raised to 2 V inducing a tunneling current increase to 315 nA. They proposed that the current produced a temperature rise and subsequent thermal and electric field induced modification. When the tunneling current reached 300 nA, an oscillation was observed, possibly the result of local melting with a Taylor[3] cone forming in the presence of the high electric field. By reducing the tunneling current to 1 nA and the bias to 100mV, the resulting feature was found to be a 35 nm wide 10 nm high mound. Four such structures were produced all similar in shape. A 0.2 eV difference

was found between the tunneling barrier heights and the surrounding surface. This was speculated to be due to surface composition changing during ion etching or segregation and electromigration during the mound production. Lines were also produced by raising the bias and the current and then moving the tip across the surface at 3 nm s^{-1}. A line was shown with a width of 20 nm, a height of 2 nm, and a length of 100 nm. Similar structures were produced on other ion etched metallic glasses such as $Fe_{86}B_{14}$. They estimated that there was a temperature increase due to the small mean free path of the electrons in the metallic glasses. Using an Ir sample they were not able to produce any features using the mentioned process. They supported their melting hypothesis by comparing the melting points (Ir 2683 K; RhZr (1340 K).

Staufer *et al.* [1991]. By increasing the tunneling potential and then the current, structures with 10 nm radius were fabricated on the surface of glassy metals. The authors suggest local melting as the fabrication mechanism. The reported tip-sample potentials were between 0.7 and 1.0 V. Currents as high as 1 mA were observed during formation. The 1 mA current remained constant while the tip withdrew 10 nm away from the sample, which suggests that the tip was in mechanical contact with the sample. They found that hillocks were sometimes inadvertently erased if another feature was fabricated nearby. Thermal conductivities and melting points were used to estimate the power necessary to melt a 10 nm radius region. These results were used to corroborate their local melting theory.

Terashima *et al.* [1990]. Voltage pulses between an HOPG substrate and tip produced nanometer structures between 0.8 and 50 nm. The holes were a few nanometers deep and partially surrounded by regions higher than the original surface plane. When the tunneling bias was raised from 20 mV (1nA) to 4 V for 10 s, a structure about 3 nm in diameter was formed. Four similar pulses of 1 s each produced four holes from 10-20 nm in diameter. Migrating Au clusters previously deposited on the surface employed the holes as nucleation sites. Attempts to alter the surfaces of Si(111) and $YBa_2Cu_3O_7$ (under air) were unsuccessful.

Terashima *et al.* [1991]. A superconducting 1 μm thin film of $Bi_2Sr_2Ca_1Cu_2O_x$ on MgO was altered with an STM. Nanometer structures between 2 and 50 nm could be fabricated using voltage pulses on a portion of the film having a flat terrace. A 10 nm structure was fabricated by raising the bias from 0.5 V to 4.5 V for 1 s. They also fabricated a 3 nm deep (*c*-axis lattice spacing) hole with a flat bottom. They suggest this to be the result of electron induced chemical etching of atomic scaled layers. The tips were made of mechanically sharpened Pt-Ir. Virtanen *et al.* [1991] Applying voltage pulses (-10 V 500 μs) at the center of STM scan lines, a 100 nm wide ditch was fabricated in a $YBa_2Cu_3O_{7-x}$ surface. Milling work mentioned in the previous section was accomplished by lowering the bias from 1.5 V to 0.4 V. This suggests an insulating barrier between the tip and sample which must be overcome before detectable current can be obtained.

Yau *et al.* [1991c]. Silicon (111) samples were chemically prepared with a final 49% HF rinse and placed into an UHV (8×10^{-9} Torr) chamber for STM modification. X-ray photoemission spectroscopy revealed the presence of oxygen and hydrocarbons adsorbed on the surface as impurities. STM imaging revealed adsorbates with an average size of 10 nm covering the surface. While operating in the constant current mode, 0.2 s voltage pulses were applied to a W tip. Increases of 0.4 nA were observed during pulsing. Mounds were generally found to be formed at voltage thresholds of ±5 V. However, if the tip was sharp enough, holes were formed. As the tip became duller both mound(s) and hole(s) were sometimes made with one pulse. As the tip degraded further only mounds were formed. An additional pulse over a mound sometimes completely or incompletely removed it, thus the process was reversible. They believe that the mounds were produced when polymerization of hydrocarbons occurred by electron exposure. The hole formation by sharp tips was explained by field evaporation. Field enhanced oxidation was thought not to happen because of the UHV environment. By keeping the bias constant at -7 V and tracing a line, a linear structure composed of discrete asperities was created. The resulting STM image actually revealed two lines which they believe were formed by two separate tips (There could possibly have been a double tip and resulting ghost imaging). They used current voltage spectroscopy to try compare the mounds to the surrounding surface. After pulsing, the amount of adsorbates was sometimes found to be low near the tip region, but after

a time the adsorbates flowed back into the region. During a period of low adsorbate count, fabrication was interrupted. The structures were found to adhere to the surface until the tip became blunt, then the structures would diffuse away. Structures made with sharp tips last for weeks. Dull tips often produced multiple structures. Pulse application within 10 nm of a previously modified region hardly affected that nearby region.

3.3 Field induced diffusion of adsorbates

Eigler *et al.* [1990]. In UHV at 4^{o} K, Xenon atoms, adsorbed onto a clean single-crystal nickel surface, were moved using the van der Waals and electrostatic forces associated with the tunneling W tip. Normal STM imaging at 0.010 V and 1 nA did not move the adsorbed atoms. But, by lowering the tip over a xenon atom by increasing the tunneling current setpoint, the atom followed the position of the tip. The xenon atoms were moved at speeds of 0.4 nm s^{-1}. Then, the tip was withdrawn by reducing the tunneling current to imaging conditions leaving the xenon atom behind on the surface. Using 35 atoms they formed the acronym IBM on the nickel surface in 14×12.5 Å letters. The atoms forming the letters were 0.5 nm apart (2 lattice spaces). They found that for any given tip and tunneling bias, there was a threshold height for parallel motion of xenon atoms to occur. They found that the polarity of the bias had no effect on the threshold tip height required for movement.

Whitman *et al.* [1991] In UHV, Cs adatoms on a GaAs surface were made to diffuse across the surface by voltage pulses. The samples

were imaged with negative sample biases of 2-3 V. The W tip was held 0.5-1.0 nm above the sample and the bias was changed to 1.0 V for 0.35 s. The result was an increase in the local Cs coverage by 70%. Similarly, using a bias of 3 V for 0.1 s produced a 50 x 100 nm region almost continuous overlayer of Cs. Chains of Cs were also transformed into a pile with a chain covered by clusters of Cs atoms. Stroscio [1991] theorized that a positive bias produces a potential gradient toward the tip causing Cs atoms to diffuse toward the tip. The absence of the same effect for a negative voltage was shown to be the result of the static and induced dipole terms canceling each other.

3.4 Field induced surface alteration within a gaseous ambient

Dagata *et al.* [1991a]. Hydrogen passivated Si substrates were modified by an STM operating in air (the gaseous oxygen in the air may be reacting with the surface). Features were patterned on the passivated Si by raising the 1.7 V imaging bias to 3.0 V (tip positive) and moving the tip along the borders of concentric squares. The resulting slightly irregular 2 nm deep lines had a FWHM (full width half maximum) of 35 nm. Time of Flight Secondary-Ion Mass Spectrometry (TOF SIMS) revealed the regions to contain more oxygen than the surrounding region suggesting oxidation of the surface had occurred. They estimated the thickness of the patterned regions to be 1-2 monolayers deep. They also found that features patterned at 2.8 V have more oxygen than features patterned at 2.2 V. This selective oxidation process has been used as a mask for the

deposition of 80 nm GaAs films[4]. The surface was then placed for 15 s in 5:3:3 HNO_3:HF:Acetic acid, and the surface was etched only in the region of pattern generation. A sulfur passivated GaAs surface was also patterned. Features as small as 8 nm were formed. The features were written at 1.2 V (4 nA) and imaged at 2.8V (0.4 nA). Ehrichs *et al.* [1988]. An organometallic gas and surface contamination were found to decompose under the application of a voltage pulse between an STM sample and W tip. Si(111) was cleaned and placed in a vacuum chamber. For imaging the tip was grounded and a -1.7 V bias was applied to the sample. Dimethylcadmium (DMCd) was introduced into the vacuum chamber to a pressure of 10^{-3} Torr from 10^{-6} Torr. Using 8 V × 10ns voltage pulses, two 1 μm wide lines were formed. Auger electron spectroscopy (AES) was performed on the lines revealing 3.57% cadmium which was not observed in a featureless area. A higher carbon content was also found. They then found that deposits were formed without the DMCd (di-methyl cadmium) vapor. They believed the deposits were due to a carbon and oxygen contamination being polymerized by the pulse. A 50 nm high dot was formed with a 4 V pulse. By cleaning the sample with an argon plasma, the contamination was reduced to the point that they were able to form 10 nm features. Using 4.5V × 400 ns pulses, they produced a 200×200 nm grid pattern out of 10-20 nm wide lines (5 vertical and 5 horizontal). Imaging the grid for 30 minutes produced no apparent feature degradation. They found that for voltage pulses less than 3 V, no surface features were formed.

At pulses above 5 V, the size of the deposit increased rapidly. Pyrolization due to surface heating and direct bond breaking were given as possible mechanisms for feature formation. Also proposed was the possibility of decomposition by photons produced from the electron current.

Ehrichs *et al.* [1990]. The STM etching of Si was reported using WF_6 gas as a catalyst. In order to reduce the amount of carbon in metallic deposits from gases, a halogen metallic gas was used. Three types of features were formed, holes, hills in holes, and hills beside holes. When -20V × 100 ns pulses were applied at a frequency of 200 Hz for 1 s between the tip and Si in a 1 mTorr ambient of WF_6, a 100 nm hill was produced beside a 100 nm hole. Using the same scheme in a 30 mTorr ambient produced a 25 nm wide 9 nm high hill inside a 50 nm wide 10 nm deep hole. This may have actually been a ring structure. Using the same parameters produced a 40 nm wide 15 nm deep hole with no hill. Changing the pulse voltage to -15 V produced a 20 nm wide 15 nm deep hole. They theorize the features were produced when the electrons had sufficient energy to dissociate WF_6 molecules adsorbed onto the surface. The hills were thought to be formed by tungsten left over from the reaction. The holes were thought to be produced by the resulting fluorine etching of the silicon surface having formed SiF_4 which is volatile. Experiments done without WF_6 result in no surface depression showing that the holes were probably not due to mechanical contact. They reference previous work done with an electron beam in which a sample

temperature greater than 50^{o} C was necessary for etching to occur.

Eigler *et al.* [1991]. A Xenon atom was transferred back and forth between a Ni(110) substrate and a W tip in a UHV environment and at 4^{o} K. They first used the tip to slide[5] the xenon atom to the edge of an atomic step. The feedback was disabled and then adjusted the tip to provide a junction resistance of 1.5 Mohm for -0.02 V tip bias. They state that the tip was 0.38 nm above the upper nickel terrace. To transfer the atom to the tip, a +0.8 V pulse was applied for 64 ms. To transfer the atom back to the surface, a -0.8 V pulse was applied for 64 ms. They have also had success with 20 ns pulses. The atom switching was confirmed with STM imaging. The switching of the xenon atom position was also detected by the tunneling current. When the atom was on the tip the tunneling current was 7 times greater than when the xenon atom was on the nickel. By switching the xenon atom between the tip and nickel terrace, bare nickel surface, and a nickel adatom, the current ratio varied from near unity to 7. Examination revealed an exponential distribution for the time delay between the start of the voltage pulse and change in conductance. This suggested that there was a probability of transfer per unit time. At smaller tip-sample separations the xenon spontaneously transferred to the tip. At larger separations the atom was found to bounce to nearby sites before transferring to the tip. Since the motion of the xenon atom was found to always be toward the positively charged electrode, ionization followed by evaporation was not thought to be the mechanism. Negative ion formation was also ruled out

because no threshold field was observed, and because xenon *6s* occupation was not likely, due to its 4-5 V resonance. They rather have suggested that heating assisted electromigration of the xenon atom was the mechanism. They believe the xenon was heated above the surrounding lattice temperature by inelastic electron scattering.

Roberts *et al.* [1991] An annealed gold surface was modified in argon at a pressure of 1.3 Pa. A small window of a larger image was scanned with a higher than normal bias. A threshold bias of 2.6±0.1 V was found to be necessary for surface modification regardless of the bias polarity. A 4.5 nm hole 1 nm deep was formed with a scanning bias of 2.8 V and was found to transform over time. A -3 V scanning bias produced a 15×30 nm rectangular hole which also changed with time. They suggested an explosive field evaporation due to local heating and estimate the temperature directly below the tip to be 1600 K (Others estimate temperature increase estimations as low as 1 K)[6]. Predicting the size of feature formation was not possible, although there was some success at predicting the formation of a hole or hill. Diffusion of hole features was also observed with the perimeter opening up as the bottom filled in with atoms from the regressing walls.

Silver *et al.* [1987] An organometallic gas was deposited on to a thin layer of HMDS (hexamethyl disilazane) coating a copper substrate. DMCd (di-methyl cadmium) was chosen for the organometallic gas because of its low dissociation energy (3.14 eV). A vacuum chamber enclosing the STM was evacuated to 10^{-3} Torr. A valve to a DMCd

reservoir was opened and the pressure increased to the 10 Torr vapor pressure of DMCd. An imaging bias below 0.01 V gave reproducible images with no visible deposits. As the biased was increased above 1 V, successive images started revealing a changing topography. The topography did not change in the absence of the gas. The W tip was brought toward the sample at 1-5 V biases. At a critical distance, a stable current started flowing. This current smoothly increased from 1-300 μA making the tip voltage drop to 0.2-1.0 V due to a 11.5 kohm current measuring resistor in the power supply. This effect only happened in the presence of DMCd implying the possible generation of a microscopic plasma between the tip and sample. An observed plasma discharge between parallel plate electrodes used for gas characterization at 4×10^{5} V m^{-1} provided credibility to the proposed plasma mechanism since STM fields are on the order of 10^{6}-10^{8} V m^{-1}. Various currents and biases produced varied deposition rates. For 270 μA current and 0.3 V bias, material more than 120 nm thick was deposited in 100 s. A 220 μA current coupled with a 0.9 V bias produce about 60 nm of deposited material. Very little, if any, deposition occurred for a 2 mV bias and a 87 nA current. A circular 40 μm deposit was obtained with a 2.6 V 72 μA plasma. AES (Auger electron spectroscopy) analysis revealed large surface contamination of oxygen and carbon in the deposit site and almost exclusively oxygen away from the site. After ion beam etching 30 nm of the deposition site, an increase in cadmium content was observed. They proposed that the carbon and oxygen could have been

due to a few days exposure to room air before analysis. Using silicon substrates and DMCd at 1 Torr, a 25 nm wide line and a 40 nm diam dot were deposited.

Yau *et al.* [1991a]. Features were produced on an HOPG surface in a gaseous trimethylaluminum (TMA) ambient. 4 V × 0.2 s pulses were applied to a tunneling tip (Au or W) to fabricate nanometer structures. The pressure of the UHV chamber containing the STM was lowered to a 2×10^{-8} Torr. Imaging of the graphite was established with a -20 to -50 mV bias and a 1 nA current. With the feedback loop active, the bias was switched to 4 V for 0.2 s. The result was contaminant deposition (50×60 nm) in almost every attempt. TMA gas (99.9995%) was introduced into the chamber to a pressure of 10^{-4} Torr. The pulse produced an observed 0.4 nA increase in tunneling current along with smaller sized features. A 40×40×10 nm deposit was formed with a 4 V × 3 s duration. They found that shorter pulses produced smaller features. After another 4 V × 0.2 s pulse, a small deposit having several components was observed. The sizes of the components were 4.5, 1.8 and 2.4 Å. They attributed these to the structure of a TMA molecule. Using a 5 V × 0.2 s pulse, a hole was formed. Similarly, three attempts made three holes. One hole, 5.5 nm in diameter and 2.7 nm in depth, was formed using the 4 V × 0.2 s pulse. No feature formation was observed for biases < 3.5 V and only depositions were formed for pulses having amplitude < 4 V. The statistical frequency of hole creation increased with increasing pulse amplitude. They found that the probability

of making a structure was 0.3 for a 0.3 nA current and 0.7 for a 1 nA current. Due to identical I-V characteristics on the HOPG before and after introduction of the TMA, no adlayers were thought to be formed on the surface. They believed that the fabrication was due to ionization of the gas molecules in the presence of the free electrons and high fields of the tunneling gap. They argued that the ionic fragments of a TMA molecule strike the HOPG surface. If the fragments had enough energy, carbon bonds were broken and a hole was developed, otherwise the fragments deposited on the surface. Although depositions were half as probable with negative pulses, hole formation was not found to occur. I(V) characteristics taken above a deposit were linear, but I(V) characteristics over the graphite showed a nonlinear region as the voltage rises.

3.5 Field induced deposition/etching within a liquid or transporting film

Bernhardt *et al.* [1990] Using Pt-Ir and W tunneling tips the surface of HOPG was modified in the presence of air and the organic fluids dimethyl phthalate and decane ($C_{10}H_{22}$). The application of a voltage pulse between the tip and sample produced hillocks and occasionally depressions. A threshold of 3-4 V was necessary for any surface alteration to occur. With an increase in amplitude there was an increase in the probability of producing a hillock. There did not appear to be any change in the voltage threshold as the initial tunneling current was varied between 0.5-2.0 nA and also for initial biases in the range 20-500 mV. Nor was there any threshold dependence on pulse durations in the range

0.2-2 μs. In fluid, the probability of producing a hillock was the same as in air. Attempts to produce a tip that did not produce hillocks in air was fruitless. A 1.7×2.5 nm hillock was produced employing a Pt-Ir tip and a 4 V × 200 ns pulse superimposed on a 80 mV bias while tunneling at 0.5 nA. An ion milled W tip was utilized for the production of a 0.9×2.1 nm hillock using a 4 V × 400 ns pulse superimposed on an 80 mV bias while tunneling at 0.3 nA. The hillocks were found to vary in size from 1-100 nm^2. All of the hillocks appeared to be featureless (which may indicate a dull featureless probe). In the presence of decane and with a cold worked W tip, a 1.7×10.2 nm hillock was formed using a 4 V × 1 μs pulse superimposed on a 160 mV bias while tunneling at 0.5 nA. The occasional production of depressions was observed. A hole, 26 nm wide × 8 nm deep, was formed with a 4.5 V × 200 ns pulse superimposed on a 160 mV bias while tunneling at 0.5 nA. Once a tip formed a depression, it was likely to form more depressions implying a significant modification of the tip. By recording the current and tip displacements after the introduction of a pulse, three types of responses were observed. All the current traces showed an initial increase then a drop to no current followed by a continuation of the initial current. The first way the tip responded was pulling away from the sample in response to the initial current rise then gradually coming closer while low tunneling currents were present and leveling to the initial position as the initial current was restored. Hillocks were sometimes observed after this response. The second response showed little initial retraction of the tip

followed by the tip moving toward the surface winding up closer as the current was restored. This also occasionally resulted in the production of a hillock. The change in tip position was thought to be due to the loss of material from the tip. The third response of the tip was an initial retraction followed by the tip moving closer to the surface with the current being restored at a position farther away from the surface. This type of response was often accompanied by the formation of a depression. The apparent increase in tip-sample distance was thought to be caused by material from the surface being deposited on the tip. The position of the tip with respect to the sample was determined by the voltage applied to the piezoelectric moving the tip. The absence of any data showing the feedback moving the tip closer to the surface during the formation of a depression was thought to indicate that the depressions were not caused by mechanical contact.

Craston *et al.* [1988] Using an electrochemical method, 1-2 μm lines were fabricated at the air interface of a Nafion thin film on a Ag

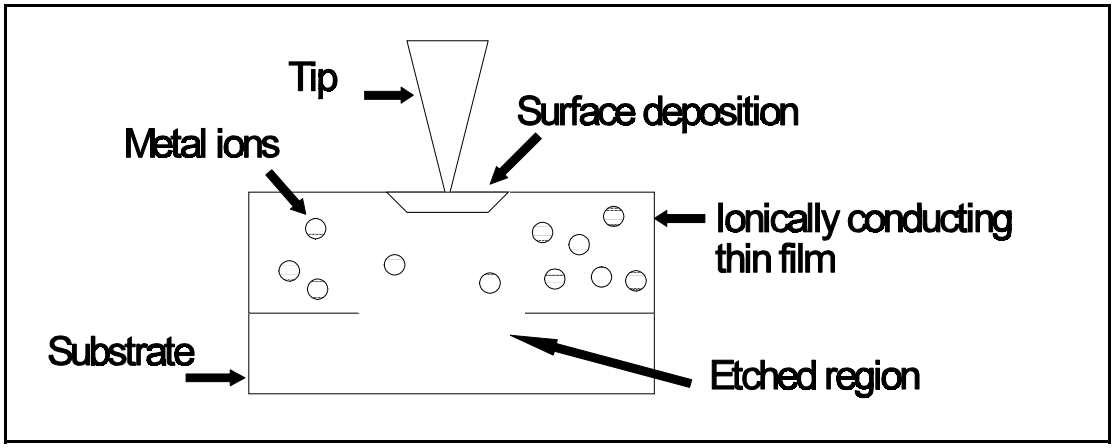

Figure 3-1. Illustration of deposition near the air interface of an ionically conducting film.

surface. The principle of the electrochemical method is illustrated in Figure 3-1. A thin polymer (faradaic conducting) film was deposited upon a conducting substrate. A bias was placed between a tunneling probe and the substrate, then the probe was lowered until a nanoamp faradaic current was detected. This current was held constant by a servo feedback loop, keeping the probe tip near the air/polymer interface. The presence of reducible ions in the polymer and a negative potential on the tip precipitated a metal deposition in the film at the tip electrode. Moving the tip parallel along the interface resulted in the fabrication of a line along the route of the tip. If the substrate was oxidizable, an etch pit formed under the tip.

The film/sample was soaked in water for 1 hr and in 50 mM $AgNO_3$ for 15 minutes before use. Experiments were performed with biases between 200 mV and 8 V. At low biases (<200 mV, 2 μm film) the tip penetrates the film scratching a line. Although the feedback was set to keep the current at 15 pA, the actual value varied from 0-1 nA during the experiment (This may indicate that the tip moved in and out of the fluid). Lines of 0.5 μm width were produced under optimal conditions. Dotted lines were produced for scan rates above 50 nm s^{-1}.

Foster *et al.* [1988] Surface alteration of HOPG in a drop of di-(ethylhexyl) phthalate was accomplished. Using an electrochemically etched W tunneling probe, the bias was raised several volts from the 30 mV tunneling bias. After applying a 3.7 V × 100 ns bias pulse during scanning, a 1-2 nm surface structural alteration was observed. The

alteration was thought to be due to an organic species from the solution being pinned to the surface. A threshold of 3.5 V with no polarity dependence was observed for surface deposition. Varying the tunneling current between 0.1 and 1 nA had no effect on the threshold. STM imaging produced no observed deterioration in the features. Applying the same bias pulse over a modified region could totally erase, partially erase or expand the feature. Partial erasure produced features as small as a benzene ring (4 Å). Proposed mechanisms were electron activation of the surface and adsorbed molecule, or electron induced dipole-dipole interaction. Many other organic species were found to react similarly.

Hüsser *et al.* [1989] Ionically conducting polymer films were used for the deposition and etching of metals. The method was described in Craston [1988]. Ag, Au, Cu, and Pd were deposited and Cu, Ag, and Au were etched. Lines submicrometer in diameter were fabricated.

The films were deposited by spincoating a drop of polymer solution on the surface of the substrate. Previous results[7] with a silver doped Nafion film and platinum tip produced lines with 1-2 μm resolution. Using a tungsten tip biased to -5 V, a 5 nA current was servoed resulting in 300 nm lines of Ag. Using an additional layer of polyimide the Ag line was removed and found to be continuously conductive. Using EDS (x-ray energy dispersion spectroscopy), the lines were found to be composed of Ag. Deposition with Cu and Cr was also produced using Nafion films soaked in an appropriate solution. For biases < 3 V, dendritic growth was sometimes observed.

Using a colloidal graphite substrate (on a glass slide) coated with a poly(4-vinylpyridine) (PVP) film containing $AuCl_4^-$, a Pt tip was biased to -5 V (1 nA) producing lines with sub-μm width. PVP films with $PdCl_4^{2-}$ also produced narrow lines. Water was necessary as a solvent for the ions in PVP.

Ag doped poly(bis-(methoxyethoxyethoxide)-phos-phazine (MEEP) films (no other solvent) were deposited on an Ag substrate. A Pt tip (5 V, 5 nA) produced lines that were not very continuous or uniform showing dendritic Ag growth. Lines were only observed if the bias was >1 V. The poor quality of the lines was thought to occur because of considerable problems with the feedback. The sticky MEEP was thought to cling to the tip as it tried to servo producing unstable tunneling conditions. By using inert Pt as a substrate, metal ions oxidized at the substrate interface were decreased, if not eliminated altogether. Nafion films containing Ag or Cu produced lines only if thin (<1 μm) films were employed. Discontinuous and non-uniform lines were made if the Nafion film was 1-2 μm thick. The culprit was thought to be gas bubbles forming at the Pt interface. They also found that they could change ion metals to produce continuous dual metal lines.

The etching of the substrates was also examined. The etching of copper surfaces was masked because of homogeneous oxidation of the surface. Ag and Au surfaces could also be etched. The resolution of the etched lines was a factor of two less than the deposited lines.

Deposition of material on the tip was not observed except for

biases around 8 V (1 μm film).

Li *et al.* [1992]. Depositions of silver were reported for an HOPG substrate in an aqueous 0.5 mM AgF plating solution. Pulses, 6 V × 50 μs (+tip), were applied between a poly(α-methylstyrene) polymer coated Pt tip and the HOPG during stationary tunneling. Protruding cylindrical features, 20-30 nm in diameter and 7 nm in height, resulted. The silver pillars did not nucleate on preexisting defects. The size and shape of an initial pillar was not altered by the fabrication of three more structures nearby. The shape of these features was unchanged even hours after formation. It was noted that several bias pulses were necessary to initialize the tip so that it produced features. After this initialization the features were produced with 90% reliability. Holes were produced during the initialization of the tip and often observed with the cylindrical features.

Further experimentation, involving variable duration pulses, showed that a shallow, 10 nm wide, pit was induced during the first 5 μs of the pulse. Increasing the duration of the pulse resulted in deposition of silver around the hole followed by an increase in height. The increase in height grew linearly over the next 25-30 μs without any associated increase in diameter. These results suggested a two-step mechanism for feature fabrication. In the first step a hole was formed which facilitates the nucleation and growth during the second step. Further work in pure water or an aqueous solution of NaF produced only pits. Reversed polarity pulses in the Ag solution did not produce mounds or holes reliably, but

micrometer sized deposition on the tip was observed during subsequent examination.

Nagahara *et al.* [1990] Using a Pt/Ir tip and Si(100) sample immersed in 0.5% HF, nanometer features were etched in the silicon. To reduce faradaic leakage current, the tip was coated with Apiezon wax, except near the tunneling tip region. The Si was degreased and etched to remove surface oxide. A tunneling bias of 1.4 V was chosen to minimize the leakage current. To eliminate photochemical effects, no light was allowed. Using a 10 hz scan rate, square features 400×400 nm and 200×200 nm were etched for 25 s each. The 400×400 nm region was 1 nm deep, while the 200×200 nm region was 2 nm deep. Above a critical scan area per unit time of 28,000 $nm^2\ s^{-1}$ the surface was imaged with no apparent etching. Scanning below 4000 $nm^2\ s^{-1}$ the depth and width remained constant. They suggested that the limiting factor was the size of the exposed tip. Increasing the tunneling current and the time the tip spends over an area was found to increase etching. Also, the etching process did not occur when distilled water or 10^{-1}-10^{-4} M H_2SO_4 was used as the liquid medium, which they believed discredits mechanical contact as the mechanism for etching. They did notice, however, that scanning areas < 400×400 nm occasionally produced degraded and streaky STM images. They attribute this to an oxide forming under the tip, which then chemically reacts with the HF producing the observed etching. By etching 20×70 nm areas a zigzag line was etched. The line etch time was 39 s. They also were able to etch 80 nm lines in

GaAs(100) to compose the letters ASU (Arizona State University).

Penner *et al.* [1991] Using electrochemically etched, poly(α-methylstyrene) polymer coated, tungsten tips, the surface of HOPG was modified while in 18 Mohm water. Application of a -4 V × 20 μs pulse between tip and sample produced a dome feature that was 0.7 nm in diameter and 0.2 nm in apparent height. Formation of similar domes with ±3.8-4.2 V pulses were possible using more than 90% of the tips tried. The domes were stable for periods >1 hr and for imaging biases up to 500 mV. A -4.2 V pulse typically formed 4 nm wide pits with monolayer heights. Continued increases in pulse amplitude resulted in monotonic increases in pit dimensions. The threshold voltage for feature formation was found to be 4.0 ±0.2 V using a variety of tips and independent experiments. Other experiments in air demonstrated daily variations as much as 5 V in the voltage threshold for feature production. In an attempt to prove that H_2O was necessary for pit formation, dry environments were also investigated. Even with pulses amplitudes as high as ±10 V, features were not produced in dry toluene or dry N_2. Introducing moisture into these environments reestablished the feature production. *n*-octane and mineral oil environments produced results similar to that in air. In H_2O, it was possible to transform the domes into 3-4 nm pits with the application of a 0.2 V pulse. They concluded that the domes were metastable intermediate structures. They suggested that the metastable structure was a 6 carbon ring transformed from the graphitic structure to diamond structure. They stated that the changed

structure was more reactive than the graphite structure. Qualitatively similar production of domes was observed for reversed bias polarities.

Rabe *et al.* [1990]. Monolayer films of octylcyanobiphenyl were deposited on the surface of HOPG. The Pt-Ir tip bias was raised to -1.7±0.1V. This threshold resulted in the formation of 1-2 nm adsorbate features on the HOPG surface. These features were only stable for <1 s. Decreasing the bias amplitude below 1.6 V caused the features to last for minutes. For 0.1-1 μs duration pulses to cause an effect, the bias amplitude had to be increased. They believed there was a metastable reaction of the film and HOPG. Decreasing the tip bias to -2 V for 2 min resulted in the formation of holes in the graphite. Holes etched at -2.5 V and -3.0 V were about 10 nm in diameter. The holes were surrounded by walls with heights less than 1 nm. The -3 V hole was several monolayers deep, while the -2.5V hole was only one monolayer deep. Larger holes were formed for a -4V bias. At a +3 V tip bias, the imaging became unstable after about a minute. Similar etch effects were found in air, water vapor and silicone oil. In 1 atm helium gas or 10 mbar dry toluene, no etching occurred up to ±4V. They concluded that for tip biases of -2 V, the results in the air, water, octylcyanobiphenyl, and silicone oil, showed that a highly reactive species was always produced. They proposed that the rest water in these fluids and an increase in bias amplitude lead to reaction products which in turn etched the graphite. They also found that these etched sites acted as nucleation centers for the crystallization of the octylcyanobiphenyl.

Schneir *et al.* [1988a]. Electrochemical deposition was produced using tunneling tips that were glass and SiO coated except for the last couple of nanometers. The tip and gold sample were covered with an electroplating solution, Orosene 999. Tunneling was achieved, then the tip was withdrawn 1 μm. With a -3 V bias applied, the tip was maneuvered back and forth along a line. The result was an electroplated line, 300-500 nm in width, 1.2μm long and >100 nm high. The experiment produced results only 2 times in 20 attempts.

Wuu *et al.* [1989] Nafion films on a Pt surface were used as an ionic conductor for the purpose of depositing polyaniline on the Pt. The 0.1 μm Nafion film was soaked in 0.1 M anilnium sulfate for 40 min. A tunneling tip was brought into contact with the film so that a 1 nA current was maintained. At tip-sample voltages above a threshold value of 5 V (sample positive), deposition of polyaniline was observed at the air/poly interface. Lower values caused the tip to scratch the Nafion film. The resolution was about 2 μm due to the thickness of the film and the electric field distribution. Attempted reversed polarity deposition produced scratch lines in the film, probably due to low conductivity polyaniline depositing on the tip.

3.6 Field and/or electron induced chemical modification

This section will report on attempts which have resulted in the chemical modification of near surface material. Stoichiometric and electronic changes of or in thin films and other surfaces will be

emphasized. Lithography has been previously achieved using focused high energy electron beams[8]. Features as small as 10 nm have been fabricated in Si using an electron beam exposed PMMA film (on SiO_2 over Si) and subsequent etching steps[9]. Using an amorphous carbon intermediate layer between a Si substrate and PMMA resist, fabrication of 15 nm AuGe lines has been achieved utilizing a 50 keV electron beam to expose the resist[10]. An STEM was used to produce lines having widths <10 nm using the acid catalyzed resist poly(p-t-butyloxycarbonyl-oxystyrene)[11]. The following reports show that the STM is also being used as a source of electrons for chemical reactions with energies below 10 eV.

Albrecht *et al.* [1988]. Poly(octadecylacrylate) (PODA) fibrils deposited by Langmuir-Blodgett techniques on graphite were modified. Using a 100 ns rectangular voltage pulse applied to the tip, breaking fibril bonds and disrupting the surface in a 40 nm region. The voltage threshold was found to be 4.1 ±0.2 V for this breaking effect.

Dagata *et al.* [1990a,b]. Si(111) samples, H-passivated in dilute HF with 10-50 nm of residual texture, were transformed. With a 3 nA tunneling current, the normal Pt-Ir tip bias of 1.7 V was raised to 3.5 V producing an alteration of the surface. Lines, 2.5 μm long, 200 nm wide, were produced side by side with a spacing of 300 nm. A 100×100 nm square was the smallest resolvable feature produced. The features appeared 1-20 nm deep when imaged with the STM. SEM revealed these structures to be sources of enhanced secondary-electron yield. STM

spectroscopy disclosed a lower work function for the modified regions. They concluded from these characteristics that a local electronic or chemical change had occurred.

They also found that biases >500 mV were required for imaging and for biases <1.7 V the tip was very close to or in mechanical contact with the sample. The feature depth appeared to increase by as much as 7 nm as the imaging bias was lowered below 1.7 V. Increasing the writing voltage above 1.7 V produced a linear increase in feature depth for air or oxygen ambient gas with no observed modification in a nitrogen ambient. The authors conclude that the features were the result of locally enhanced surface oxidation. They also found that the features were selectively etched by a 15 s dip in HNO_3:HOAc:HF (5:3:3).

Dagata *et al.* [1991b]. Various films of MBE (molecular beam epitaxy) grown Al_xGa_{1-x} and In_yGa_{1-y} III-V semiconductors were modified using an STM. Images of the surface were obtained at 3.8 V (tip) and 0.4 nA current. A series of 2 μm long 85 nm wide lines were written at 3 lines per sec with a bias of 4.2 V in air. The lines showed residual surface roughness and were somewhat irregular. The apparent height of the lines changed with writing bias. Investigating the mechanisms of modification, it was found that As_2O_3 and In_2O_3 were depleted by desorption under low electric field conditions, which were typical for imaging. A high electric field was thought to induce a reaction at an underlying GaAs or InGaAs layer resulting in a strongly bonded oxide layer.

Dujardin *et al.* [1992] The STM dissociation of individual adsorbed decaborane ($B_{10}H_{14}$) molecules using the low energy field-emission electrons. Decaborane was admitted to a UHV chamber and allowed to condense on 7×7 Si (111). With low exposures, 0.01 L (torr s), the decaborane preferably adsorbed near defects. At higher exposures, 0.1 L, adsorption was observed at a variety of sites with a tendency to adsorb over center Si atoms. Conductance spectroscopy revealed the adsorbed molecule to be an insulator with a band gap of 2 eV. A bias of 2 V and a current of 200 pA was used for imaging. They imaged a region with an adsorbed molecule (7 Å wide), then scanned the region again with a bias of 4 V, and again imaged the region for comparison. They found "displacement of adsorbed molecules, dissociation and fragmentation, and cluster formation". At higher surface coverage (0.1 L) clustering occurred for groups of molecules adsorbed on large flat terraces (instead of molecules adsorbed near defects). After scanning a region including a molecule with an 8 V bias, two distinct features appeared, suggesting a dissociation of a molecule. Another region containing two protruding features was scanned with an 8 V bias. The result was elimination of the features and nearby Si atoms. Since scanning at high biases was not found to alter any bare silicon, the molecules were thought to dissociate and tie up dangling Si bonds. The probability of dissociation was found to be 0.1 at 4 V increasing to 0.8 at 8 V. Since the fields were a factor of 5 smaller than necessary for field dissociation, the mechanisms thought to be low energy field-emission electrons.

Jahanmir *et al.* [1989]. Three protruding lines were written on a 20 nm *a*-Si:H thin film on Si with a series of nine voltage pulses (10 V, 35 μs) for each line. The lines were 1.1 μm long and 140 nm wide with an apparent height of 15 nm. The W STM tip was held in a constant position during voltage pulsing by disabling the servo feedback electronics. Maximum current detected during modification was 100 μA. Differences in I-V characteristics indicated that the lines were more conductive than the initial surface. The linewidths were found to correspond to the average tip radius for two different radius tips. They theorize that the apparent height of the lines was due to a change in conductance produced by a phase transformation of the thin film from amorphous to crystalline (This is probably unlikely considering the 15 nm feature height).

Jahanmir *et al.* [1990]. The local conductance of a 2.3 nm film of oxide on a silicon substrate was changed by a 6 V, 1 mA, 35 μs voltage pulse. The surface became rectifying after the voltage pulse.

Ringger *et al.* [1985, 1986]. Using an STM with a W tip, the surface of glassy $Pd_{81}Si_{19}$ has been modified in a 10^{-8} Torr vacuum. The tip was scanned at 100 nm s^{-1} with a bias of 100 mV and a current of 10 nA. Subsequent viewing of an STM scanned region by an SEM revealed lines with a spacing of 16 nm. XPS studies revealed the surface to contain about two monolayers (liquid) of hydrocarbons and carbon oxygen species on top of 3 nm of SiO_2. SEM revealed no deposits at the end of lines suggesting the lines were not mechanically formed. The lines

were thought to be due to a contrast of material conduction. Going further, they propose that the lines were made conducting due to polymerization of the hydrocarbon film.

$$solid) + H_2(gas) \Rightarrow xAg(solid) + H_2Se \qquad \textbf{(3,3)}$$

Utsugi [1990] Alteration of 15 nm of $Ag_{1.9}Se$ formed on a $Ge_{0.1}Se_{0.9}$ film on an unidentified substrate is reported. Biasing a Pt STM tip to +3.5 V and scanning in a computer controlled grating pattern (60 nm line, 100 nm spacing) produced grooves 15 nm deep ($Ag_{1.9}Se$ thickness). Lines as small as 13 nm in width were used to form the letters NTT. Although continuous lines were produced with constant biases, voltage pulses produced no alterations. Effects were observed for +2 to +5 V biases. When negative biases were used no surface alteration was observed. In a 5×10^{-3} torr vacuum, even biases up to +5 V produced no concave formations. In hydrogen gas, they found a logarithmic dependence of the growth rate of the depth of a concave formation with the applied voltage. They suggest that H_2(gas) in the air was responsible for the work done. The following chemical reaction was proposed for the degeneration of the surface:
They suggested that it was the bias which segregated the Ag from the Se allowing the Se to react with the hydrogen in the air ambient.

3.6.1 Energetic electron induced changes within a film

Marrian *et al.* [1990, 1991]. The negative acting *e*-beam resist P4BCMU (polydiacetylene with urethane substituents) was exposed with electrons from an STM tip. The STM was operated in the field emission

mode (V greater than barrier height) and in a 10^{-8} Torr vacuum. An LB film (<75 nm) was deposited on silicon. Negative biases were applied to the tip. Low biases caused the tip to drag in the resist and higher biases caused exposure of the resist. For 25 nm and 75 nm films, adequate imaging potentials were -3 V and -7 V respectively. The resist was exposed by ramping the bias at 40 V s^{-1} so that the current would remain constant and electron dosage could be determined. The bias was held constant at the exposing voltage for 10 ms and then ramped back down. Dots of about 8 nm height were produced with voltages from -20 to -30 V. A threshold for exposure was found to be about -8 V with dot diameter increasing with a more negative bias. The minimum diameter was about 20 nm. Currents from 50 pA to 0.5 nA fell within experimental error so that no current dependence could be detected. The lack of current dependence caused suspicion of a thermally based mechanism for formation. Attempts to write lines resulted in variably sized raised features. Depressed features were also formed with sharp tips.

McCord *et al.* [1986]. Using an STM operating in the field emission mode, where electrons tunnel from the tip into the vacuum, a contamination resist was deposited on Si, Au on Si, Al on Si, Cr on Si, and Pt on Si thin films. In order to prevent the metal films from pulling away from the substrate, the beam energies were kept below 20 eV. A Vacuum of 3×10^{-5} Torr prevented unstable currents due to ionization of gases and adsorbed molecules. Square regions were exposed to a

100 nA, 10-1000 eV, SEM beam revealing buildup of contamination at all energies. Attempts at lithography with the STM initially required electron doses of 0.1 C cm^{-1} to produce visible line patterns. These doses required an hour to write a few 10 μm lines. At a current of 60 nA and energy of 10 eV lines were produced on Au films at a rate of 250 nm s^{-1}. Subsequent etching produced 100 nm wide gold lines. A LB film of docosenoic acid on an Al film was exposed with a 25 nA beam of 25 eV electrons. Using a writing speed of 500 nm s^{-1}, and subsequent development and etch, 100 nm wide lines of poor quality were produced. McCord *et al.* [1988]. PMMA films were exposed in UHV using an STM operating in the field emission mode. The film thickness was limited to a few tens of nanometers to assure complete penetration of electrons and prevent penetration of the tip into the film. They found that the film should be no thicker than 1 nanometer for each volt between the tip and sample voltage. For an electron dose $>10^{-2}$ C cm^{-2} having a 25 eV energy, the PMMA was crosslinked producing a negative resist. Writing at 1 μm s^{-1}, a 30 V, 10 pA beam produced 20 nm wide lines. Lower doses and lower voltages produced positive resist action in a Cellosolve-methanol solvent. This action was thought to be due to chain scission. Lines, 22 nm wide and 10 nm high, were fabricated using a liftoff technique. It was also possible to expose resists with a reverse polarity voltage (exposing electrons emitted from the surface). The field in the resist was about 1 V nm^{-1}. This reversed exposure eliminates problems associated with secondary and backscattered electrons broadening the

exposure width. For electron energies from 40-100 eV, reversed exposure provides much better resolution. Instabilities in the beam current due to ion desorption from the resist were reduced with reversed exposure. This enabled the writing speed to be increased to 10 μm s^{-1}.

Zhang *et al.* [1989] LB deposited resist films of PMMA and poly(vinyl cinnamate) on Cr were altered with an electron beam produced by an STM. Tip biases varied from 5-100 V and currents from 5-1000 pA. Lines were patterned with electron doses of 10^2-10^4 nC cm^{-1} which exceed conventional doses for resist patterning. After developing and baking, the PMMA was coated with 8 nm of Au and examined in a SEM. The poly(vinyl cinnamate) samples were wet etched with chromium etchant then the film removed. Using a 30V × 30 pA exposure, lines having a width of 30 nm were formed. The resist was removed in the exposed areas after development (positive resist action), although the resist was supposed to be negative. This may have been due to accidental exposure to light with subsequent breaking of cross-linking by the energetic electrons. Lines having widths of 80 nm were etched into the chromium. The larger widths were due to isotropic etching. Double lines were also formed. These were probably due to tips with a double tunneling asperity. Linewidths were consistently smaller when a negative sample bias was used. This was thought to be caused by the transverse spreading of electrons entering the film.

3.7 Illumination-assisted field-induced surface lithography.

The use of light for generating patterns on surfaces has long been established. The limitation of such features is limited by the wavelength of the light. As a result, features below 100 nm are difficult to achieve using such techniques. Building optics to direct such light is also a difficulty. Directing a KrF excimer laser (248 nm) into a Talbot interferometer, sub-100nm line patterns have been directly ablated into polyimide[12].

A theoretical consideration of light induced damage near a nanometer scale inhomogeneity such as a metal STM tip has been given by Shtokman [1989]. The theory is based upon an enhanced field effect near the tip.

Lin *et al.* [1987] A glass sheathed Pt tunneling probe was held about 1 μm away from the surface of GaAs in an electrolyte solution (5 mM NaOH, 1 mM EDTA[13]). With the application of a -4 V bias to the tip relative to the sample and the simultaneous irradiation of light from a tungsten-halogen lamp, the surface of the GaAs was selectively etched. Using this process 0.3-2 μm wide lines were produced. The 2 μm line was somewhat discontinuous, possibly because of bubble formation. The different linewidths were produced by different tip sizes. The whole surface of the GaAs showed some etching. Similar etching results were achieved in organic solvents. One of these was acetonitrile with nitrobenzene or an alkaline halide as an added species.

Thundat *et al.* [1990] GaAs(100) surfaces were used as a substrate for plating Au from a buffered acidic (3.5 pH) solution of gold cyanide. Acidic solutions down to a pH of 3.0 reportedly do not produce cyanide gas. An Apiezon coated Pt-Ir tip was brought to within tunneling range of the GaAs with a tunneling bias of 0.1 V. The tip was then withdrawn a few hundred Angstroms from the surface. The surface was illuminated with white light and the bias was increased to 4 V for 1 min. The surface was then imaged with 0.1 V bias. They found that gold dots were formed beneath the tip if the GaAs was *p*-type. For *n*-type GaAs, no deposits were formed directly under the tip. Instead,an annular region of small 15 nm Au hills were formed away from the tip. The 0.1-10 μm dimensions of the gold dots were dependent on the amplitude and duration of the pulse. Without the presence of light, no gold features were deposited. The localized deposition was explained to be due to the presence of a localized depletion region under the tip. Photogenerated electron-hole pairs in the depletion region provided an electron source for Au reduction at the surface resulting in the deposition of Au.

Using different solutions of NaOH as the electrolyte medium, studies of the photocorrosion of *p*-GaAs(100) were performed. STM images of surfaces etched using a Pt counterelectrode and using the tunneling tip were examined. The surfaces were potentiostatically etched while illuminated with white light. Surfaces etched by the tip (-0.1 V tip, 1 mM NaOH) were found to be much smoother than surfaces etched by a counterelectrode (0.1 V sample, 1 M NaOH). Continued STM scanning

(-0.1 V) of the surface etched with the counter electrode caused a flattening of the surface. For surfaces etched with the counterelectrode and positive sample potentials, the absence of light did not seem to affect the process. Features etched by the STM were less pronounced if etched in the dark. They suggested that the presence of holes at the interface weakens the bonding producing a corroded surface. Repeated STM scanning of the same area caused the surface to become less conductive. By circulating the NaOH or moving the tip, proper tunneling was restored.

Yau *et al.* [1991b]. Laser radiation and an STM operating in a Trimethylaluminum (TMA) ambient were combined to produce deposition on an HOPG surface. A XeCl pumped dye laser was pulsed (18 ns) with a wavelength of 440 nm. The laser was focused on to the tunneling region of the STM. The chamber housing the STM was evacuated (10^{-8} Torr) and then filled with TMA to a pressure of 10^{-2} Torr. The HOPG was imaged with tip biases between -20 and -50 mV. Biasing the tip positive (0.8-3.0 V, 1 nA), a laser pulse was delivered to the tunneling region resulting in deposition. A 15.8×15.8 nm feature was produced for a 3 V bias. A 1 V bias spawned a 1 nm region with two 5×4 Å structures. These were thought to be four or five aluminum atoms. A 14×13 Å deposit was formed with a 1.1 V bias. Current-voltage measurements showed a linear relationship above the deposits while a non-linear relationship was observed above the HOPG. They were also able to remove deposits with an additional laser pulse while the tip was over the

deposit. They also demonstrated the ability to fill a 30 nm hole with continued pulsing of the laser. No depositions were accomplished without the presence of the TMA. By detuning the laser away from aluminum resonance (430 nm), deposition was rarely observed. The proposed mechanism involves the ability of the laser to induce multiphoton fragmentation and ionization of the TMA. The field of the STM was thought to have guided the molecular fragments to the surface.

3.8 Localized electrostatic charge implantation in films

No papers were found which report the direct use of an STM for deposition of charge. However, there are papers which address nanometric charge storage with a scanning force microscope (SFM)[1]. The SFM is based on the bending of a cantilever which has a typical spring constant of 0.1-100 N m^{-1}. The cantilever has a sharp probe on the end. The electrostatic, magnetic, or atomic forces on this probe produce a bending of the cantilever. This nanometric bending of the cantilever can be detected by an STM probe above the cantilever, capacitance between the cantilever and a fixed electrode, a reflected laser lever action, or by laser interferometry. The SFM is servoed to a preset force or force gradient. The motion of the SFM probe is used to determine constant force or force gradient topography of a material by scanning in the same manner as an STM.

Barrett and Quate [1991] Thin films of silicon nitride on silicon dioxide on silicon were charged using an SFM probe. The presence of the

charge in the nitride changed the charge in the Si depletion layer. The presence of charge was detected using capacitance techniques. Pulses, -40 V × 100 μs, were applied to the probe causing charging of the nitride. The pulses produced 170 nm FWHM regions of charge. The regions were also erased with the application of a reversed polarity voltage pulse. The threshold for writing was found to be -25 V. And a minimum write time was determined to be 20 μs and thought to be limited by electronics. The erasing time was determined by the intermediate oxide layer. A chemically produced 1-2 nm oxide needed a 10 V × 20 μs pulse for erasure, while a dry thermal 5 nm oxide required a 40 V × 1 ms pulse for erasure. Charging occurred every time for 202 attempts. Dull tips produced larger charged regions than sharper tips. The smallest bits that were written were 75 nm across. They separated charge effects from topography effects by using simultaneous force and capacitance measurements. The half life of charge for the chemical oxide barrier was about 1 hr, while charge separated by the thermal oxide showed no decay over seven days. Minimum size for a charge affected region was calculated to be several hundred Å.

Stern *et al.* [1988] and Terris *et al.* [1990] By the application of a voltage pulse (100 V × 25 ms) to the probe of an SFM, a charged region was generated in a 1 mm PMMA film. The scanning height was approximately 100 nm before charging. The charge was localized to a 2 μm region. Bias affected force contours confirmed that the region was charged. The charge was observed to decay over a 1 hr time period.

Sapphire produced similar results. Any induced charging of mica or quartz decayed before contours were obtained.

3.9 Magnetic alteration

Moreland and Rice [1990] Using a triangular shaped Fe iron film for a tunneling detector, the CoCrTa film of a computer memory hard disk was magnetically altered. The aluminum substrate disk had a base film of NiP, and a 1 μm intermediate layer of CoCrTa, and a 1 nm carbon lubricating layer on the surface. The Fe iron film was 5 μm thick and was mounted at an angle with respect to the surface and with a point toward the surface. The Fe bent in the presence of the magnetized film necessitating a change in the servo mechanics to maintain a constant tunneling current. By using a magnet mounted near the top of the Fe film, the magnetization of the disk was altered. The extent of magnetization was affected by the strength of the magnetization in the iron film, the duration of the magnetic recording process, and the tunneling current. With a tunneling current of 0.4 nA and a scan time of 1 line s^{-1}, an 8×8 μm^2 area was magnetized. The tunneling probe had to move 50 nm toward the sample to compensate for the bending of the Fe triangle. By operating a Pt-Ir tip at various biases over the surface, and subsequent magnetic imaging revealed the magnetization of the surface was not produced by the tunneling current. Using a 100 nm Au layer on the tip, sample, or both did not affect the magnetic recording process. The smallest region magnetized was 500×500 nm with 20 nm resolution.

3.10 Summary and discussion

State of the art reports on lithography with a tunneling tip have been presented. The scope and results of the literature are briefly summarized in Tables 3.1 - 3.11 for each specific lithograpy type. The reports covered a diversity of methods and results. The methods had varied results depending on such things as material of tip and sample, and cleanliness and sharpness of the tip.

Mechanical contact methods often resulted in tip changes and unpredictability of hole or hill formation. Unpredictable formation would prevent those schema from being used as a memory since bit making must be a predictable process. Tip changes upon contact suggest that, for any method, care should be given to prevent the tip from contacting the surface while moving the tip toward the substrate for writing or reading memory bits. When they are comparable in size, a convolution of the tip and bit affects the apparent dimensions of the manufactured bits. Tip changes could also affect the addressability of a memory scheme.

Using bias pulses to induce surface changes was also reported. In many cases surface alteration was achieved only with a bias pulse above a certain threshold. This threshold was often reported as being dependent on the history of the tip. Surface alteration was also found to be statistical near the threshold. This is unfortunate since it is near the threshold where the smallest surface features are produced and we desire minimum sized bits for maximum storage density. We also desire to be able to be sure a given set of alteration parameters will produce a definite

result. None of the STM experiments reported a 100% success rate although some individual tips produced surface alterations above 99% of the time. Reports disclosed that the predictable formation of a hole or hill was not always possible. Most of the works involving Au and Pt surfaces revealed surface diffusion of atoms during normal scanning. This would make these surfaces unusable as a memory dependent on field induced topography since corruption of the stored information could result from diffusion. Some reports suggested a current dependence on formation of surface features. Some ambient effects, which may affect memory reliability, were also reported on the formation of features. Other experiments involving ambient effects on tunneling currents are reported in Chapter 7.

Experiments showing the diffusion of adsorbates due to increased electric fields showed a statistical transfer of material. This suggests that adsorbate features would not be advisable as memory bits since they may move around. A more detailed report of surface features diffusing over time during normal scanning is included in Chapter 4.

Experiments performed under liquids, involving voltage pulsing, often revealed a difficulty in predicting a hole or hill type surface feature. Variable current responses to similar pulses were mentioned demonstrating unreliability. These may be limited by coating of tips to prevent leakage currents. Also tunneling at high fields in a gas was demonstrated to produce a plasma between the tip and substrate.

Field induced chemical modifications such as bond dissociation and

cross-linking in polymeric films, and amorphous to crystalline phase changes along with absorption and desorption of material were demonstrated.

Light was also shown to be capable of inducing surface modifications. Since a combination of both bias and illumination were necessary, the size of the manufactured features was not diffraction limited. In one case, the changing of the wavelength by 10 nm determined whether or not a feature would be produced. The light was thought to induce hole-electron pairs which weakened bonds and induced reactions.

Charged regions were produced in silicon nitride using a force probe and in photoresist using a tunneling probe. The decay of charge in the photoresists was on the order of minutes which would impede its use in a memory while the charged regions in the nitride were considerably more durable.

A magnetized tunneling probe was also found capable of magnetizing 500 nm regions of a surface even when covered with 100 nm of gold.

This summary shows feasibility along with some problems associated with certain methods. The results are general with certain materials behaving differently for a given surface alteration method. For a more detailed summary of how individual materials fare for use in a nanomemory see Chapter 5, Scanning Tunneling Lithography: Material Précis.

Table 3-1. Mechanical contact surface alteration literature summary.

Authors	Sample	Tip	Feature Type	Feature Lateral Size	Other
Abraham..	Gold	W	Hole/hill	50 nm	UHV, tip distortion
Garfunkel..	$Rb_{0.3}MoO_3$		Hole/Line/ Square	6 nm	Stable features
Gimzewski..	Ag on Si	Ir	Hill, Hole	10 nm	Tip Degradation
Harmer..	$YBa_2Cu_3O_{7-x}$		Hole	25 nm	Poor conductivity
Jaklevic..	Gold	W	Hole	20 nm	UHV, Surface Migration
Marchon..	Rhenium	W	Hill	2-5 nm	hills not Re
McCord..	CaF	W	Lines	360 nm	Surface not conducting
Stroscio..	CO and Pt on Pt, Xe and Ni on Ni		atoms	atomic	UHV, 4^oK
van Loenen..	Silicon	W	hole/hill	10 nm	UHV
Virtanen..	$YBa_2Cu_3O_{7-x}$	Pt/Ir	Grooves	100 μm	Transformation over 1 hr
Yokohata..	Gold	Pt	Indents	30-300 nm	Tip displacement

Table 3-2. Field induced material transport literature summary, Part I.

Author	Sample	Tip	Feature Type	Feature Width	Pulse Voltages, currents and durations	Interesting notes
Akari..	WSe_2	Au	hole	5 nm	4-6 V, <200nA, 10-400 ns	Holes grew over time
Albrecht..	HOPG in air HOPG in UHV	W	holes none	2-10 nm	3-8 V, 1-100 μs	Threshold dependent on tip; inconsistent formation
Becker..	Ge in UHV	W	hill	8 Å	-4 V	inconsistent formation
Casillas..	Ti(O_2) on Pt on mica	Pt-Ir	hole	5-36 nm	±2 cycling, 250 ms	different I(V) curves
Emch..	Au on mica		hills/holes	5-10 nm	3-5 V, 10 ns	tip dependent threshold unpredictable hill or hole surface diffusion
Heinzelmann..	$HoBa_2Cu_3O_{7-x}$		hole	10-80 nm	4 V, 10 nA, 5 s	2 V threshold
Hoffman-Millack..	Au	W	hole	60 nm	2 V stepped, 60 ms	hole filled in after 50 min
Li..	Au	W	holes	2-8 nm	> 2.7 V	varying threshold
Lyo..	Si	W	hill or hole	1-5 nm	±3 V	hill removal possible
Mamin..	Pt and Si Au	Au W	hills holes	15-30 nm	±3.5-4.0 V, 10 ns	hills bigger near threshold, hills could be removed and redeposited, observed tip alteration
Marchon..	atomic S on Re under oil	W	hole scattered hills	50 nm 1-10 nm	3 V, 100 nA, 2 s -3 V	attempts in air were unfruitful
McBride..	Au Au	W Pt	hills holes/hills hills	15 nm	(hills -3.8 V, 150 μs) (both -4 V, 250 μs) (hills ±3.8 V)	hills formed when pulse current duration exceeded 200 μs, field threshold of 2.3 V nm^{-1}
Miller..	HOPG	Pt-Ir	hills/holes	1-200 nm	2.7-8.0 V	changing threshold

Table 3-3. Field induced material transport literature summary, Part II.

Author	Sample	Tip	Feature Type	Feature Width	Pulse Voltages, currents and durations	Interesting notes
Mizutani..	damp HOPG	Pt	holes	1-10 nm	3.5 V, 350 μs	80 % success
Ohmori..	Pd and Pt		surface diffusion		150 mV, 2 nA	impurities on samples
Parkinson..	InSe, ZrS_2, $TiSe_2$, $SnSe_2$, SnS_2, $NbSe_2$, TaS_2, $MoSe_2$, WSe_2, MoS_2, WS_2, PtS_2, $ReSe_2$, WTe_2, $MoTe_2$	W or Pt	hole	500 nm	< ±100 mV	Normal tunneling produced holes
Rabe..	Ag on mica		holes/hills	10 nm	5 V, 100 ns	unpredictable hole/hill type
Saulys..	$Na_{0.9}Mo_6O_{17}$	Pt-Ir	holes	5-10 nm	0.6-2.5 V, seconds	surface transformation during imaging
Schimmel..	WSe_2	W or Pt-Ir	hills/rings	1-6 nm	2.3-5.8 V, 20 ms	structures were formed and imaged in the constant height mode of operation
Schneir	HOPG Au under grease		hole hills/holes	1-9 nm 5-10 nm	3.2-4.0 V, 0.5 s 3.0 V	some damage existed beyond the hole; unpredictable hole/hill formation surface diffusion reported
Shedd..	Au HOPG		holes holes/hills	 20 nm	3-5 V 0.05-3.5 V	
Shenn..	HOPG	W	holes	1-10 nm	30-180 V, 0.1-0.5 μs	0.04 Torr vacuum, tip dependent threshold
Sommerfeld..	Au and Pt	Pt-Rh	hills	5 nm	5 V, 20 ns	Au threshold, 2.8 V, Pt threshold, 4.3 V, surface diffusion observed

Table 3-4. Field induced material transport literature summary, Part III.

Author	Sample	Tip	Feature Type	Feature Width	Pulse Voltages, currents and durations	Interesting notes
Staufer..	$Rh_{25}Zr_{75}$ $Fe_{86}B_{14}$ glassy metals		hill lines hills	35 nm 20x100 nm 20 nm	2 V, 315 nA 0.7-1.0 V, 1 mA	possible taylor cone formation UHV Erasure of nearby hills
Terashima.. [1990]	HOPG		holes	1-50 nm	4 V, 1-10 s	unsuccessful alteration of Si and $YBa_2Cu_3O_7$
Terashima.. [1991]	$Bi_2Sr_2CaCu_2O_x$ on MgO	Pt-Ir	hole	2-50 nm	4.5 V, 1 s	
Virtanen..	$YBa_2Cu_3O_{7-x}$		ditch	100 nm	10 v, 0.5 s	1.5 V or greater must be used to image
Yau..	Si(111) in UHV	W	hills/holes lines/ asperities	14 nm	±5 V, 0.2 s	hills would diffuse away, holes which were made only with sharp tips lasted for weeks, adsorbates were necessary for hill formation

Table 3-5. Field induced diffusion of adsorbates literature summary.

Author	Substrate	Adsorbate	Tip	Feature size	Notes and information
Eigler..	Ni in UHV at 4^o K	Xenon atoms	W	Atomic	When current was increased above 1 nA, the atoms followed the tip
Whitman..	GaAs in UHV	Cesium	W	50 nm covered	3 V 0.1 s pulse caused the Cs to move towards the tip with no effect for negative pulse; Cs chains were also broken up;

Table 3-6. Field induced surface alteration within a gaseous ambient literature summary.

Author	Sample	Ambient	Tip	Feature Type	Feature Width	Pulse Voltages, Currents, and Durations	Notes and Comment
Dagata..	H passivated Si	air ($O_{2)}$		lines	35 nm	2.2-3.0 V continuous	TOF SIMS revealed more oxygen in region. selective etching possible
Ehrichs.. [1988]	Si (111)	DMCd vacuum	W	lines hill	1 μm 10-50 nm	8 V, 10 ns 4 V	They found that the DMCd was not necessary; C,O polymerization possible; 3 V threshold
Ehrichs.. [1990]	Si	WF_6 (1 mTorr) WF_6 (30 mTorr)		hole/hill hill/hole hole	100/100 nm 25/50 nm 20 nm	-20 V, 100 ns -20 V, 100 ns -15 V, 100 ns	Results without WF_6 showed no holes suggesting fluorine etch
Eigler..	Ni (110)	Xe in UHV at 4^o K	W	atom	atomic	8 V, 20-64 ms	The xenon was transferred between sample and tip
Roberts..	Au	Argon (1.3 Pa)		hole	4.5 nm	2.8 V	Filling of holes observed
Silver..	HMDS on Cu	DMCd	W	hills	120 nm 60 nm 40 μm	0.3 V, 270 μA, 100 s 0.9 V, 220 μA 2.6 V, 72 μA	AES revealed large carbon contamination in feature area
Yau..	HOPG	vacuum TMA	Au or W	hills hills hole	60 nm 1-5 nm 5 nm	4.0 V, 0.2 s 4.0 V, 0.2 s 5.0 V, 0.2 s	3.5 V threshold statistical hole creation

Table 3-7. Field induced deposition/etching within a liquid or transporting film literature summary.

Author	Sample	Liquid/film	Tip	Feature Type	Feature Width	Pulse Voltage, Current, and Duration	Notes and Comments
Bernhardt..	HOPG	dimethyl-phthalate decane	Pt-Ir W	hills hills hole	1-100 nm 10 nm 26 nm	4 V, 200 ns 4 V, 1 μs 4 V, 200 ns	Tip dependent hill/hole formation, tip changes observed
Craston.. Hüsser..	Ag	$AgNO_3$- NaFion	Pt	lines	1-2 μm	0.2-8.0 V, 0-1 nA	Deposition at air/polymer interface, Unstable current, broken lines for rates > 50 nm s^{-1}
Foster..	HOPG	diethylhexyl-phthalate	W	hill	1-2nm	3.7 V, 100 ns	Deposition may be organic, 3.5 V threshold, erasure possible
Hüsser..	graphite Ag	PVP ($AuCl_4^-$) MEEP	Pt W	lines lines	sub-μm non uniform	-5 V, 1 nA 5 V	Ag, Cu. Pt and Au etched, Ag, Au, Cu deposited, dendritic growth for < 3 V
Li..	HOPG	aq AgF H_2O, NaF	Pt	columns pit pit	20-30 nm 10 nm	6 V, 50 μs 6 V, 5 μs	Stable with nearby production, Columns grow on holes, Polarity dependent
Nagahara..	Si(100) GaAs	aq HF	Pt-Ir	squares lines	200-400 nm 80 nm	1.4 V, 25 s	Etching not possible in H_2O od H_2SO_4
Penner..	HOPG	DI H_2O	W	hill hole	0.7 nm 4 nm	±4 V, 20 μs -4.2 V	4 V threshold which varies with tip, No pits formed with N_2 or dry toluene
Rabe..	HOPG	octylcyano-biphenyl	Pt-Ir	adsorbate hole	1-2 nm 10 nm	1.7 V -(2-3) V, 2 min	Air, H_2O, silicone oil similar etch, no etching in helium or dry toluene
Schneir..	Au	Orasene 999		line	300-500 nm	-3 V constant	2 successes in 20 attempts
Wuu..	Pt	anilnium sulfate in NaFion	Pt W	line	2 μm	5 V sample positive	Deposition of polyaniline observered at the air/poly interface

Table 3-8. Field and/or electron induced chemical modification literature summary.

Author	Modified Substance	Tip	Modification Extent	Modification Sort	Modification Parameters	Notes and Comments
Albrecht..	PODA on graphite		40 nm	Broken fibrils	4 V, 100 ns	4.1 ±0.2 V threshold
Dagata.. [1990a,b]	H-Si on Si(111)	Pt-Ir	200 nm groove 100 nm square	Chemical change maybe oxidation	3.5 V constant	Features etched in HNO_3:HOAc:HF modification in air or O_2, no modification in N_2
Dagata.. [1991b]	Al_xGa_{1-x} In_yGa_{1-y} MBE on GaAs		85 nm lines	Oxidation	4.2 V	low field oxide desorption high field oxidation
Dujardin..	$B_{10}H_{14}$ on Si(111)		1 nm	Energetic electron dissociation	4-8 V	Probability of dissociation was 0.1 at 4 V and 0.8 at 8 V
Jahanamir.. [1989]	*a*-Si-H on Si	W	10 nm lines	Conductance increased	10 V, 35 μs, 100 μA	Linewidth equals tip radius, (phase transformation theorized)
Jahanamir.. [1990]	SiO_2 on Si			Conductance changed	6 V, 35 μs, 1 mA	Surface became rectifying
Rinnger..	$Pd_{81}Si_{19}$	W	16 nm lines	Oxidation	100 mV, 10 nA	Hydrocarbons also observed
Utsugi..	$Ag_{1.9}Se$ on $Ge_{0.1}Se_{0.9}$	Pt	13-60 nm grooves	Selenide hydrogenation	2-5 V	No etching for neg bias, H_2Se(gas) theorized
Marrian..	P4BCMU		20 nm dots	electron exposure	-(20-30) V, 10 ms	Bias ramped, -8 V threshold
McCord.. [1986]	Si; Au, Al, Cr, Pt on Si		100 nm lines after etch	contamination buildup	10-1000 eV, 25-100 nA	0.1 C cm^{-1} threshold, docosenoic acid also used
McCord.. [1988]	PMMA		20 nm lines 22 nm	resist crosslinked; chain scission	30 V, 10 pA, 1 μm s^{-1} lower voltage and doses	Possible to expose resist with reverse polarity decreases linewidth
Zhang..	PMMA, PV-cinnamate		30 nm after etch	electron exposure of resist	5-100 V, 5-1000 pA, 10^2-10^4 C cm^{-1}	Linewidths smaller with negative bias (smaller transverse spread)

Table 3-9. Illumination-assisted field-induced surface lithography literature summary.

Author	Surface	Ambient	Tip	Light Source	Feature Type	Feature Size	Parameters	Notes and Comments
Lin..	GaAs	NaOH, EDTA	Pt	Tungsten halogen	Etched lines	0.2-2 μm	-4 V	Linewidth equals tip radius Also used organic solvents
Thundat..	n-GaAs p-GaAs p-GaAs	AuCN NaOH	Pt-Ir	White light	gold dots hills away from tip Etching	0.1-10 μm 15 nm smoothing	4 V, 1 min 0.1 V	Features less pronounced if done in dark, NaOH required circulation
Yau..	HOPG	TMA		XeCl laser (440 nm)	hill	1-16 nm	1-3 V, 18 ns light	Linear conductance above features; No features without TMA; 430 nm light deposits rare

Table 3-10. Localized electrostatic charge implantation in films literature summary. Atomic Force Probes used.

Author	Substrate	Feature Extent	Pulse Parameters	Comment and Notes
Barrett..	SiN on Si	170 nm FWHM charged regions	-40 V, 100 μs	-25 V, 20 μs threshold, erasure possible, 75 nm smallest region 100% charging for 202 attempts, Chemical oxide 1 hr charge half life, Thermal oxide charge 7 day stability
Barrett	Chemical SiO_2 Thermal SiO_2		10 V, 20 μs erasure 40 V, 1 s erasure	
Stern.. Terris..	PMMA	2 μm	100 V, 25 ms	1 hr charge decay, sapphire gave similar results, No detectable charging of mica or quartz

Table 3.11 Magnetic Alteration.

Author	Substrate	Feature Extent	Parameters	Comment and Notes
Moreland..	CoCrTa film	200 nm - 8 μm square	Magnet applied to tip	The Fe tip was bent in a cantilever style so that it would bend in the presence of a magnetic field necessitating a servo response, 100 nm Au layer did not hinder magnetization

3.11 Additional papers

Due to the lapse of time between completion of the thesis and presentation, recent papers were not included for the defense. Many of these papers are presented in this section with a brief overview of the work.

Barniol *et al.* [1992] HF-treated Si was altered under air with -1.4 V imaging conditions. The surface had not been rinsed in DI water. The mechanism is reported to be a tip-induced oxidation effect.

Chen and Ahmed [1993] PMMA resist was exposed with a 80 V electron beam. Subsequent etching produced silicon pillars less than 10 nm wide.

Dagata *et al.* [1992] Nanolithography on III-V semiconductors. MBE arsenic and chemical sulfur capping were shown to passivate GaAs. The S-capped surfaces were thought to be too rough for nanolithography. The As capped surface were oxidized using STM biases of 3.8-6.5 V. Resolution of features was found to be dependent on tip shape and varied from 50 to 200 nm. Vacuum environments were thought to be necessary for atomic manipulation.

Day *et al.* [1993a] Carbon deposits (44 nm) were produced above a 4 V threshold with a monolayer film. The writing speed was 1 μm s^{-1}.

Day *et al.* [1993b] Selective oxidation of silicon was obtained while scanning an atomic force probe over the surface. The oxidation occurred when the probe had a potential between 3 and 25 V. 100 nm lines were

formed at a speed of 100 nm s^{-1}.

Garcia [1994] Hydrated purple biological membrane sheets were mechanically altered producing nanometer scale marks.

Heyvaert *et al.* [1992] $YBa_2Cu_3O_7$ was etched with an STM tip. For biases below 1 V, the etching occurred at edges only. For biases above 1 V, etching was nondiscriminating.

Hosaki *et al.* [1992] Using a voltage pulse, surface sulfur atoms were removed from MoS_2 using a tungsten STM tip. The tip was reported to be 0.3 nm above the surface while a -0.5 V 70 ms pulse was applied. The pulse also had a 0.1 ms spike which extended the bias to -5.5 V. Using successive pulses, the letters PEACE 91 HCRL were produced by removal of atoms. The experiment was performed at room temperature and at a vacuum of 10^{-6} Pa. They suggest a field evaporation mechanism.
They also found that they could produce a 4 nm hill with mechanical contact.

Huang *et al.* [1992] Using pulses <1 ms in duration, 1 nm holes were manufactured on the surfaces of MoS_2 and $SnSe_2$. Hole formation thresholds were found to be 3.5 V for MoS_2 and 1.4 V for $SnSe_2$. Erasure of holes by removal of layers was found to occur using biases above 4.5 V for MoS_2 and 1.7 V for $SeSn_2$.

Mamin *et al.* [1994] Gold bumps on gold were formed on the fly with 4 V pulses between the tip and sample. Due to servo-pulse interaction, time between pulses was limited to 1 ms. The writing was about 90% reliable.

Ostrom *et al.* [1992] What was thought to be Si nanocolumns were formed on Si with 3-7 V 1 sec pulses. The probe was also found to lengthen by several tens of nanometers which prompted the view that the structures were Si.

Ross *et al.* [1993] Square regions of surface modification were produced at the surface of a self-assembled monolayer of $HS(CH_2)_{17}CH_3$ on Au(111) using an STM tip. Defect structures, about 5 nm in diameter were observed on the surface before modification. Surface alteration was observed for a 300 mV bias while scanning. The regions showed a pile of material at the edges of the scanned regions. Using a 3 V bias produced features as small as 25 nm with no apparent pile up at the edges. They suggest that the tip may be scanning within the monolayer.

Silva *et al.* [1992] Au films on mica were mechanically machined to produce insulating gaps between conducting lines and regions. Fabrication of insulated wires and pads was demonstrated.

Stockman *et al.* [1993] STM was used to expose c-tricosenoic acid on a Au film in a nitrogen ambient at -10 V. After developing in ethanol and argon milling, 15 nm lines were formed.

Sugimura *et al.* [1993] Tip anodization of titanium was observed. The process could be limited to a 30 nm region at best. It was found that the process was dependent on humidity. Less resolution was produced at higher humidities. The tip was moved at a rate of 1 μm s^{-1}

Thibaudan *et al.* [1994] A silicon surface was etched in a Ferrocene $(C_5H_5)_2$ environment. The 50,000 Langmuirs of ferrocene was

deposited on a boron doped silicon surface. At a threshold of -1.7 V in a 10^{-7}-10^{-4} vacuum, the surface was etched by what was thought to be field ionization with a FeSi volatile by-product. Lines of 3 nm width were produced.

Wang *et al.* [1992] Monatomic stripes several hundred nanometers in length and 4 nm wide and 2-4 nm spacing were formed on reconstructed Au (111) surface. Normal STM scanning along the [1,1,-2] direction produced the features. The tip was tungsten.

Wang *et al.* [1993] A 150 nm × 150 nm top monolayer of Au was moved to the edges of underlying layers in about an hour of continuous scanning.

This page intentionally left blank.

This page intentionally left blank.

[1] For more detail see Sarid, Dror, *Scanning Force Microscopy*, (Oxford University Press, New York, 1991).

[2] Possibly meaning an oxidation type chemical reaction, i. e. ionization and evaporation.

[3] Taylor, Geoffrey, "Disentigration of water drops in an electric field", Proc. R. Soc. A **280**, 383 [1964].

[4] Dagata, J. A., Tseng, W., Bennet, J. Schneir, J., and Harary, H. H., "Nanolithography on III-V semiconductor surfaces using a scanning tunneling microscope operating in air", J. Appl. Phys. **70,** 3661 (1991b).

[5] Eigler, D. M., and Schweizer, E. K., "Positioning single atoms with a scanning tunneling microscope", Nature **344**, 524 (1990).

[6] Marella and Pease [1989], see also Li *et al.* [1989] and Staufer *et. al.* [1987, 1991].

[7] Craston, Derek H., Lin, Charles W., and Bard, Allen J., "High Resolution Deposition of Silver in Nafion Films with the scanning tunneling microscope", J. Electrochem. Soc. 785 (Mar 1988).

[8] For more detail see pages 442-446 of Sze, S. M., *Semiconductor Devices, physics and technology, (Wiley & Sons, New York, 1985).*

[9] Pan, X., Allee, D. R., Broers, A. N., Tang, Y. S., and Wilkinson C. W., "Nanometer scale pattern replication using electron beam direct patterned SiO_2 as the etching mask", Appl. Phys. Lett. **59,** 3157 (1991).

[10] Shimizu, Kazuhiro, Nakakita, Hideaki, and Oda, Shunri., "Nanometer Patterning by Electron Beam Lithography Using an Amorphous Film as an Intermediate Layer", Jap. J. Appl. Phys. **30,** 890 (1991).

[11] Umbach, C. P., Broers, A. N., Koch, R. H., Wilson, C. G., and Laiowitz, R. B., "Nanolithography with a high resolution STEM", IBM J. Res. Develop. **32**, 454 (1988).

[12] Phillips, H. M., Callahan, D. L., Sauerbrey, R., Szabo, G., and Bor, Z., "Sub-100 nm lines produced by direct laser ablation in polyimide", Appl. Phys.Lett. **58,** 2761 (1991).

[13] Acetic acid, (ethylene dinitrilo)tetra.

Chapter 4.

Scanning Tunneling Lithography: Experiments

The purpose of this chapter is to present basic experimental results regarding the alterability of a surface using a tunneling probe. This chapter will begin with a theoretical overview of quantum mechanical electron tunneling through a square potential energy barrier and its application to STM. Knowledge of the related tunneling parameters are necessary for a better understanding of surface alteration experiments. After this knowledge is reviewed, various surface alteration experiments will be reported.

4.1 Quantum mechanical electron tunneling

An electron has been demonstrated to act not only like a particle (classically) but also like a wave (interference and diffraction). A probability interpretation provides the means for interrelating the particle and wave nature of electrons. Similar to the electric field strength of an electromagnetic wave, an electron with a constant linear momentum, *mv*, and energy, *E*, is attributed a simple harmonic *wave function*, Ψ, where

$$\begin{aligned}\Psi(x,t) &= \sin 2\pi\left(\frac{x}{\lambda}-\nu t\right) + i\cos 2\pi\left(\frac{x}{\lambda}-\nu t\right) \\ &= e^{ikx}\, e^{-\frac{i}{\hbar}Et} = \psi(x)\,\psi(t)\,.\end{aligned} \qquad \textbf{(4-1)}$$

The position of the electron is given by x, the de Broglie wavelength and

frequency are respectively $\lambda = \frac{h}{mv}$ and $\nu = \frac{E}{h}$, t is the time, and where $k = \frac{2\pi}{\lambda}$ and h is Plank's constant. By using this equation to solve Schrödinger's equation,

$$-\hbar^2 \frac{\partial^2 \Psi(x,t)}{\partial x^2} + V(x,t)\Psi(x,t) = i\hbar \frac{\partial \Psi(x,t)}{\partial t}, \qquad \textbf{(4-2)}$$

the probability of an electron to be found at a position inside or beyond a classically forbidden potential barrier, V(x,t), can be determined. This probability, P, is defined by the equation

$$P(x,t) = \Psi^*(x,t)\,\Psi(x,t). \qquad \textbf{(4-3)}$$

Assuming that an electron is incident on a time independent square potential barrier as shown in Fig. 4:1, then Schrödinger's equation for the electron reduces to Eqn. (4-4).

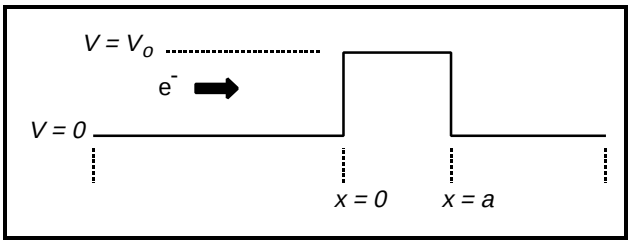

Figure 4:1. Electron incident on a potential energy barrier V_o greater than electron energy, E.

$$-\frac{\hbar^2}{2m}\frac{d^2\psi(x)}{dx^2} = E\,\psi(x), \quad \textit{for } x < 0 \textit{ and } x > a$$
$$-\frac{\hbar^2}{2m}\frac{d^2\psi(x)}{dx^2} = (E - V_o)\,\psi(x), \quad \textit{for } 0 < x > a\ . \qquad \textbf{(4-4)}$$

After calculating the probability amplitudes of the incident and reflected waves for each of the regions, one can calculate the probability

flux transmitted through the barrier. This transmission coefficient[1], T, is given as

$$T = \frac{[\textit{probability at } x<0\,]\cdot v_{x<0}}{[\textit{probability at } x>a\,]\cdot v_{x>a}}$$

$$= \left[1 + \frac{\left(e^{\kappa_o a} - e^{-\kappa_o a}\right)^2}{16\frac{E}{V_o}\left(1-\frac{E}{V_o}\right)}\right]^{-1}, \quad \textit{where } \kappa_o = \sqrt{\frac{2m(V_o-E)}{\hbar^2}} \qquad \textbf{(4-5)}$$

$$\approx 16\frac{E}{V_o}\left(1 - \frac{E}{V_o}\right) e^{-2\kappa_o a}, \quad \textit{if } \kappa_o a >> 1.$$

The barrier region between a STM tunneling tip and a conducting sample is an example of a potential barrier. The potential barrier, V_o, of this region is related to the work functions of the sample (ϕ_s) and tip (ϕ_t), and also the bias, V_b, between the tip and sample. This work function, ϕ, is the amount of energy necessary for an electron (at Fermi energy, E_F) to escape from the surface into a vacuum. Work functions for the elements with clean surfaces range from 2-6 eV. Using V_o-E_F=4 eV and no applied bias, we obtain a value for k_o=1.15/Å. This implies that for tip-sample separations greater than an Angstrom, T is proportional to $e^{-2\kappa_o s}$, where s is the tip-sample separation and is taken to be equivalent to the barrier thickness. The current, I, which flows between the sample and tip will be proportional to T. The proportionality constant will depend on the electron density at the surface of the electron source.

Since tip and sample usually have different work functions, the

barrier is nonuniform. For $eV_b<\phi_o=(\phi_t+\phi_s)/2$, the barrier height can be estimated using the WKB[2] integral approximation to $V_o=\phi_o-eV_b/2$, where e is the charge of an electron. For $V_b<<\phi_o$, Simmons [1963] estimated the current density, J, to be:

$$J = \left(\frac{3e^2}{2h^2}\right)\left(2m\phi_0\right)^{½}\frac{V_b}{s}\,e^{\frac{-4\pi}{h}(2m\phi_0)^{½}s} \qquad \textbf{(4-6)}$$

From Eqn. (4-6), there are three interrelated variables which pertain to tunneling microscopy, *s*, V_b, and I (or J). The current can be calculated from I=J×A, where A is the effective tunneling area under the tip. Using a tunneling area of 1 Å^2, and calculating ϕ_o=5.3 eV from the work functions of a Pt tip and a graphite sample, tunneling currents vs. tip-sample separation, I(s), plots were obtained. Fig. 4:2 shows I(s) plots for 1, 10, and 100 mV tip-sample biases. The natural log of the currents of Fig. 4:2 are plotted in Fig. 4:3, showing a slight deviation from a straight line due to the 1/*s* term in the current.

The three interrelated variables of the tunneling equation yield three possible tunneling configurations. The first is applying a constant current and servoing s to keep V_b constant. This method was used by the topografiner but is not used for STM imaging. The second is the normal topographic operation of a scanning tunneling microscope, where V_b is fixed and a constant tip-sample distance, *s*, is obtained by servoing the probe to maintain a constant current value, I. STM images produced from topographic data will be called *Z-images* for the purpose of discussion. The third configuration is the current imaging operation of an STM where

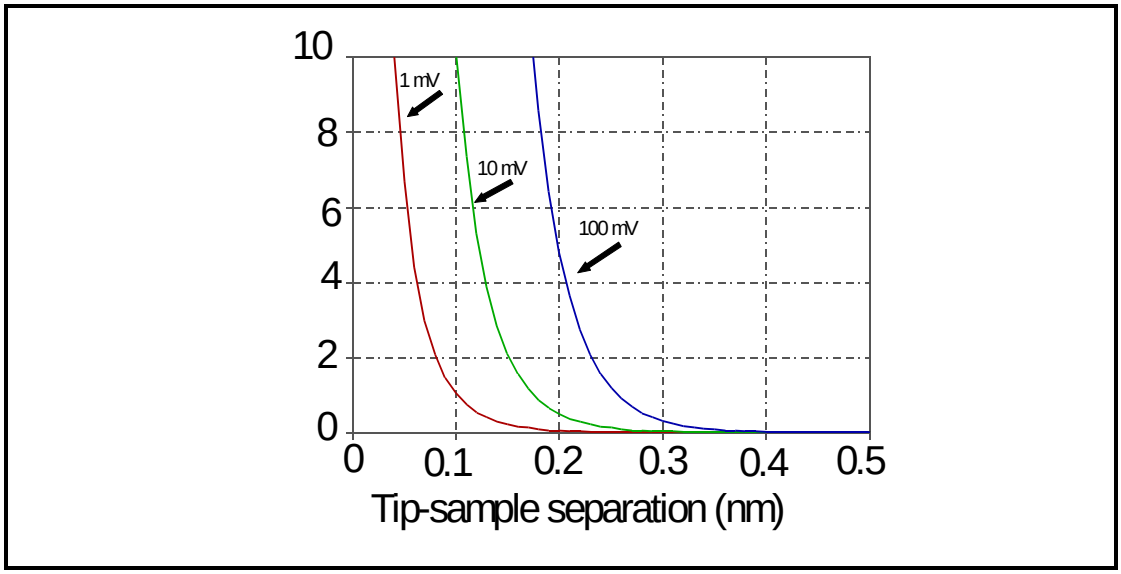

Figure 4:2. Plotted theoretical currents for various biases.

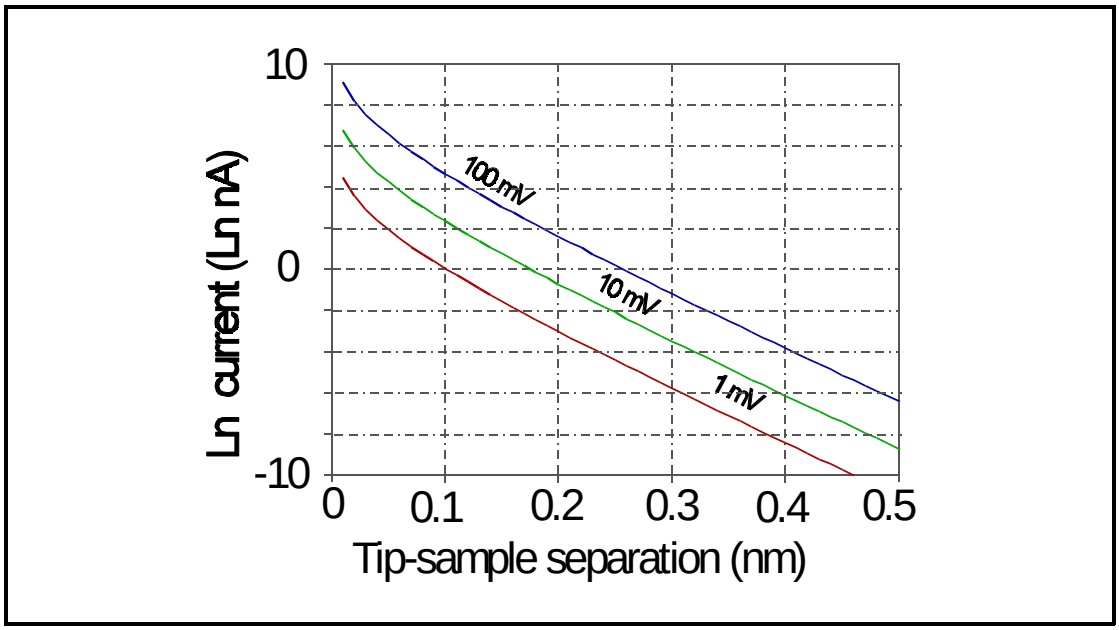

Figure 4:3. Natural log of currents in Fig. 4:2.

the gain of the feedback electronics is kept low so that the position of the probe is not allowed to change rapidly. The current is recorded and a theoretical height is calculated from the natural log of the current. Current imaging is only used for obtaining the electronic structure on an atomic

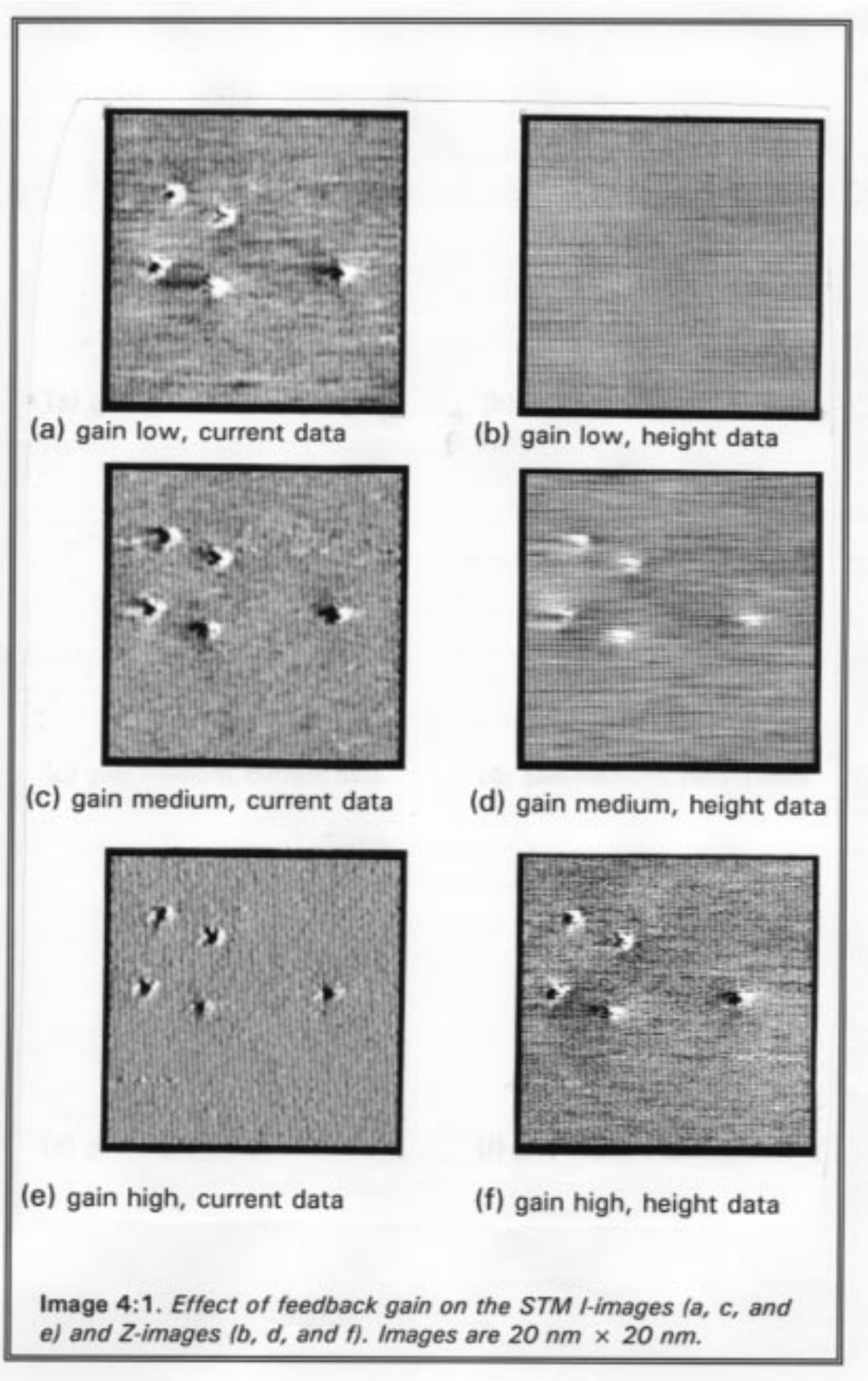

Image 4:1. *Effect of feedback gain on the STM I-images (a, c, and e) and Z-images (b, d, and f). Images are 20 nm × 20 nm.*

scale or for viewing defects having atomic dimensions on flat surfaces. STM images produced from current data will be termed *I-images* for the purpose of discussion. Image 4:1 shows the effect that the feedback has on the appearance of a nonuniform surface for both Z-images and I-images.

4.2 Alteration of a graphite surface

This section describes the results of experiments designed to produce a topographical alteration of the surface of highly oriented pyrolytic graphite (HOPG). The STM used for these experiments was a commercially available Nanoscope II. A breakout box was constructed so that there was access to the sample bias wire and ground wire. This access allowed control of an external bias with a superimposed voltage pulse to facilitate surface modification. All biases mentioned were applied to the sample with the tip grounded through a 1 MΩ resistor. Except where specifically noted, the voltage pulses were produced with a Leader LFG-1310 or a Wavetek Model 23 function generator.

The HOPG sample was chosen for several reasons. One is the presence of flat crystalline regions on the surface with areas extending over 1 μm^2. Since HOPG is a two-dimensional layered material, fresh surfaces are easily prepared by cleaving with a piece of tape. The surface is also relatively immune to oxidation at room temperatures.

Image 4:2 shows how the surface of HOPG looks when scanned with an STM. The greyscale I-images show the areas as lighter which

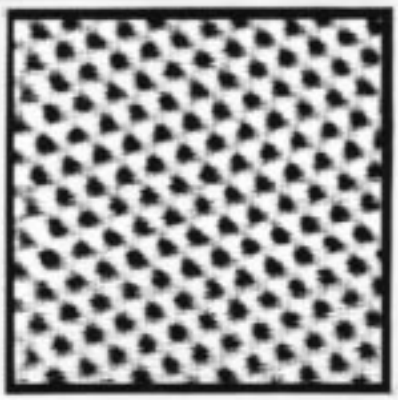

(a) 3 nm × 3 nm, I-image

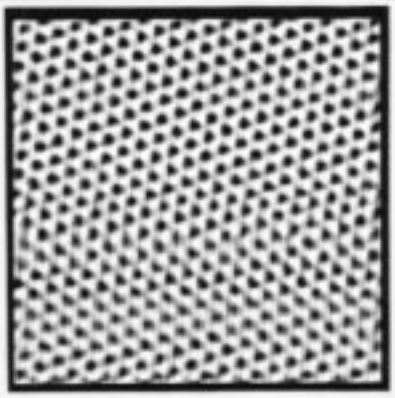

(b) 5 nm × 5 nm, I-image

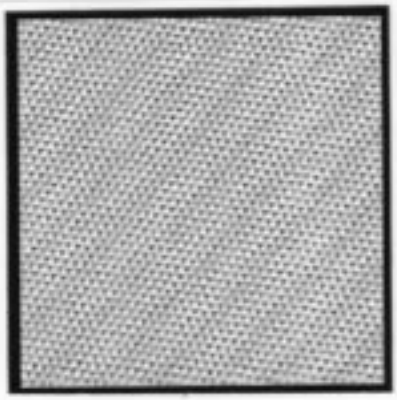

(c) 10 nm × 10 nm, I-image

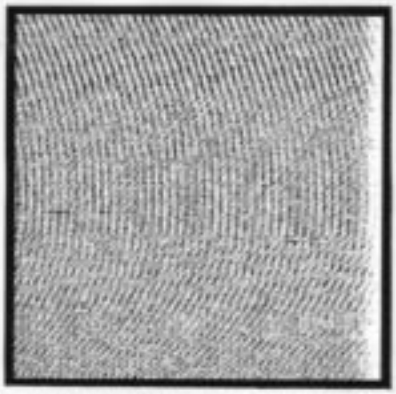

(d) 100 nm × 100 nm, I-image

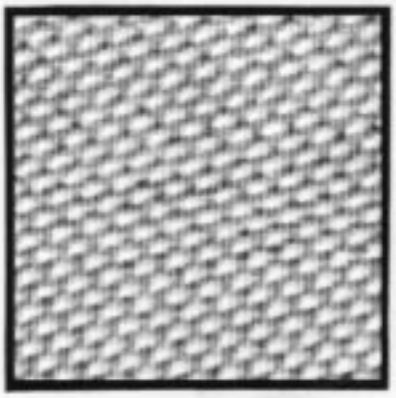

(e) 3 nm × 3 nm, Z-image

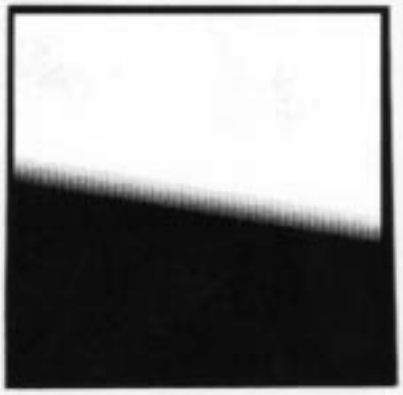

(f) 100 nm × 100 nm, Z-image

Image 4:2. STM images of HOPG. (b), (c) and (d) have been filtered to remove noise. (e) has also had a tilt correction to better reveal the atomic resolution. (f) has tilt included.

have higher conductivity and hence higher currents. The darker regions indicate regions where the current was lower. For the Z-images, the greyscale relates the displacement of the tip necessary to maintain a constant current. Image 4:2(a) reveals a trigonal pattern with saddle points and holes between the more conducting points. There is discussion[3] on whether the highest conductive regions (lightest) are above atoms that have a vertical nearest neighbor on the closest plane or on the second closest plane with the saddle points above the other atomic position. Notice that Image 4:2(d) has corrugations. These are not due to true current corrugations but to a combination of aliasing due to data acquisition and feedback effects. Notice also that atomic resolution in not discernible in that image. Image 4:2(e) minimum to maximum (i. e. darkest to lightest) distance is about 2 Å.For atomic resolution images, I-images can provide more detail than Z-images. Notice that for the 3 nm images, the I-image reveals the saddle points better than the Z-image. Image 4:2 (b), (c), and (e) have been filtered to remove noise. Image 4:2(e) has also had a tilt correction. Image 4:2(f) shows a 100×100 nm Z- image with the sample tilt not subtracted from the data.

4.2.1 Initial investigative experiments

Due to its simplicity, we choose to investigate field induced modification produced by application of a voltage pulse between the tip and sample. This gave us four parameters that could be varied to effect surface alteration. These are the initial current, initial bias, and pulse magnitude and duration.

For our first set of experiments, the bias was set to 20 mV and the feedback electronics were servo controlled to maintain a 2 nA tunneling current (i. e. I_{set} = 2 nA). Using a Pt-Ir[4] tip, tunneling on HOPG, the effect of a 2.75 V square pulse superimposed on the bias was examined. For pulse durations of 2, 20, and 100 μs, there was no observable effect. When a 200 μs pulse was applied, a 40 nm hole with a raised rim was formed. An STM image obtained with the same tip as that used for alteration is shown in Image 4:3(a).

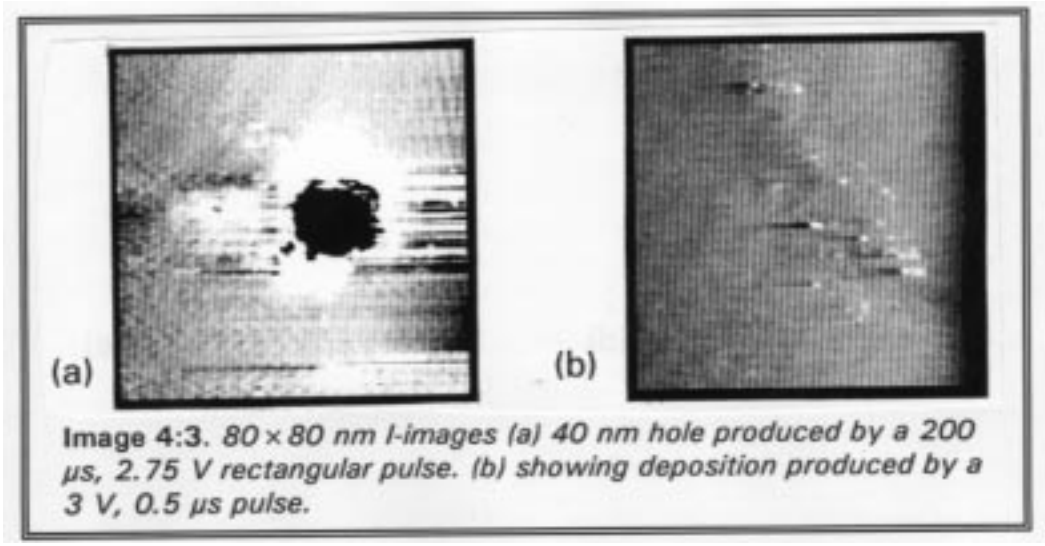

Image 4:3. *80 × 80 nm I-images (a) 40 nm hole produced by a 200 µs, 2.75 V rectangular pulse. (b) showing deposition produced by a 3 V, 0.5 µs pulse.*

A 3 V × 0.5 μs pulse superimposed on a 20 mV bias while tunneling at 2 nA produced scattered deposition on the surface over an 80×80 nm region. This deposition is recorded in Image 4:3(b). After reducing the pulse amplitude to 2 V, no surface alteration was visible. The tip-surface separation was reduced by increasing the tunneling current (I_{set}) to see if the 2 V pulse could produce surface alteration at smaller separations. For I_{set} = 8 nA, 12.87 nA, and 14.6 nA no change in surface appearance was observed. The change in servo current from 2 nA

to 14.6 nA would produce a decrease the tip-sample separation, $\delta s \approx \frac{1}{2\kappa_{\emptyset}} \approx 0.5\,\text{Å}, \; for \; s > \frac{1}{\kappa_{\emptyset}}$. (see the calculated currents in Figs. 4:2 and 4:3). This 0.5 Å displacement may denote a substantial percentage of *s*, effecting a significant change in the surface fields in addition to more than an order of magnitude in pulse current.

Increasing the amplitude of the 0.5 μs pulse to values less than 3 V produced no visible surface alterations. When the square pulse amplitude was increased to 4 V, some scattered deposition was observed. These results suggest that the pulse amplitude must be greater than 3 V for surface alteration to occur with a 0.5 μs pulse.

4.2.2 Pulse duration effects

The effect for 100, 50, 10, 5, 0.5, and 0.05 μs pulse durations of a 4 V pulse amplitude are shown in Image 4:4. The original surface was defect free. At this pulse amplitude (4 V), holes were produced until the pulse duration was decreased from 10 to 5 μs, then an apparent deposition on the surface is obtained. It took two pulses for modification to occur for the 0.05 μs pulse and then only scattered modifications were observed, Image 4:4(f).

4.2.3 Initial current inconsistency

A 400 μs × 4 V pulse was applied onto the 20 mV sample bias with different set currents. The results are shown in Table 4-1. These results seem contradictory since a decrease in current should have drawn the tip away from the sample causing a decreased surface field producing

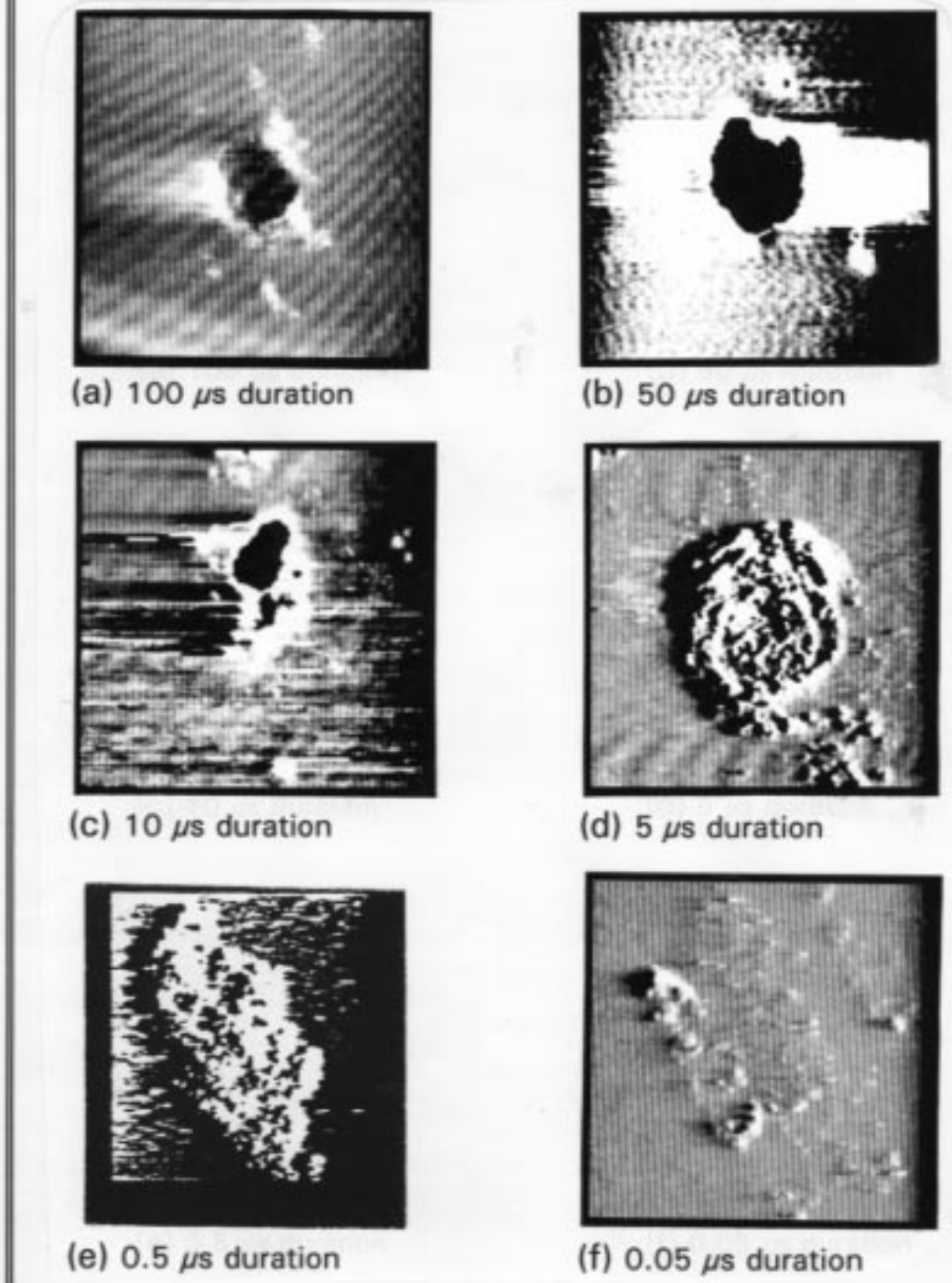

Image 4:4. *80×80 nm I-images of surface modifications produced by 4 V rectangular voltage pulses of various duration.*

Table 4-1. Setpoint current effects on surface alteration for a 4 V × 400 μs pulse applied on a 20 mV bias.

I_{set}	*Effect of Pulse*
2.0 nA	10 nm hole with damage extending 20 nm
0.5 nA	10-15 nm hole with damage extending 40 nm
8.0 nA	60-80 nm altered region

less alteration, but we see that the alteration extent was not directly related to the current magnitude. A change in the tip (geometric and/or electronic) and resulting field transformation may have been the cause of this apparent contradiction. The effect of tip motion due to instrument dynamics is discussed in Chapter 6.

4.2.4 Pulse amplitude threshold for alteration

The results for a series of alteration attempts using various pulse amplitudes and currents are recorded in chronological order in Table 4-2. As shown, an attempt using an 8 V × 200 μs pulse to produce alteration with I_{set} = 2 nA was unfruitful for V_b = 20 mV. I_{set} was then decreased to 0.5 nA. When the 8 V pulse was reapplied, the 150 nm hole shown in Image 4:5 was produced. Again this seems to be counterintuitive since the decrease in the set current should have withdrawn the tip from the sample and decreased resulting fields.

Image 4:5. *Altered region produced with an 8 V pulse. 300 nm × 300 nm I-image.*

Table 4-2. Surface alteration results for a 200 μs pulse on a 20 mV bias for various pulse amplitudes and setpoint currents.

Attempt	I_{set}	**Pulse Height**	**Alteration Extent**
1	2.0 nA	8 V	none
2	0.5 nA	8 V	150-200 nm (Image 4:5)
3	5.0 nA	< 3 V	none
4	5.0 nA	3.5 V	100 nm
5	2.0 nA	3.5 V	40 nm
6	0.5 nA	3.5 V	20-40 nm
7	0.5 nA	3.25 V	none for 3 attempts
8	0.5 nA	3.6 V	30 nm
9	0.5 nA	3.5 V	30 nm on third try

Reducing the amplitude to < 3 V and increasing I_{set} to 5 nA produced no alteration. Increasing the pulse amplitude to 3.5 V produced a 100 nm altered region. Reducing I_{set} to 2 nA produced a 40 nm damaged region. Decreasing I_{set} farther to 0.5 nA produced a 20-40 nm region. After decreasing the amplitude to 3.25 V, three attempts to alter the surface proved fruitless. Increasing the amplitude to 3.6 V produced a 30 nm altered region. Reducing the amplitude to 3.5 volts produced a 30 nm surface alteration only on the third try. These results suggest two things, first, for this experiment there was an alteration threshold near 3.5 volts for the pulse (holding pulse width constant), and second, near the threshold the alteration process is unreliable in nature. Thresholds near 3.5 V for alteration have been observed by others also.[5]

4.2.5 Initial bias effects

This next experimental series of pulses was devised to determine the effect of initial sample bias, V_b, on producing an altered surface. With I_{set} = 2 nA, a 3.5 V × 5 μs pulse was added to V_b. The extent of the altered region of the surface was investigated for $-1 < V_b < 3.7$ V. Table 4-3 contains a list of the extent of surface alteration for associated initial biases. Resulting surface alterations are shown in Images 4:6 and 4:7. The varied appearance of the produced altered regions reveals the uncertainty in surface alteration.

In order to get a better grasp of the alteration size as a function of initial bias, the data in Table 4-3 has been graphically represented in Fig. 4:4. Two different tips were used in the experiments and are shown on the graphs in Fig. 4:4 using different symbols. Both tips produced <10 nm features for $-0.8 < V_b < 0.25$ V. But, one tip also produced 80-100 nm features at these biases. The graphs illustrate that different tips have different alteration effects and also that each tip can produce varied or unreliable results. The formation of a hole or hill was not predictable.

When the voltage pulse was applied upon V_b = -0.7 V with I_{set} = 2 nA, the mound structure in Image 4:7(l) was produced. However, using the same initial bias and pulse after changing I_{set} to 4 nA, the two holes shown in Image 4:8(a) were produced. Image 4:8(b) is a more detailed view of one of the holes revealing the diameter of the hole to be less than 2 nm. The production of two holes suggests the presence of a second

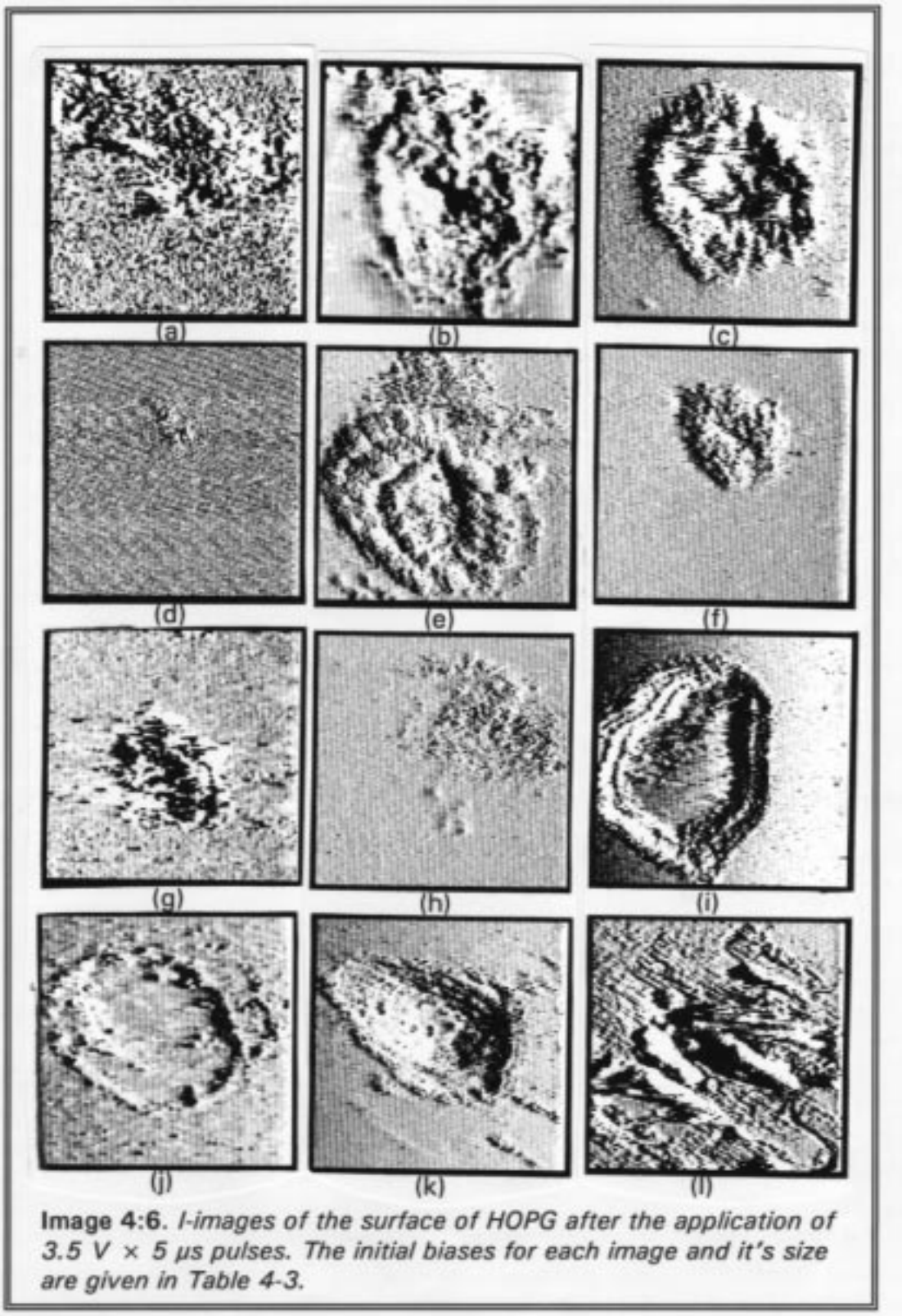

Image 4:6. *I-images of the surface of HOPG after the application of 3.5 V × 5 µs pulses. The initial biases for each image and it's size are given in Table 4-3.*

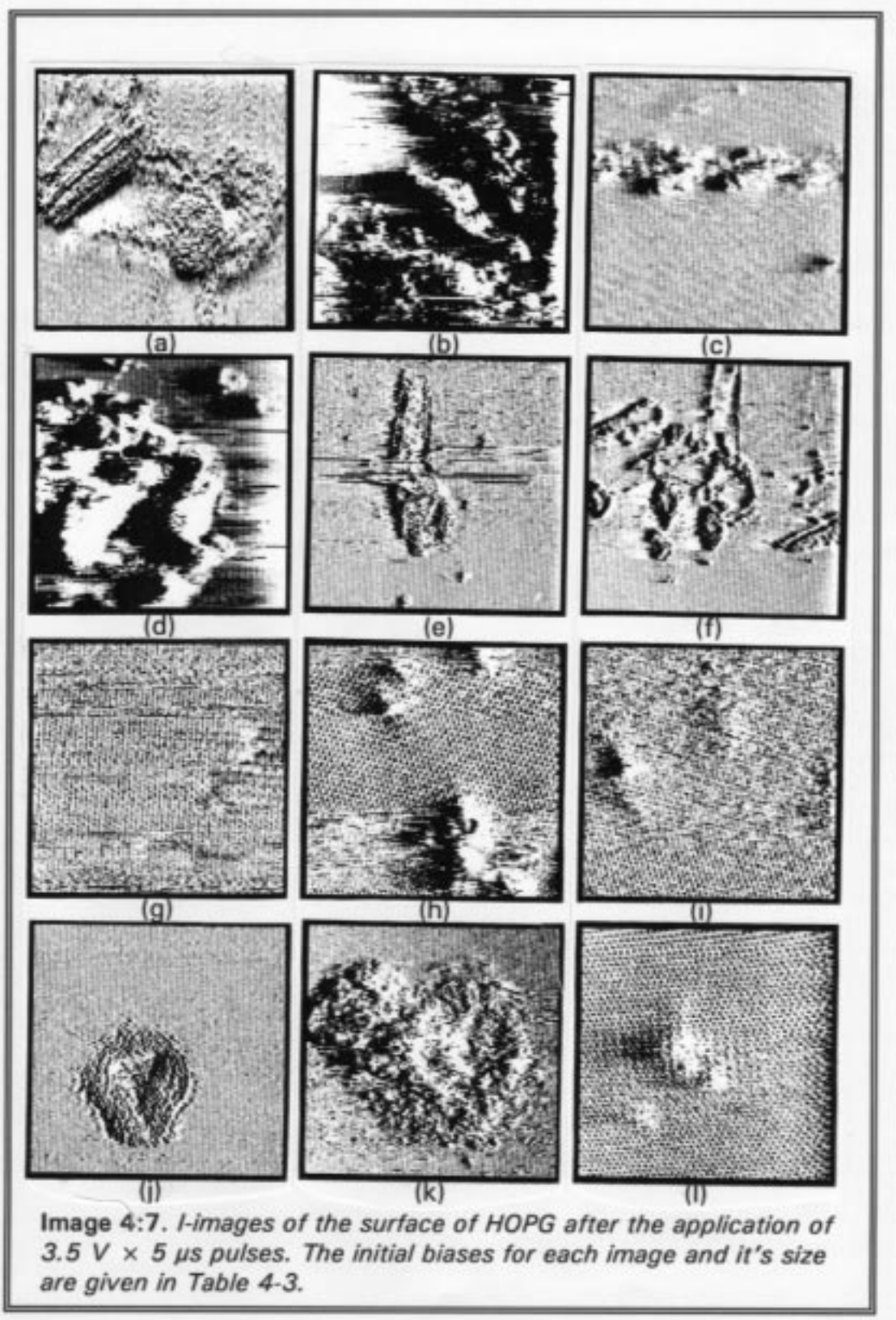

Image 4:7. *I-images of the surface of HOPG after the application of 3.5 V × 5 µs pulses. The initial biases for each image and it's size are given in Table 4-3.*

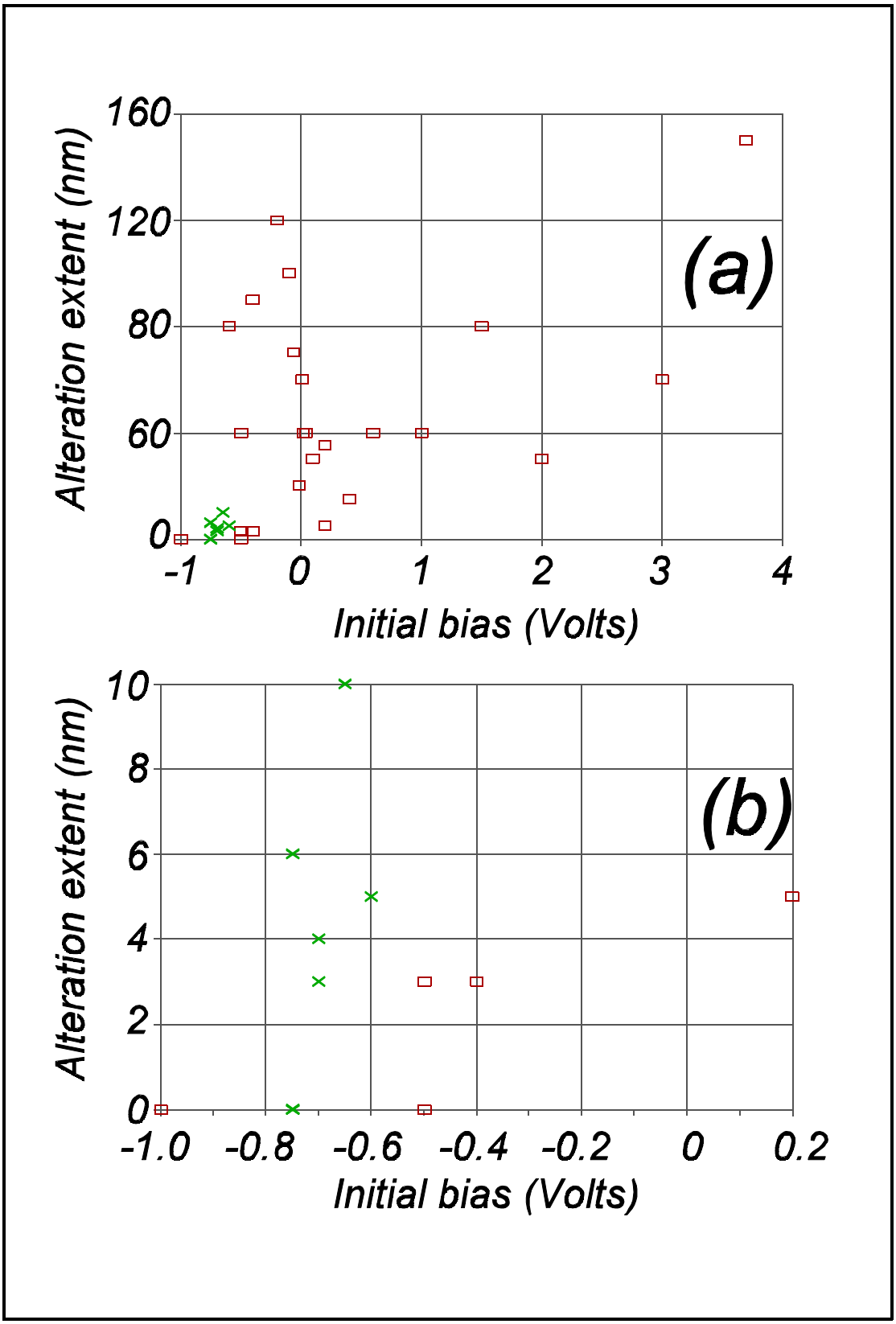

Figure 4:4. Alteration extent for changing initial bias from Table 4-3. (a) shows all the data and (b) shows alterations of less than 10 nm extent. Different symbol styles signify different tips.

Table 4-3. *Extent of damaged region as a function of initial bias for a pulse with a 3.5 V amplitude and a 5 μs duration.*

V_b (mV)	Alteration extent (nm)	Image	Image size nm × nm
0.020	40	4:6(a)	80 × 80
0.040	40	4:6(b)	80 × 80
0.100	30	4:6(c)	40 × 40
0.200	5	4:6(d)	20 × 20
0.200	35	4:6(e)	40 × 40
0.400	15	4:6(f)	40 × 40
0.600	40	4:6(g)	80 × 80
1.000	40	4:6(h)	40 × 40
1.500	80	4:6(i)	100 × 100
2.000	30	4:6(j)	40 × 40
3.000	60	4:6(k)	80 × 80
3.700	150	4:6(l)	200 × 200
0.010	80 × 40	4:7(a)	80 × 80
-0.020	400	4:7(b)	400 × 400
	<<< The graphite sample was moved at this point >>>		
-0.020	40 × 10	4:7(c)	40 × 40
-0.060	40 × 5	none	
-0.060	70	4:7(d)	80 × 80
-0.100	50 × 150	4:7(e)	200 × 200
-0.200	120	4:7(f)	200 × 200
-0.500	none for 2 attempts		
-0.500	3	4:7(g)	10 × 10
-1.000	none		
-0.500	none		
-0.400	several 3 nm	4:7(h)	10 × 10
-0.400	couple 3 nm	4:7(i)	10 × 10
	<<< next day >>>		
-0.400	90	4:7(j)	200 × 200
-0.600	80	4:7(k)	100 × 100
	<<< changed to new tip >>>		
-0.700	none		
-0.650	10		
-0.700	couple 4		
-0.750	none for 3 attempts		
-0.700	4	4:7(l)	10 × 10

nearby protruding tip. Alternatively, if alterations were produced by a changing field at the surface rather than the field itself, the production of two holes can also be explained. In line with this reasoning, it was also found that a triangular pulse could sometimes produce three mound shaped features. Of course, this also could be attributed to multiple tips.

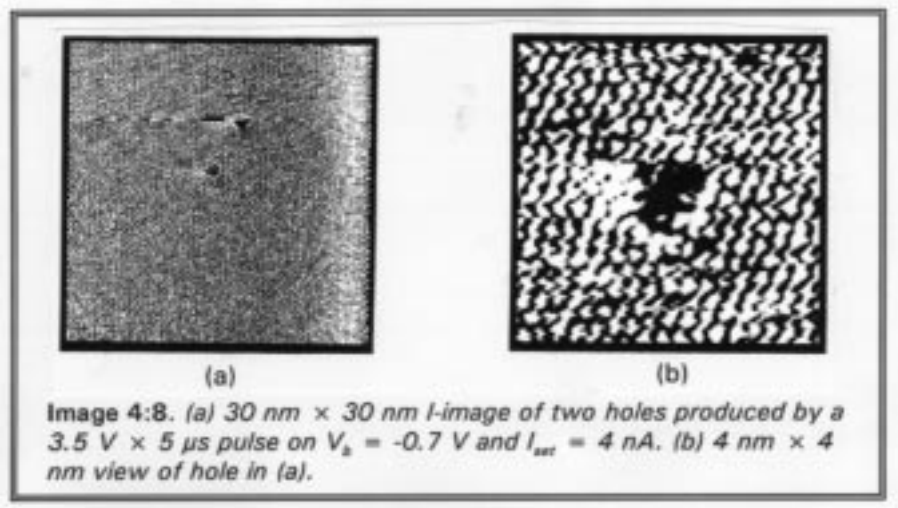

Image 4:8. *(a) 30 nm × 30 nm I-image of two holes produced by a 3.5 V × 5 µs pulse on V_b = -0.7 V and I_{set} = 4 nA. (b) 4 nm × 4 nm view of hole in (a).*

Leaving I_{set} = 4 nA, changing V_b to -1 V, and applying the pulse produced no surface alteration for 3 attempts.

4.2.6 Other experimental observations

Noticing a minimum in alteration dimensions near V_b = -0.7 V, the sample bias was set at this value and the pulse duration was varied producing the surface features shown in Image 4:9. All of the pulses produced surface features on the order of 4 nm or less.

Changing tips and using a 0.1 μs duration pulse, the effect of changing initial bias and pulse amplitude on the alteration dimensions was investigated. Pulses of this duration or less were found to deviate from a

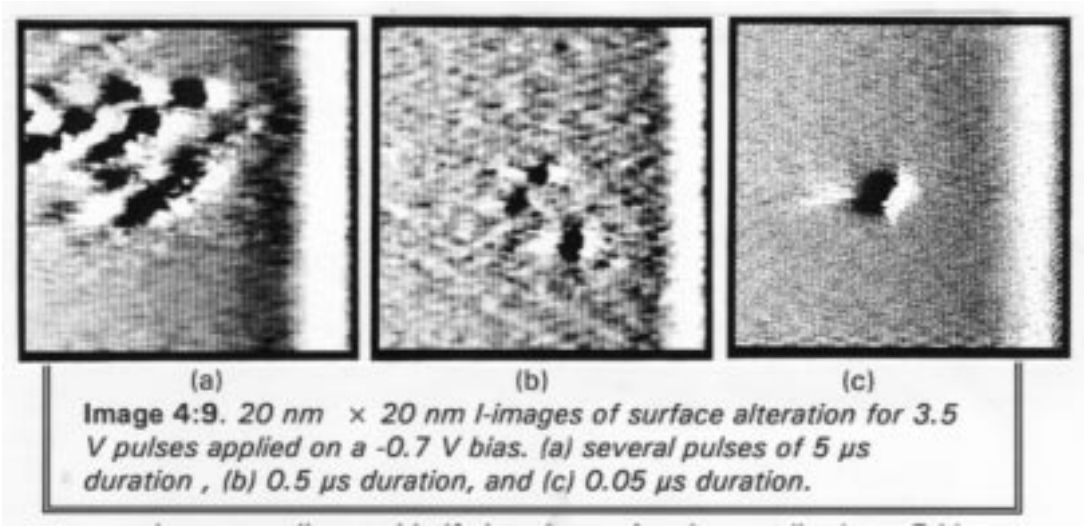

Image 4:9. *20 nm × 20 nm I-images of surface alteration for 3.5 V pulses applied on a -0.7 V bias. (a) several pulses of 5 μs duration , (b) 0.5 μs duration, and (c) 0.05 μs duration.*

square shape to a distorted half-sine shape. A pulse amplitude > 5 V was necessary for this tip to produce any surface features. For a 5.7 V pulse amplitude and V_b = -0.7 V, the alteration size varied from 0 to 40 nm. This further demonstrates a reliability problem in feature production for certain parameters. Changing the initial bias in the range -650 < V_b < -300 mV, the produced feature size was consistently 40 nm, larger than we desire for a bit size.

Attempts to produce surface alteration using a ramped voltage pulse were unsuccessful for 1 ms ramps as high as 5.2 V and for initial biases ranging from -5 V to 100 mV.

4.2.7 Pattern generation

Noticing that the smallest features were produced near V_b = -0.7 V for most of the previous experiments, this parameter was kept constant for other experiments. A 3.5 V × 0.05 μs pulse produced the 1-2 nm feature in Image 4:10. In an effort to see if it was possible to produce a regular array of bits (i. e. altered areas) on the HOPG surface, the tip was repeatedly pulsed and moved to manufacture the 40 nm

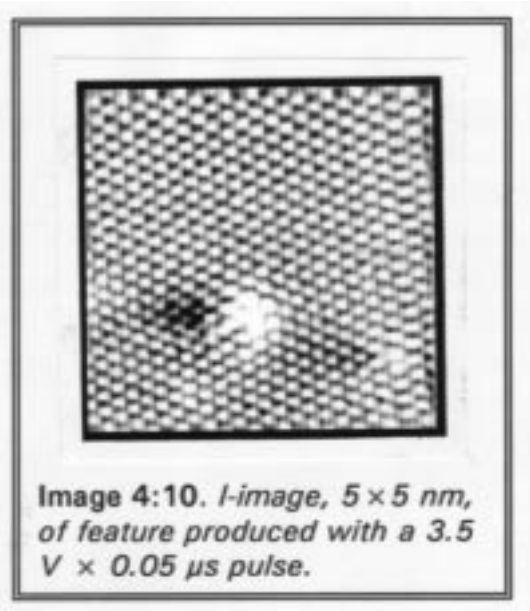

Image 4:10. *I-image, 5 × 5 nm, of feature produced with a 3.5 V × 0.05 µs pulse.*

L-shaped structure seen in Image 4:11(a) and (b). The pulse had a sine wave shape. Initially, the pulse amplitude required to make the individual bits of the 'L' was 3.3 V. As the formation of the 'L' progressed, it was necessary to increase the amplitude to continue making the bits. With the completion of the 'L', the amplitude had been increased to 4.6 V. The necessity of increasing the amplitude further demonstrates the unreliability of feature production. This also implies that surface or tip properties changed during the progression.

The bits were placed to within 5 nm of the desired position causing the 'L' to have a line thickness of about 10 nm. Continuing the process produced the U-shape shown in Image 4:11(c). After the completion of the 'U', V_b was changed to +20 mV then back to -0.7 V. This resulted in degradation of the 'U' to the degree that only a few of the bits comprising the 'U' were still visible, Image 4:11(d). Whether the bits evaporated into the ambient, diffused away, or were plowed by the tip is not known.

4.2.8 Durability of bits

The dissipation of the bits led to surface diffusion investigations. Image 4:12 demonstrates the volatility of bits on HOPG. Image 4:12(a)

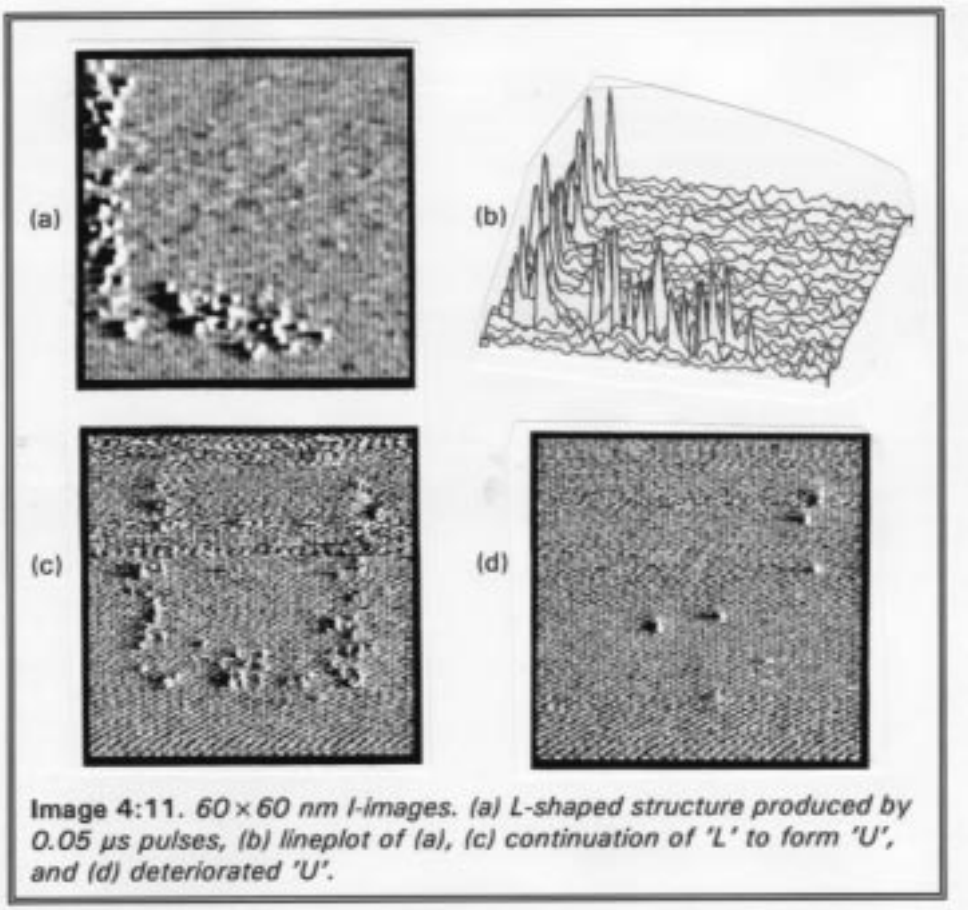

Image 4:11. *60 × 60 nm I-images. (a) L-shaped structure produced by 0.05 μs pulses, (b) lineplot of (a), (c) continuation of 'L' to form 'U', and (d) deteriorated 'U'.*

shows a pattern of bits manufactured with 3.7-3.8 V × 5 μs pulses superimposed on V_b = -0.7 V. I-images for times 41, 83, 93, 124, and 165 s after the initial image are shown in Image 4:12(b-f). One of the bits is shown moving over time while two do not appear to move and one vanishes from the image area. A similar time delay series of unstable bits, manufactured in a experiment six weeks later, are shown in Image 4:13, the seven original bits disappear one at a time until there are only two left. The total time between the first and last images was 6 minutes. Images 4:12 and 4:13 both show the diffusion of what appear to be mounds of material that were deposited from the tip or ambient.

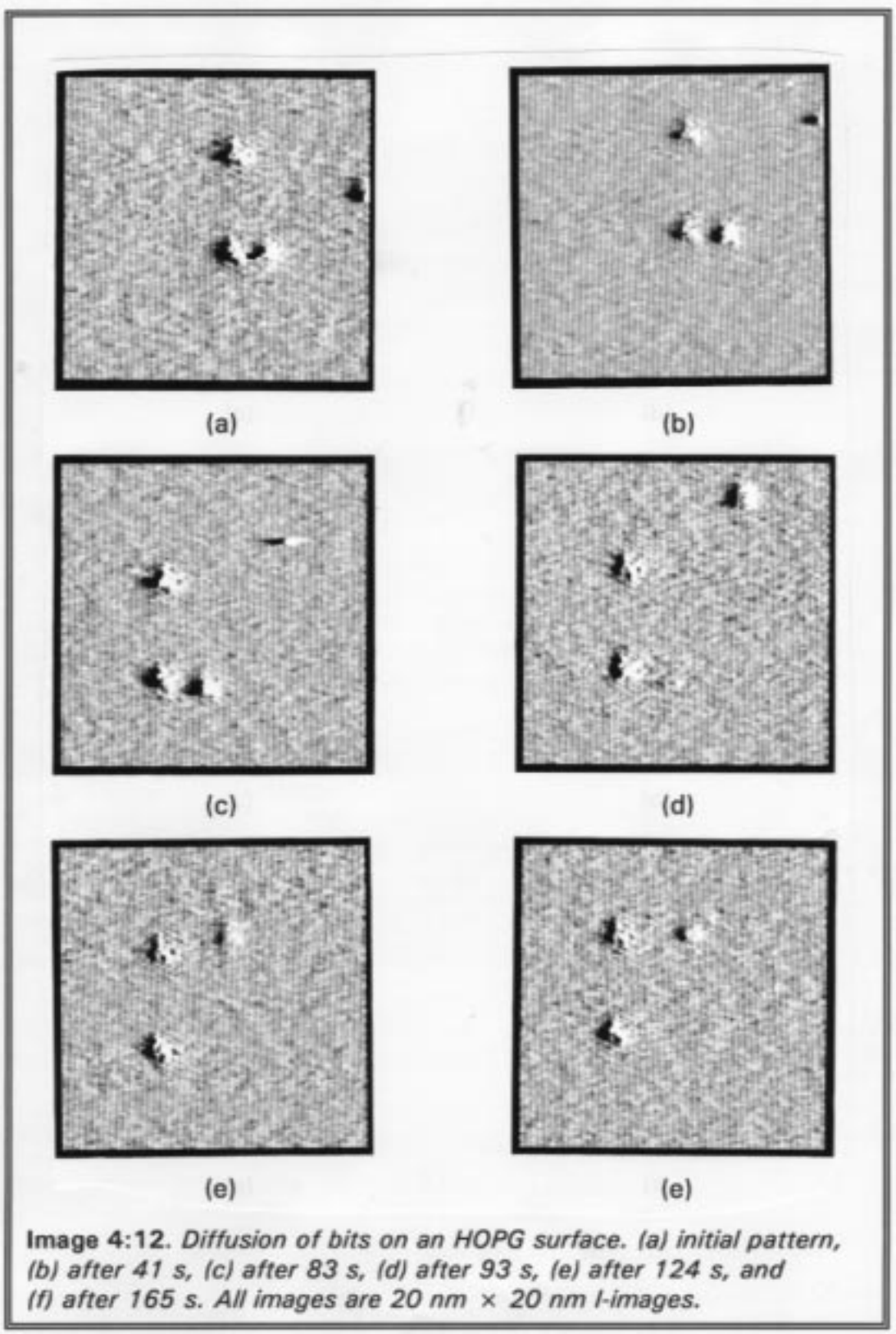

Image 4:12. *Diffusion of bits on an HOPG surface. (a) initial pattern, (b) after 41 s, (c) after 83 s, (d) after 93 s, (e) after 124 s, and (f) after 165 s. All images are 20 nm × 20 nm I-images.*

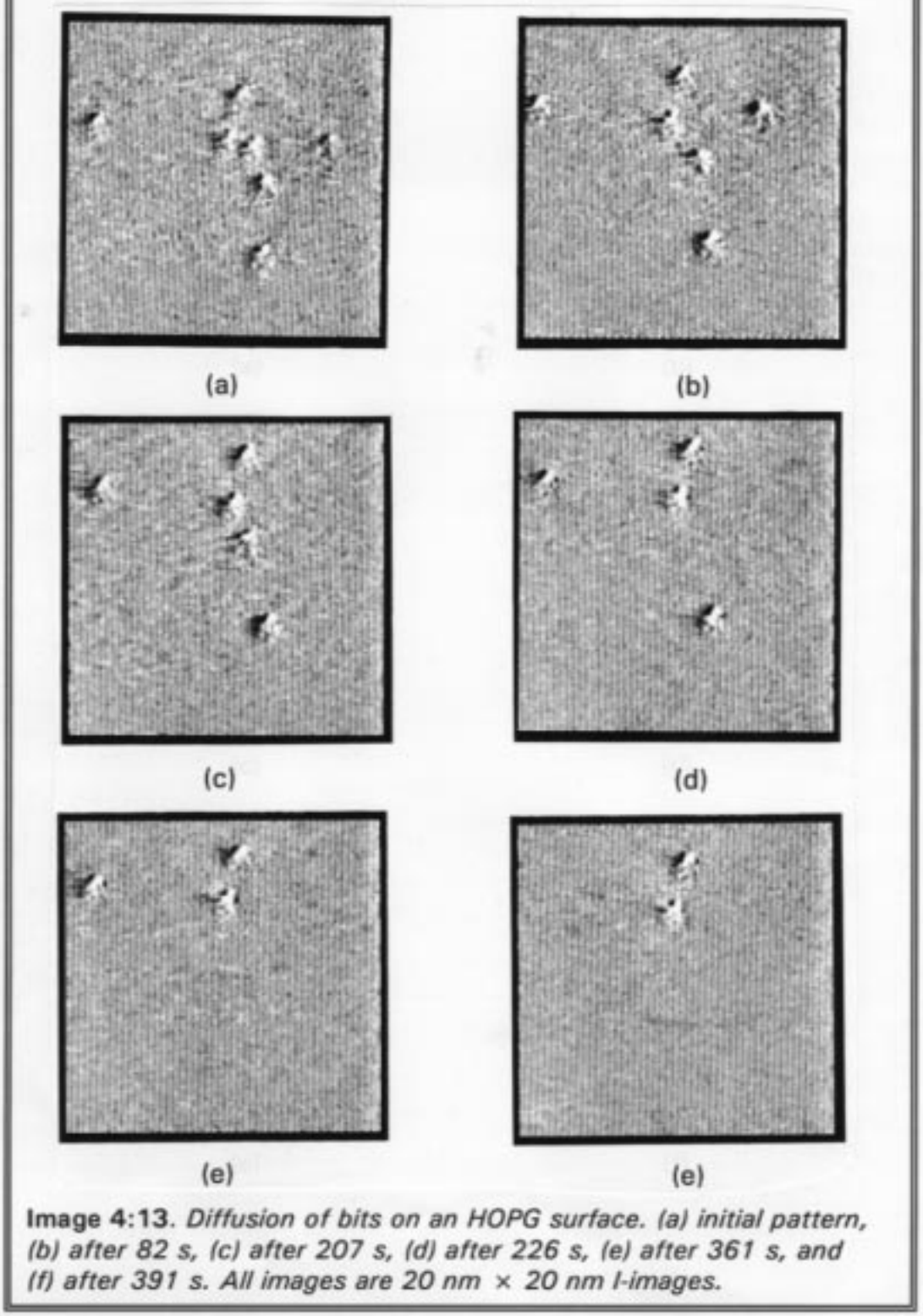

Image 4:13. *Diffusion of bits on an HOPG surface. (a) initial pattern, (b) after 82 s, (c) after 207 s, (d) after 226 s, (e) after 361 s, and (f) after 391 s. All images are 20 nm × 20 nm I-images.*

The same effect is demonstrated for holes in Image 4:14(a-c). The time from the first to last image of hole assimilation was about 33 min. Some of the mounds of Image 4:12 diffused across the surface on the order of seconds while the mounds of Image 4:13 and the holes of Image 4:14 were stationary until their quick assimilation. The material that appears on the rim of the hole in Image 4:14(d) could diffuse or be pulled by the tip into the hole causing its disappearance. These results demonstrate that the features made in this manner would not be feasible for use as bits since they are not durable, even for a short while.

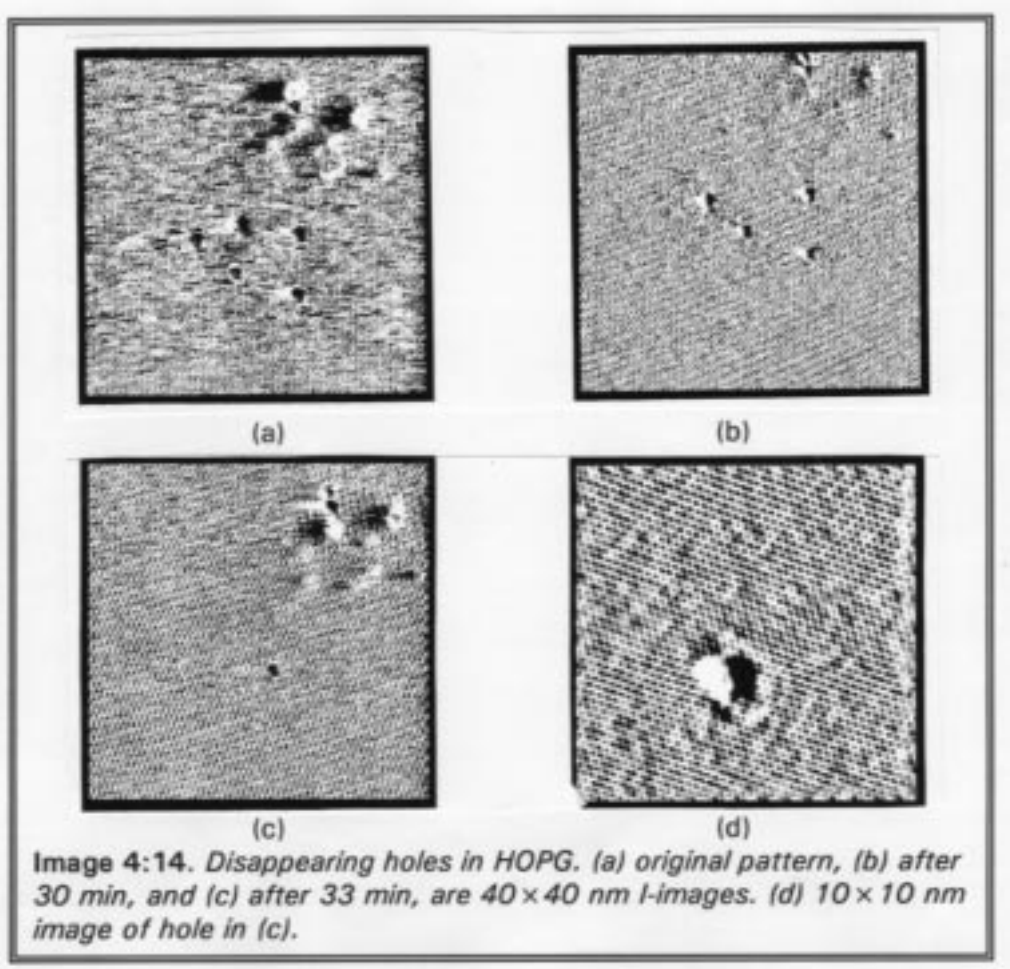

Image 4:14. *Disappearing holes in HOPG. (a) original pattern, (b) after 30 min, and (c) after 33 min, are 40×40 nm I-images. (d) 10×10 nm image of hole in (c).*

4.2.9 Results with a data acquisition board

Manufacturing features was also possible with pulses generated by a Data Translation DT2821 data acquisition board. The Asyst[6] program used to produce the sample bias and pulse amplitude and duration is given in Appendix A. The program allowed the trailing edge of a pulse to be ramped slower than the leading edge. The digital to analog (D/A) circuit of the board was checked and found to have a slew rate of about 4 V/μs. The duration of the pulse was limited to the 10 μs maximum clock rate of the board. The D/A system of the board could output up to ±10 V with a 12 bit resolution.

Image 4:15(a) and (b) show 2-3 nm holes made with a 3-4 V × 10 μs pulse. Keeping the pulse parameters and V_b constant, I_{set} was varied to produce the features in Image 4:15 (c-f). Image 4:15 (c) and (d) both had I_{set} = 2 nA and the pulse produced features approximately the same 1-2 nm size. The 30 nm hole in Image 4:15 (e) was made with I_{set} =0.5 nA and the small feature of Image 4:15(f) with I_{set} = 8 nA. As previously mentioned, one would expect the size of a feature to be larger when the tip was closer (i. e. I_{set} is larger), the inverse was observed. The change in feature type from mound to hole was also counterintuitive. The apparent mound (higher conductive region) of Image 4:15(c) still retained the corrugations of the graphite lattice. This suggests that the greater conductance may be due to an atom or atoms between lattice planes. Bryant[7] *et al.* [1986] show the effect a gold atom has when it is below the first plane of graphite atoms and suggest using a linear combination

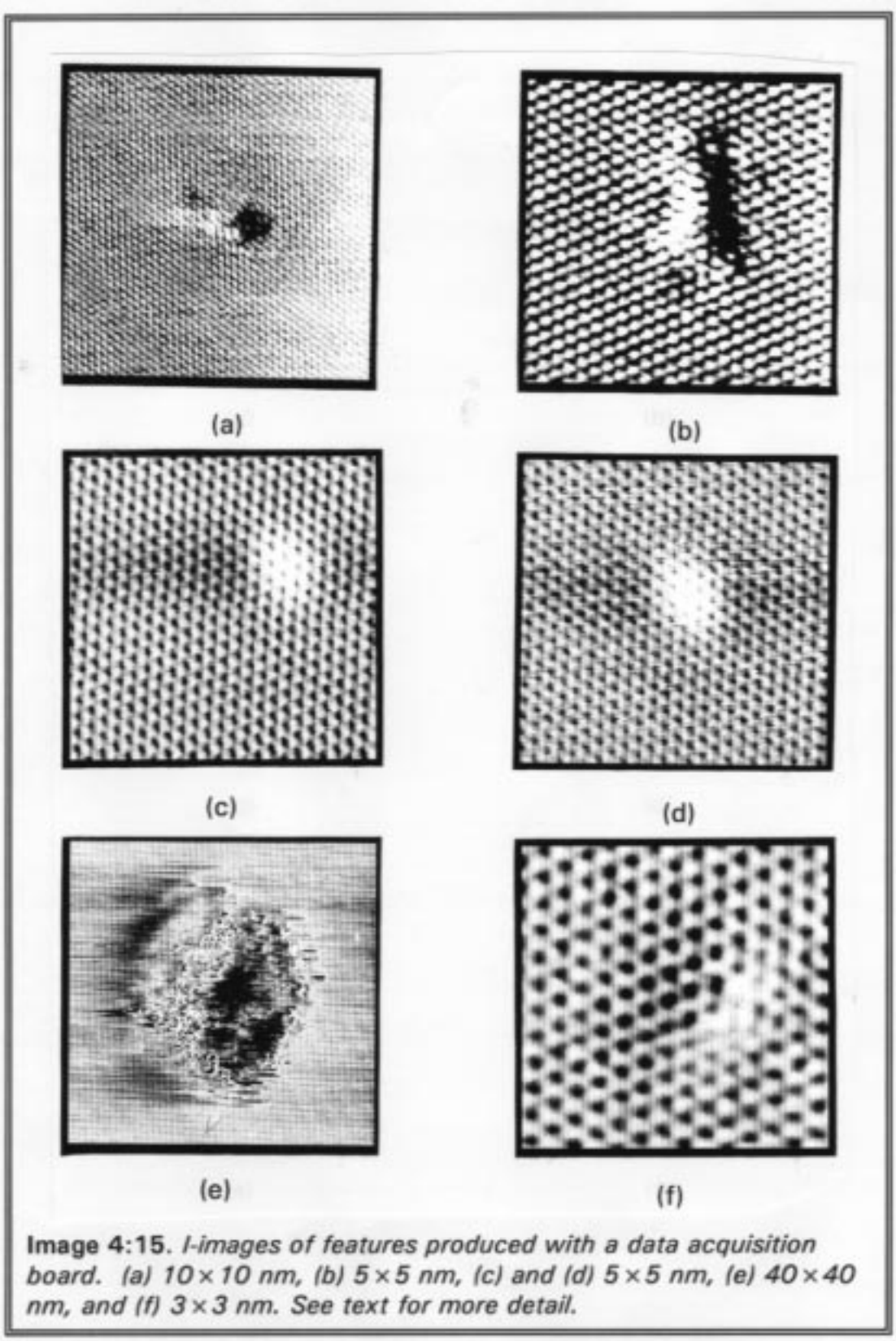

Image 4:15. *I-images of features produced with a data acquisition board. (a) 10×10 nm, (b) 5×5 nm, (c) and (d) 5×5 nm, (e) 40×40 nm, and (f) 3×3 nm. See text for more detail.*

of atomic orbitals (LCAO) approach to find the effect an intercalated atom has on the tunneling properties. The lattice structure of the region could also be retained if there was no real deposition, but only a slight deformation of the first graphite layer due to high fields during the application of the pulse.

The smallest feature yet produced, shown in Image 4:15(f), is also shown by a lineplot in Image 4:16 , which reveals it to be a single atom on the surface either from the tip or a nearby lattice site. The extended effects are probably due to conduction between this atom and nearby tip atoms (i. e. atom imaging tip).

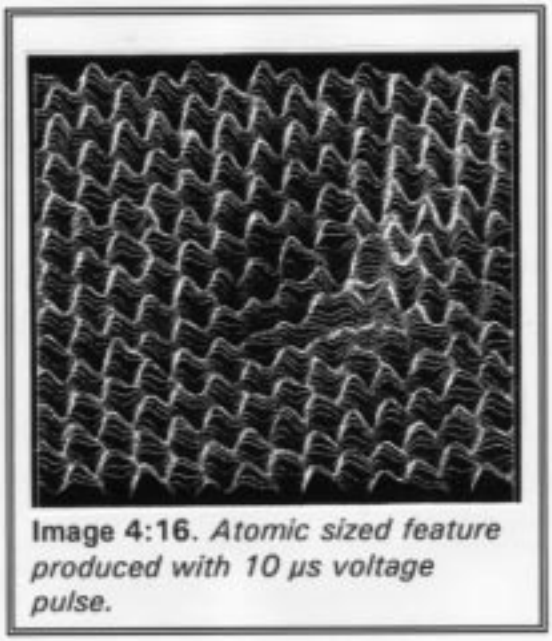

Image 4:16. *Atomic sized feature produced with 10 µs voltage pulse.*

4.2.10 Sample-hold circuit for feedback limitation

Although the gain of the feedback electronics was kept low to try to prevent any tip displacement during the pulsing, the response of the tip to the induced currents during pulsing was unknown. These currents often exceeded 100 nA.

In order to prevent these induced current effects on the tip position, the sample hold (S/H) circuit of Fig. 4:5 was introduced at the output of the current to voltage converter. The S/H circuit kept the current near the setpoint during pulsing and, therefore, preventing tip servo

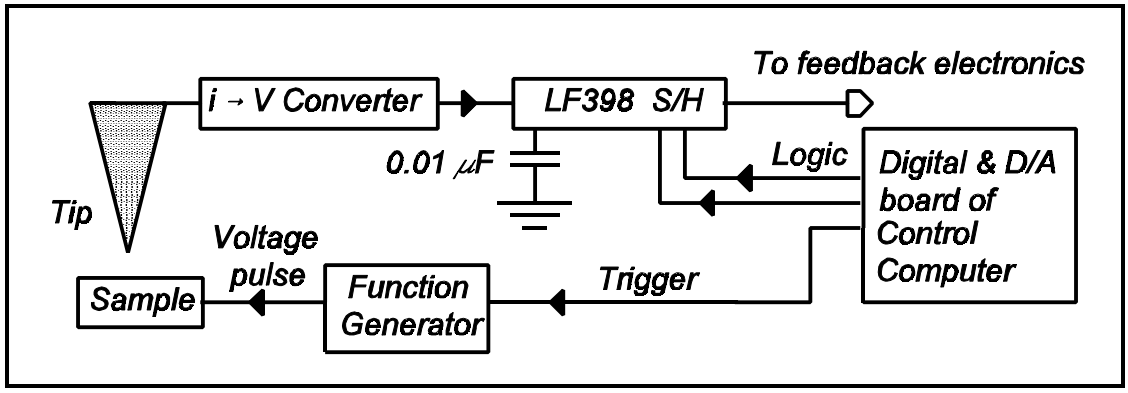

Figure 4:5. Diagram illustrating a sample/hold setup used to limit feedback response during voltage pulsing.

motion. Although there were 100 mV spikes in the output of the S/H converter when switching between sampling and holding, no surface alteration was observed when the S/H was switched without the concurrent application of a voltage pulse.

Using an electrochemically etched tungsten tip and a 4 V peak × 3.3 μs pulse on a -0.75 V sample bias, alteration experiments were performed. There was no alteration observed for a sinusoid pulse, but using a triangular pulse, the ringed hole feature in Image 4:17(a) was produced. The S/H circuit was holding during the pulse and for 0.5 ms afterward. After moving the tip to a nonaltered area, the pulse was reapplied with the S/H sampling. The resulting alteration of 20×80 nm deposition is shown in Image 4:17(b). After changing to another W tip, the pulse produced the two 15 nm deposition features shown in Image 4:17(c) with the S/H holding. Allowing the S/H to sample, the pulse produced 30 nm ring of deposition shown in Image 4:17(d). Expanding the imaged region, Image 4:17(e) shows more of the surrounding area of the feature in Image 4:17(d). It shows a second ring feature about the same size and 50 nm away. The second ring is either a ghost image or a

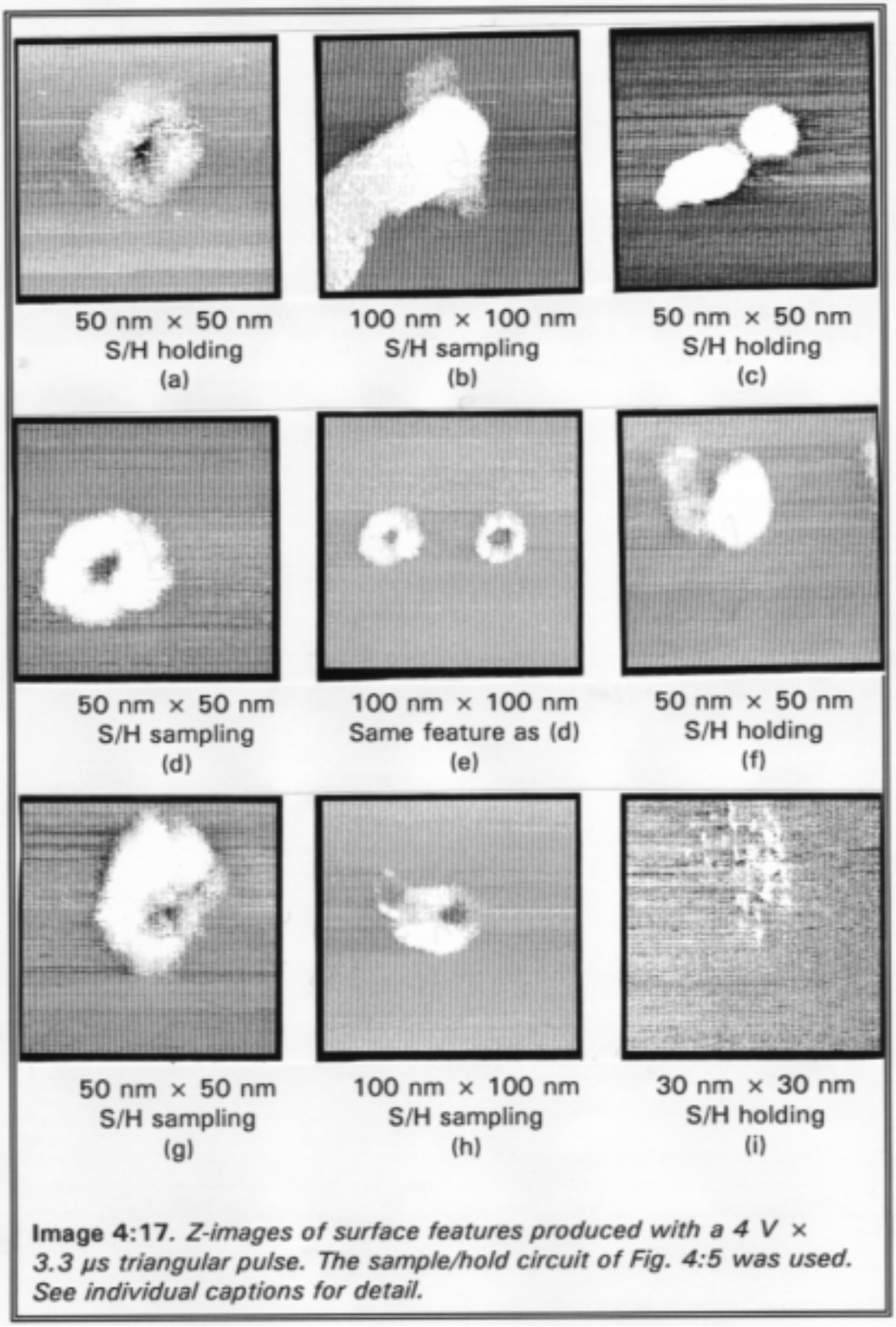

Image 4:17. *Z-images of surface features produced with a 4 V × 3.3 µs triangular pulse. The sample/hold circuit of Fig. 4:5 was used. See individual captions for detail.*

similar feature produced by another tip on the probe. Since the features are so similar, it is more likely that the second ring is fictitious.

Changing the duration of the S/H holding time to 1 ms, while keeping the pulse parameters constant, the pulse produced the 15 nm mound in Image 4:17(f) while the S/H was holding. Allowing the S/H to sample, the pulse produced the ringed hole in Image 4:17(g).

After changing W tips and increasing the S/H holding time to 2 ms, the first pulse with the S/H holding produced no surface alteration, but the second pulse produced the 25 nm feature shown in Image 4:17(h). With the S/H sampling, the pulse produced scattered deposition over a 15 nm region [See Image 4:17(i)]. The imaging resolution became poor after this pulse and remained that way until the application of another pulse. After this, a pulse applied with the S/H holding produced no surface alteration. Then, a pulse applied with the S/H sampling produced a 50 nm mound.

More experiments were carried out with a 150 Ω × 0.1 μF RC (resistive-capacitive) ac filter placed in the output of the S/H circuit, providing a cutoff frequency $(2\pi RC)^{-1}$ of 10 kHz. The reason was to assure that the previously mentioned switching "glitches" would have no effect. Using a 3.3 μs triangular pulse with peak amplitude of 3.5 V or less produced no lasting surface alteration.

Using the S/H with the RC filter, a +5 V × 17 μs symmetric triangular (positive half) pulse was applied on a 0.7 V sample bias. The tip was W and had been dipped in HCl to remove any surface WO_3. With

the S/H holding for 1 ms after the pulse, a 10 nm hole surrounded by a 50 nm diameter ring was produced.

A voltage pulse with an sharp leading edge and a triangular trailing edge *(sawtooth)* was used in conjunction with the S/H circuit and a W tip. For I_{set} = 1 nA and V_b = 0.6 V, a 4 V × 10 μs pulse produced the 15 nm hole in Image 4:18(a) using a 1 ms hold time. Using the same parameters at a different spot produced the 15 nm hole in Image 4:18(b). Increasing V_b to 1 V, and keeping the other parameters the same, the 15 nm hole in Image 4:18(c) was induced. Repeating the pulse at another location produced the 15 nm hole shown in Image 4:18(d). Varying the time of the pulse showed a 3.3 μs pulse producing the <10 nm hole of Image 4:18(f) and a 1.7 μs pulse producing a 100 nm hole.

Using these parameters with a chemically etched Pt-Ir tip[8] produced a 15 nm alteration on the first pulse, 30 nm on the second, none on the third and fourth, and 50 nm on the fifth attempt. Although there is a steady increase in feature dimension, it is an undesirable inconsistency.

4.2.11 Unreliable bit-size with similar pulses

Returning to a W tip that had been dipped in HCl, rinsed in deionized (DI) water, and blow dried with nitrogen from a tank, the 3.3 μs pulse was applied with I_{set} = 0.5 nA. Fifteen attempts were made to alter the surface with the pulse. The results were, in order, a 10 nm hole, a 10 nm hole, no effect, a 10 nm hole, no effect, a 15 nm hole, spotted deposition, a 15 nm hole, a 15 nm hole, ring of deposition, a 15 nm hole,

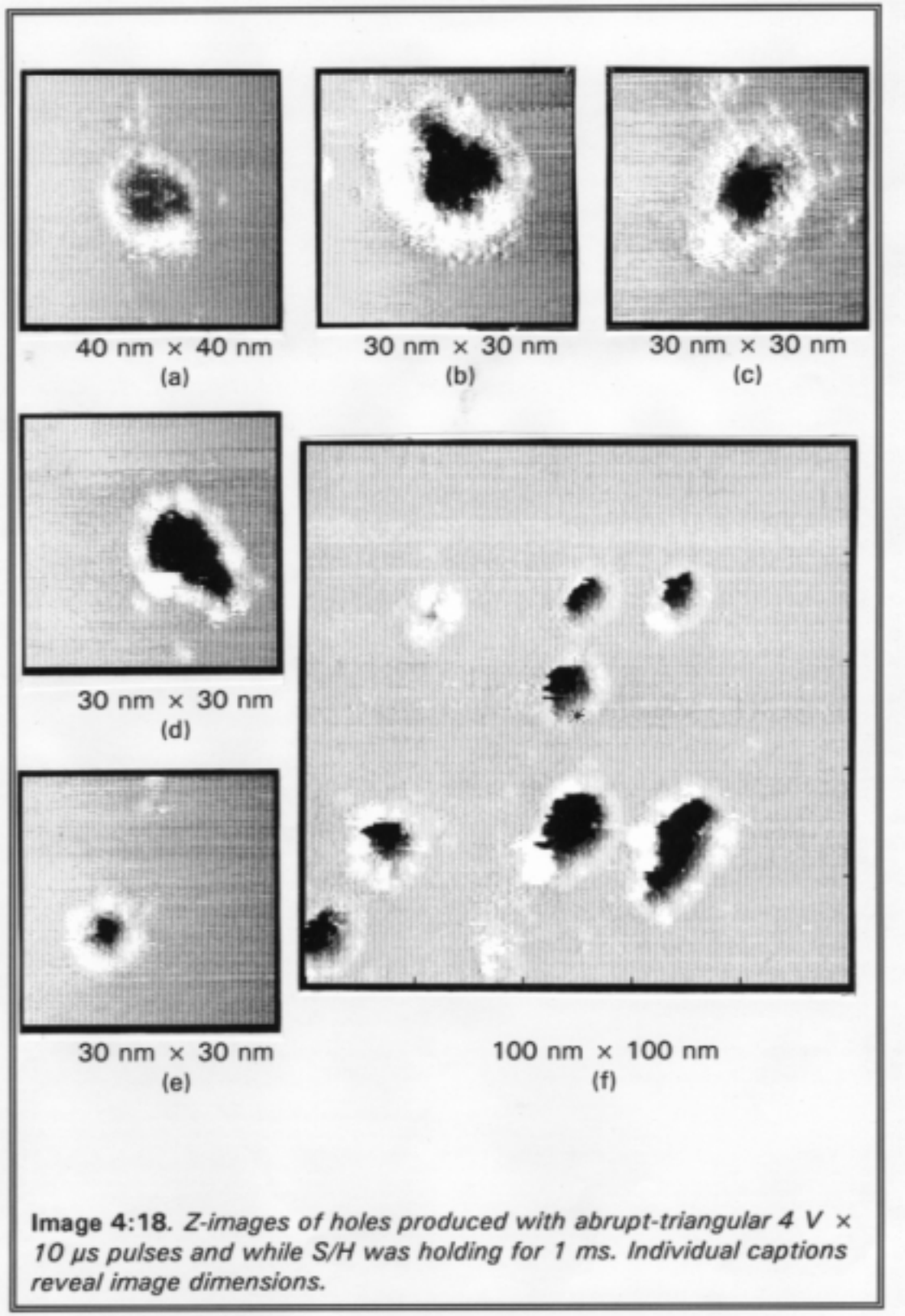

Image 4:18. *Z-images of holes produced with abrupt-triangular 4 V × 10 µs pulses and while S/H was holding for 1 ms. Individual captions reveal image dimensions.*

no effect, a 15 nm hole with scattered deposition, a 20 nm hole, and a 20 nm hole. With this series of holes, the 'I' shape shown in Image 4:18(f) was constructed. The 'I' shape was produced from top-left to bottom-right. Notice the enlargement of the holes as the construction progressed. An attempt to produce surface alteration under a nitrogen ambient produced a 500 nm altered region.

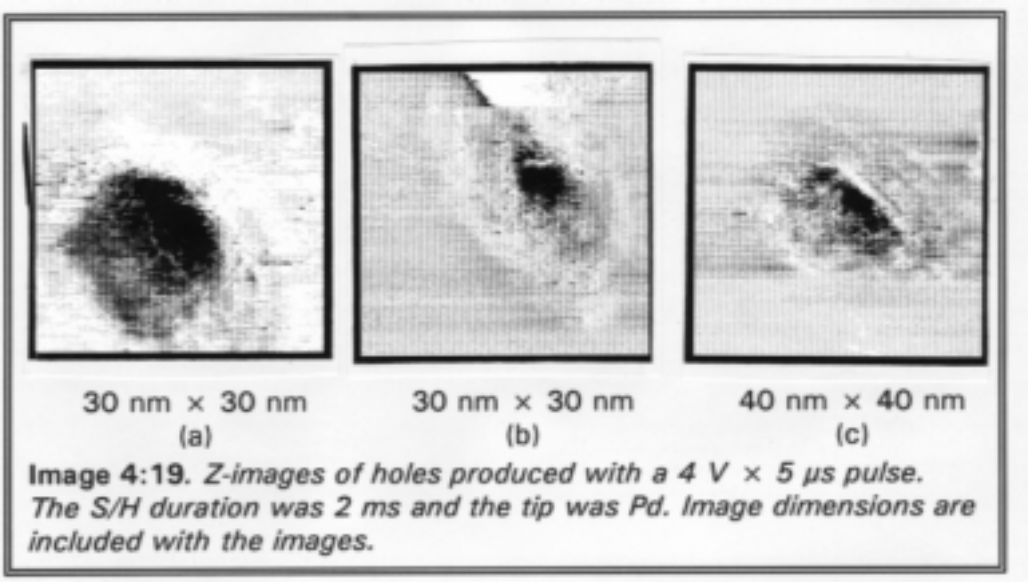

Image 4:19. *Z-images of holes produced with a 4 V × 5 μs pulse. The S/H duration was 2 ms and the tip was Pd. Image dimensions are included with the images.*

Using a 5 μs × 4 V sawtooth pulse with a 2 ms S/H hold time and a mechanically sharpened[9] Pd tip, the holes shown in Image 4:19 were produced.

The tip was changed to a Pt-Ir[4] tip. With I_{set} = 0.5 nA, a 5.5 V × 3.3 μs sawtooth pulse on a 74 mV sample bias produced the 10×25 nm feature shown in Image 4:20(a). V_b was increased to 1.1 V and the pulse applied producing the 10 nm hole seen in Image 4:20(b). The pulse was reapplied seven more times producing, in order, no effect, scattered damage [Image 4:20(c)], no effect, a small disappearing mound, two

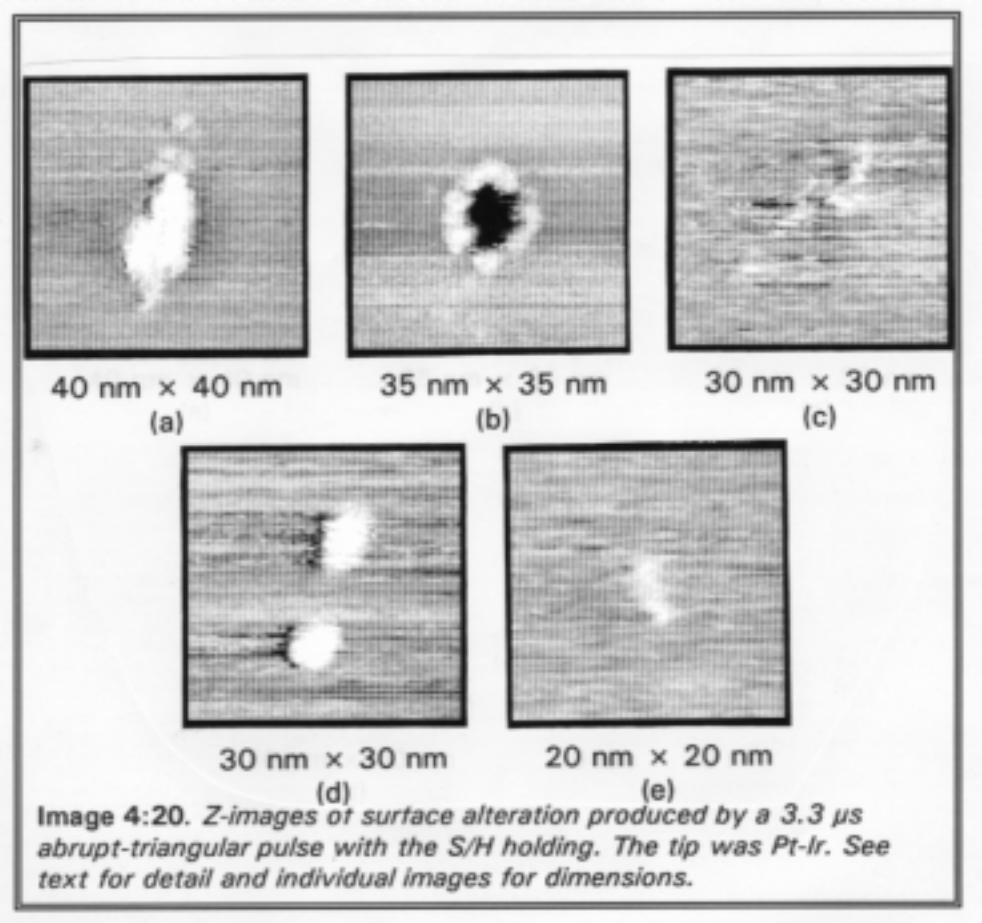

Image 4:20. *Z-images of surface alteration produced by a 3.3 μs abrupt-triangular pulse with the S/H holding. The tip was Pt-Ir. See text for detail and individual images for dimensions.*

5-7 nm mounds [Image 4:20(d)], no effect, and the 3-4 nm deposition shown in Image 4:20(e). This again demonstrates the irreproducibility of feature formation for a Pt-Ir tip.

4.2.12 Alteration under deionized water

Alteration was also attempted under DI water without the S/H circuit. The surface appearance of the HOPG under water before the application of a pulse is seen in Image 4:21(a). Setting appropriate values for the tunneling current was difficult due to a 9 nA leakage current which existed due to the finite conductivity of the water. Results varied from no observed effects for ±18 V pulses to the scattered damage

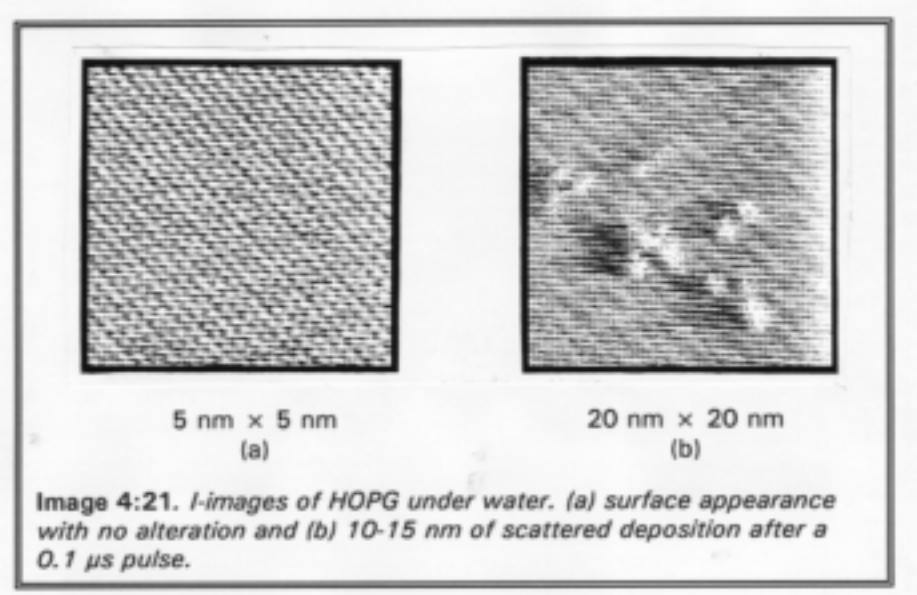

Image 4:21. *I-images of HOPG under water. (a) surface appearance with no alteration and (b) 10-15 nm of scattered deposition after a 0.1 μs pulse.*

shown in Image 4:21(b). For pulses applied with frequencies greater than 700 kHz, the current would more often than not start oscillating between ±2 nA with a frequency of 2.8 Mhz. The oscillation continued regardless of I_{set} or feedback gain values and even if the tip-sample separation was more than several μm. The feedback was digitally controlled by a computer with an update frequency of about 60 kHz, so the oscillation could not be caused by the feedback. The probable cause was uncontrollable induced ac crosstalking in the STM head. Some theoretical and experimental electrical analyses of the STM head are given in Chapter 6.

4.3 Surface alteration of a platinum thin film

A thin film sandwich structure consisting of platinum on chromium on highly polished glass was manufactured to be tested for use as a

possible substrate for writing nanometer scale bits.

Pt was selected for the surface film because of its ability to resist oxidation. The glass substrate was selected because of its ability to be polished to a very smooth surface. An intermediate layer was needed because Pt films adhere poorly to glass. Cr provided the necessary adhesion for both the Pt and the glass. It was desired to have a Pt layer thin enough to be able to field evaporate nanometer scale patches, leaving the Cr to oxidize, manufacturing a less conducting nanometer scale memory bit.

Cr was sputter deposited to a thickness of about 100 Å onto a highly polished glass substrate and then Pt was sputter deposited to a thickness of about 10-20 Å. The deposition was made for us by Tony Lefkow at the Thin Film Center of the University of Wisconsin. The Cr was simultaneously deposited upon a glass microscope slide to characterize the intermediate Cr plating process of the Pt-Cr-glass sandwich structure. While examining the samples, it was noted that they were not as transparent as expected suggesting that the thin films may have been thicker than desired. A second deposition was made to assure the integrity of the samples.

The optimum tunneling bias was found to be -300 mV for both the Pt-Cr-glass samples and the Cr on the glass slide. The Cr was probably covered with thin layer of CrO_x due to ambient oxidation. The optimum tunneling currents were 0.1 nA for the chromium surface and 0.2 nA for the platinum surface.

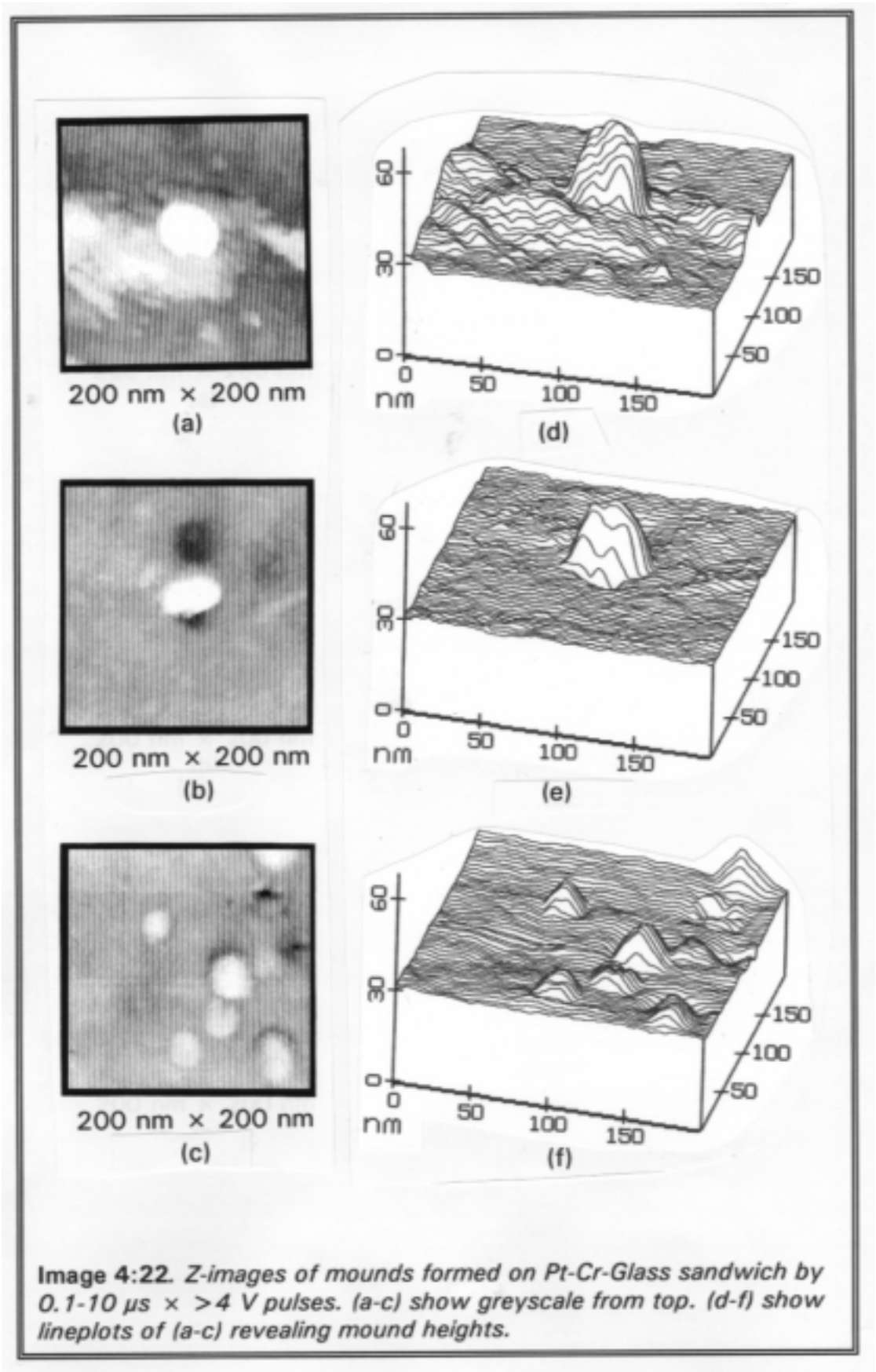

Image 4:22. *Z-images of mounds formed on Pt-Cr-Glass sandwich by 0.1-10 μs × >4 V pulses. (a-c) show greyscale from top. (d-f) show lineplots of (a-c) revealing mound heights.*

Surface alteration was induced by voltage pulses superimposed on the tunneling bias. Pulse times from 0.1 to 10 µS with amplitudes from 1-10 V were used. We found that mounds from 20-200 nm in size could be manufactured. No reliable combination of pulse times and amplitudes was found which would mark the surface. All of the results were intermittent. It was necessary, however, to use amplitudes greater or equal to 4.0 V to achieve the alteration of the surface. The surface alteration almost invariably included a hill formation regardless of the pulse time. Image 4:22(a-c) shows greyscale Z-images of mounds formed on the surface. Lineplots corresponding to these mounds, shown in Image 4:22(d-f), reveal the mounds were 10-30 nm in height. Multiple pulses produced the multiple mounds seen in Image 4:22(c) At shorter pulse times (greater frequencies), and positive substrate bias and pulse, the mounds would usually be accompanied with an underlying hole structure. Examples of these mound in hole features are shown in Image 4:23(a-f). Image 4:23(d-f) are lineplots of the greyscale images shown in Image 4:23 (a-c), respectively.

4.3.1 Shrinking platinum bit

A mound in hole structure was STM imaged over time to see if the structure was stable. The mound was found to decay progressively over time. The changing shape can be seen in Image 4:24. Image 4:24(a-b) shows the initial feature. Image 4:24(c-d) is after 43 seconds. Notice the mound shrinking in height and length. Image 4:24(e-f) shows the structure after about 9 minutes. The mound no longer protrudes above

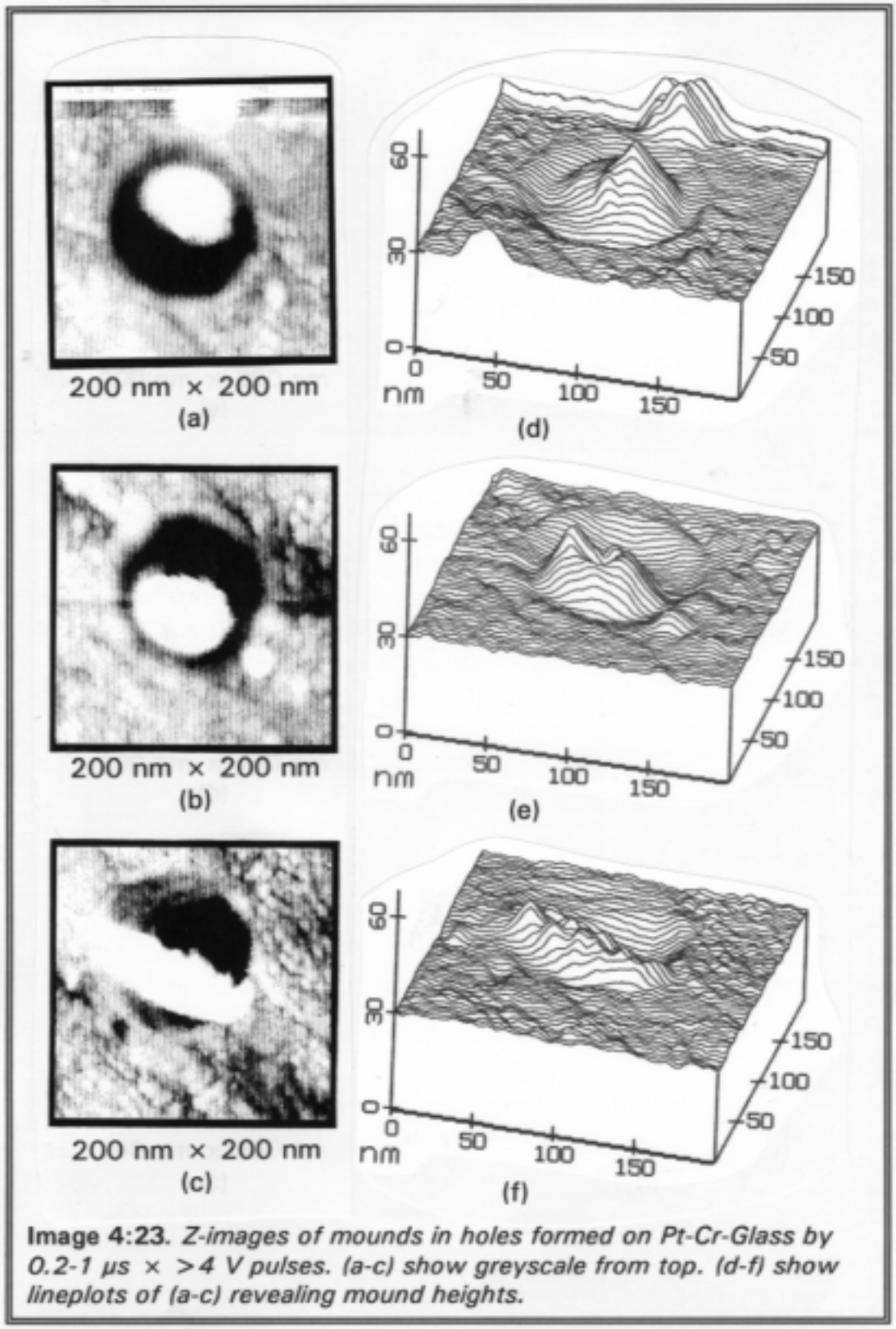

Image 4:23. *Z-images of mounds in holes formed on Pt-Cr-Glass by 0.2-1 μs × >4 V pulses. (a-c) show greyscale from top. (d-f) show lineplots of (a-c) revealing mound heights.*

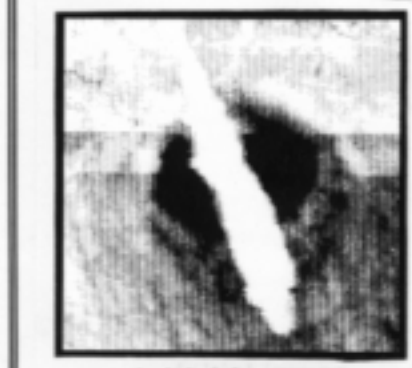

Initial image
200 nm × 200 nm
(a)

After 47 s
200 nm × 200 nm
(b)

After 9 min 14 s
200 nm × 200 nm
(c)

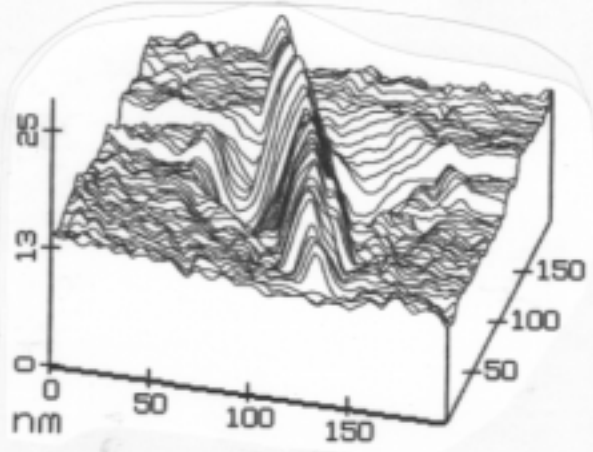

(d)

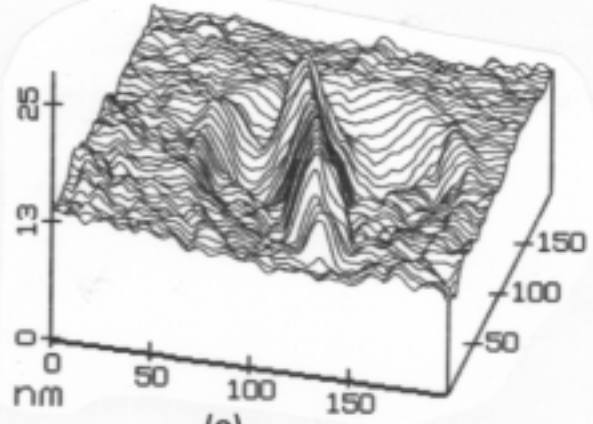

(e)

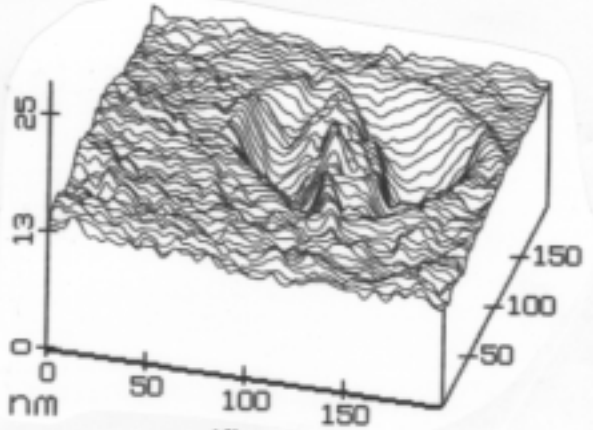

(f)

Image 4:24. *Z-images of progressive diffusion for a mound in hole formed on Pt-Cr-Glass. (a-c) show greyscale and (d-f) show corresponding lineplots. Scales and times are shown with images.*

the rim of the hole and the hole itself is smaller.

In order to see if the tip became shorter after a mark was made on the surface, a voltage pulse was applied while Image 4:25(a-b) was taken. Image

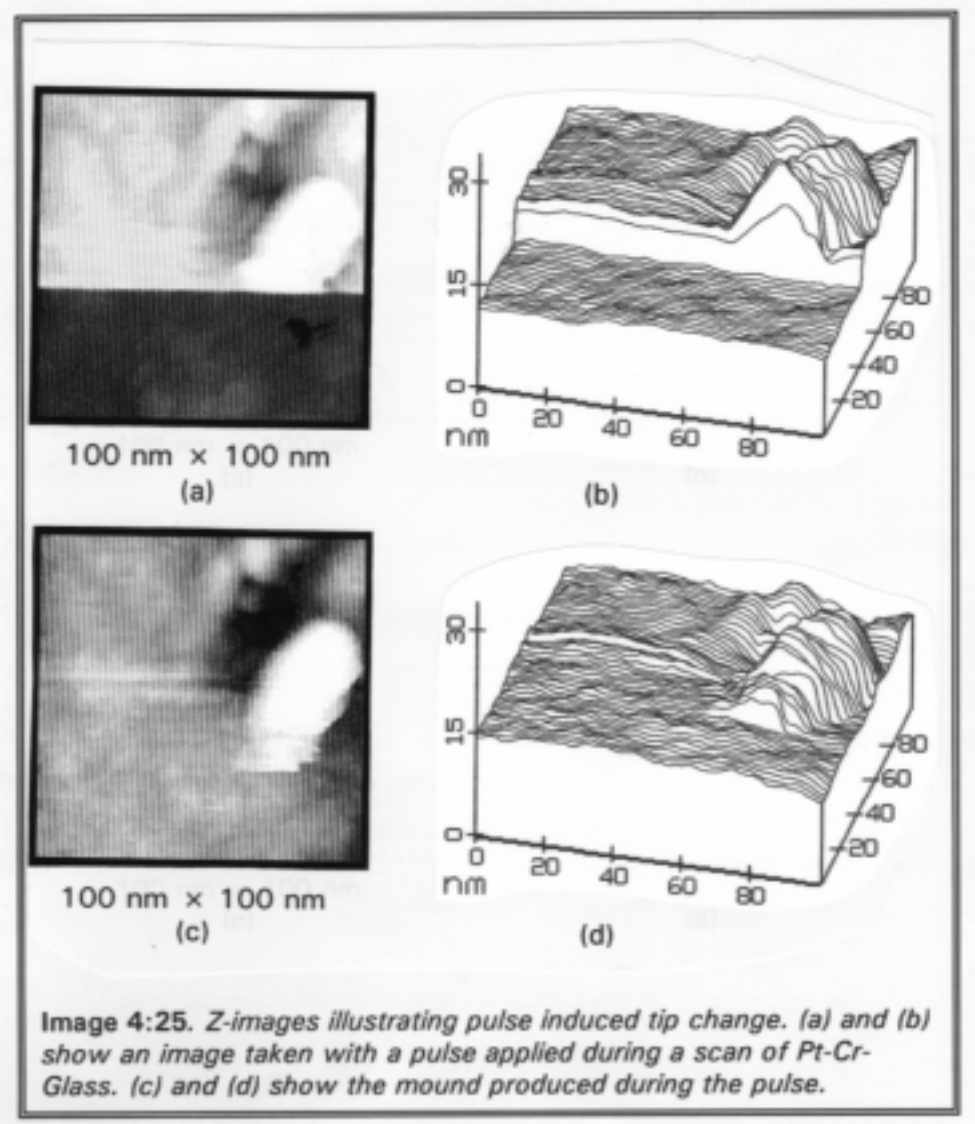

Image 4:25. *Z-images illustrating pulse induced tip change. (a) and (b) show an image taken with a pulse applied during a scan of Pt-Cr-Glass. (c) and (d) show the mound produced during the pulse.*

4:25(a-b) reveals that the tip apparently became about 5 nm longer as a result of the modification. Image 4:25(c-d) shows the mound that was formed during the voltage pulse.

4.3.2 Model for platinum bit formation

Since there appears to be a mound of material deposited on the surface, a question arises as to the source of the mound because the tip also became longer. This may be explained by the model shown in Fig. 4:6 where the deposition causes contact between the tip and sample. This contact need not arise from any motion of the tip due to feedback effects. Instead the tip

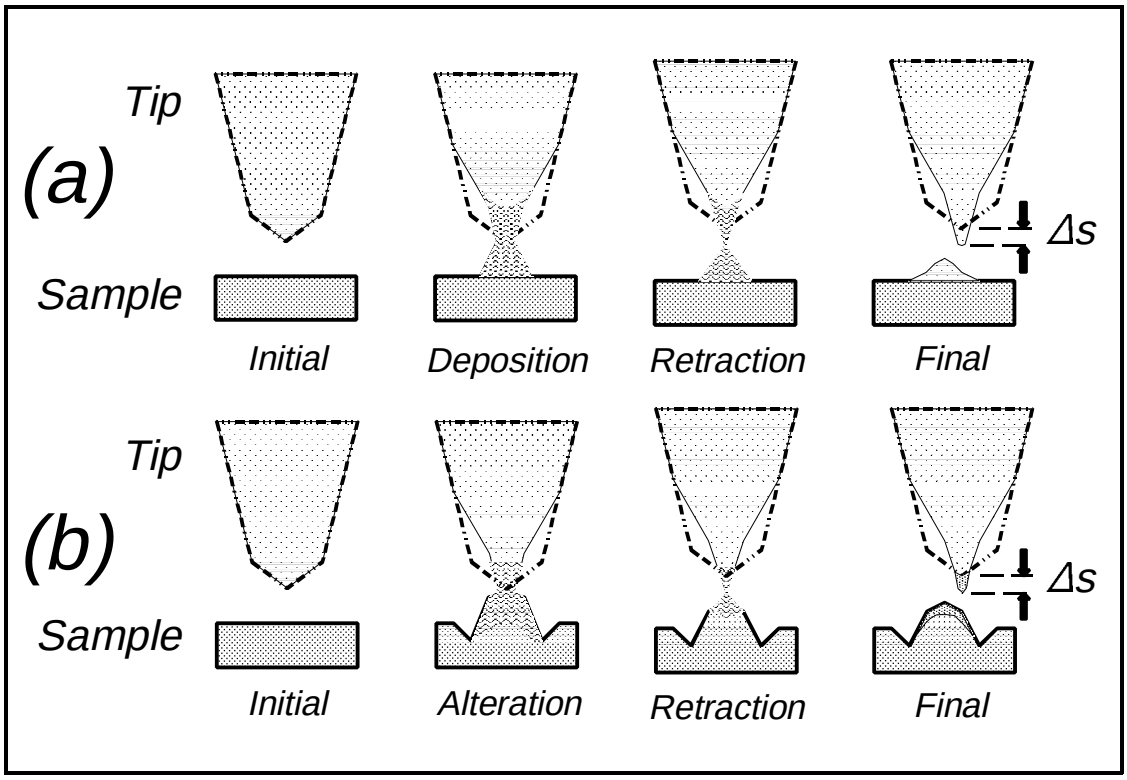

Figure 4:6. Illustration of tip extension formation (a) during mound formation, and (b) during mound in hole formation. Dotted lines show initial tip shape for comparison. See also Landman [1990].

gives up the material as is illustrated in Fig. 4:6(a). As the deposition material from the tip moves toward the surface, the tip becomes elongated causing a bridge between the tip and sample. The bridge increases the current which causes the feedback to retract the tip and break the bridge with the sample while sharpening and

elongating the tip by $\triangle s$ at the same time. This could also account for the lack of reliability of the alteration process. At positive sample biases, material may also be taken from the sample for the bridge resulting in the hill in hole combination shown in Fig. 4:6(b).

The results fell far short of our desired nanometer scale holes for oxidation. The observed diffusion of the platinum mound cast doubts on this particular thin film structure being used for a field-induced memory device.

Vibration was minimized by placing the stiff STM head on a three inch granite pad which rested on three pneumatic supports. In addition, the STM was located on the bottom floor of the building which was built upon bedrock. The low vibration levels were confirmed by the consistent noise free images obtained.

4.4 Summary

This chapter reported various results of altering surfaces by increasing the bias between a tunneling probe and sample. A review of quantum mechanical tunneling theory was presented and theoretical currents were plotted as a function of tip-sample spacing for various biases. The theory revealed three variables for tunneling. The parameters are tip-sample spacing, bias, and current. Setting any two of these parameters determines the other.

We had the goal of determining a process which would repeatably and consistently alter a surface using a voltage pulse between the tip and

sample. Four parameters were varied to determine their effect on the field induced alteration experiments. They are initial tunneling current and bias, and the amplitude and duration of the pulse superimposed on the initial bias.

An HOPG sample and Pt-Ir tip were used for various investigations. We expected to find that decreasing the initial current for a given pulse would result in a smaller alteration region, since, theoretically, the tip should withdraw from the sample and result in a reduced electric field for a voltage pulse. However, we found that decreasing the current often resulted in a larger altered area. But, it was not consistent this way either with larger currents sometimes inducing larger alteration regions.

We found that alteration regions were diverse in appearance. Some appeared as holes, some as hills, some as hills in holes, and some as scattered deposition.

We also observed that for each different tip, there was a pulse amplitude threshold which must be reached before any observable surface transformation occurs. This threshold varied from near 3 V to above 5 V. We also found that near the threshold, alteration was intermittent for similar pulses.

The results also show that there are certain initial biases which produced nanometer scaled alteration regions. This bias was -0.7 V for the Pt-Ir/HOPG combination. However, at this bias feature production was intermittent. But, using this bias, we were able to produce an L-shaped pattern with sequential biasing and lateral tip motion. In spite of this

apparent success, we found that the pulse amplitude had to be significantly increased as the structure was formed in order to continue the process. We also found, using a tungsten tip, that holes formed in an I-shaped pattern using the same pulse, increased in size as the process was continued.

We also noted that the features which were induced were not always stable. Features that appeared as hills moved around and disappeared in a mater of a couple of minutes. Apparent 2 nm holes were observed to dissipate over a half hour time span.

These results suggest that the production of a field induced nanomemory using an HOPG substrate is not at all feasible due to unreliability and inconsistency of feature formation, and poor durability of some surface features.

Attempts at producing features on platinum on chromium thin film on glass showed similar problems. The features produced were at least 20 nm in extent. The features were also observed to autotransform in time indicating non-durability. These experiments also demonstrated that a Pt-Ir tip can also be altered during pulsing. This could result in corrupted addressing if used in a nanomemory.

In conclusion, we found that the method and materials used showed no real promise for incorporation into a nanomemory due to problems of reliability, consistency, and durability.

[1] Eisberg, Robert and Resnick, Robert, *Quantum physics of atoms, molecules, solids, nuclei, and particles,* (Wiley & Sons, New York, 1974) page 218.

[2] Wentzel-Kramers-Brillouin (WKB) Approximation, see page 2 of Wolf, E. L., *Principles of electron tunneling spectroscopy*, (Oxford University Press, New York, 1985).

[3] Batra, P., Garcia, N., Rohrer, H., Salemink, H., Stoll, E., and Ciraci, S., "A study of graphite surface with STM and electronic structure calculations", Surf. Sci. **181,** 126 (1987). (See also J. Vac. Sci. Technol. **A6(2)**, 313 (1988).

Selloni, A., Carnevali, P., Tosatti, E., and Chen, C. D., "Voltage-dependent scanning-tunneling microscopy of a crystal surface: Graphite", Phys. Rev. **B 31**, 2602 (1985); Erratum: Phys Rev B **34(10)** 7406 (1986),

Tománek, David, Louie, Stephen G., Mamim, H. Jonathon, Abraham, David W., Thomson, Ruth Ellen, Ganz, Eric, and Clarke, John, "Theory and observation of highly asymmetric atomic structure in scanning-tunneling microscopy images of graphite", Phys. Rev. **B 35**, 7790 (1987).

Tartar, R. C., and Rabii, S., "Electronic properties of graphite: a unified theoretical study", Phys. Rev. **B 25**, 4126 (1982);

[4] Mechanically formed Digital Instruments Nanotips.

[5]. Threshold on graphite:

Albrecht, T. R., Dovek, M. M., Kirk, M. D., Lang, C. A., Quate, C. F., and Smith, D. P. E., "Nanometer-scale hole formation on graphite using a scanning tunneling microscope", Appl. Phys. Lett. **55,** 1727 (1989);

Roberts, C. J., Davies, M. C., Jackson, D. E., Tendler, S. J. B., and Williams, P. M., Controlled nanometer-scale line and symbol formation on graphite in air using a scanning tunneling microscope, J. Phys.: Condens. Matter **3**, 7213, (1991);

Bernhardt, R. H., McGonigal, G. C., Schneider, R., and Thomsom, D. J., "Mechanisms for the deposition of nanometer-sized structures from organic fluids using the scanning tunneling microscope", J. Vac. Sci. Technol. **A 8,** 667 (1990).

Threshold on other materials:

Rabe, Jürgen P., Buchholz, Stefan, and Ritcey, Anna M., "Reactive graphite etch and the structure of an adsorbed monolayer - a scanning tunneling microscope study", J. Vac. Sci. Technol. **A 8,** 679 (1990);
Rabe, Jürgen P., and Buchholz, Stefan, "Fast nanoscale modification of Ag(111) using a scanning tunneling microscope", Appl. Phys. Lett. **58,** 702 (1991).

[6] An interactive programming environment for data acquisition marketed by Keithley instruments.

[7] Bryant, A., Smith D. P. E., Binnig G., Harrison, W. A., and Quate C. F., "Anomalous distance dependance in scanning tunneling microscopy", Appl. Phys. Lett. **49**, 936 (1986).

[8] Controlled Geometry tips from Materials Analytical Services.

[9] The tip was sharpened by cutting at an angle with a pair of stainless steel medical scissors.

Chapter 5.

Scanning Tunneling Lithography: Material Précis

This chapter describes the propensity of individual materials for use as a nanomemory component. An individual summary of how each material fares in the areas of alterability, reproducibility, durability, and readability of these alterations are discussed. This authors work, along with work reported in the literature summarized in Chapter 4, are gleaned for relevant information to provide the necessary basis for evaluation. Full reference citations can be found in the thesis bibliography.

Observation by an STM normally suggests that surface alteration is readable as a bit, especially on flat crystalline surfaces. The technique of applying a voltage pulse to produce this alteration is hereafter referred to as *pulsing.* The alteration produced by any mechanism is also referred to as a "*bit*".

This chapter will consider the materials cited in the investigation of Chapters 3 and 4 individually and combine important memory related properties in a series of tables.

5.1 $Ba_2Sr_2CaCu_2O_x$ Terashima [1991].

A pulse with one second duration was required to produce a 10 nm structure. This long writing time renders it useless for writing bits in a reasonable amount of time.

5.2 Calcium fluoride McCord [1987].

The tip had to penetrate a 20 nm CaF film in order produce tunneling. Particulates were observed on the tip which would corrupt

addressing schemes. The sample is not conducting enough to be read by STM.

5.3 Cesium Whitman [1991].

Under UHV, Cs atoms were caused to diffuse across the surface of GaAs. Continuous overlayers were produced by voltage pulsing. The scheme provides a way to alter the surface. The reproducibility would depend on the amount of Cs located nearby. Also, since the Cs does diffuse so well, bits would not be durable because nearby voltage pulses would corrupt them. The only positive aspect is that the difference in substrate and bit material is advantageous for reading by ac methods. The vacuum requirement prevents a practical memory design.

5.4 Cobalt chromium tantalum film Moreland and Rice [1990].

The film was altered magnetically and read by a force probe. The smallest bit size was 500 nm with 20 nm resolution. The bit size of 500 nm is too large for the proposed memory, but, if it can be reduced to the 20 nm resolution, the size could be workable.

5.5 Decaborane Dujardin [1992].

Displacement, clustering, and fragmentation of 7 Å bits of $B_{10}H_{14}$ on Si were observed at biases > 4 V. The size is excellent for a memory, but the fact that it can be displaced casts doubt on the durability of any bits made with it.

5.6 Doped and undoped gallium arsenide III-V semiconductors Dagata [1991b, 1992], Lin [1987], Thundat [1990].

Films of In and Al doped GaAs films were modified by increased

tunneling bias. As_2O_3 and In_2O_3 were depleted under low biases. Higher biases produced strongly bonded oxidation at underlying layers. Lines, 85 nm in width, were irregular showing that the process is not consistent enough for writing.

Lines were electrochemically etched in GaAs with the application of a -4 V bias and in the presence of laser irradiation. Minimum line width was 300 nm, too large for proposed memory bits. Using this scheme, fabricated bits would not be durable since the whole surface of the GaAs showed signs of etching.

Readability would be poor under NaOH since, in order to maintain a stable tunneling current, circulation of the solution was required, which is not pragmatic for the desired small size of a nanomemory.

In an gold cyanide solution, gold dots and rings as small as 100 nm were deposited on GaAs by a 4 V × 1 min pulse during illumination with white light. The light was necessary to the formation of dots. The 100 nm dot size is larger than desired. Application of light may not be too great a burden for a memory since low cost semiconductor diodes are readily available. The time of writing is too long and is probably related to the chemistry involved. Of course, the use of a liquid in a memory leads to problems of evaporation and replenishment.

5.7 Germanium Becker [1987].

An 8 Å bump was formed with a -4 V pulse, excellent for a memory bit. However, surface transformation was not always reproducible.

5.8 Glassy metals Staufer [1987, 1991].

Under UHV, mounds as small as 35 nm in diameter were produced on $Rh_{25}Zr_{75}$ with a 2 V bias which also produced an instability in the current. A tip speed of 3 nm/s was used to produce 20 nm wide lines. The speed would be detrimental to memory writing time. The production of mounds was also tip dependent with Ir tips not producing any alteration. Alteration was also possible on $Fe_{86}B_{14}$. In experiments which produced 20 nm hills, the tip was found to withdraw 10 nm suggesting intimate tip-sample contact. Inadvertent erasure of a bit if another bit was manufactured nearby suggests that the bits are not durable enough for a memory structure.

5.9 Gold Abraham [1986], Emch [1989], Hoffmann-Millack [1990], Jaklevik [1988], Li [1989], Mamin [1990, 1994], McBride and Wetsel [1991], Roberts [1991], Schneir [1988b], Shedd [1990], Silva [1992], Sommerfeld [1990], Wang [1992, 1993], Yokohata [1990].

Indention produced 10-300 nm holes. During indention, a reported 50 nm of damage surrounding 10 nm holes could affect nearby bits. Holes, 5 nm in width, produced by indentation filled within minutes to hours. The tip sometimes changed relative positions after indention which prohibits readability by corrupting any addressing scheme. Buckling of the tip was reported to have produced lateral tip displacements up to 250 nm for the largest indentation.

Hills and holes were fabricated with voltage pulses. The voltage threshold for modification was dependent on the cleanliness of the tip.

Tip change was observed for contaminated tips. Some pulse voltages produced only hills near the threshold voltage, while a 0.2 V change in voltage produced both holes and hills. Since threshold voltages varied over 2 V for different tips and samples, a knowledge of the alteration type is not predictable. Holding the bias at 2 V for an extended time was shown to alter the surface suggesting that there could be long time operation effects on the integrity of the surface which would in turn corrupt memory storage.

Most reports show atoms diffusing over time to fill in produced holes. A 10 nm hole dissipated and crystal steps moved 10 nm in 20 s. A 30×60 nm hole filled in completely within an hour. This shows that nanometer scale bits in Au would not be durable even for a short time. Some holes produced with rims were found to endure for over two hours, but hole formation for this surface was also inconsistent.

Some tips were found to change with the application of a pulse. This would corrupt the addressing, affecting the readability.

Under fluorocarbon grease, a 10 nm hole was made by raising the bias until the feedback caused the tip to pull away. Predetermination of mound or hole formation was not possible, indicating irreproducibility.

Gold tips were used as deposition sources to produce 15-24 nm mounds on Pt and Si by pulses with durations as small as 10 ns. At a 10 ns writing rate, a megabit memory could be theoretically written in less that a second. It was also reported that the duration of the induced current pulse had to exceed 200 μs for alteration, increasing the megabit

writing time to about 3 minutes. The bit sizes are marginal for our standards but still allows a bit density a factor of 10^4 greater than is currently available. The production of thousands of bits did not degrade one tip's ability to write, revealing excellent alterability. However, the tips did not always produce mounds but sometimes produced holes, an intolerable characteristic for the desired reproducibility. Static discharges remote from the STM also produced deposition adding an unknown factor in the alterability. The observed occasional transformation of the tip would destroy the readability.

Under an electroplating solution, Orosene 999, > 300 nm lines were formed, too large for memory structures. The plating was not reproducible, forming structures in only 2 of 20 attempts.

5.10 Hexamethyl disilazane (HMDS) on copper Silver [1987].

At biases above 1 V the surface was found to alter in the presence of DMCd. An observed 300 μA current indicates a plasma which would not be limited to the tunneling regions. This increased area results in depositions of many micrometers in width. This is unacceptable for a memory where the desired bit size is around 2 nm.

5.11 Highly oriented pyrolytic graphite Albrecht [1989], Bernhardt [1990], Foster [1988], Li [1992], Miller and Hocken [1990] (and this thesis), Mizutani [1990], Penner [1991], Rabe [1990], Schneir [1988a], Shedd [1990], Terashima [1990], Yau [1991a,b].

Holes as small as 2 nm and as large as 200 nm were produced by pulsing. There was a tip-dependent amplitude threshold necessary for

formation. Reports of this threshold varied, but the magnitudes were always greater than 2.5 V with some tip-sample configurations not producing any bits for amplitudes as high as 10 V. Near the threshold, the formation of mounds instead of holes was often observed. Mounds were typical with negative pulses applied to the sample. This thesis found mounds to be irreproducible by showing the necessity of increasing the pulse amplitude to continue mound formation. This thesis also shows these mounds to diffuse within minutes indicating that they would not be durable enough for a memory. The mounds diffused almost immediately when the bias was switched from negative to positive for a couple of seconds and then back to negative. Although longer times were necessary, holes were also observed to disappear. Other reports claim stability of features. One possible explanation for mound stability could be in the material of the feature. If one feature is produced from tip material, while another is the result of contamination in the ambient, their surface diffusivities would also be different. This would be particularly true if one was charged and the other was not charged.

Using positive voltages, the predetermined reproducible formation of a mound or hole was not possible. The hole sizes were not found to be reproducible but were often observed to increase in size with the number of bits produced. Given the same pulse parameters, this thesis shows holes varying in size from 1-20 nm. This irreproducibility is more than sufficient to make a memory inoperable. Although one tip successfully produced 496 holes out of 498 tries, not all tips produced bits.

Bits were made with pulse durations from 10 s to 10 ns. Bigger holes were not always associated with longer pulses. For pulse durations greater than 100 μs, the time to write 10^6 bits limits its capacity to be used as a high density memory.

UHV, and UHV vented to benzene or pure oxygen or 100 L water inhibited hole formation. In UHV, contamination deposits of 50 nm mounds were observed for 0.2 s pulses. A sample that had been stored in a container with water prior to alteration produced 10 nm bits during only 80% of the trials showing limited reproducibility. At a vacuum of 0.04 torr, increased pulse amplitudes were also required for successive alterations, illustrating irreproducibility at this pressure. The changing daily ambient also played a role. Some experiments suggest that H_2O in the ambient is necessary for hole production[1].

Under DI H_2O, domes as small as 7 Å were produced having durability >1 hr under normal imaging conditions. The use of water leaves something to be desired since the medium would have to be replenished due to evaporation. The re-ionization of the water over time would produce an unacceptable changing of parameters necessary for alteration. Coating of the tip except for the last few nm is also necessary due to higher leakage currents.

In a 10^{-4} torr TMA (trimethylaluminum) ambient, pulsing produced features dependent on pulse duration. For 0.2 s pulses, Angstrom scale features were produced. The feature size is sufficient to produce an advanced memory, but the 0.2 s time required to write on the surface

makes it impractical. The reproducibility of features was also found to be unreliable in nature so that there is no assurance of alteration. In a 10^{-2} torr TMA ambient, an 18 nS × 440 nm (Al resonance) light pulse was used in conjunction with a 0.8-3 V bias. The result was deposits as small as 1 nm for a 1.1 V bias, excellent for a nanomemory bit size. By changing the light wavelength to 430 nm, deposition was rare. The effect of the light on reproducibility was not mentioned. The deposition showed linear I-V measurements while the HOPG I-V was nonlinear. This would be excellent for an ac reading scheme.

Alterations in organic fluids, dimethyl phthalate, and decane were clouded by the fact that similar features were produced in air with similar pulse parameters. One experiment showed, however, that once a tip produced a hole it was likely to form more holes indicating a tip dependence on alterability.

Under a drop of di(-ethylhexyl) phthalate, voltage pulses wrote features as small as 1-2 nm which could be erased or partially erased. The structures were not found to deteriorate during imaging. This provides an excellent write-read scheme. The 100 ns pulse required is also favorable for a memory. The reproducibility question was not addressed fully. The effect of subsequent voltage pulses was not consistent. Although this scheme seems promising, the reproducibilty may inhibit it from producing a viable memory. Experiments showing non-durability of bits on HOPG suggest using another substrate. There will also be a problem of maintaining the ambient over a long period of time.

Pulsing produced 1-2 nm adsorbate features in a monolayer octylcyanobiphenyl film on HOPG. The duration of the adsorbate features varied from < 1 s to several minutes for others, not durable enough for memory. Holes, 10 nm in width were formed with 2 s duration pulses. This writing time would be to long for a memory.

Also reported was the inability to alter the surface under 1 atm of helium and 10 mbarr of dry toluene.

In a AgF solution, 50 μs pulses produced 30 nm mounds on 10 nm holes. The holes were produced during the first 5 μs of the pulse. Several pulses were necessary to initialize the tip, demonstrating that the tip had to be conditioned just right for alteration. The feature size may be acceptable for a first generation memory. The features demonstrated durability by not changing shape on the order of hours and being unaffected by nearby depositions. The 90 % success at reproducing the structures was good, but for viability would have to be increased to enable memory segments to accurately store information (possibly by read-rewrite scheme). It may be that an initial hole is necessary for formation. The main problem is maintaining the stability of the AgF solution over long time periods. The process needs to be characterized for the same tip over days and weeks.

5.12 $HoBa_2Cu_3O_{7-x}$ Heinzelmann [1988].

High biases applied for 5 seconds altered the surface. Repeating the process produced alteration from 10-80 nm. The time of alteration and inconsistency make it impractical for writing bits.

5.13 Ionically conducting films: nafion on silver, $AgCl_4^-$ and $PdCl_4^-$ doped PVP on graphite, Ag doped MEEP on Ag Craston [1988], Hüsser [1989].

Silver lines were electrodeposited at the surface of the Nafion films. Optimal conditions produced 0.5 μm line widths. These dimensions are two orders of magnitude greater than desired. Also, The writing speed of 50 nm/s is too slow to be used for writing.

The doped PVP films produced sub-μm lines, not small enough for memory bits. The MEEP films were sticky to the tip and not consistently alterable, producing discontinuous lines.

5.14 Nickel and platinum surface diffusion Stroscio [1991].

Atoms of Xe, Ni, Pt, and CO adsorbates were moved along the surfaces of Ni and Pt in UHV. The process allows atomic scaled bits to be manufactured. A knowledge of the position of an atom is necessary before you can move them, so that, a reservoir of atoms is necessary.

A necessary motion between reservoir and memory area would slow the writing of the memory down extensively. These atomic particulates require impractical low temperatures to be stable and thus durable.

5.15 Palladium Ohmori [1991].

Over a 250 minute period, grooves and hills were observed to flatten out during 2 nA STM imaging. This shows that Pd bits would not be durable.

5.16 Palladium silicide Rinnger [1985, 1986].

In a 10^{-8} torr vacuum, the surface of $Pd_{81}Si_{19}$ was modified while

STM scanning at 100 mV. This shows that biases higher than 100 mV must be used to read any bits fabricated in this material. The vacuum would have to be eliminated to produce a practical memory, but this may result in oxidation of the Si causing further reading problems.

5.17 Platinum Ohmori [1991], Sommerfeld [1990], and this thesis.

Four pits were observed to grow during STM imaging. A 40×150 nm mound that extended 20 nm above a 100 nm wide pit was observed to decay in height to the level of the pit edge in 9 min. The pit also filled in during this time. This surface diffusion indicates that bits would not be durable on Pt.

Pulsing a thin film of Pt on Cr on glass produced hills and hole-hill structures with a minimum size of about 40 nm. This is too large for practical use in a nanomemory. The writing time of 10 μs is sufficient for a memory. The tip, however, was found to change shape which would affect the readability through corrupted addressing. Biases of 2 V were observed to alter the surface if the tip was left at the same place for an extended time, which casts more doubt on the durability of a surface under imaging conditions.

Anilnium sulfate, $(C_6H_5NH_3)_2SO_4$, doped Nafion films were used to deposit polyaniline on Pt. The resolution of deposition was about 2 μm, much larger than the desired bit size.

5.18 Poly(octadecylacrylate) Albrecht [1988].

Fibrils on HOPG were broken with 100 nS pulses. The pulse duration is more than adequate for writing. The altered region extended

40 nm, more than desired for the proposed memory. Reading the bit would be difficult due to the unpredictable structure of the bit.

5.19 Purple bronze, $Na_{0.9}Mo_6O_{17}$ Saulys [1991].

A several second pulse applied to the cleaved sodium surface of purple bronze, produced 5-10 nm holes. The holes were not found to be durable but grew and coalesced during subsequent scanning. The long pulse duration used for formation of holes could not be used to produce a practical memory.

5.20 Resists Chen [1993], Marrian [1990], McCord [1986, 1988], Stern [1988], Terris [1990], Zhang [1989].

Dots, 20 nm wide, were produced in a LB P4BCMU negative resist film on Si at 10^{-8} torr. The writing time of 10 ms is too long for a viable memory, requiring about 3 hr to write 10^6 bits. The vacuum also prohibits its use as a viable memory.

Contamination resists were deposited on Au, Al, Si, and Pt thin films. The necessary vacuum of 0.03 mTorr is not practical for a memory. Lines were written at 250 nm/s, equal to about 10 ms for a 2.5 nm bit. This is an excessively long writing time for memory. The lines were 100 nm wide which is much larger than the desired 2.5 nm bit size.

Writing in PMMA at 1 μm/s, 20 nm wide lines were produced. The process would produce a 20 nm bit size which is a tolerable memory bit size. However, the necessary vacuum makes it impractical. The writing time for 10^6 bits would be about 8 hrs, too long for a workable memory. The alterations were discerned after etching, which is not practical for a

user programmed memory.

Using a force probe, a 25 ms × 100 V pulse produced a 2 μm charged region. The charging was not durable but decayed over 1 hr. The writing time and bit size are too large for the desired memory.

5.21 Rhenium (0001) Marchon [1988].

Touching the crystalline surface with a W tip produced 2-5 nm hills. The hills were found to differ electronically from the bare surface suggesting the ability to read by ac conductance methods. The necessary touching would slow the memory down and alter the tip, corrupting readability.

5.22 $Rb_{0.3}MoO_3$ Garfunkel [1989].

Holes, 6 nm across, were formed by indentation. Features produced by abrasion did not degrade over a 4 hr time period. Indentation may require a long writing time and probable tip degradation.

5.23 Silicon Barniol [1992], Dagata [1990a, 1991a], Day [1993b], Ehrichs [1988, 1990], Jahanamir [1989], van Loenen [1990], Lyo [1991], Nagahara [1990], Ostrom [1992], Silver [1987], Terashima [1990], Yau [1991c].

Holes, 10 nm in width were produced by repetitively indenting Si under UHV. Mechanical contact would eventually change the tip and corrupt the addressing so that it would not be readable.

Using 30 ms voltage pulses, single atom displacement was observed. For 200 ms pulse durations and sharp tips, holes were formed. Additional pulses dulled the tip, facilitating the production of both

mounds and holes and then only mounds as pulsing continued. The alteration supports very high density memory, but the time for writing 10^6 bits exceeds 8 hr.

The production of mounds was also linked to the amount of nearby adsorbates which limited the reproducibility of alteration. The mounds were found to contain Cd, C, and O when DMCd was used as an ambient. These different materials could be used to enhance readability. The fact that bare silicon is only available in UHV prevents it from being seriously considered as a memory substrate. Attempts to alter the surface of Si(111) under air were unsuccessful (probably due to the native oxide).

High tunneling biases produced oxidation of hydrogen passivated Si. Structures 35 nm wide were formed. Due to the oxidation, higher biases are required for reading. This necessary high reading bias would corrupt any memory structure by causing oxidation in other passivated areas.

Under an HF solution, the surface of silicon was etched a couple of nanometers deep using tunneling bias of 1.4 V. For tip biases < 1.7 V, the tip may have been contacting the sample. For biases > 1.7 V the bias produced etching. There seems to be no region where some surface alteration is not achieved so that it would not be possible to read the data without corrupting it using STM. Times for etching were too large for memory feasibility. The use of HF as a medium is not tolerable because it reacts with the Si even without a bias. Using H_2SO_4 as a medium was

unsuccessful.

Using WF_6 (1 mtorr) as a catalyst, Si surfaces were altered by pulsing. The result was 20-40 nm hills, holes and combinations. The 1 s pulse times used for writing is too long to be feasible for memory. The low pressure ambient restricts its use as a memory. The unpredictability of type of alteration does not satisfy the reproducibility requirements of a memory.

Amorphous Si:H was altered with 10 V, 35 μs pulses. The time is adequate for writing. The features were 140 nm wide, too large for the proposed memory bit density.

The local conductance of a 2.3 nm thin film of SiO_2 was produced by a pulse. The imaging of such a film is difficult at best, not lending itself to readability.

5.24 Silicon nitride Barrett and Quate [1991].

Using a force probe, 100 μs × -40 V pulses were used to charge the nitride. Capacitance detection was used for reading. A working memory has been demonstrated for this scheme. A thermally grown silicon oxide layer was used to prevent discharging. The smallest charged regions produced were 75 nm, too large for the proposed nanomemory.

5.25 Silver Gimzewski [1987], Rabe [1991].

Hills, 10 nm wide, and indentations were produced by tip contact to Ag on Si film. The production of a hill or hole was dependent on the cleanliness of the tip-sample system for Ag on Si films. Holes < 1 nm deep formed in Ag on Si annealed out within seconds of production.

Using a Ag on Mica film that was flat to within 1 nm, 100 ns pulses produced nine holes (10 nm) and two hills for eleven attempts exemplifying irreproducibility. The current only changed for about 20 μs, demonstrating an excellent writing speed. The flat surface would provide excellent readability and the bit size could would allow 2500 bits/μm^2.

5.26 Silver selenide $Ag_{1.9}Se$ Utsugi [1990].

With a constant bias, 15 nm grooves were produced in a 15 nm $Ag_{1.9}Se$ film. The width of the grooves suggests a tolerable bit size for a nanomemory. The alteration was not possible in a 5 mtorr vacuum. The H_2 in the air was suggested as being necessary for alteration. If so, the changing air ambient could play a role in reproducibilty. Pulsing did not alter the surface indicating that this design is not fast enough for writing a memory.

5.27 Sulphur on rhenium under silicone oil Marchon [1988].

Alteration was made under silicone oil but was not possible in air. The 30×50 nm hole is too large for a nanomemory bit particularly since it was only 6 Å deep which would make reading difficult by tip displacement. If the bottom of the hole was void of sulphur however, ac reading techniques could be employed. The 2 s time required to produce a bit would require an impractically high 23 days to write 10^6 bits.

5.28 Tianium and Titanium oxide on platinum on mica Casillas [1991], Sugimura [1993].

Cyclic pulsing at ±2 V produced 5 nm disc shapes. Different electronic properties were found above the discs and unmodified surface

which provides a possible readability scheme. It was necessary, however, to cycle the pulses for 0.25 s. To write one million bits at this rate would take a week which is not practical.

The anodization of titanium was found to be limited to 30 nm, borderline for a memory bit size. The process was also found to be humidity dependent which indicates the ambient would have to be controlled to produce a workable memory.

5.29 Two dimensional materials : InSe, ZrS_2, $TiSe_2$, $SnSe_2$, $NbSe_2$, TaS_2, $MoSe_2$, WSe_2, WS_2, PtS_2, $ReSe_2$, WTe_2, and $MoTe_2$ Huang [1992], Parkinson [1990], Schimmel [1991].

The surface of these materials were observed to nucleate etch pits that grew during STM imaging. Imaging for 8 hr produced 500 nm square regions 20 layers deep. This eliminates these materials as memory substrates because the reading would corrupt any manufactured bits. The W and Mo samples only pitted for biases greater than 1 V, which may allow these materials to work in a memory. Huang [1992] reports thresholds for MoS_2 and $SeSn_2$.

5.30 Tungsten diselenide Akari et al. [1991], Parkinson [1990], Schimmel [1991].

A 2-5 nm hole was manufactured by pulsing. The hole changed in shape to a triangle and began enlarging. Due to hole growth during subsequent scanning, bits produced on this surface would not be durable. The necessary pulse duration for alteration changed depending on the sharpness of the tip suggesting the alteration process is unreliable.

Ring shaped structures on WSe_2, produced by pulsing, were 6 nm in diameter. Producing 100 such rings produced no degradation in the imaging ability (or readability) of the tip. The durability of bits was confirmed by observing a feature for two days with no apparent changes. The 20 ms duration for pulses require a minimum of 5 hr to write 10^6 bits.

5.31 Xenon Eigler [1990, 1991].

Xenon atoms were moved around at a rate of 0.4 nm/s at 4 K under UHV. Although atomic sized bits could be produced, the ambient renders it impractical for a memory. Also, the time to move the bits would require too much writing time.

The ability of a Xenon atom to transfer between the tip and substrate could cause problems with the durability and readability of a memory structure.

5.32 $YBa_2Cu_3O_{7-x}$ Harmer [1991], Heyvaert [1992], Terashima [1990], Virtanen [1991].

Normal STM imaging was found to alter the surface producing holes which coalesce. Rough surfaces (600 nm) of the oxide were STM milled to a flatness less that 15 nm. Grooves were found to change in appearance for up to one hour after production illustrating the lack of durability for this surface. Since normal STM imaging alters the bits, you would not be able to read the information without corrupting it.

For 4 V pulses lasting about 10 s, alteration was not observed in air. Using 10 V pulse amplitudes, a 100 nm ditch was produced. The

reports indicate that there is an insulating barrier at the surface which facilitates alteration through contact. This contact would change the tip and corrupt the readability.

5.33 Précis tables

This section contains Tables 5-1 to 5-6 which provide an overview of relevant memory related aspects of substrate-ambient-tip stratagems for surface alteration.

The **Sample**/*tip* column gives the surface material of the substrate and the tip material. The ambient column reveals any gas or liquid which covers the tip and sample.

The alterability of the surface is related to the bit type, bit size, megabit time, and mechanism. The bit type column tells whether the proposed bit formation is a mound extending above the surrounding surface, a hole extending below the surrounding surface, a line regardless of the concave or convex shape, a charged region, a magnetized region, or any other similar attribute. The bit size column gives an estimated bit size that could be produced with the alteration strategy. The megabit time is the estimated time that would be required to make 10^6 alterations of the surface. These have been calculated from reported fabrication rates and pulse durations.

The mechanism column describes the alteration strategy. A mechanical mechanism means that indentation or mechanical contact was used for alteration. An electrical mechanism means that the bias was increased or pulsed to produce the alterations. A chemical mechanism

means the chemical composition of the surface was somehow changed by the ambient and/or bias. An illumination mechanism means that light was used in conjunction with other methods to produce alteration.

The reproducibility column gives information on how well the alteration could be repeated and the parameters which were observed to affect the alteration. The durability column shows any observed dissipation or diffusion in bit structure over time. The readability column describes the possible ways in which the alteration could be read as a data bit. Z means the changing tip height may provide the criterion for bit existence. I means the changing tunneling current could be a criterion, and ac means that the ac conductance of the tunneling junction could provide the criterion.

The summary tables were examined for materials which would fulfill the following requirements:

1] Ambient: no vacuum, liquids, or nonatmospheric gases, which would introduce packaging problems.

2] Bit size: less than 100 nm, which may be possible with present techniques.

3] Megabit writing time on the order of a few minutes.

4] No mechanical contact techniques, it wouldn't take much tip movement to corrupt the addressing.

5] The bit features must be durable over time and with nearby bit formation.

6] The process must be reproducible with predictable results.

7] The process for reading the bits must not be able to erase or change them.

None of the schema, with the exception of the charge techniques, fulfill all of the above criteria. Problems associated with writing time, durability, reproducibility, readability, ambient impracticality, etc. restrict their use. Even the most inert materials are revealed to lack durability.

Since the most promising techniques, electrical charging of thin films and maybe magnetization (if the bit size can be reduced), use force probes instead of tunneling probes, these may be required in place of or in addition to tunneling techniques. There are some types of experiments which have not been tried, however. Perhaps the mechanisms would work more favorably in a positive vapor pressure. It may be possible to hermetically seal a memory device in an inert or other ambient with relatively inconsequential expense. Experiments involving the effects a nitrogen ambient has on tunneling are reported in Chapter 7. A conceptual design for a tunneling based magnetic memory which doesn't require the deposition or removal of material is given in Chapter 10. These proposals may lay the foundation for future research.

The next few chapters focus on related areas which require understanding in order to produce a nanomemory. Some of the considerations will involve things which become important provided that a writing technique can be perfected. Others involve more theoretical aspects which allow us to better understand the processes which are

involved. These in turn may reveal new areas of investigation or explain problems and inconsistencies encountered in previous experiments.

In section 3.11 additional papers were added to the thesis. These will be discussed here as to their viability as a basis for a memory scheme.

The **HF covered Si** of Barniol [1992] was altered while imaging. This would make it unfeasible since the reading of nonaltered surface could change the state.

The **PMMA** resist of Chen [1993] would not work as a direct write memory since developing and etching is required. However, the 10 nm Si pillars may be useful for laying down a memory pattern.

The **III-V semiconductors** of Dagata [1992] showed that the resolution of features depended on tip shape which would cause problems of predetermined bit size. Also the 50 nm minimum size of features is much larger than desired for bit size.

The **carbon deposits** of Day [1993a] would be unworkable due to writing speed.

The **Si oxidation** of Day [1993b] has feature resolution too large (100 nm) for use as bits.

Mechanical alteration used by Garcia [1994] on **biological membranes** would not be practical since the mechanical contact would alter the tip over time and corrupt addressing.

The etching of **$YBa_2Cu_3O_7$** by Heyvaert [1992] would not work for making bits since all biases produced some sort of etching.

The work by Hosaki [1992] on removal of surface S atoms from **MoS_2** showed promise in some areas, but the vacuum required limits its use. Also the pulse shape irregularity would cause problems in an integrated system.

The time of bit formation on **MoS_2 and $SnSe_2$** would require about 10 minutes to write a megabit of information for the work of Huang [1992]. The time is too long for a memory.

Mamin's [1994] work on **Au** deposition also required excessive times between feature formation. Also the reliability of 90% would need to be increased for a useful scheme.

Columns formed on **Si** by Ostrom [1992] also required an excessive time for feature formation (1 sec).

Probable intimate tip-surface contact using **$HS(CH_2)_{17}CH_3$** monolayers by Ross [1993] limits this for use as a memory.

The mechanical machining of **Au films** by Silva [1992] is not thought to be feasible due to tip alteration and addressing corruption.

The method of Stockman [1993] for making 15 nm features on **Au films** is not practical due to the necessity of additional processing steps.

The feature production speed of 1 μm s^{-1} by Sugimura [1993] for anodization of **Ti** would be prohibitive in the production of a memory.

Ferrocene thin films on Silicon were used as lithographic masks by Thibaudan [1994]. Due to additional processing and high vacuum the method would not be feasible.

Au surface modification by Wang [1992, 1993], produced by

normal scanning, again demonstrates that gold surfaces could not be used due to data corruption by reading methods.

[1] Albrecht [1989], Mizutani [1990], Rabe [1990], and Tendler [1992].

Table 5-1. Chart summarizing the relevant properties of sample/ambient/tip stratagems for use in a memory configuration. See text for more explanation.

Sample/*Tip*	Ambient	Bit Type	Bit Size (width)	Megabit Time	Mechanism	Reproducibility	Durability	Readability
$Ba_2Sr_2CaCu_2O_x$ /*Pt-Ir*	Air	Hole	10 nm	10 days	Electrical			Z
CaF	Air	Hole	360 nm		Mechanical			Insulating
Cs/*W*	UHV	Mound	50 nm	4 days	Electrical		Diffuses	ac, Z, I
CoCrTa	Air	Mag	500 nm		Magnetic			20 nm res.
GaAs (doped)	Air	Hole	85 nm	4 hours	Elec-Chem			Z
GaAs/*Pt*	NaOH EDTA	Hole (Lines)	300 nm-2 μm		Electrical, Chemical, and Illumination	Discontinuous Lines	NaOH etches surface	NaOH affects tunneling
	AuCN	Mound	100 nm	2 years				Z
Glassy Metals: **$Rh_{25}Zr_{75}$**	UHV	Mound	35 nm	2 months	Electrical	No features for Ir tips		Z
$Fe_{86}B_{14}$	UHV	Mound	20 nm		Electrical		Erasure from nearby pulse	Z
Gold	Air	Holes	5-300 nm		Mechanical		Rapid filling by diffusion	Tip changes observed
	Air	Hole & Mound	$\geq$10 nm		Electrical	Threshold and type uncertainty	50 nm damage for 10 nm hole	
	Grease	Hole	10 nm		Electrical	Type uncertainty		

Table 5-2. Continuation of chart summarizing the relevant properties of sample/ambient/tip stratagems for use in a memory configuration. See text for more explanation and detail.

Sample/*Tip*	Ambient	Bit Type	Bit Size (width)	Megabit Time	Mechanism	Reproducibility	Durability	Readability
Pt and Si → /*Gold* ←	Air	Mound	15-24 nm	3 minutes	Electrical	90-100% for particular tips Sometimes hole formation		Z, ac Tip changes
Au	Orosene 999 (Liquid)	Lines	300 nm		Electroplate	2 out of 20 success rate		
HMDS	DMCd (gas)		several μm		Electrical plasma			
HOPG/*Pt,W*	Air	Mound & Hole	2-200 nm	$\geq$ 10 seconds	Electrical	Threshold, size, type, & tip variations	Dissipation & diffusion of features	Z, I
	UHV vent to O_2, H_2O or benzene	No holes						
HOPG soaked in H_2O	Air	Holes	2-10 nm	6 minutes		80% hole formation		
HOPG	DI H_2O	Mound	$\geq$ 7 Å				Over 1 hour	
	Drop of Di-ethylhexyl phthalate	Mound	$\leq$ 1 nm	0.1 second		Variation in subsequent pulsing	No imaging deterioration	

Table 5-3. Continuation of chart summarizing the relevant properties of sample/ambient/tip stratagems for use in a memory configuration. See text for more explanation and detail.

Sample/*Tip*	Ambient	Bit Type	Bit Size (width)	Megabit Time	Mechanism	Repro-ducibility	Durability	Read-ability
HOPG	TMA gas 10^{-4} Torr	Mound	< 1 nm	2 days	Electrical	Statistical		Z, I, ac
		Hole	5 nm					
	10^{-4} Torr 10^{-2} Torr	Mound	1 nm	< 1 second	Electrical & Illumination	Rare without Illumination		
	AgF liquid	Mound on hole	30 on 10 nm	1 minute	Electro-chemical	90% formation	Stable for hours even with nearby deposition	Z, ac
HOPG/*Pt-Ir*	Octylcyano-biphenyl monolayer	Mound	2 nm	10 sec	Electrical		< minutes	Z
		Hole	5 nm	2 weeks				
	1 atm He or 10 mbar dry toluene	None						
$HoBa_2Cu_3O_{7-x}$	Air	Hole	10 nm	5 weeks	Electrical	Inconsistent		
Ionically conducting films **Nafion on Ag** **doped PVP on graphite** **Ag doped MEEP on Ag**		Lines	500 nm	1 week	Electro-chemical	MEEP produced irregular lines		ac
Ni, Pt, Xe, and CO adsorbates on Ni & Pt	UHV	Atoms	Atomic	Years	Electrical		Needs 4^o K for stability	Z. I, ac

Table 5-4. Continuation of chart summarizing the relevant properties of sample/ambient/tip stratagems for use in a memory configuration. See text for more explanation and detail.

Sample/*Tip*	Ambient	Bit Type	Bit Size (width)	Megabit Time	Mechanism	Reproducibility	Durability	Readability
Pd and Pt /*Pt-Ir*	Nitrogen						Grooves and hills flatten with 250 minutes STM	Tip changes
$Pd_{81}Si_{19}$	UHV						100 mV STM alters surface	
Pt on Cr on Glass / *Pt-Ir*	Air	Mound in hole	40 nm	10 seconds	Electrical	Varied bit shapes and sizes	Mound degradation	Z, Tip changes
Platinum	Anilnium/ Nafion	Lines	2 μm		Electro-chemical			
Poly(octa decylacrylate) on HOPG	Air	Broken Fibrils	40 nm	1 second	Electrical			Erratic bit formation
Purple bronze $Na_{0.9}Mo_6O_{17}$ /Pt-Ir	Air	Holes	5 nm	1 month	Electrical		Holes grow and coalesce during STM	Reading corrupts bits
$Rb_{0.3}MoO_3$	Air	Holes	6 nm		Mechanical		Durable over 4 hours	
P4BCMU Resists	UHV	Lines after etching	20 nm	3 hours	Electrical			
	UHV		20 nm	8 hours	Electrical			
PMMA	UHV	Charge	2 μm		Electrical		Charge decay	ac, Force

Table 5-5. Continuation of chart summarizing the relevant properties of sample/ambient/tip stratagems for use in a memory configuration. See text for more explanation and detail.

Sample/*Tip*	Ambient	Bit Type	Bit Size (width)	Megabit Time	Mechanism	Reproducibility	Durability	Readability
HOPG	UHV	Lines and Mounds of Contaminates	50 nm	2 days	Electrical		See HOPG	Z, I
Au, Al, Si, & Pt	10^{-5} Torr		100 nm	3 hours	Electrical			Z, I
Rhenium /*W*	Air	Mound	2-5 nm		Mechanical			Z, I, ac
Silicon	UHV	Holes	10 nm		Mechanical			Z
	UHV	Atom	Atomic to nm	8 hours	Electrical	Mound/hole uncertainty		Z
	DMCd 1 mTorr	Mound	10 nm	1 second	Electrical			Z, I, ac
	WF_6 gas 1-30 mTorr	Mound in holes	20-40 nm	2 months	Electrical			
/*Pt-Ir*	dilute HF	Holes	200 nm		Elec-Chem		HF etches Si	Z
	Air or O_2	Mound			Oxidation		Tip touches in air	
	Nitrogen	None						
Si:H	Air	Mound	35 nm		Oxidation		Oxides hinder tunneling Si:H will eventually oxidize	
Si:H amorphous	Air	Lines	140	1 minute	Elec-Chem			
Silicon Nitride Silicon Dioxide	Air	Charge	75 nm	1 minute	Electrical	100%	1 week+ (Thermal SiO_2)	ac, Force

Table 5-6. Continuation of chart summarizing the relevant properties of sample/ambient/tip stratagems for use in a memory configuration. See text for more explanation and detail.

Sample/*Tip*	Ambient	Bit Type	Bit Size (width)	Megabit Time	Mechanism	Repro-ducibility	Durability	Read-ability
Silver Selenide $Ag_{0.9}Se$ /*Pt*	Air & H_2	Lines	15 nm		Electrical; No effect w/ pulsing			
	5 mTorr	None						
Sulfur on Re	Silicone oil	Hole	40 nm	23 days	Electrical			Z, I, ac
	Air	None						
Ti(O_2) on Pt	Air	Holes	5-36 nm	1 week	Electrical (ac)			I, ac
Tungsten Diselenide/*Au*	Air	Holes	5 nm	1 second	Electrical	Time varies with tip	Holes grow and fuse	Z, I, ac
	Air	Rings	6 nm	5 hours	Electrical		> 2 day stability	
$YBa_2Cu_3O_{7-x}$	Air	Flatten			Mechanical		STM may alter surface	
	Air	Grooves	100 nm	1 month	Electrical			
2-D Materials: InSe, ZrS_2, $TiSe_2$, $SnSe_2$, $NbSe_2$, TaS_2, $MoSe_2$, WSe_2, WS_2, PtS_2, $ReSe_2$, WTe_2, and $MoTe_2$		Holes			STM imaging produced surface wear and pitting			

Chapter 6.

Mechanical and Electrical Design Considerations

It has been shown that nanometer scale structures can be manufactured on HOPG via scanning tunneling microscopy (STM) techniques using a high frequency voltage pulse superimposed on the normal STM tunneling bias. Considered here are the factors which will affect the magnitude of the voltage pulse actually reaching the tip and the response of the necessary current to voltage electronics.

6.1 Potential degradation

In order to determine the effect of the STM head on surface alterability, experiments and theoretical calculations are used to estimate the percentage of the high frequency voltage pulse actually appearing across the tunneling region, i. e. the region between the tip and the sample surface. In order to achieve this goal, the ac equivalent parallel capacitances and resistances of the Nanoscope II STM head "A" were measured as a function of frequency. These measurements provided a basis for designing a theoretical lumped parameter electrical model of the analyzed STM head. From the theoretical circuit, voltage drop percentages were calculated as a function of frequency.

6.1.1 Parallel capacitance and resistance measurements

The ac equivalent parallel capacitances and resistances were measured using an HP4284A LCR meter. There were three nodal points of measurement on the Nanoscope II STM head "A". These are

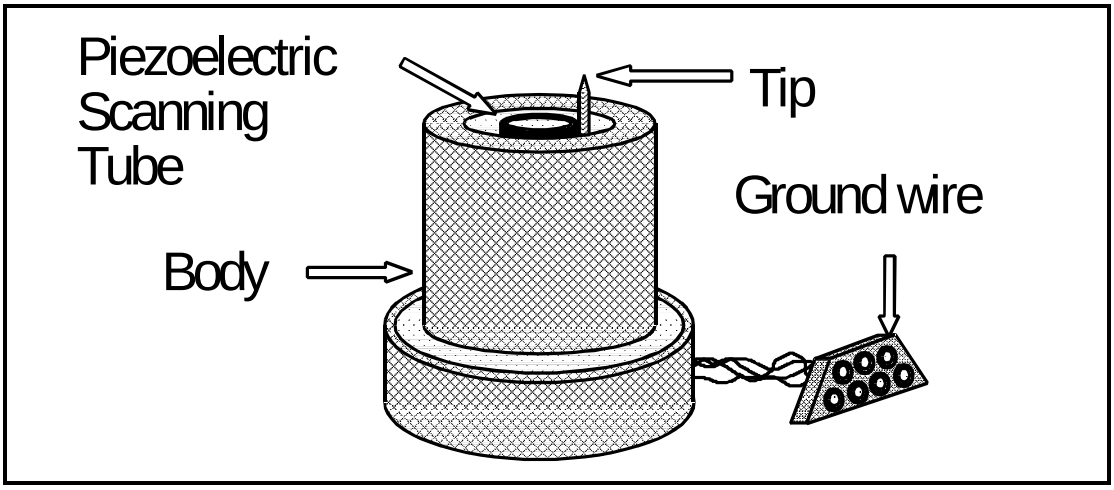

Figure 6:1. Drawing of Nanoscope II head 'A' showing points (tip, body, and ground wire) used for ac electrical measurements.

designated in Figure 6:1 as tip, body, and ground wire. Measurements were taken with an ac amplitude of 200 mV while the frequency was varied from 100 Hz to 1.0 MHz. The measured capacitances and resistances are listed in appendix B, Table b-1, for measurements between two of the three nodes while leaving the third node floating. Table b-2 of appendix B gives the measured capacitances and resistances between one of the nodes and with the other two nodes electrically connected.

6.1.2 Theoretical circuit development and measurement comparison

From the measured values, the equivalent electrical circuit of Figure 6:2 was developed. A basic knowledge of the mechanical and electronic design of the head provided insight into the theoretical circuit design. Resistor R_2 is the input resistor of the current to voltage (I:V) converter. The C_5 capacitance is produced by the interaction between the body and the wire which goes from the tunneling tip to the I:V converter. The wire actually passes through an insulated cylindrical hole in the Invar

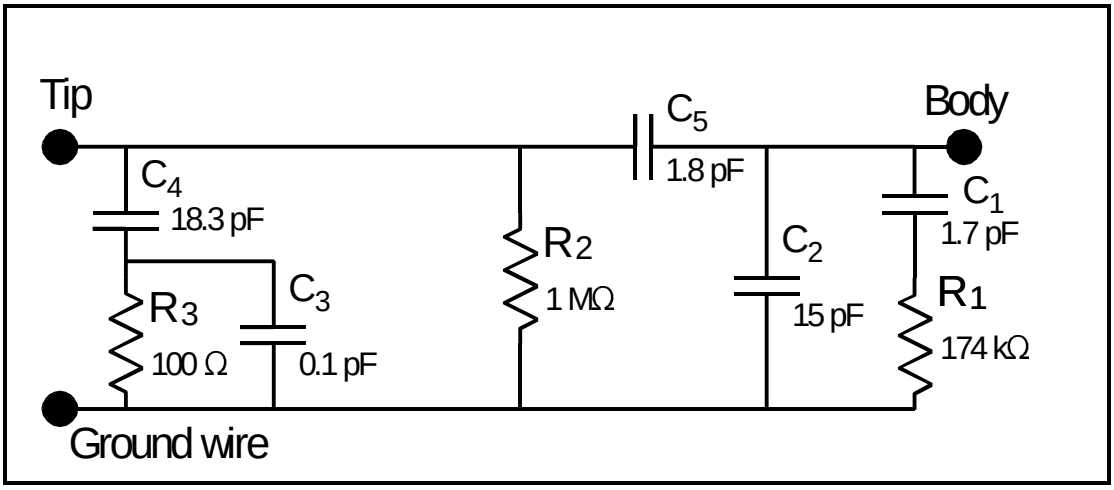

Figure 6:2. Theoretical circuit diagram for the Nanoscope II head 'A' disconnected from the microscope base and control electronics.

body effectively constructing a cylindrical capacitor. Capacitance C_4 and C_3 along with resistor R_3 are probably due to the input impedance of an op-amp in the I:V electronics. The theoretical circuit was derived by starting with the known position and value of R_2, then added the known position of C_5. Several designs for the rest of the circuit were examined for the other values, but not entirely blindly. The measured data showed that at low frequencies the resistance between the body and ground approached immeasurably high values. This indicated a series capacitor model. This left two simple models to examine. The known series capacitor could have been in series with a parallel resistor-capacitor network or in parallel with a series parallel resistor network. The circuit shown gave the best theoretical fit to the measured data.

The node to node measured and theoretical parallel capacitances and resistances as a function of frequency for the circuit in Figure 6:2 are plotted in Figure 6:3. The theoretical and measured capacitances and resistances from one node to the connected other two nodes are plotted

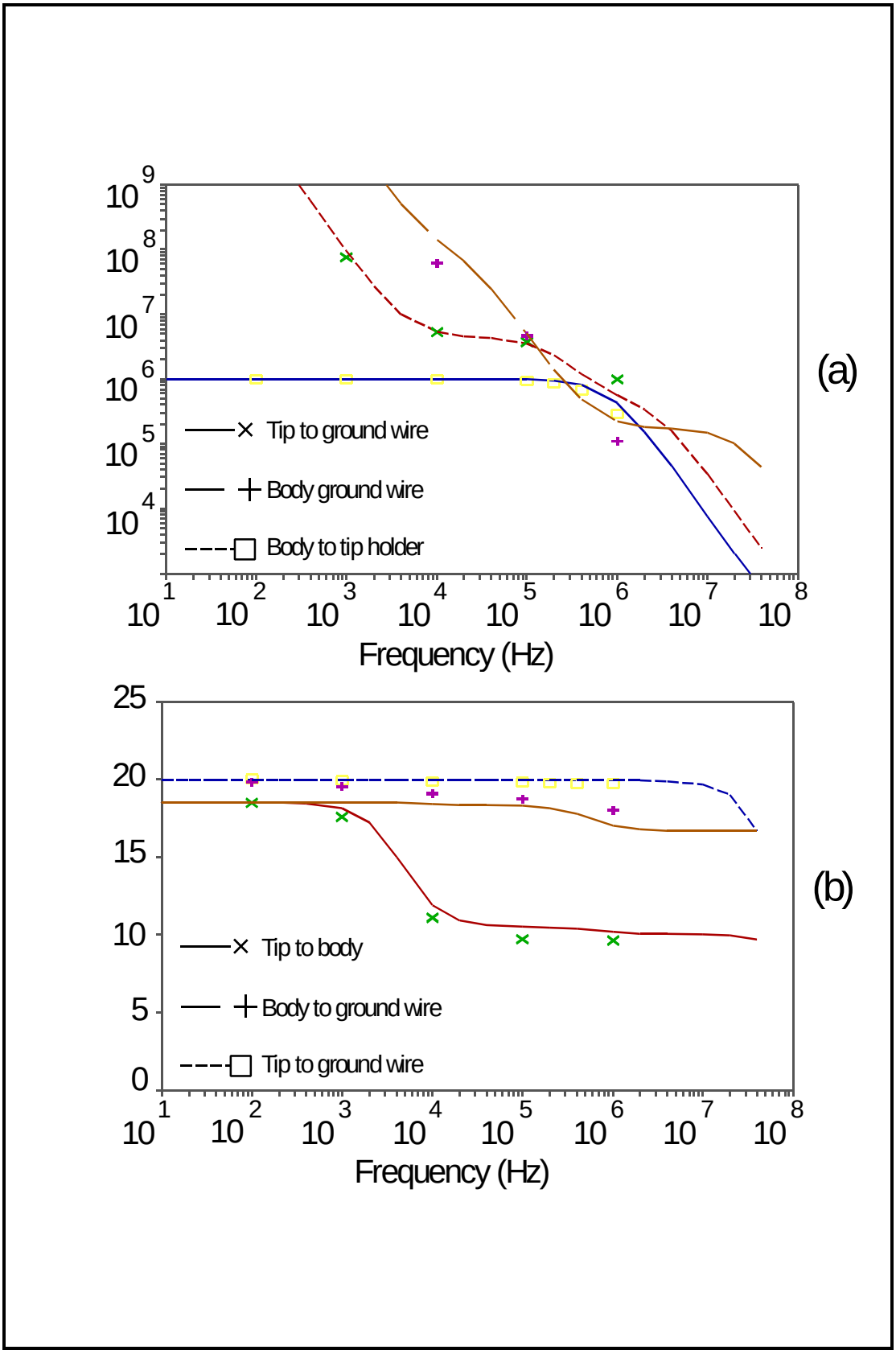

Figure 6:3. Measured (symbols) and calculated (lines) resistances (a) and capacitances (b) vs frequency. Measurements are taken with one node floating.

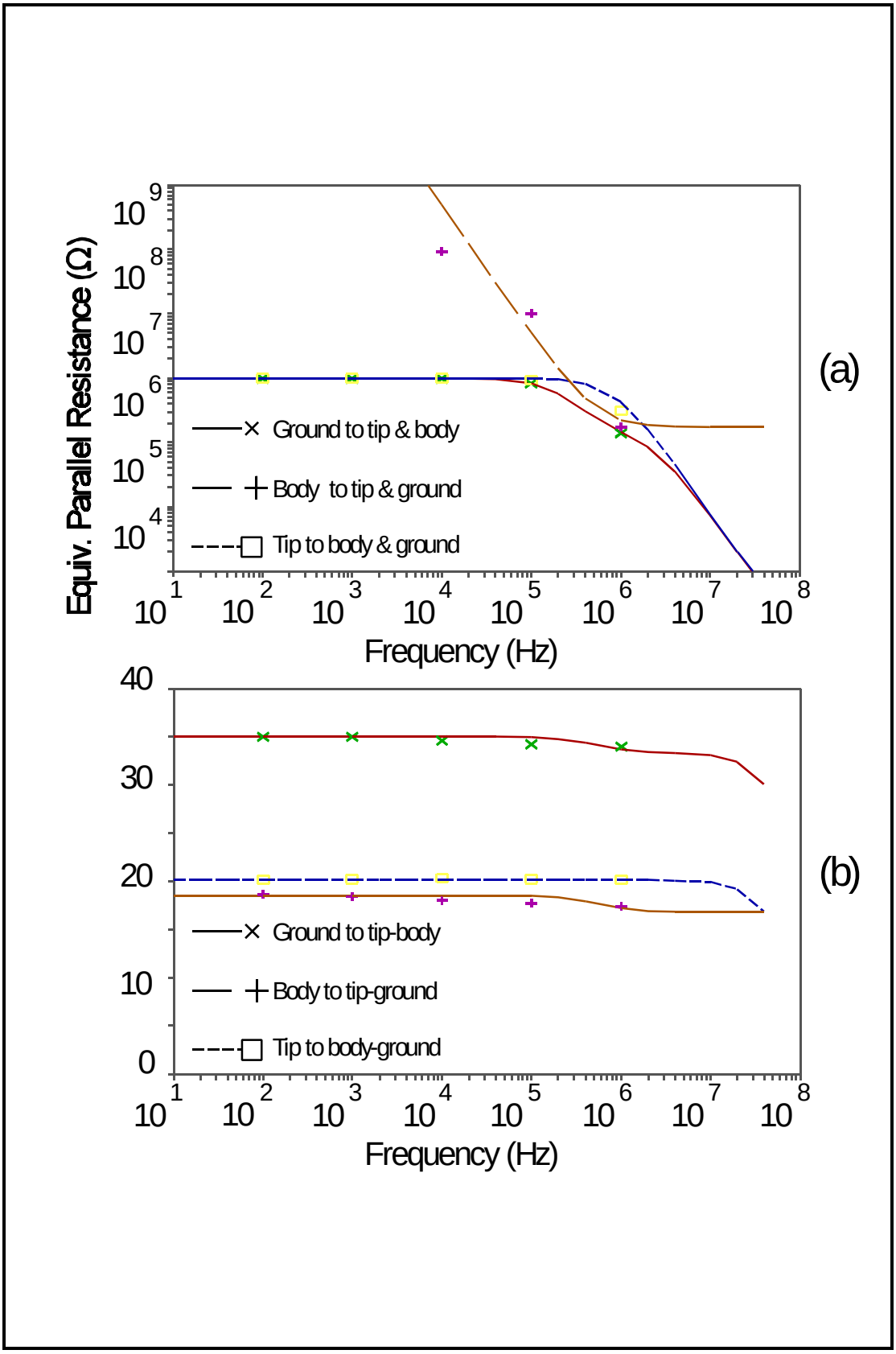

Figure 6:4. Measured (symbols) and calculated (lines) resistances (a) and capacitances (b) vs frequency. Measurements are taken between one node and the connected other two nodes.

as a function of frequency in Figure 6:4. The Asyst computer program used to calculate the theoretical values is contained in appendix A.

The theoretical circuit of Figure 6:2 was expanded to include the tip to sample capacitance and tunneling resistance along with the capacitance between the sample holder and the body of the STM head. This expanded circuit is diagrammed in Figure 6:5. The tunneling resistance (R_2) was estimated to an upper limit by assuming a tunneling bias of one volt and a common tunneling current of one nanoamp. Dividing the bias by the current yields a resistance of 10^9 Ω.

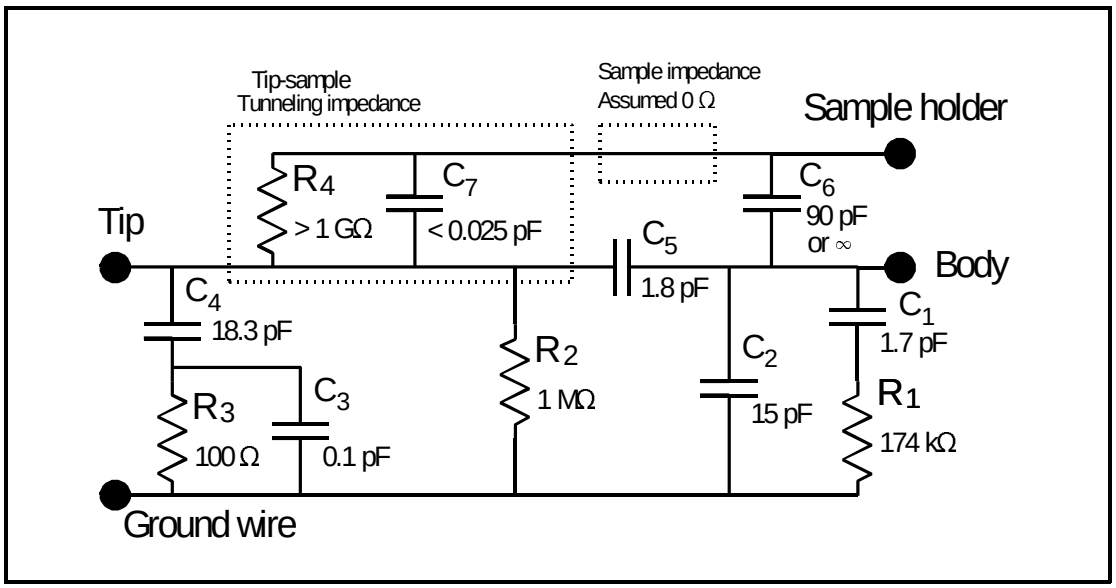

Figure 6:5. Theoretical circuit diagram for the Nanoscope II 'A' STM head including tunneling and sample holder impedances.

6.1.3 Calculation of tip-sample capacitance

The capacitance, C_7, between the tip and sample was estimated by first calculating the potential function, then deriving the electric field function. A surface integration of the field gives the charge on the tip surface. The charge is then differentiated with respect to the voltage to

determine the capacitance.

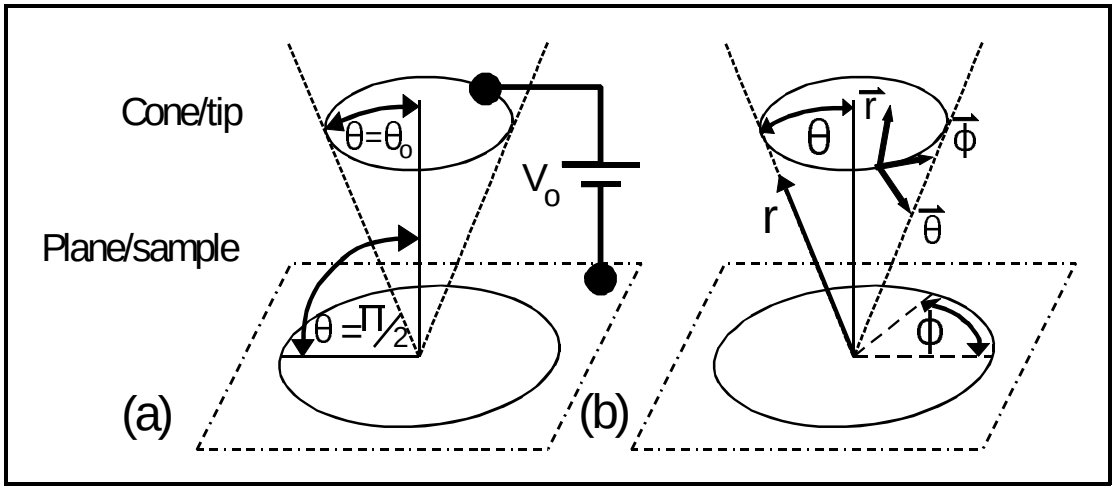

Figure 6:6. (a) Tip and sample geometrical structure, and (b) spherical coordinate description, for STM tip to sample potential, electric field, charge, and capacitance calculations.

In order to calculate the potential function, electric field function, charge, and capacitance between the tip and sample, the physical geometrical shapes must be known. Although no two STM tips are exactly alike, we will assume the tip has a basic conical structure. For the majority of applications presented in this thesis, samples are generally flat over a large area giving rise to a planar structure. The structure is illustrated in Figure 6:6 using spherical coordinates to describe the structure mathematically. The surface of the tip is described mathematically by $\Theta=\Theta_o$, where Θ_o is a constant (a cone), and the sample surface is mathematically described $\Theta=\pi/2$ (a plane). We have allowed the tip and the sample to mathematically touch where r=0 to greatly simplify the solution. The actual tip-sample separation is theoretically on the order of Angstroms which produces negligible change in the total capacitance. This geometry also produces an upper limit on the value of capacitance for the situation where the tip fits entirely inside

the theoretical cone.

6.1.3.1 THE POTENTIAL FUNCTION

Assuming an air gap, void of charge between the sample and tip, the potential in this region is described by Laplace's equation $\nabla^2 V(r,\theta,\phi)=0$, where $V(r,\Theta,\phi)$ is the function describing the potential between the tip and sample. Laplace's equation in spherical coordinates is:

$$\frac{1}{r^2}\frac{\partial}{\partial r}\left(r^2\frac{\partial V}{\partial r}\right) + \frac{1}{r^2\sin\theta}\frac{\partial}{\partial\theta}\left(\sin\theta\frac{\partial V}{\partial\theta}\right) + \frac{1}{r^2\sin^2\theta}\frac{\partial}{\partial} \qquad \textbf{(6-1)}$$

Since the potential is symmetrical in r and ϕ, $V(r,\Theta,\phi) = V(\Theta)$ and Equation (6-1) reduces to:

$$\nabla^2 V = \frac{\partial}{\partial\theta}\left(\sin\theta\frac{\partial V}{\partial\theta}\right) = 0. \qquad \textbf{(6-2)}$$

Solving equation (6-2) with the boundary conditions, $V(\Theta_o) = V_o$ and $V(\pi/2) = 0$, yields the following potential equation:

$$V(\theta) = V_o\left[\frac{\ln(\csc\theta - \cot\theta)}{\ln(\csc\theta_o - \cot\theta_o)}\right]. \qquad \textbf{(6-3)}$$

This equation is graphed in Figure 6:6 for a one volt potential between the tip and plane and for several values of Θ_o . Notice that the inner potential starts deviating from a linear shape as the cone angle becomes smaller.

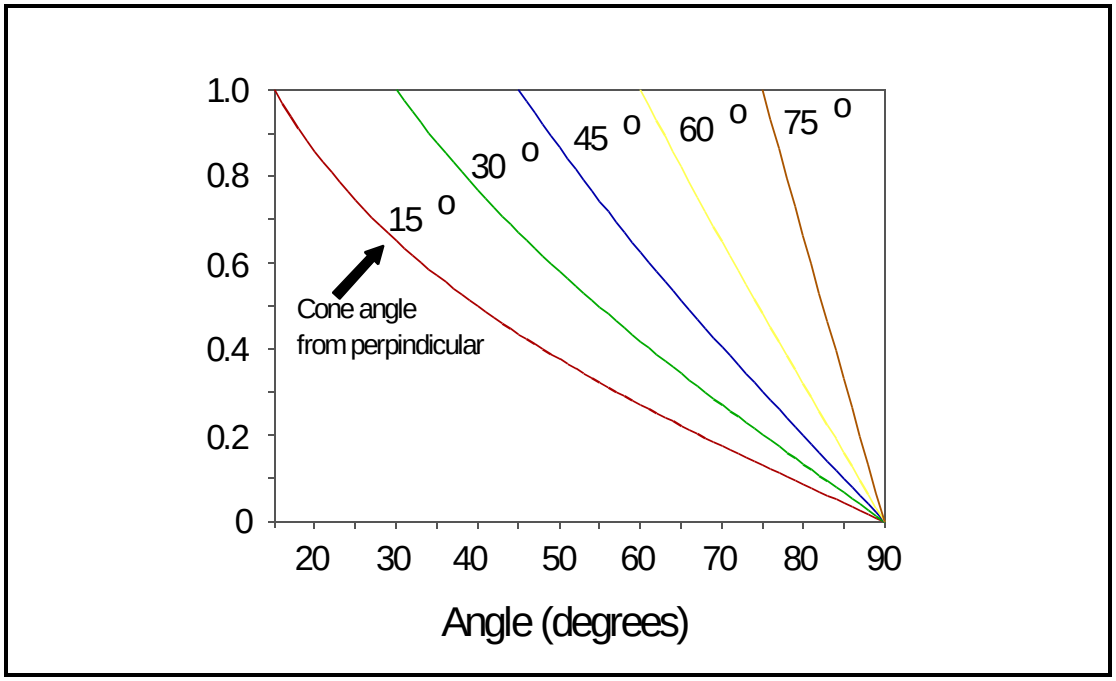

Figure 6:7. The potential as a function of angle between a conical tip and planar surface for various values of cone angle Θ_o. Θ is measured normal to the plane.

6.1.3.2 THE ELECTRIC FIELD VECTOR FUNCTION

Knowing the potential function we can calculate the electric field function $E(r,\Theta,\phi) = -\nabla V(r,\Theta,\phi)$ yielding:

$$\vec{E}(r,\theta,\phi) = -\left[\frac{\partial V}{\partial r}\vec{r} + \frac{1}{r}\frac{\partial V}{\partial \theta}\vec{\theta} + \frac{1}{r\sin\theta}\frac{\partial V}{\partial \phi}\vec{\phi}\right] = \frac{-V_o}{r\sin\theta\ \ln(\csc\theta_o - \cot\theta_o)}\vec{\theta}. \quad \textbf{(6-4)}$$

This is shown graphically in Figure 6:7 for a 1 V applied potential and at a radius of 1 μm with a 15^o cone angle.

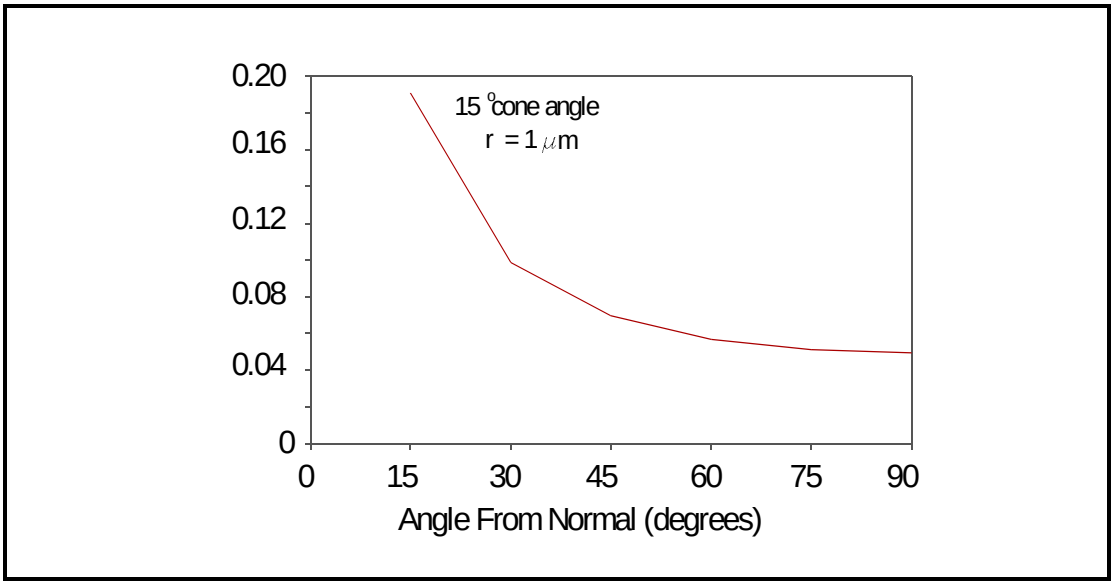

Figure 6:8. The electric field as a function of angle between a conducting cone and plane with a 1 V applied field, a 15° cone, and at a radius of 1 μm. The angle is measured normal to the plane.

6.1.3.3 THE CHARGE ON A LIMITED CONE

In order to calculate the capacitance, the charge, Q, on the tip as a function of V_o must be known. Using Gauss's law and setting a limit on the extent of the tip at r_o, we have the equation:

$$
\begin{aligned}
Q &= \epsilon_o \int_{S'} \vec{E} \cdot da' \\
&= \epsilon_o \int_0^{2\pi} d\phi \int_0^{r_o} \vec{E} \cdot r \sin\theta \; dr \; \vec{\theta} \\
&= \frac{-2\pi\epsilon_o V_o}{\ln(\csc\theta_o - \cot\theta_o)} \int_0^{r_o} dr \; \vec{\theta} \cdot \vec{\theta} \\
&= \frac{-2\pi r_o \epsilon_o V_o}{\ln(\csc\theta_o - \cot\theta_o)},
\end{aligned}
\qquad \textbf{(6-5)}
$$

where the volume S' is chosen to include the surface of the tip and the surface area of S', da', is divided into areas chosen to be normal to the spherical coordinate vectors. The dielectric constant of the region

between the cone and plane is that of air, ϵ_o = 8.86 pF m^{-1}. The areas bounding the volume are the surfaces of constant Θ (one inside and one outside the tip), r=0, r=r_o, ϕ=0, and ϕ=2π. The extent of the cone has been limited to r_o because real tips are limited by their construction from wire or in some cases thin rod stock.

6.1.3.4 THE CAPACITANCE OF THE CONE-PLANE STRUCTURE

Now that the charge, Q, on our tip is known as a function of V_o, the capacitance $C(r_o,\Theta_o,V_o)$ can be determined by differentiating the charge, C, with respect to the potential, V_o, producing the equation:

$$C(r_o,\theta_o,V_o) = \frac{dQ}{dV_o} = \frac{-2\pi r_o \epsilon_o}{\ln(\csc\theta_o - \cot\theta_o)}. \qquad \textbf{(6-6)}$$

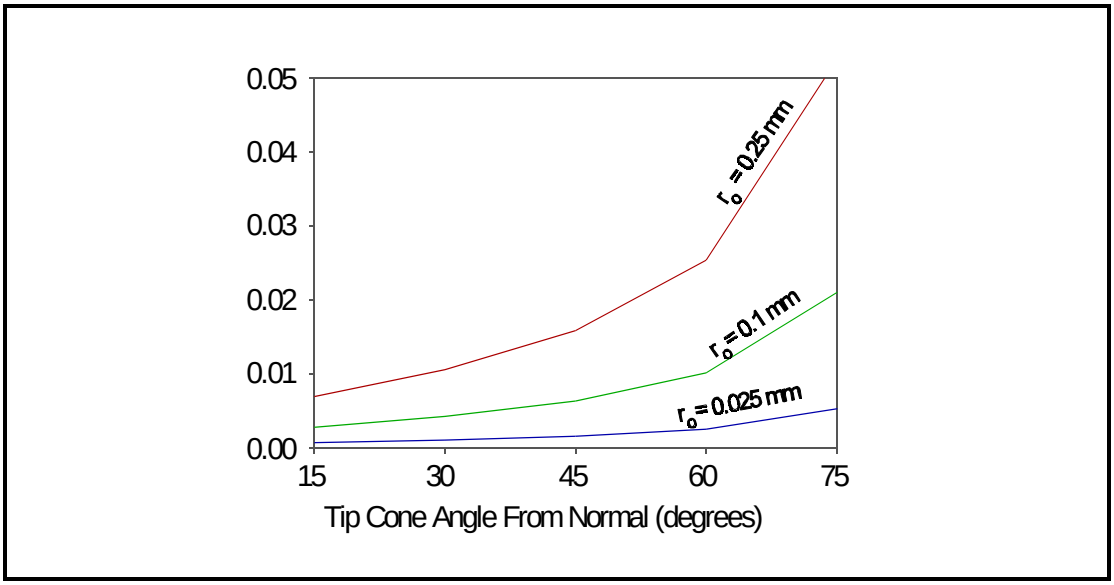

Figure 6:9. Calculated capacitance between a conical tip and a planar sample as a function of cone angle. The capacitance is graphed for three values of radii.

Capacitance values between the tip and sample as a function of cone angle, Θ_o, are graphed in Figure 6:9 for V_o = 1 V, and for

r_o = 0.25 mm, 0.10 mm, and 0.025 mm. By letting Θ_o vary between 30^o and 60^o and letting r_o vary between 0.01 μm and 0.25 mm, we obtain lower and upper limits for the capacitance of the tip, 4×10^{-7} pF and 2.5×10^{-2} pF, respectively.

The body to sample holder capacitance, C_6, was directly measured for the insulated holder and found to be 90 pF. When an uninsulated holder is used, the impedance associated with C_6 approaches zero Ω (C_6 becomes ∞ for practical purposes). The internal impedance of the sample along with the bias contact are assumed to be zero Ω for our calculations. Such things as ohmic contact problems, semiconductor type samples, and thin film type samples may cause the sample impedance to be large enough at high frequencies to degrade the potential drop across the tip-sample interface.

6.1.4 Potential drop across the tunneling junction region

The response of a voltage pulse was estimated to be approximately the same as a continuous ac signal with a period equal to the pulse duration and having an amplitude equal to that of the pulse. From the circuit of Figure 6:5, the theoretical percentage of the amplitude of an ac voltage signal can be calculated. The percent ac voltage drop across the tunneling gap for the components of Figure 6:5 is plotted in Figure 6:10 as a function of frequency. The three curves are for using an uninsulated sample holder, an insulated sample holder, and an insulated sample holder with the body grounded. Changing the tunneling capacitance, C_7, from 4×10^{-7} pF to 2.5×10^{-2} pF (calculated upper and lower limits) produced

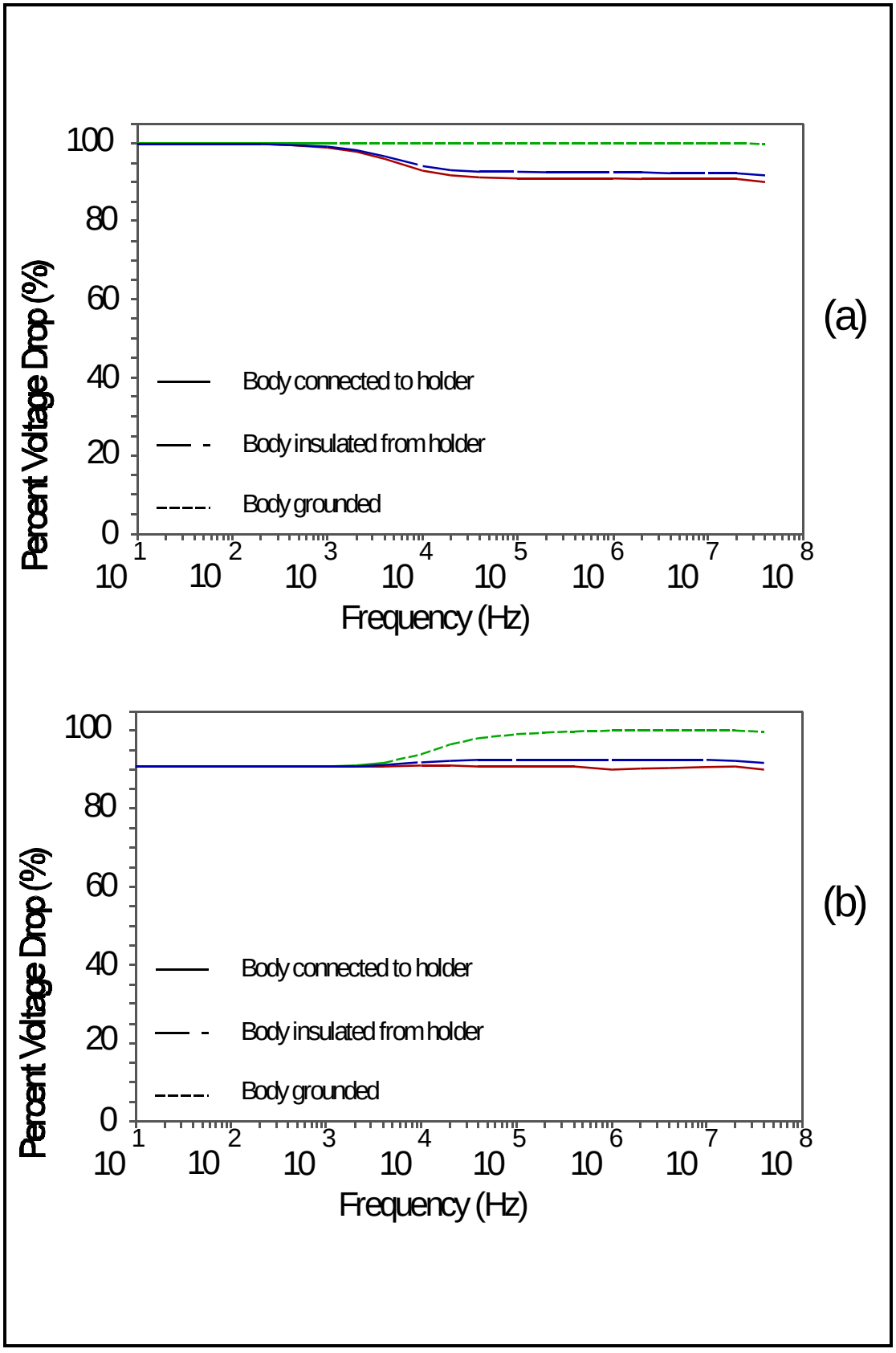

Figure 6:10. Voltage percentage appearing across tunneling region vs frequency for (a) components of Fig. 6:5, and (b) with $R_2=10^7$ Ω. Legend shows body and holder specifics.

negligible changes in the percent ac voltage dropped across the tunneling region. Changing the tunneling resistance, R_4, had an effect only for lower resistances. For $R_4 = 10^8\ \Omega$, there was a negligible change in the percent ac voltage dropped across the tunneling region. Figure 6:10 shows the plot of the percent ac voltage drop across the tunneling region with the same configurations as in Figure 6:5, but with $R_4 = 10^7\ \Omega$. The decrease in the percent voltage dropped for low frequencies appears across the I:V conversion resistor, R_2 ($10^6\ \Omega$). The greater the value of the capacitor C_5, the greater the potential degradation for higher frequencies. At low frequencies and with the body not grounded, the potential degradation can be estimated by Ohm's law with resistor R_2 and the tunneling resistance R_4 in series. At higher frequencies, the capacitors C_5 and C_4 in series determine the potential degradation across the tunneling region. Since capacitance C_5 may change with the ambient pressure, temperature, and humidity, the percent voltage drop across the tunneling junction may also change. For minimal potential degradation, the design criterion should be $R_4 >> R_2$ and $C_4 >> C_5$, with C_5 as small as possible.

6.1.5 Cabling (transmission line) degradation

The impedance between the input and ground of the cable connecting the voltage pulse source to the STM head was measured to determine if there would be any signal degradation in the cable. The measurements are plotted in Figure 6:11. Figures 6:11(a) and 6:11(b) show the impedance and equivalent parallel capacitance, respectively, of

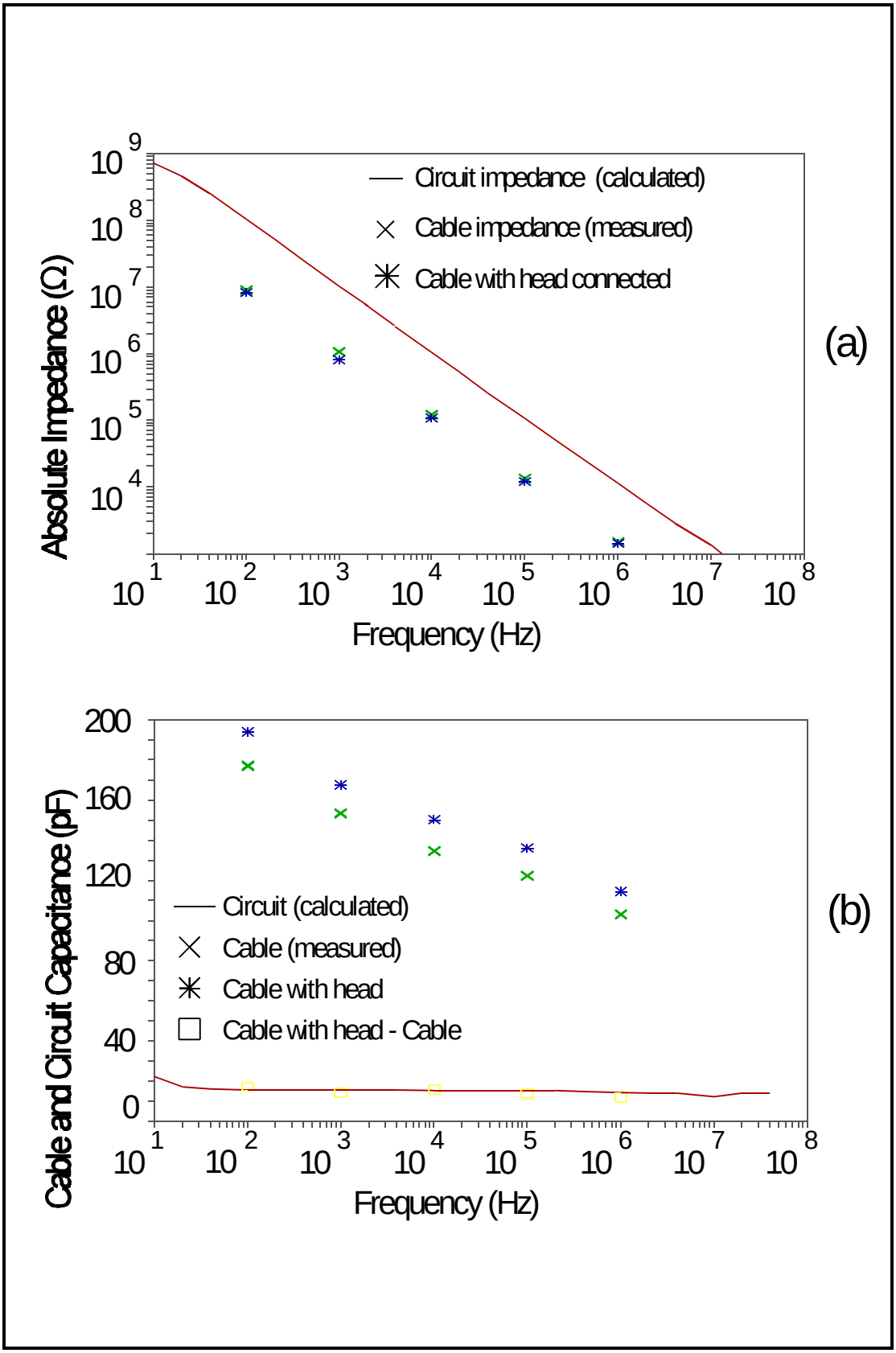

Figure 6:11. Cable measurements and circuit calculations for impedance (a) and capacitance (b) vs frequency. Comparison is made with the head connected and disconnected.

the cable with the head disconnected, the cable with the head connected, and the calculated impedance of the head. In addition, Figure 6:11(b) shows the difference of the capacitances of the cable with and without the head connected (labeled as Cable with head - Cable). Additionally, Figure 6:11(b) shows the measured capacitance of the circuit. Since this lines up with the difference of the cable capacitance, with and without the head connected, the cabling impedance is determined to be primarily acting in parallel with the head. This results in the same potential across the cable and circuit.

6.1.6 Voltage source output impedance degradation

The output resistance of most function generators is 50 Ω, and the output impedance of the DT2821 digital to analog board is given as 0.1Ω. For both impedances, the degradation of the potential at 1 MHz (Z cable + head = 1400 Ω) is less that 0.1 %. If we used a frequency which reduced the cable+head impedance to 100 ohms (probably near 100 MHz if the trend in the data is followed), there would be an additional reduction of the potential by 10 % for the function generator considering a 90^{o} phase shift between source and circuit impedance.

6.2 Output theoretical gain of I:V Converter

Since we have determined that 90 % of the voltage appears across the tunneling junction, we wish to determine the effect of the 10% stray voltage on the response of the STM. The potential is dropped across the resistor R_2 of Figure 6:5. This resistor is used in the op-amp circuit of

Figure 6:12 to convert the current through the tunneling region to a voltage which feeds a digital feedback loop. The R-C filter of Figure 6:12 is sometimes included in the circuit to further reduce the gain.

The output of this circuit is equal to the potential dropped across R_4 times the gain of the op-amp circuit. The gain of the circuit as a function of frequency is plotted in Figure 6:13. Common voltage thresholds for nanomodification pulses are around 3 volts. At frequencies greater than 50 kHz this should result in 0.3 volts across R_2. For a 1 MHz pulse this should result in an additional output of 0.7 volts (gain = 2.5) with no RC filter, and 0.003 volts (gain = 0.013) if the RC filter is in the circuit. At 100 kHz (an

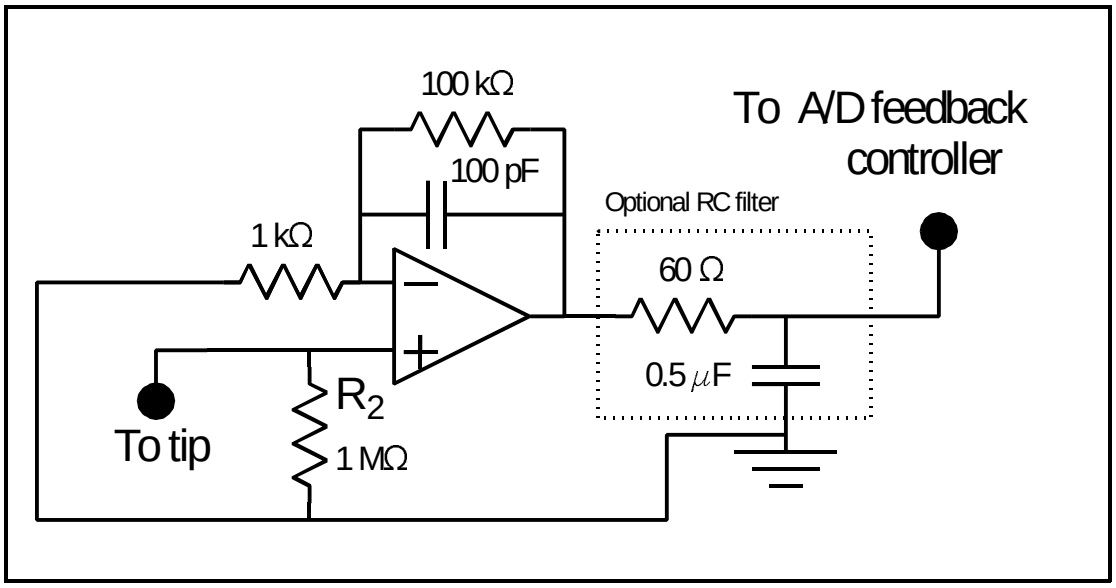

Figure 6:12. Circuit diagram of the I:V converter used in the Nanoscope II STM head 'A' with optional external RC filter.

observed threshold for modification of non-square wave pulses) the gains are 16.7 and 0.88 with and without the RC filter, respectively, producing apparent I:V voltages of 5 volts and 0.26 volts. It is called apparent because the output voltage is not produced by the

tunneling current. The smaller additional voltages would not result in damaging tip displacements since the STM responds logarithmically to the change in current. The 5 volt change would make the tip pull away from the sample initially, then move toward the surface after the pulse due to a deficiency in current.

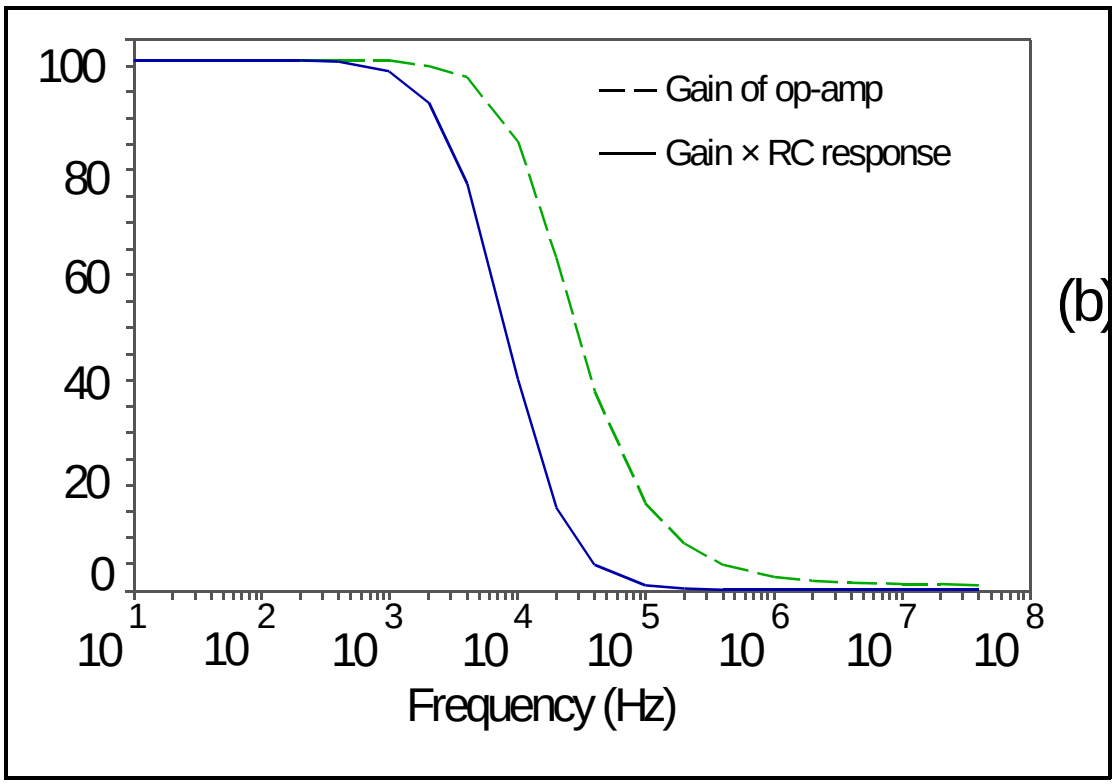

Figure 6:13. The gain of the op-amp circuit shown in Fig. 6:12 with and without the RC filter attached to the output.

Also important to consider is the effect a pulse, instead of a continuous wave, has on the output. A test was performed to see the actual response of the I:V circuit with the tip separated from the sample a sufficient amount to inhibit tunneling. The results for the 20 μs pulse shown in Figure 6:14(a) are shown in Figure 6:14(b-d) (hand sketched from an oscilloscope). With the body floating and no RC filter, the 6.35 V observed value for the initial peak of the I:V response shown in

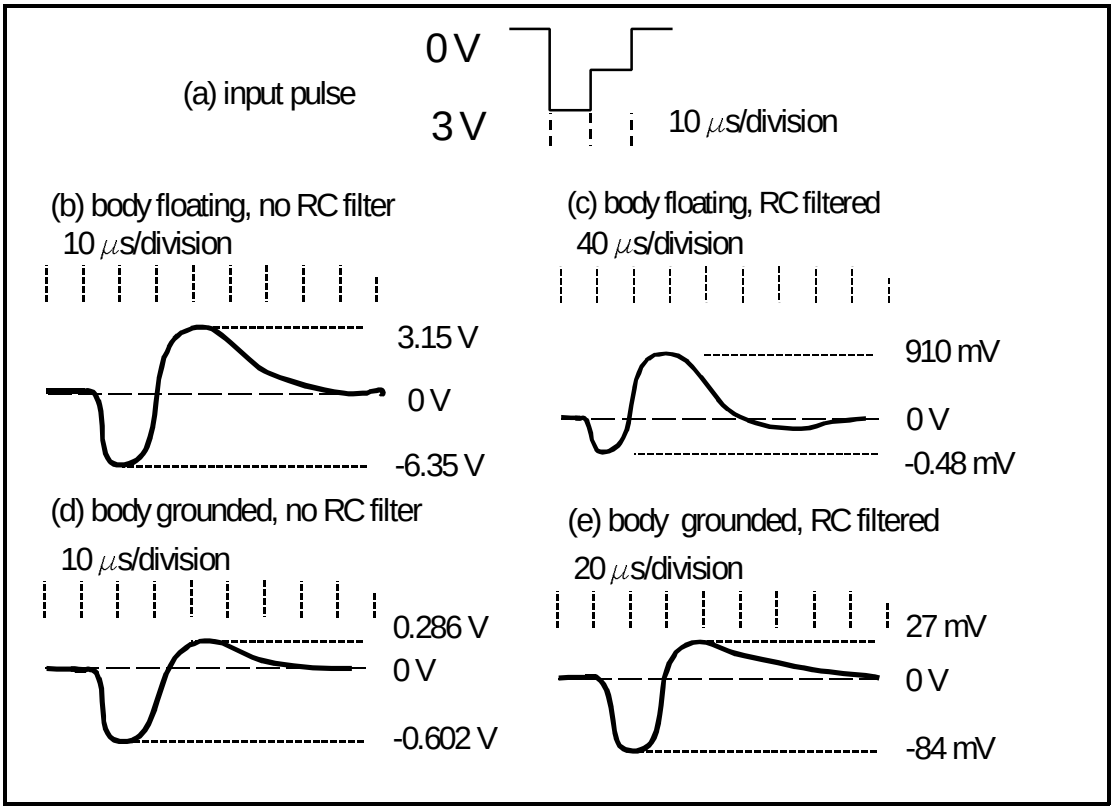

Figure 6:14. Input pulse (a) and it's effect on the output of the I:V converter (b-e) as hand sketched from an oscilloscope trace. See individual captions for more detail.

Fig. 6:14(b) compares favorably with the 5 V predicted value. Similarly, with the body floating and the RC filter in the circuit, the initial peak value of 0.48 V shown in Fig. 6:14(c) was not far from the predicted value of 0.28 V. Figs. 6:14(d) and (e) show that the response was limited to millivolt values when the body was grounded. More important is the fact that the response of the I:V reverses polarity before it comes back to an equilibrium value. Such a reversal could cause the perceived current to drop (or even reverse) affecting the servo feedback. This could not have affected the alteration experiments when the S/H circuit was being used, but could have affected other alteration experiments. This is not thought to have been the case since the feedback gains were set low enough to

prevent any rapid displacement of the tip. For STM's with logarithmic amplifiers, a voltage reversal could cause a saturation of the log amp. If the log amp can not quickly recover, the resulting feedback could force the tip into the sample. This was not possible for the Nanoscope since there is an absolute value circuit and the log of the current is performed digitally.

Alteration was also possible when the body was grounded and the RC circuit was present. In this situation, the I:V response would have been on the order of 100 mV. This would result in a tip displacement of 0.3 nm if the feedback was operating in the constant current mode, which it was not. Since the feedback was operating at low gain (constant height), there would be no significant tip displacement. Since nanomodification has been achieved for 1 & 10 MHz pulses, and with or without the RC circuit and body grounded, it is evident that surface modification is not always caused by the tip touching the sample due to feedback response motion.

6.3 Experimental response of I:V converter during modification

We have shown the response of the I:V converter with a large separation between the tip and sample. Figure 6:15 shows the effect of a voltage pulse on the output of the I:V converter during tunneling. The graphs were hand sketched from an oscilloscope trace. The applied pulse shape is shown in Fig. 6:15(a) and the response of the I:V converter is shown in Figs. 6:15(b), (c), and (d). Low feedback gains were used to

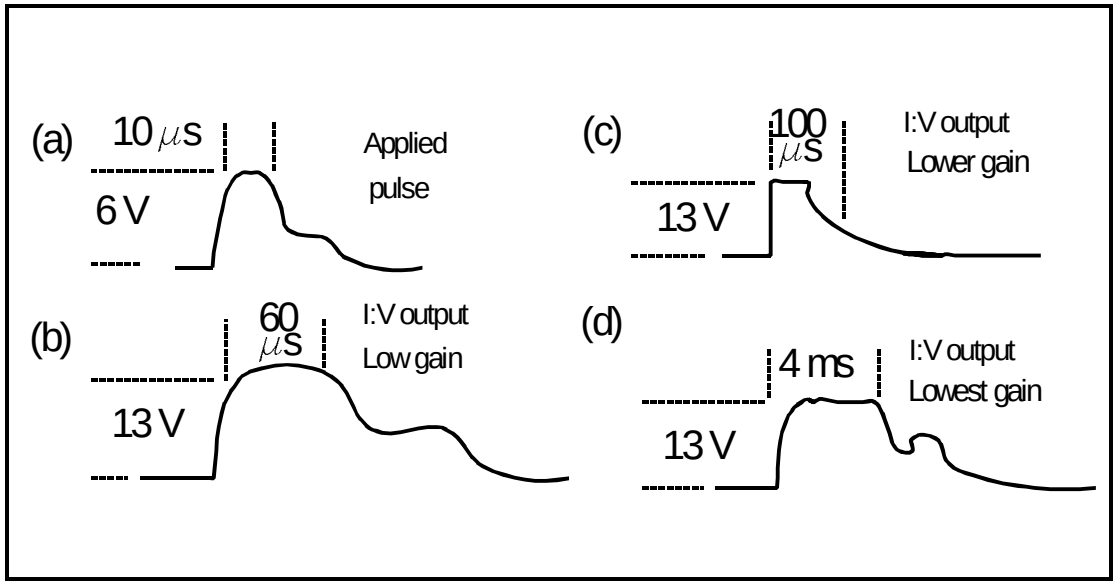

Figure 6:15. Effect of modification pulse on I:V converter output. (a) is the input pulse, (b), (c), and (d) are the resulting voltage outputs for low, lower, and lowest feedback gains.

assure a stable response. The converter reached its maximum of 13 V for all gains. The lowest gain required more than 4 ms to recover while the minimum response time was about 60 μs. The I:V converter without the added RC filter has a response time of $2\pi RC = 63$ μs. This minimum response will limit the time to produce 10^6 bits to a 63 second minimum. This is quite slow compared to the state of the art magnetic writing speeds of 10 ns/bit[1] for permanent archival. This means that multiple write heads or arrays would have to be incorporated to match the speed. Also, to increase the writing speed the design could utiliuze a smaller response time. This may not be possible and still keep the feedback stable and the tunneling gap constant.

6.4 Summary of electronic criterion for a tunneling nanomemory

The design of the STM and I:V converter have been shown to electronically affect the percent of the voltage pulse appearing across the tunneling junction. The stray pulse voltage has also been shown to affect the observed tunneling current. The electronic design of the I:V converter also effects the speed with which a memory bit can be written. The design of a nanomemory should include the criterion specified in Table 6-1.

Table 6-1. Some electronic design criterion for a tunneling based nanomemory.

1. The input resistance of the I:V converter should be much less than the resistance of the selected tunneling gap.
2. The capacitance from the substrate to the tip and/or wires leading to the I:V converter should be minimized.
3. The input capacitance of the I:V converter should be much greater than that from the sample to the tip and I:V input wire.
4. The electronic response time of the I:V converter should be less than the desired memory writing and reading time.

[1]Scott, James F., and Paz de Araujo, "Ferroelectric Memories", Science **246**, 1400 (1989).

Chapter 7.

I(S) Characteristics and Environmental Effects

Accurate measurement of surface structure heights with a scanning tunneling microscope (STM) requires a knowledge of tip-sample interaction. For measurements other than atomic resolution the STM operates by endeavoring to keep the tip-sample tunneling current constant by analog or digital feedback circuits. In order to obtain repeatable measurements, the repeatability of I(s) characteristics must be determined.

There are devices that have been conceived which would operate with a tunneling sensor[1] as the position sensitive transducer. Among these devices are patents for a magnetometer[2], a tunneling microphone[2], and the nanomemory[3] design which we have been considering. A knowledge of the relationship between the current, I, and the displacement, s, of the tip is integral to designing stable feedback circuits for these devices that can repeatably place the tip at a given height above the sample with maximum speed.

Accurate assessment of the expected operation of a transducer is necessary for design purposes. Consider the previously mentioned memory concept. The production of bits may require a repeatable separation between the tip and surface for the modification strategy to work. The reading of atomic scale bits from a memory structure using tunneling technology requires an apriori knowledge of the relationship

between the height of the tip above a sample and the corresponding tunneling current. Since two ways to read a bit using tunneling technology are with changes in height or changes in current, uncertain I(S) characteristics could change the requirements for the detection of a bit.

This chapter describes experiments relating to the I(s) relationship, that is, the dependence of the tunneling current, I, on the displacement, s.

7.1 X-ray calibrated I(s) apparatus

A monolithic x-ray interferometer[4] was utilized as the heart of a device to accurately measure the tunneling current between a sample and probe as a function of sample-tip displacement. The interferometer is constructed from a single crystal silicon monolithic flexure and a translation motion of 20 nm is provided by an electromagnetic force actuator. The probe was mounted in a reduction lever mechanism and brought to within tunneling range using a screw positioned wedge. Using this system open-loop, manual adjustment to within 20 nm was readily achieved. Using the actuator, sample displacement was controlled with subangstrom resolution and a precalibration accuracy of better than 50 pm.

7.1.1 Apparatus design for displacement and tunneling

The apparatus was designed for measuring the tunneling current as a function of displacement between a sharp probe and a conducting sample. The principles of operation are demonstrated schematically by

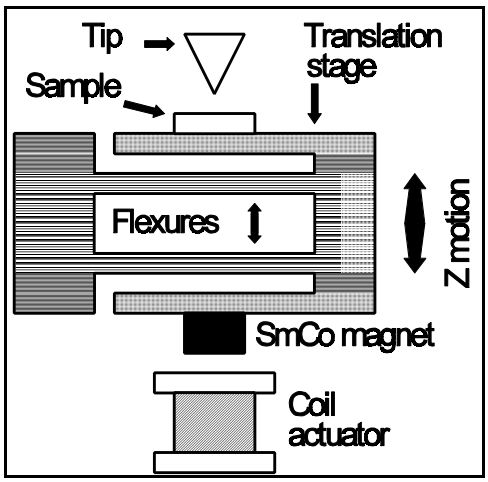

Figure 7:1. Schematic drawing for illustrating the operation of the tunneling apparatus.

Figure 7:1. Sample displacement of 20 nm is provided by a simple linear flexure translation stage. The sample is bonded upon the translation stage collinear with the actuator by using a silver paint which also served as a conduction path to the sample. A SmCo permanent magnet is rigidly attached opposite the sample on the flexure stage. Surrounding this, but not touching, is a uniformly wound circular cylindrical solenoid coil. Current through the coil produces a magnetic field inducing a force on the magnet which bends the flexure springs. It has been shown that the force/current characteristic of this actuator system is relatively insensitive to axial motion of the magnet relative to the coil[5]. The flexure stage was designed, built, and calibrated x-ray interferometrically by researchers at the University of Warwick.

The monolithic flexure stage was machined out of single crystal silicon. Figure 7:2 shows a schematic diagram of the flexure stage (not to scale). The x-ray interferometer consists of three blades. The x-rays are incident at an angle of about 6^{o} upon the first blade which, acting as a *splitter*, divides the beam into transmitted and refracted components. These beams are incident on the second blade which refracts the beams to act as a *mirror*. The third blade, acting as *analyzer*, interferometrically recombines the beams to form moiré fringes. If the crystal lattice of all

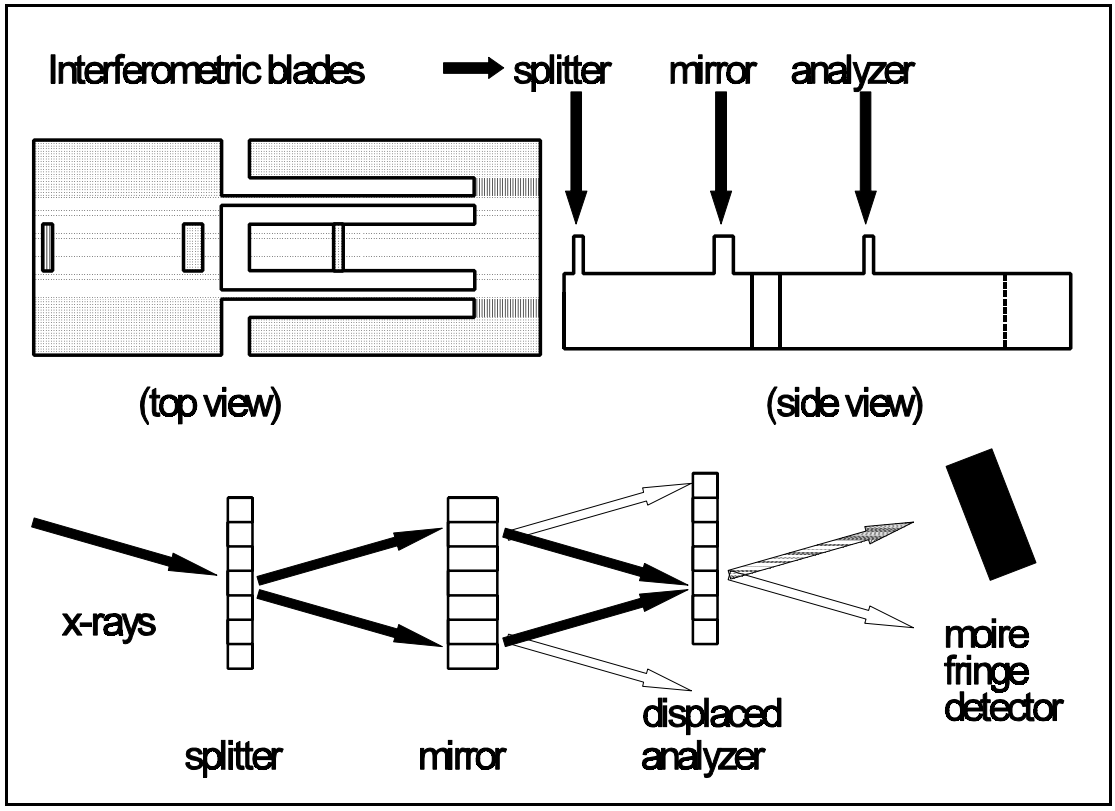

Figure 7:2. Drawing showing the interferometric design of the flexure stage.

three blades are aligned, the count of x-ray intensities of the emergent beam can be used to monitor fractional crystal lattice displacement as the right blade is laterally displaced relative to the other two. The flexure stage was kinematically mounted on a block of aluminum to which the coil was attached.

The tunneling probe assembly was designed to mount kinematically on the top of the flexure stage. This structure incorporated the tunneling probe along with coarse and fine positioning devices. Coarse adjustment was required to bring the tip to within a couple of micrometers of the sample and fine adjustment required to bring the tip to within the 20 nm range of the flexure stage. To provide thermal stability, the basic

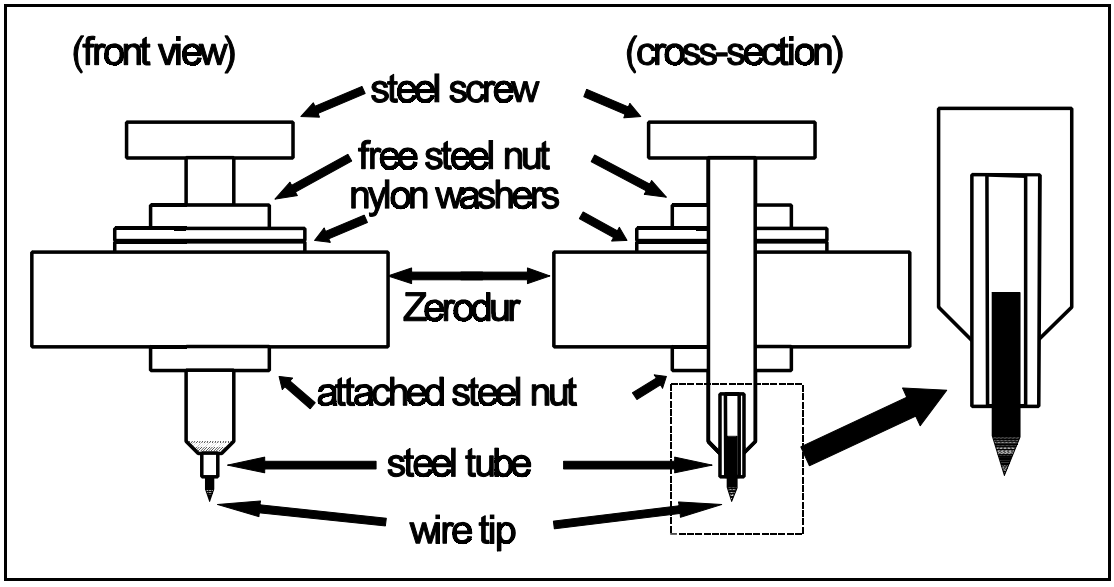

Figure 7:3. Tunneling probe mount with coarse adjustment. The cross-section with expanded area shows the tip inside the tube.

structure was made of the low thermal expansion glass ceramic Zerodur. Figure 7:3 illustrates the mounting and coarse positioning of the tunneling probe. Mechanically sharpened 0.254 mm wire tunneling tips are held in a stainless steel tube by frictional forces. The tube is mounted by cyanoacrylate (i.e. super-glue) into a center drilled steel screw. The probe is moved up and down with respect to the Zerodur mount by turning the screw. Only the bottom steel nut is fastened to the Zerodur. This sets a reference point for thermal expansion at the bottom of the Zerodur mount, i.e. only the part of the probe below the Zerodur is contained in the thermal loop of the tunneling structure. The nylon washers act as a spring to preload the screw and nut preventing hysteresis and increasing the stiffness of the structure. The upper nut also slides across the nylon washers with nominal friction assuring the two nuts do not lock up the screw thereby preventing adjustment. The design of the coarse

adjustment also facilitates the exchanging of wire probes during experimentation.

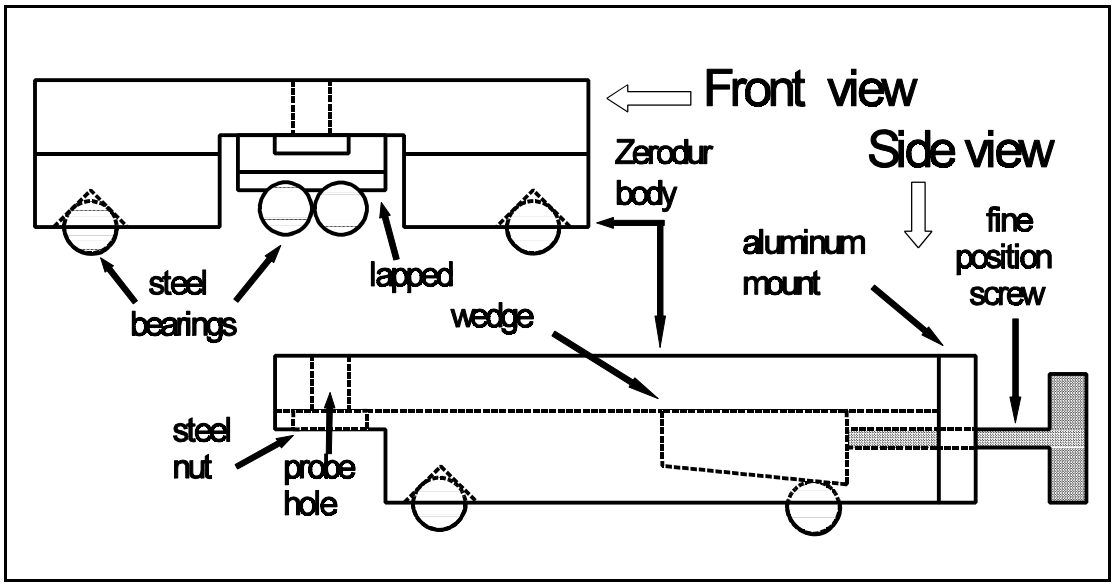

Figure 7:4. Schematic of body structure which kinematically rests via bearings on the translation stage. The screw-wedge structure for fine tip-sample adjustment is shown with the side view.

The basic body structure into which the tunneling probe was mounted is shown in Figure 7:4. The tunneling probe of Figure 7:3 is mounted through the probe hole into the steel nut of Figure 7:4. The attached steel nut of Figure 7:3 is the same as that indicated in Figure 7:4. The fine position screw has a thread spacing of 0.5 mm. The wedge has an aspect ratio of about 100:1. As the screw is turned, the wedge increases the spacing between the double ball bearings resting on the translation stage and the Zerodur body. This in turn causes the body to tilt on the front ball bearings lowering the tunneling probe. The relative spacings of the probe hole, and front and back bearings produce a lever action when the probe is tilted with an attenuation of about 5:1. The combined screw-wedge-lever action produces a fine adjustment of

1000 nm for each screw revolution. The screw head was marked for 80 equal rotational divisions, producing a scale of about 12.5 nm per division. The 4 cm length of the wedge provides a fine adjustment range of about 80 micrometers. Since the fine adjustment was manual, any upward hand motion affects the tip sample separation. For example if the operators hand caused the Zerodur body to raise 1 μm, the tip would move closer to the sample by at least 100 nm, 5 times the maximum displacement of the translation stage. This motion would force the tip into the sample corrupting both sample and tip. To reduce influence of the manual adjustment, an elastic band was connected to the coil mount, wrapped over the Zerodur body and interferometer, and connected on the other side to produce a preload force which would have to be overcome by the operator before motion was produced.

To increase surface flatness, the region of the body forming a counterface for the sliding wedge was high-speed diamond ground. Additionally, the wedge was lapped to decrease surface roughness and waviness which would corrupt the fine adjustment motion and increase friction.

Steel ball bearings were chosen as kinematic rests in order to match the thermal expansion of the probe structure and sample. Conical holes 2.5 mm deep (45^{o} angle from normal) were ground into the body with a diamond grinder. Similarly, the translation stage support had 45^{o} V-grooves machined into the top of it. The balls were placed between the conical holes and grooves. Simple geometrical analysis shows that the

thermal expansion of the structural loop from the bottom of the groove to the top of the hole will equal the thermal expansion of the steel ball times $\sqrt{2}$. Since the sample and tip material, and their respective length and thickness are variables in the thermal loop, exact determination of correct ball size was not possible. Assuming thermally similar materials, the estimated distance between the top of the attached nut of the probe and the bottom of the sample ($\approx$7mm) divided by $\sqrt{2}$ provides the estimated 5 mm diameter of the ball. The Zerodur body was not included in the calculation since it has a negligible thermal expansion coefficient (10^{-7}/^{o}C). The 2.5 mm of silicon from the bottom of the kinematic groove to the top of the silicon stage was also neglected having a thermal expansion coefficient about 1/3 that of the steel in the probe.

The complete coil-stage-probe structure was mounted on a sand filled optical bench. The bench was connected to a 2 m × 1 m × 0.7 m concrete block that was in turn supported by a pneumatic vibration isolation system. Previous calibration of the x-ray interferometer showed an open loop accuracy of better than 20 pm.[4]

The flexure stage was computer controlled using a Metrabyte μDash 16 digital to analog (D/A) conversion board & supporting electronics. The D/A output was connected to a Darlington pair current amplifier feeding one terminal of the actuating coil while the other terminal was grounded. The 12-bit D/A board had an output of ±10 volts. An 8 V output displaced the stage 20 nm. This provided a least significant bit (lsb) resolution of about 0.025 nm.

The tunneling circuit diagram is shown in Figure 7:5. The 9 volt supply is a battery which provides the sample bias producing the tunneling current.

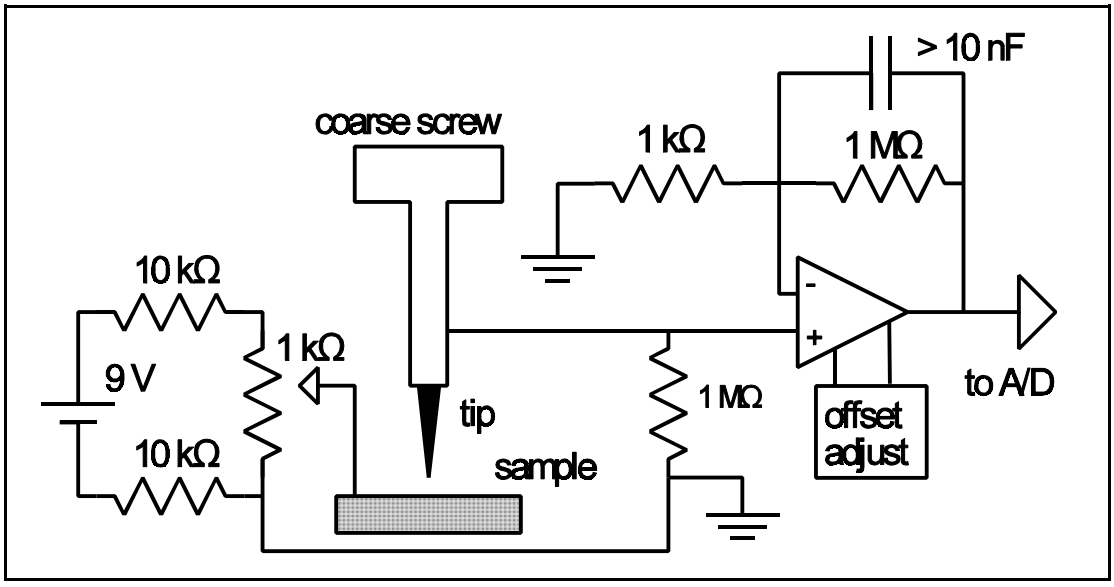

Figure 7:5. Electronics of the current to voltage converter.

The bias can be reversed by switching the leads of the battery. The tunneling current flows through the coarse positioning screw and a 1 megohm resistor. The potential drop across the 1 megohm resistor is multiplied approximately 1000 times by the op-amp circuit. Data from the output of the op-amp is recorded using an analog to digital (A/D) acquisition board controlled by the computer. The current to voltage conversion of the circuit is 1 volt/nanoamp. Due to the high gain of the circuit, and the antenna shape of the probe, electrical shielding of the setup was necessary. The shield was made of aluminum and covered all sides of the setup except where the fine adjustment screw extended to enable acess to manual adjustment. Experiments were done to test the integrity of the shield and these results are discussed in the following

section.

Coarse adjustment of the probe was performed while viewing the tip-sample spacing with a 30×, long focal length microscope. After coarse adjustment was made, the shield was mounted and grounded.

A computer program[6] was used to displace the translation stage over its 20 nanometer extension range while sampling the current/voltage value to detect the onset of a sufficient tunneling current. If, after a complete 20 nm translation of the specimen toward the probe, no tunneling current was detected, a manual adjustment was made to the fine adjustment screw, and the procedure repeated until a tunneling current was detected. The current data for each position of the stage was measured and recorded.

7.1.2 Design integrity evaluation

The design of the system must have sufficient integrity to provide confidence in measurements. Effects of electrical shielding, electronics stability, and thermal drift were evaluated to determine the integrity.

The output of the current to voltage converter was analyzed using an Advantest TR9403 digital spectrum analyzer. The tunneling probe was withdrawn from the sample a sufficient distance to prevent tunneling. Power spectrum plots were obtained for the setup with and without the electrical cover shield in place. Figure 7:6(a, c, and e) are spectrum plots for the shield removed and for frequency ranges of 100 Hz, 500 Hz, and 50 kHz respectively. Figure 7:6(a) shows a very sharp peak at 50 Hz, which corresponds to the power line frequency (England). The second

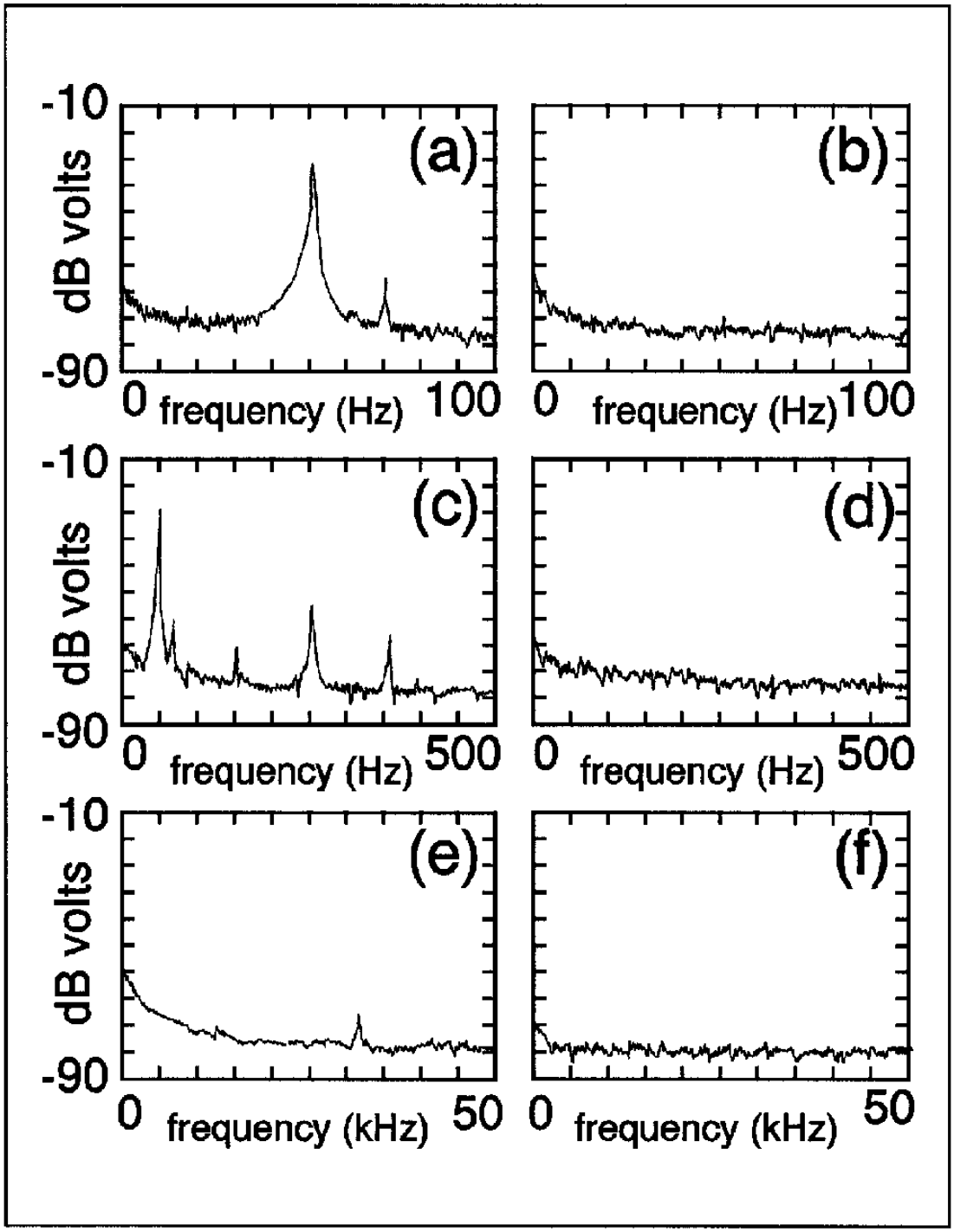

Figure 7:6. Power spectrum plots of the I:V converter output. (a), (c), and (e) were taken with the cover shield removed. (b), (d), and (f) were taken with the cover shield in place.

peak at 70 Hz is due to the refresh rate of the nearby computer monitor. Amplitude peaks for the first, third, fifth, and seventh order harmonics of the power line frequency are revealed in Figure 7:6(c). The peak around 31 kHz in Figure 7:6(e) corresponds to the horizontal sweep frequency of the computer monitor. Figures 7:6(b, d, and f) are power spectrum plots, corresponding to Figures 7:6(a, c, and e) respectively, with the cover shield in place. Figure 7:6(b) shows a barely detectable peak at -70dB for 50 Hz. The absence of any other detectable peaks in these plots demonstrate the effectiveness of the cover shield to remove noise induced into the probe by ambient electrical fields.

Figure 7:7 (a) and (b) shows power spectrum plots while ramping the coil voltage during translation stage motion. There is the small peak for 50 Hz at -65 dB. The frequency domain for Figure 7:7(a) is from 0-100 Hz and 7:7(b) is from 0-1 kHz.

Figure 7:8(a) is a plot of the output of the current to voltage converter over a 40 second period while there is no tunneling. It shows that there is about a 20 mV drift of the output due to the electronics circuit corresponding to an apparent current of 20 pA.

The tunneling probe was adjusted to bring a mechanically sharpened Pt-Ir tip[7] within tunneling range of an highly oriented pyrolytic graphite (HOPG) sample. Figure 7:8(b) is a graph of the I:V converter as a function of time while keeping the output voltage to the coil constant. The coil voltage was held at a value which produced 2 nanoamps of tunneling current. Along with some random drift corresponding to about

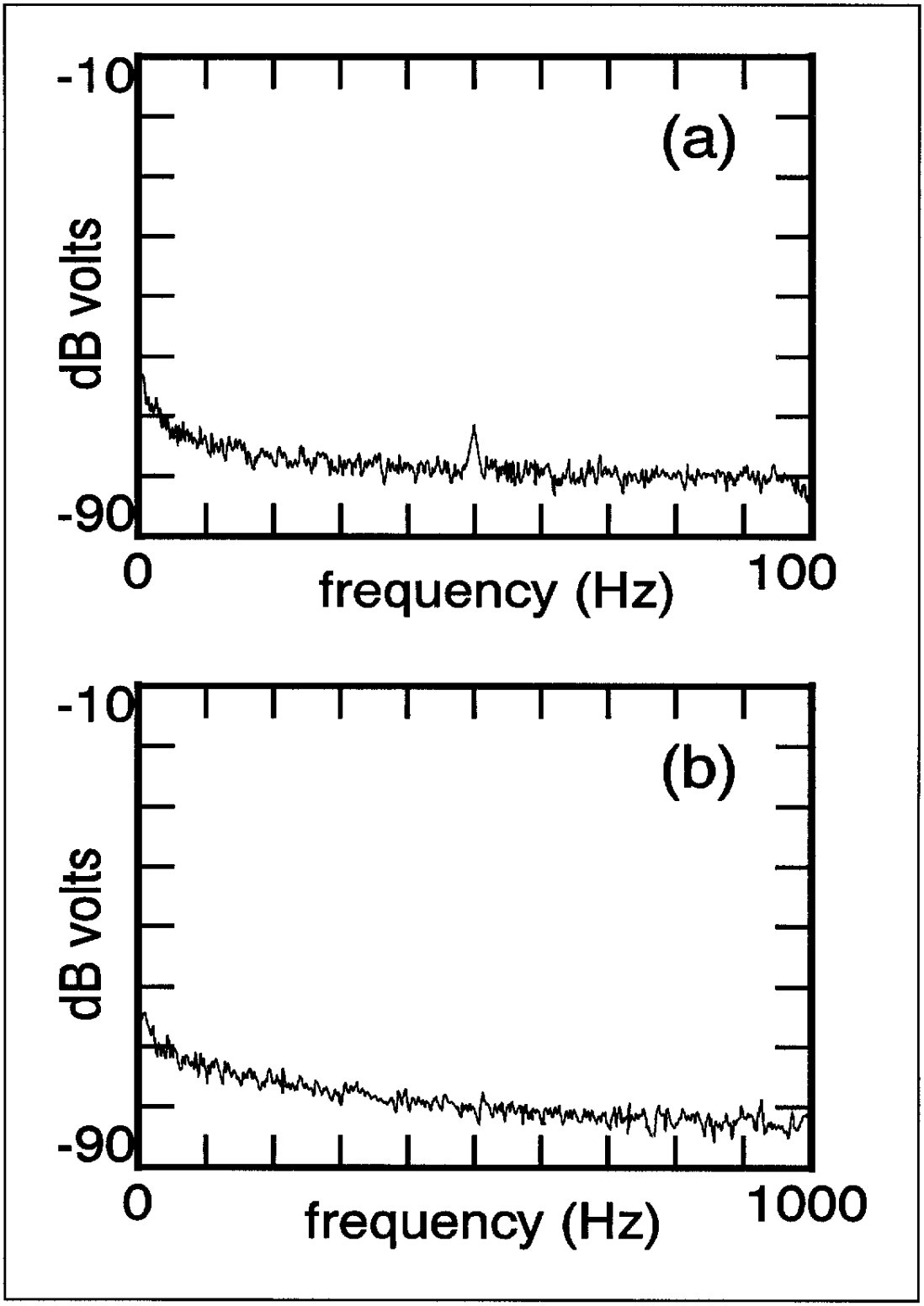

Figure 7:7. Power spectrum plot of the I:V output taken while sweeping the coil voltage. Frequency range is 100 Hz in (a) and 1 kHz in (b).

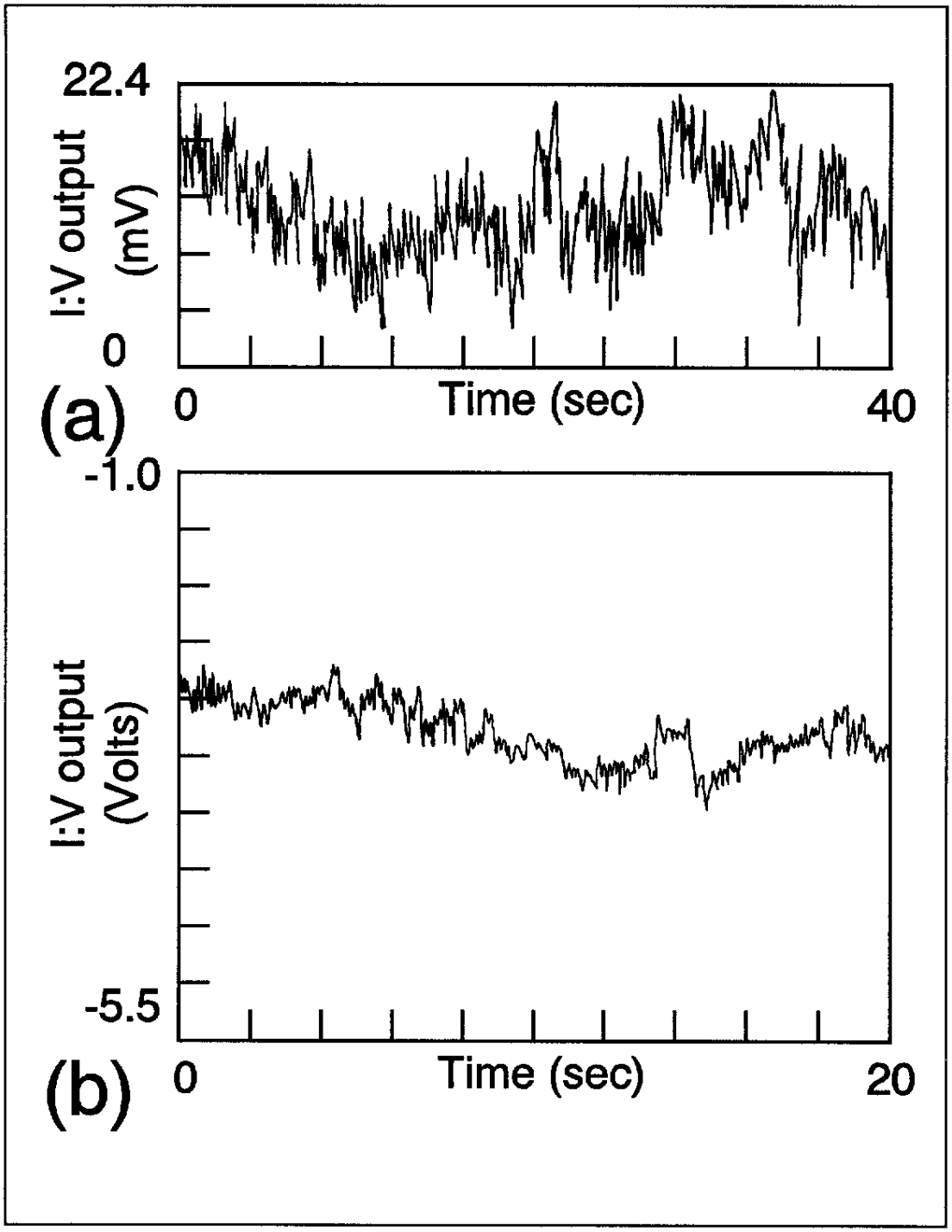

Figure 7:8. (a) I:V output with no tunneling over 40 second time period. (b) I:V output during tunneling for 20 second time period.

1.0 nanoamps, there appears to be abrupt changes in the current of around 0.4 nanoamps. The random drift may be due to thermal expansion of the materials. The abrupt changes in tunneling current between 6 and 8 seconds may be due to tip-sample electronic interaction effects. Power spectrum plots during tunneling would sometimes contain sharp peaks.

Figure 7:9 shows a tunneling curve and subsequent power spectrum plot for a Palladium-HOPG tip-sample system. The flexure was displaced to provide a tunneling current of 4 nanoamps. After the proper tunneling current was achieved, the power spectrum measurements were taken. This plot shows peaks at slightly less than 50 Hz and 100 Hz. A possible source for mechanical vibration is a nearby machine shop and a nearby road outside the building. Other I(s) curves and their power spectrums at maximum currents are contained in Appendix C.

The thermal stability is demonstrated in Figure 7:10(a) which shows six I(s) curves of data taken over a 15 min period. Notice the 1.5 nm maximum shift in displacement necessary to achieve the maximum current. Thermal stability is also established by the fact that the probe-sample separation was observed to remain within the 20 nm range of the translation stage over a five hour period.

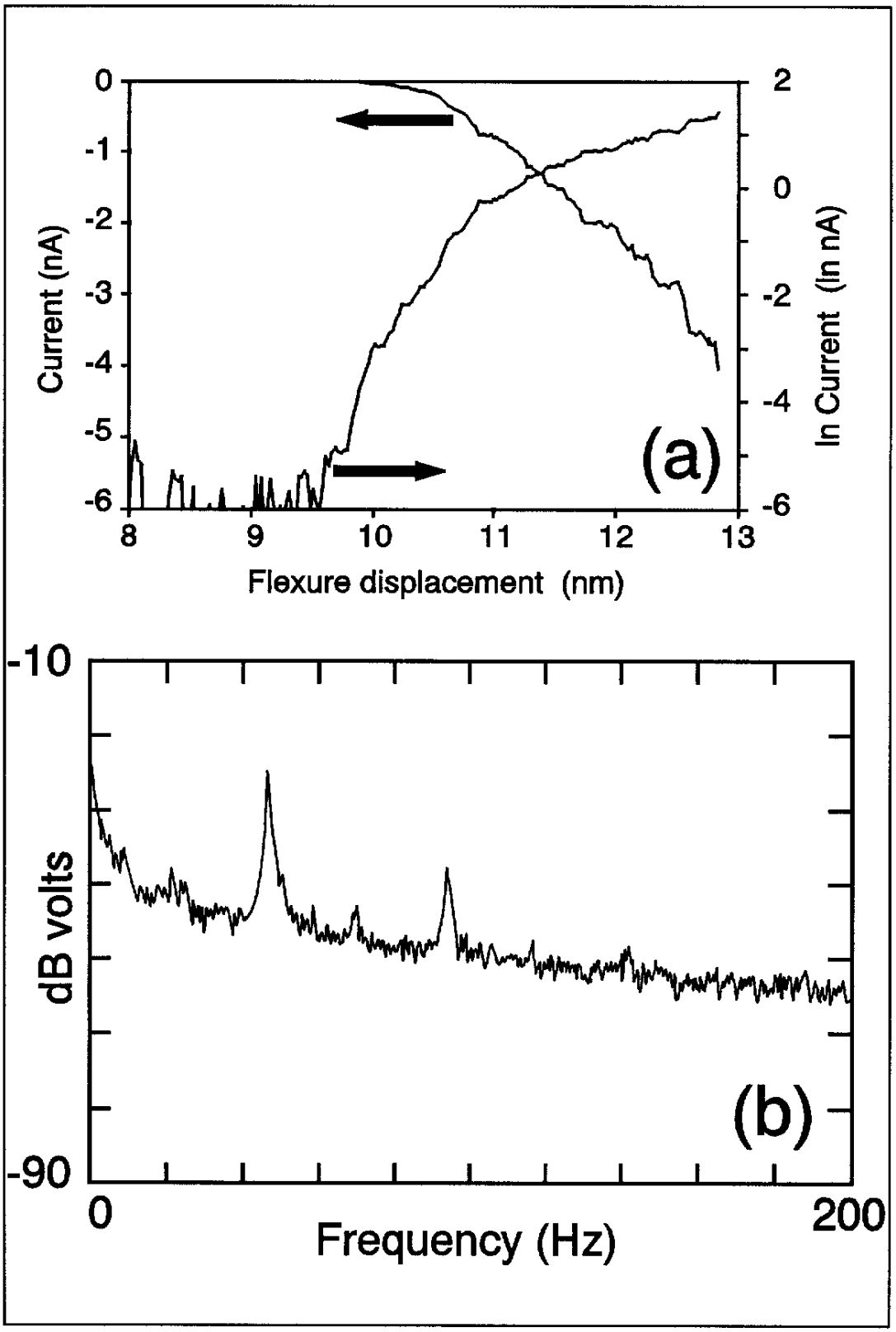

Figure 7:9. (a) Current and it's natural log versus flexure displacement for a Pd-HOPG system. (b) The power spectrum from the I:V converter for the maximum current in (a).

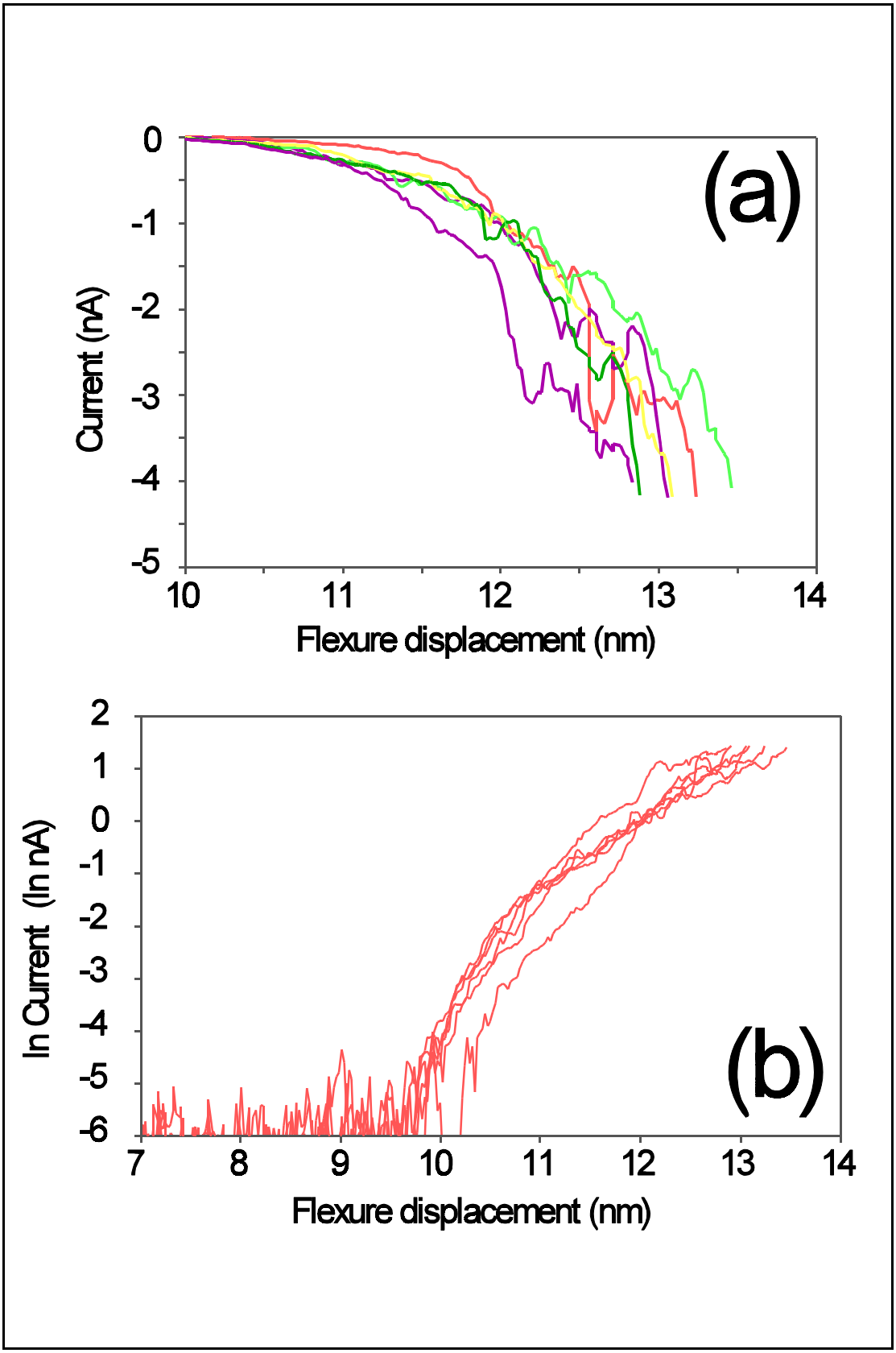

Figure 7:10. Six I(s) data sets taken over a 15 min period with the same tip are shown in (a) with there natural logs in (b). Total variation is less than 1.5 nm Illustrating thermal stability.

7.1.3 I(s) characteristics from data

Data sets were collected under ambient conditions at room temperature. Theoretically, we have previously shown in chapter 4 that the current should depend exponentially on the separation. This relationship is given mathematically by

$$I(s) = \frac{A}{s} e^{-\kappa s}, \ \kappa \approx 23 \ nm^{-1}. \qquad \textbf{(7-1)}$$

For separations, s, larger than 4/k, the slope of the natural log of the current should be equal to -k. This should be true regardless of your position over the surface. Figure 7:10(b) contains plots of the natural logarithms of the I(s) curves in Figure 7:10(a). Notice that the ln plots do not all appear the same. Indeed, not only do the slopes vary, but many plots contain multiple slopes. Least squares fits to the linear portions of these curves are plotted in Figure 7:11. The slopes of the lines are given with each plot and vary from 0.88 nm^{-1} to 5 nm^{-1}. These slopes are considerably lower than the calculated theoretical value of 23 nm^{-1} for an electron barrier of 5.3 eV (average value of work functions of Pt and graphite). Low barrier heights have been reported elsewhere.[8]

Similar results were obtained with different tip materials. Figure 7:12(a) shows plots of I(s) data taken with Pt-Ir, Ag, and Pd tips. The natural log of these data is plotted in Figure 7:12(b). The slopes for each line are shown on the graph in units of nm^{-1}. Appendix C contains more than 50 additional plots of of I(s) and ln I(s) data for Pt-Ir, Ag, and tips and the same HOPG sample. These not only include "good" data sets but also those in which there is apparent noise and other problems. Data with

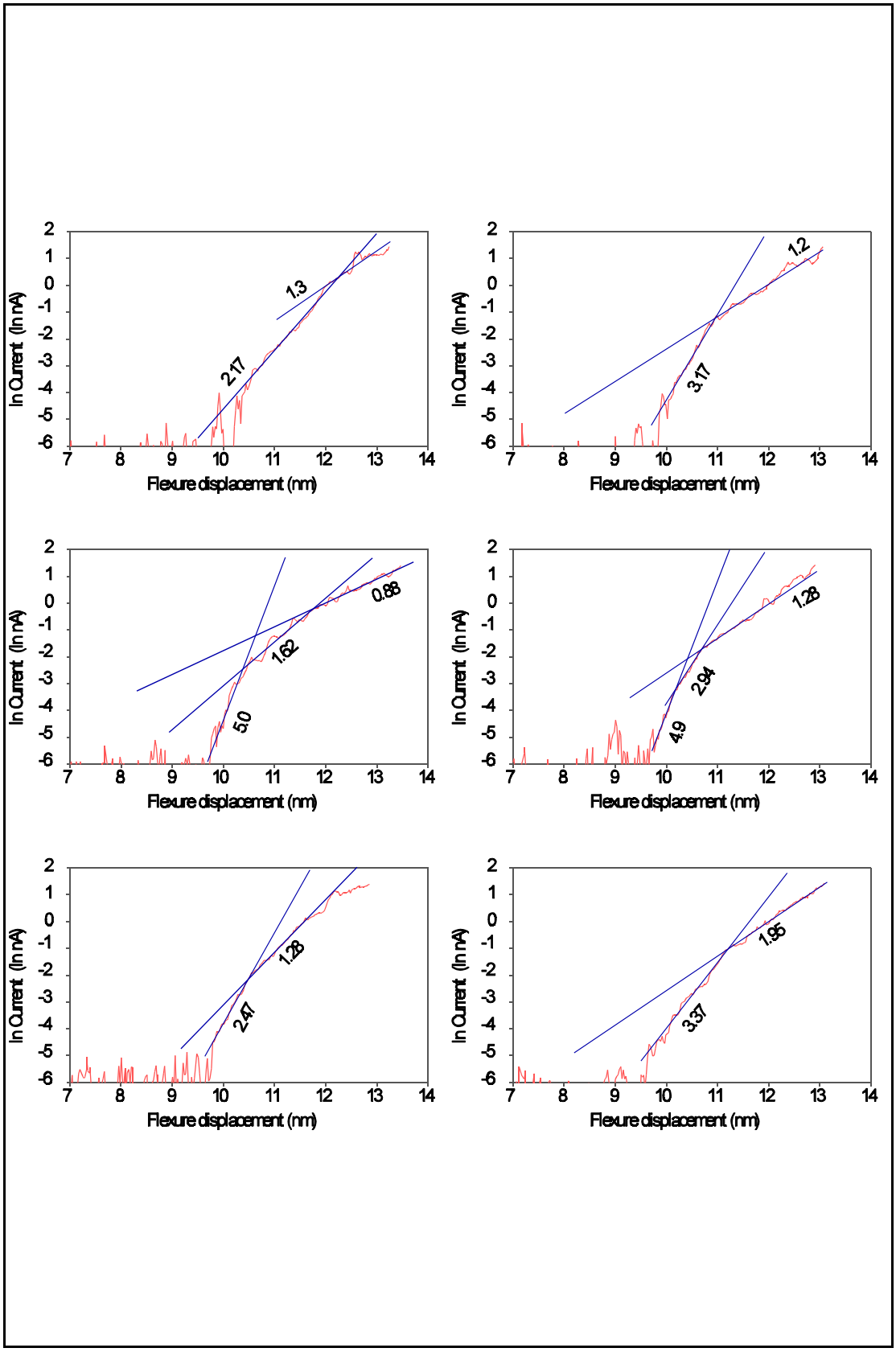

Figure 7:11. Plots of the natural log of the tunneling current versus flexure displacement using the same Pt tip and HOPG sample. Slopes are given for lines in nm^{-1}.

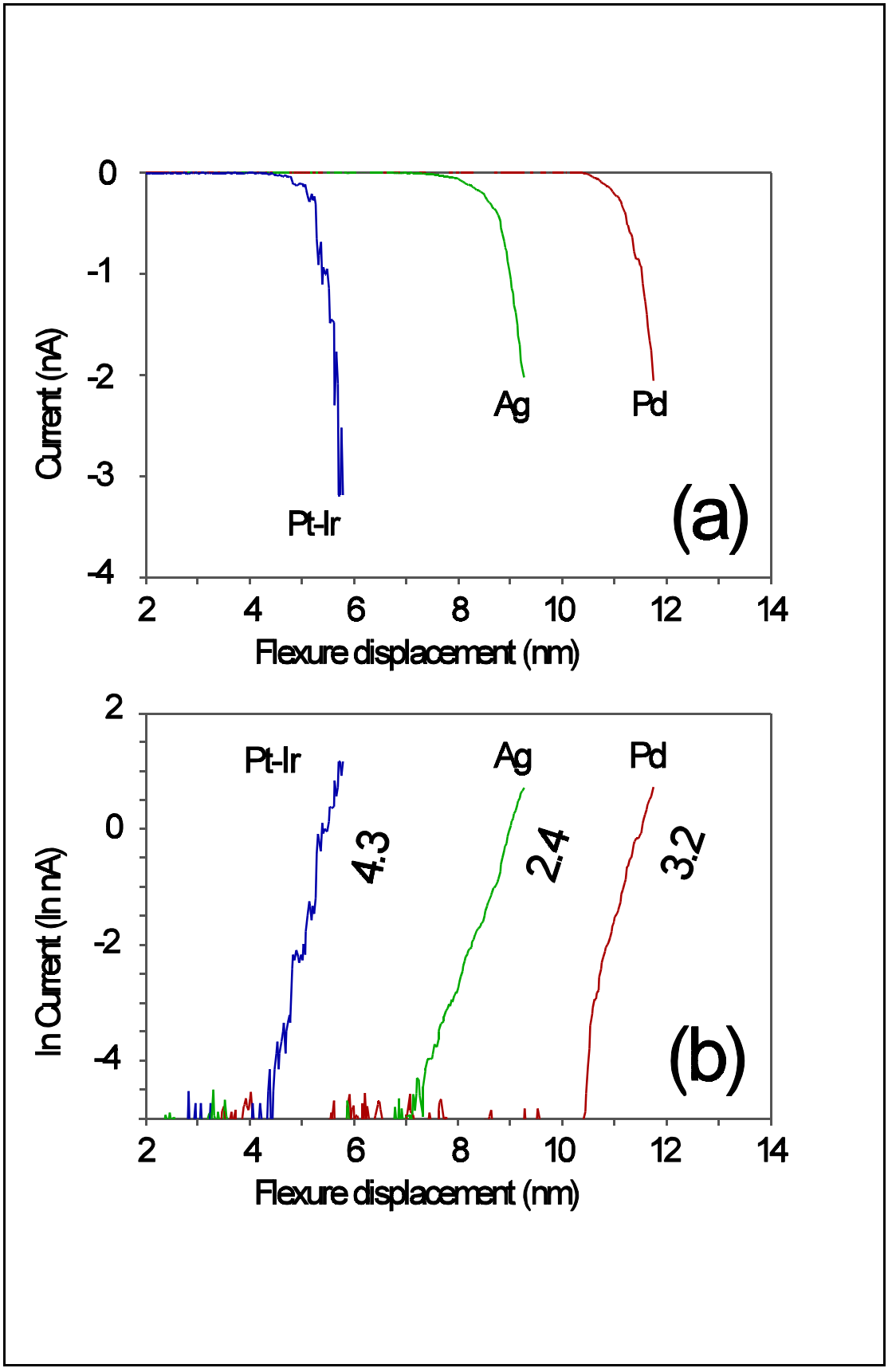

Figure 7:12. (a) current data and (b) natural log of the current versus flexure displacement for Pt-Ir, Ag, and Pd tips. The slopes have nm^{-1} units.

the same Ag tip showed variations in slope from 0.6 to 7.2 nm^{-1}. This may have been due to oxidation effects in the air ambient.

Since Pt and graphite are two materials that are inert in a room air ambient, we expect the combination to produce the most consistent I(s) data. The experimentation shows that I(s) are similar but not repeatable for a specific tip and highly variable for different tips. This causes problems if it is necessary to position the tip a repeatable distance away from the sample in order to manufacture a bit.

The nanometric shape of the tip may also play a role in non-ideal I(s) plots. Viewing various mechanically cut tips varied in a scanning electron microscope revealed that the tips were irregular on a micrometer scale. This, of course, does not necessarily infer similar geometries on a nanometer scale.

7.2 Results from Nanoscope II

The commercially available Nanoscope II STM is also capable of generating I(s) characteristics. This section describes experiments in air for the Nanoscope. The STM has the advantage over the x-ray calibrated instrument because surface images can also be obtained. These images can be used to ascertain the integrity of the tip. The STM has the disadvantage of having a z-axis that is more difficult to calibrate accurately.

7.2.1 STM z-axis calibration

The z-motion of the Nanoscope is produced by a tube made of a piezoelectric ceramic. In order to obtain reliable I(s) data it was necessary to affirm the z-axis calibration. We desired to evaluate the calibration reported by the manufacturer using the height of a monolayer step on an HOPG sample. Using the STM, we observed that the minimum observed height of steps was about 6.5 Å. This is roughly equal to twice the interlayer separation (3.35 Å) of graphite. Heights were only less than 6 Å when the STM image revealed multiple tunneling points[9].

There were three possible reasons for the observed step height. First, the graphite surface may prefer a double step to a single step. Second, a contamination particle could be between the tip and sample as suggested by Mamin *et al.* [1986]. This contamination contact would push the surface down as the tip approached the surface. Third, the reported calibration of the STM could be wrong.

The contamination theory was eliminated due to observed steps near 6 Å for many tips. The contamination is not likely for all the tips and the 6 Å spacing should have changed considerably with each tip depending on the variability of the contamination. The manufacturer was contacted about their calibration procedure. After discussion, they recalibrated a similar STM head using a known step and found that the true calibration was probably 40% less than their reported value. This calibration led to a measured step height near 4 Å. Since our STM head would have a slightly different calibration than theirs, we adjusted the

calibration to yield the step height to be the expected 3.35 Å. This step height would be accurate only if the electron states are similar on both sides of the step. Vertical linearity problems of piezoelectric had been minimized by Digital Instruments in the software. If contamination were causing a surface deflection, calibration from an atomic step height would also eliminate displacement errors if the contact was not localized at the tunneling point.

7.2.2 STM I(s) characteristics and atomic resolution

For an HOPG sample and Pt-Ir tip like that used in the previous section, the I(s) characteristics shown in Fig. 7:13 were obtained with a -40 mV sample bias and averaged over 5 data sets to remove noise. The ln I(s) characteristics show slopes higher than those in Fig. 7:11 obtained using the x-ray calibrated tunneling apparatus. STM images taken after the I(s) curves of Fig. 7:13(a-c) and before the curves in (d-f) are shown in Image 7:1. The images have not been filtered to remove any noise. Notice that the atomic corrugations are more discernible when the current is higher. The 0.2 nA, 1.0 nA, and 5.0 nA z-images have vertical atomic corrugations of 0.3 Å, 0.4 Å and 1 Å respectively.

One may expect the best images when the slope of the ln I(s) curve is nearest the theoretical 23 nm^{-1}, but this is not the case. Figure 7:14 contains an STM z-image and ln I(s) curves taken immediately preceding the image. Although the slopes are high, 8.9-16.9 nm^{-1}, the image shows very poor resolution. We have found this to be consistently the case when images are taken at currents that have

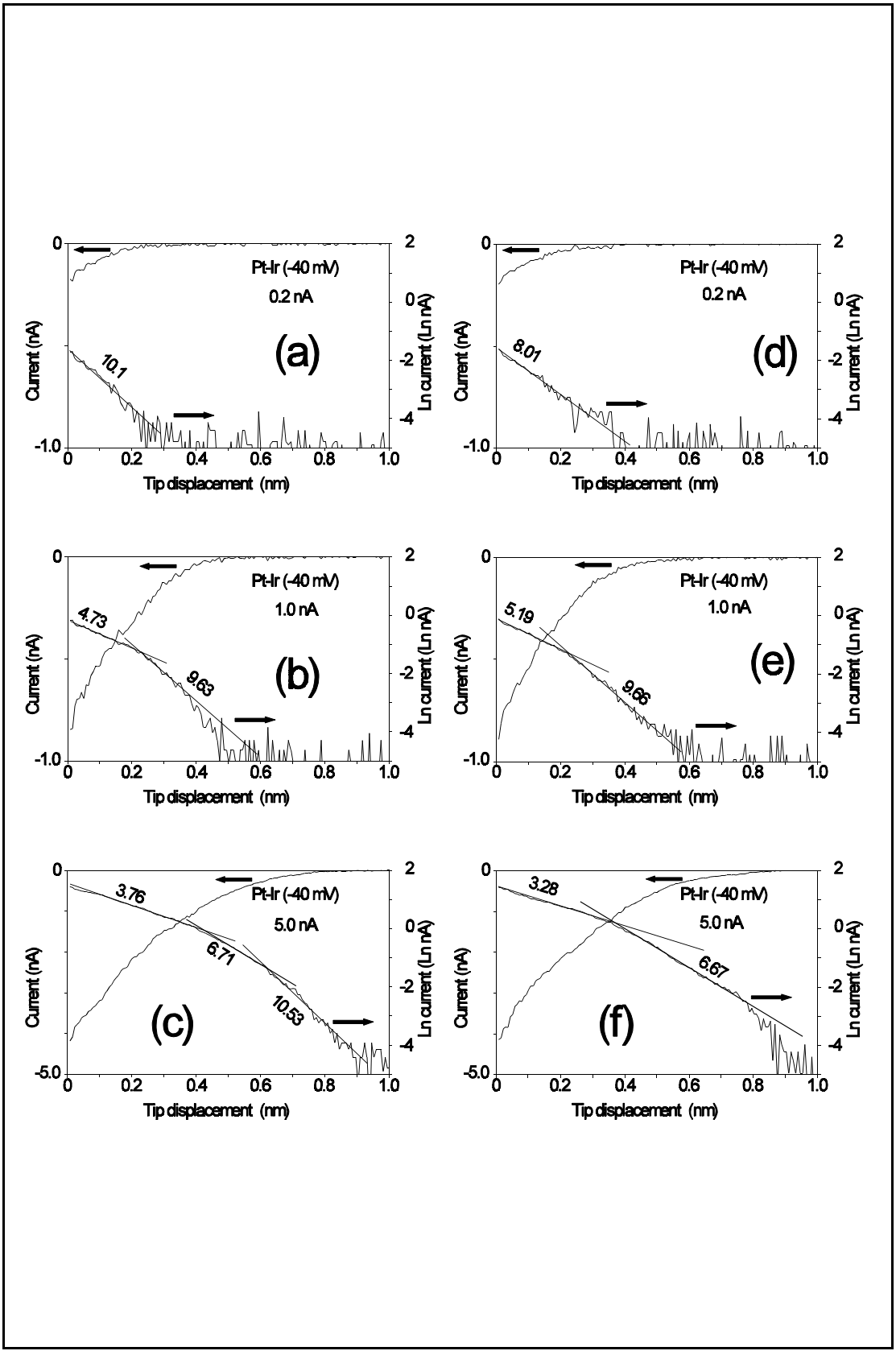

Figure 7:13. I(s) and Ln i(s) curves versus tip displacement taken with STM. Slopes to the Ln plots are given in nm^{-1}. Images taken at the maximum currents in (a-c) are shown in Image 7:1.

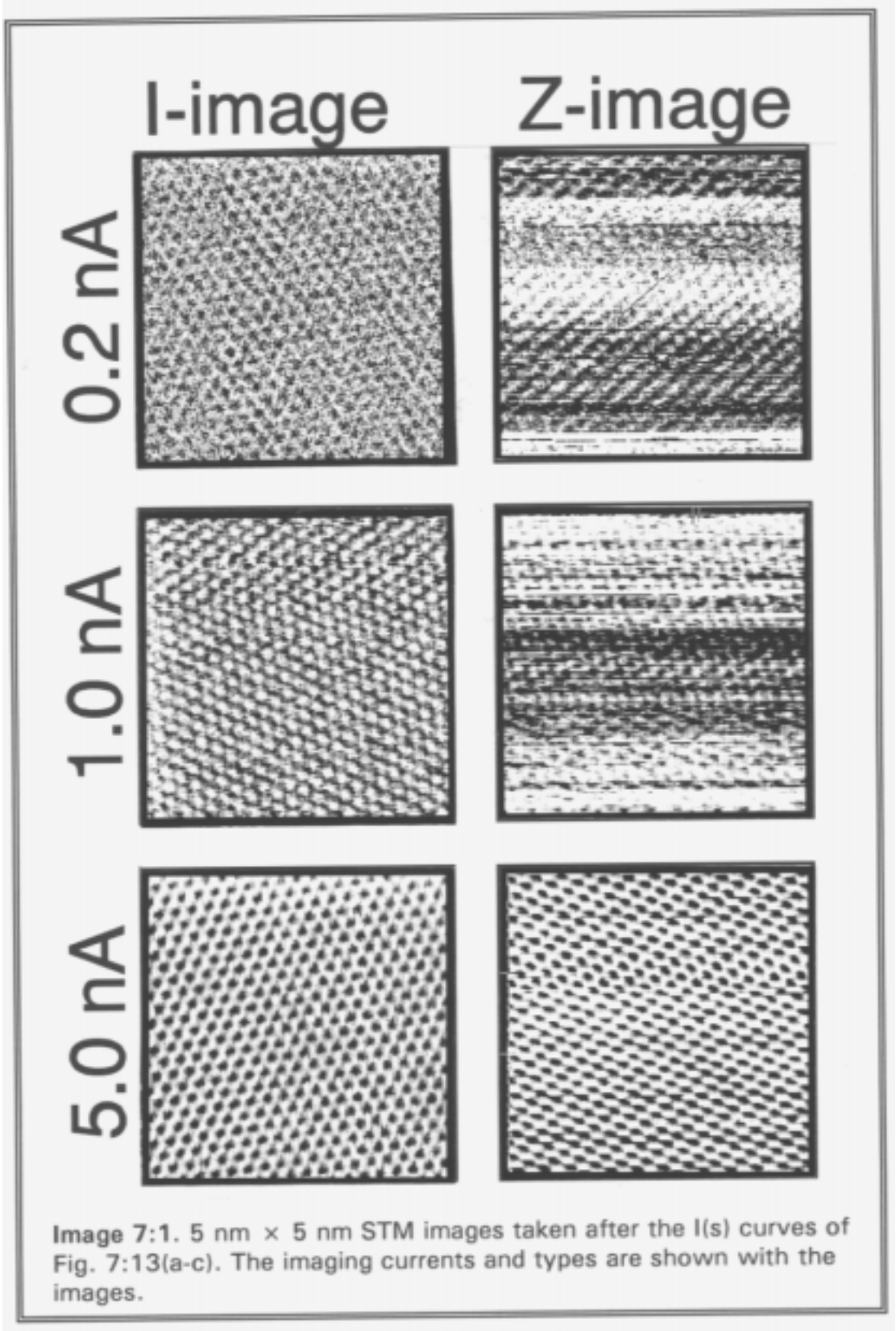

Image 7:1. 5 nm × 5 nm STM images taken after the I(s) curves of Fig. 7:13(a-c). The imaging currents and types are shown with the images.

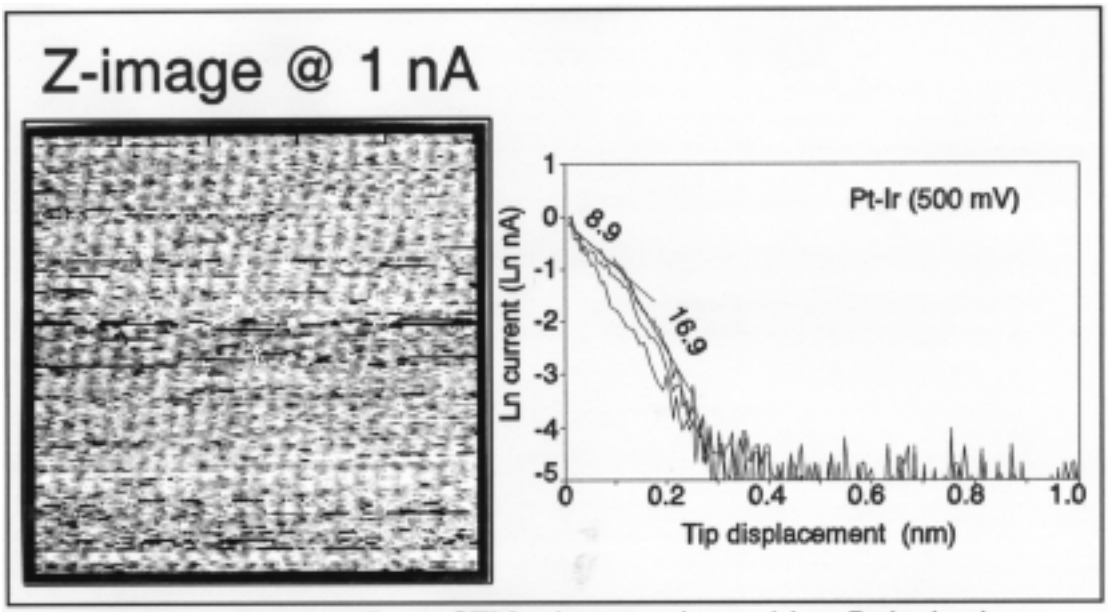

Figure 7:14. A 5 nm × 5 nm STM z-image taken with a Pt-Ir tip that produces Ln I(s) curves with high slopes. Slopes are in nm^{-1}.

corresponding high ln I(s) slopes at those currents. Notice also that the slopes of the ln I(s) curves at 0 (1 nA) have values differing by a factor of two even though the same tip is used and only a few minutes have elapsed between the data sets. This effect is common although not always as pronounced with most tips. This implies that the apparent barrier height which is related to the slope of ln I(s) curve would not be useful for reading memory bits.

7.2.3 Bias and pulsing dependence of I(s) characteristics

The effect of bias and pulsing on I(s) characteristics was determined by looking at I(s) curves for -50 mV and -500 mV before and after a voltage pulse was applied between the tip and sample. An electrochemically etched Pt-Ir tip[10] was used to give assurance of a small tunneling area. The tip gave accurate values for an HOPG atomic step and atomic resolution was achieved. The results are shown in

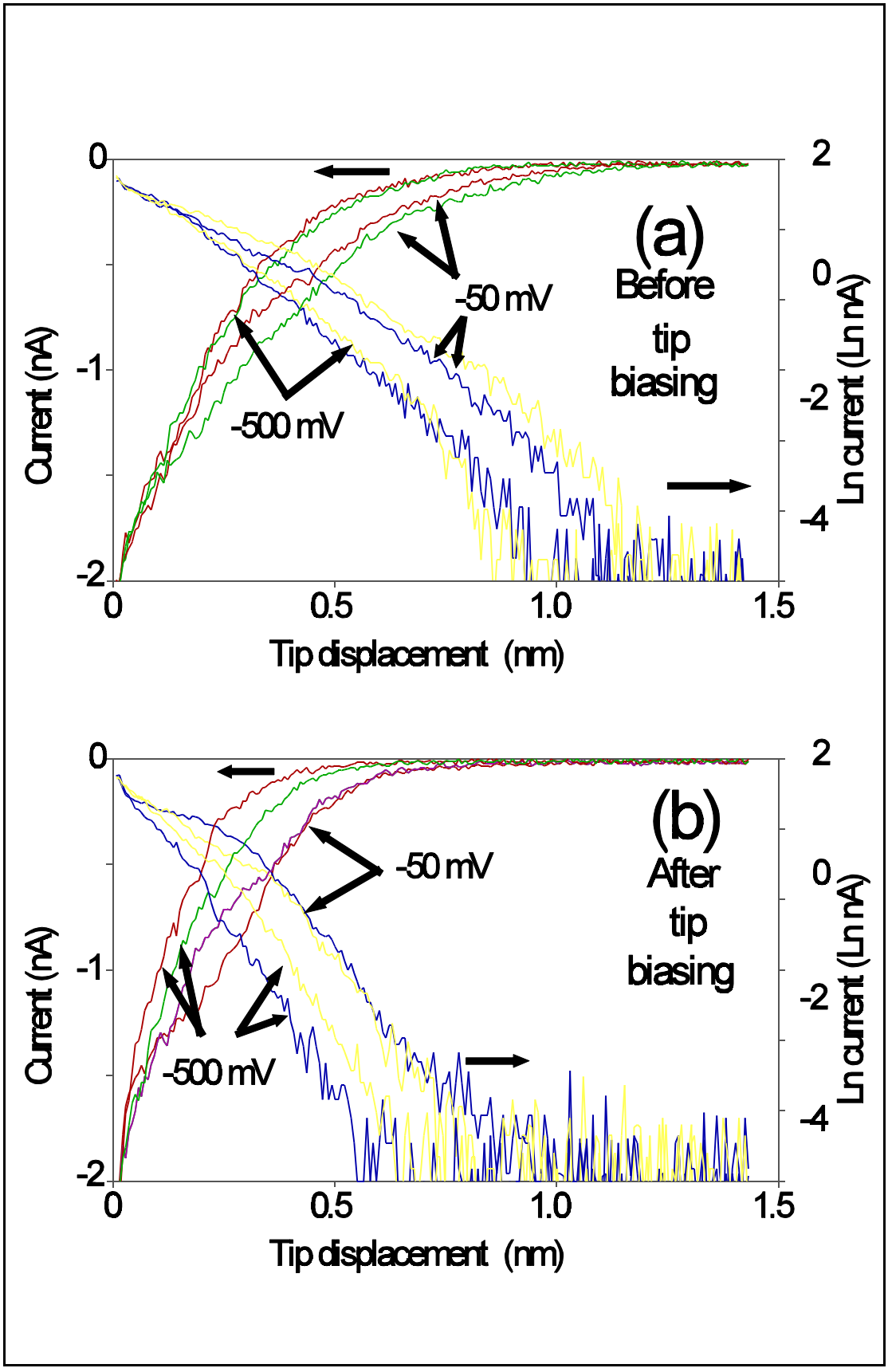

Figure 7:15. I(s) characteristics at -50 and -500 mV for an etched Pt-Ir tip. (a) is before and (b) is after an extended duration several volt tip bias.

Figure 7:15. Two I(s) curves are shown for each bias. ln I(s) curves are also plotted for easier comparison of slopes. Figure 7:15(a) shows the I(s) characteristics which reveal that the -500 mV curves have higher slopes. The higher bias does not necessarily mean that the field between the tip and sample is higher due to work function effects. A several volt bias was applied for several seconds which could simulate aging due to long term operation as a memory. I(s) curves after the bias are seen in Fig. 7:15(b). The -500 mV still produces steeper curves, but the -50 mV curves are steeper than those of the -500 mV curves before the bias. Imaging atomic steps after the bias revealed that there was a second tunneling point on the tip which probably affected the I(s) curves. Since the ln I(s) curves are steeper farther away from the sample, this second tip may have allowed the tip to be farther away from the sample for a given current, resulting in steeper slopes. This may be the reason that tips which produce steep I(s) curves have poorer resolution. Appendix C contains other I(s) and ln I(s) curves and their slopes for lower and higher initial currents. The major impact of this study shows that the distance between the tip and sample for a given current is likely to vary with tip and sample materials, tip geometry, and surface or tip contamination. The next section reveals that the I(s) characteristics also vary with changing ambient.

7.2.4 Ambient effects on I(s) characteristics

This study summarizes investigations into the ambient gas effects on I(s) characteristics. I(s) curves were taken for mechanically sharpened

Pt-Ir tips HOPG sample. The Nanoscope II STM was mounted inside a polycarbonate vacuum jar in order to be able to change ambient gases. The setup designed to switch the ambient is illustrated in Figure 7:16. The valves allow the ambient to be switched between filtered nitrogen or compressed air, nitrogen or air bubbled through deionized water, or a vacuum down to -29" Hg (≈25 Torr). Room air can also be introduced by disconnecting an appropriate tube and controlling the air flow through a valve.

The STM was operated in the spectroscopic mode to obtain I(S) characteristics for the various ambient gases. An average over twenty-five I(S) curves was obtained in order to significantly reduce the noise level. A fresh surface of the HOPG was obtained by placing a piece of tape on the surface and peeling it off, thus cleaving a slice from the

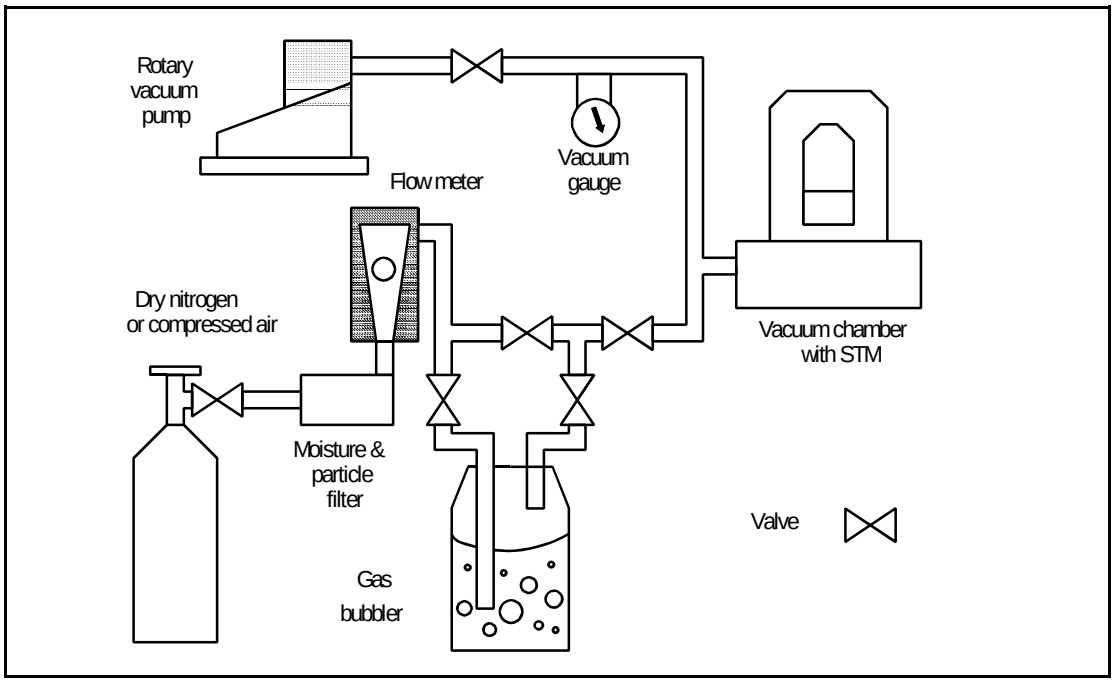

Figure 7:16. The laboratory apparatus setup used for switching tunneling ambient gases.

surface.

Measurements were taken with the sample at a potential of +50 mV. Initial I(s) curves were taken after atomic resolution imaging was demonstrated. Then, the ambient gases were sequentially introduced and characteristic current data recorded. The most profound changes occurred while switching between N_2 bubbled through DI water and a vacuum near -29" Hg. Graphs of the data are shown in Figure 7:17.

Analysis of the natural log data shows that the initial I(S) data set after the cleave and in air has the highest slopes (-10.2 and -6.74 nm^{-1}). Most of the data taken during this relatively low vacuum show slopes near -3.9 nm^{-1} (-3.89, -3.93, -3.85, and -3.21). The slopes increased the longer the ambient was at a vacuum near -29" Hg. The I(s) curves taken when nitrogen was bubbled through deionized water ambient were significantly more elongated than those taken with vacuum. The moisture may be responsible for the expanded curves during bubbling. Since the vapor pressure of water is between -28" Hg and -29" Hg at room temperature, the vacuum may be evaporating most of that deposited from the ambient onto the surface or tip.

Other experiments with a -40 mV (reversed polarity) bias showed the curves elongating with the introduction of nitrogen or nitrogen bubbled through DI water. However, the restoration of steeper I(s) characteristics was not consistently produced with a vacuum. One possible explanation is that the negative bias decreased the current forcing the tip into the sample causing irreversible changes. Another is

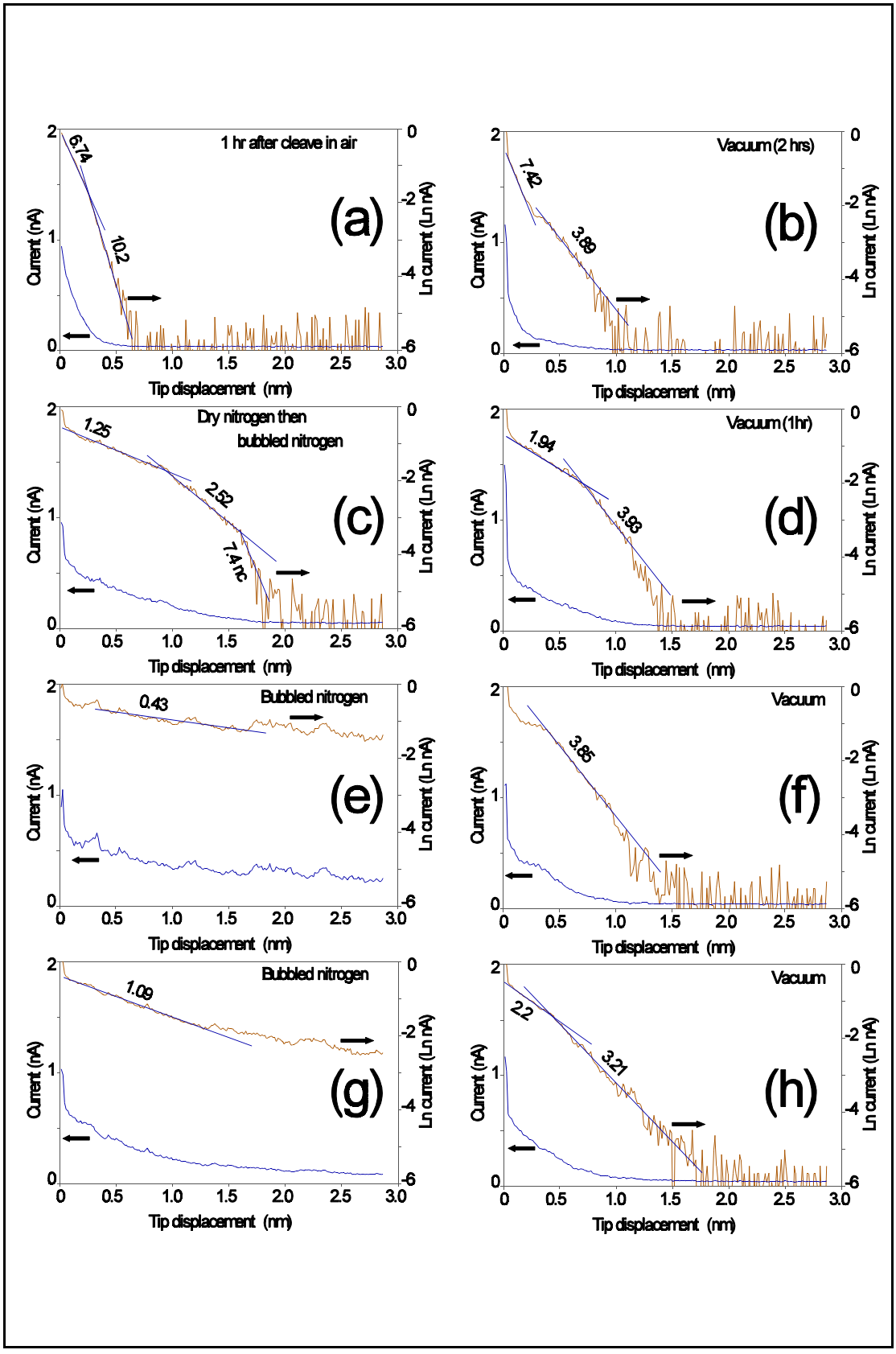

Figure 7:17. I(s) and Ln I(s) curves taken for various ambients. The ambients are shown for each graph. The sequence of ambients reflects the sequence of graphs (a-h). Slopes are reported in nm^{-1}.

that the direction of the current affects the evaporation of surface moisture on the tip or sample.

The results of this investigation show that the ambient plays a definite role in determining the I(s) characteristics. This in turn will affect the separation between the tip and sample for a given tunneling current.

7.3 Summary and Significance of results

We have shown that tunneling I(s) characteristics vary depending on several things. These are listed in Table Table 7-1. One is that the I(s) characteristics vary between individual tips due to material and geometric reasons. A second is that each individual tip shows similar, but slightly varying I(s) curves over time. A third factor causing variation is the magnitude of the applied bias. A fourth variation is the history of the tip and is revealed with the application of a voltage pulse. And a fifth parameter is the ambient condition. All of these things cause the I(s) characteristics to alter which produces an unpredictable spacing between the tip and sample.

Table 7-1. Parameters which affect the I(s) characteristics.

1] Individual tip variation (material, geometry etc.)
2] Tip variation over time.
3] Applied bias.
4] History of tip (voltage pulses and tip-sample contact)
5] Ambient conditions (gas, contamination, etc.)

This unpredictable spacing will affect the write and readability of the proposed memory. The uncertain separation will produce a corresponding uncertain electric field strength thus effecting surface modification. Voltage pulses also effect the I(s) curves and, thus, the spacing which in turn affects the modification. This may account for the necessity of changing the parameters to continue making modification which was reported in Chapter 4.

The effect on readability is demonstrated by Figure 7:18. Using a tunneling probe as a detector of memory bits one would have to take into account the changes in the I(s) characteristic. For example, if the height of the probe changed from 1 to 2 nanometers then there could be a 2 nm change in apparent width of a nanometer scale memory bit as shown in Fig. 7:18. Also, changes in the probe geometry (dull or sharp) could amplify the problem.

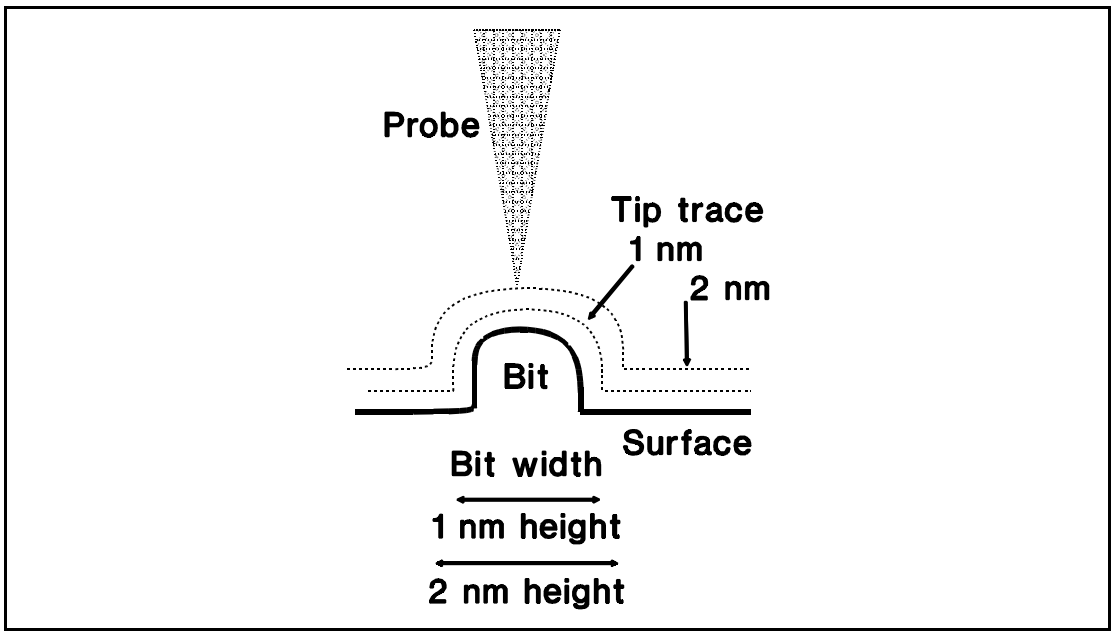

Figure 7:18. Illustration showing the apparent change in width of a surface feature for different probe scanning heights.

[1] Bocko, Mark F., Stephenson, Kendall A., and Koch, Roger H., "Vacuum Tunneling Probe: A Reduced-Back-Action Transducer", Phys. Rev. Lett. **61**, 726 (1988); Bocko, Mark F., "The scanning tunneling microscope as a high gain, low noise displacement sensor", Rev. Sci. Instrum. **61**, 3763 (1990).

[2] Wandass, Joseph H., Colton, Richard J., and Murday, James S., "Magnetic field sensor and device for determining the magnetostriction of a material based on a tunneling tip detector and methods of using same", U. S. Patent #US5103174

[3] Quate, Calvin F., "Method and means for data storage using tunnel current data readout", U. S. Patent # US4575822, Mar. 11, 1986.

[4] Chetwynd, D. G., Cockerton, S. C., Smith, S. T., and Fung, W. W., "The design and operation of monolithic x-ray interferometers for super-precision metrology", Nanotechnology **2**, 1 (1991).

[5] Smith S. T., and Chetwynd, D. G., "An optimised magnet-coil force actuator and its application to linear spring mechanisms", Proc. Inst. Mech. Eng. **204(C4)**, 243 (1990).

[6] Written by Salam Harb at University of Warwick.

[7] Commercially available from Digital instruments.

[8] Batra [1988], Wang [1990], Binnig [1984], Gimzewski [1987], Coombs [1986], and Lang [1988] (theoretical).

[9] Another example of a tip tunneling through multiple points is given in Chapter 9.

[10] Longreach Scientific Co., Orr's Island, Maine.

Chapter 8.

I(s) Electronic Considerations

In previous chapters ln I(s) graphs were shown which were not linear. This nonlinearity is not in agreement with simplified tunneling theory. One speculation for the cause of this has already been mentioned, that of intimate tip-sample contact. The purpose of this chapter is to show that a nonlinear curve can be theoretically predicted using more detailed quantum theory. Also, experiments will be reported which suggest that the tunneling current is affected by the electronic states of surface electrons. These results are used to explain ln I(s) slopes which are not continuous but tend toward discrete values.

8.1 Tunneling revisited

In tunneling theory, like other theories, assumptions are made to gain simplified practical approximate solutions. As these solutions are pushed to their limits, the approximations no longer hold and significant departures from experimental results may be observed. A common basic assumption of tunneling theory is that the barrier changes abruptly at the electrode surfaces and is constant or linear in between. Another assumption is that a squared hyperbolic sine term is sufficiently large to be approximated as exponential. If the tunneling bias is held to a low constant value, these assumptions yield the approximated[1] tunneling equation

$$I(s) = \frac{I_o}{s} e^{-2k_o\sqrt{\phi_o}s}, \qquad \textbf{(8-1)}$$

where I_o, k_o, and ϕ_o are intrinsic constants. The 1/s tunneling prefactor was supplied by Simmons for the theoretical current flow between two parallel planar electrodes separated by a distance s. For platinum and graphite electrodes this produces a ln I(s) equation of the form

$$\ln I(s) = A_o + \ln(\frac{1}{s}) - 23 \cdot s, \quad \textit{and its derivative} \quad \frac{d \ln I(s)}{ds} = \frac{-1}{s} - 23 \text{ nm}^{-1}, \qquad \textbf{(8-2)}$$

where s is in nm, and A_o is a constant. This equation has a slope magnitude that is always greater than 23 nm^{-1} and increases at smaller separations. This is the opposite of what has been observed experimentally. This discrepancy can be reconciled if one considers the fact that the barrier potential is not constant, but changes significantly as the electrode spacing decreases below 1 nm.

8.1.1 Barrier calculation using image charge potentials

The barrier potential energy, $\phi(x,s)$, at a position x between electrodes of spacing s is

$$\phi(x,s) = \phi_{im}(x,s) + \phi_v(x,s) + \phi_w(x,s) - E_F \; . \qquad \textbf{(8-3)}$$

where ϕ_{im} is the image charge potential of the electron between the tunneling electrodes, $\phi_v(x,s)$ is the potential function due to a bias between electrodes, ϕ_w is the potential function due to the work function[2] difference between the electrodes, and E_F is the Fermi energy.

The difference in work functions, ϕ_w, between a platinum tip (ϕ_t = 5.65 eV) and a graphite sample (ϕ_s = 5 eV) is 0.65 eV.

The classical solution for the image potential of an electron between

$$\phi_{im}(x,s) = \frac{-e^+}{4\pi\epsilon}\left[\frac{1}{2x} + \sum_{n=1}^{\infty}\left(\frac{ns}{n^2s^2-x^2} - \frac{1}{ns}\right)\right], \qquad \textbf{(8-4)}$$

two infinite equipotential conducting planes is given by the equation

where ϕ_{im} is in eV, s is the spacing between electrodes, and x is the position of the electron between the electrodes. ϵ is the dielectric constant of the region between the electrodes (normally that of free space) and e^+ is the magnitude of the charge on an electron. This solution is cumbersome to work with, although a summation of the first 10 terms yields 0.1% accuracy. Simmons suggested the approximate equation

$$\phi_{im}(x,s) \approx -1.15\,\frac{Ln(2)\,e^+}{8\pi\epsilon}\,\frac{s}{x(s-x)}. \qquad \textbf{(8-5)}$$

This solution is adequate for s > 1 nm, but it is near or below this region which tunneling occurs. Also as $s \to \infty$, this equation **does not** reduce to the classical equation of an electron near a single conducting grounded plane

$$\phi_{im}(x,s) = \frac{-e^{+}}{8\pi\epsilon x}. \qquad \textbf{(8-6)}$$

As a much better fit to the numerical solution, the following approximate equation[3] is introduced.

$$\phi_{im}(x,s) \approx \frac{-Ln(2)\,e^{+}}{8\pi\epsilon}\left(\frac{s}{x(s-x)}\right) e^{\left(\frac{0.55(s-2x)^2}{s^2+0.5(s-2x)^2}\right)}. \qquad \textbf{(8-7)}$$

This equation was deduced by the application of appropriate boundary conditions and the observed exponential error between the numerical solution and Simmons' approximation. Modifying Eqn. (8-5), the 1.15 prefactor that Simmons introduced to make his equation fit the data was dropped. Then an exponential multiplicative term was included to account for the observed error. The exponential power argument had to obey certain conditions. Symmetry is one such condition, that is, the value of ϕ at x must be the same at s-x. Also, as $s \to \infty$, the exponential term must reduce to $[Ln(2)]^{-1} \approx e^{0.55/1.5}$ so that Eqn. (8-7) reduces to Eqn. (8-6) for an electron near an infinite conducting plane. Equation (8-7) does indeed have symmetry and reduces to the classical equation for an electron near a plane.

The numerical summation [Eqn. (8-4) n=1 to 500], the Simmons equation [Eqn. (8-5)], and Equation (8-7) are plotted in Fig. 8:1 (a) and (b) for s=1 nm and s=0.5 nm respectively. The bold dash-dot line in Fig. 8:1 (a) and bold line in Fig. 8:1(b) represent the Fermi energy, E_F of a graphite electron. The area above E_F and below the potential is related to

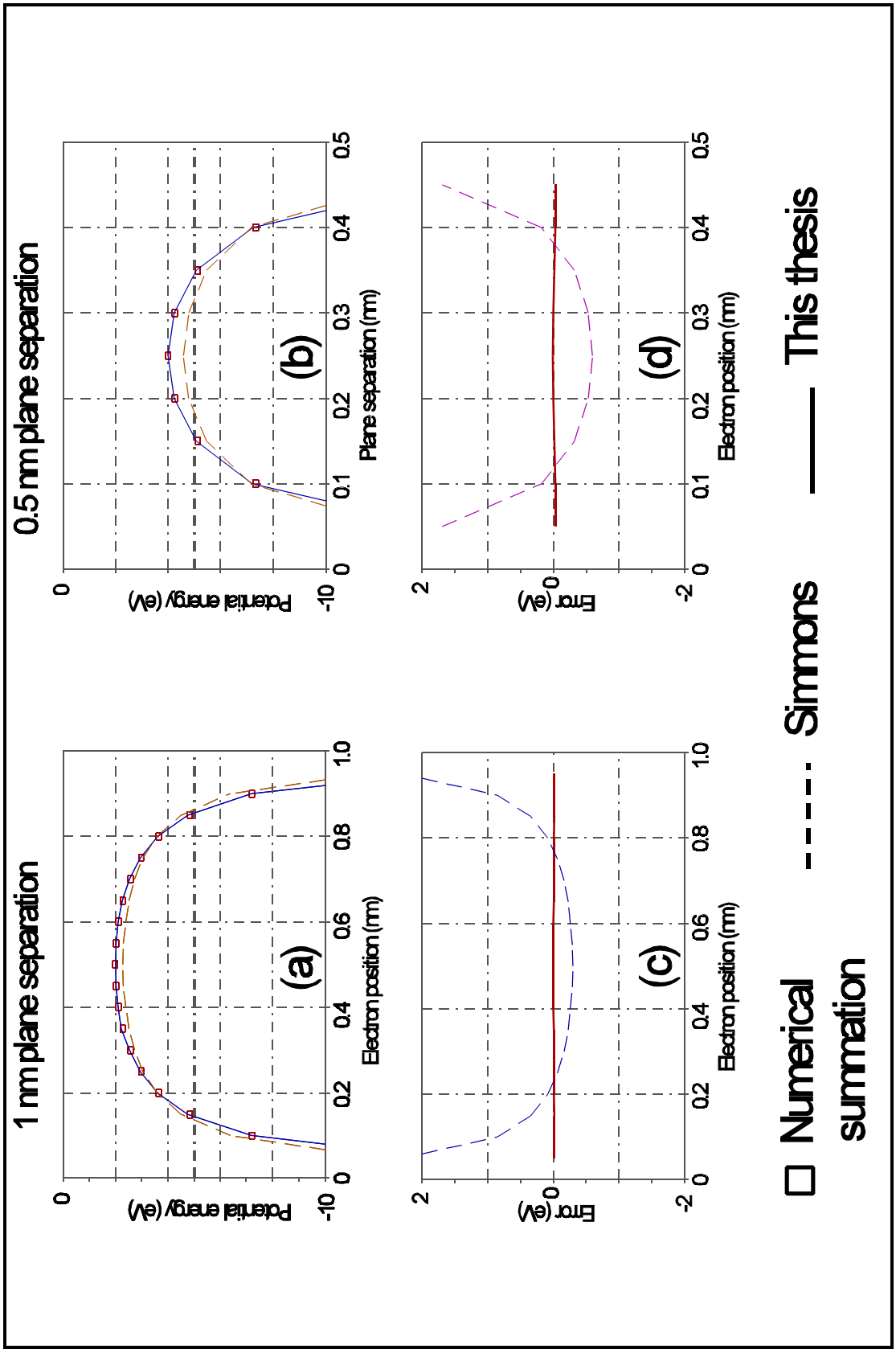

Figure 8:1. Electron image potentials calculations (a) and (b) and estimation errors (c) and (d) between two planes using equations (8-4) (numerical), (8-5) (Simmons), and (8-7) (this thesis).

the barrier integrity, B(s) [$\phi^{½}$s term of Eqn. (8-1)] and is defined more rigorously in Equation (8-8) . Figure 8:1(b) shows that the Simmons equation produces a significantly incorrect evaluation of the barrier at 0.5 nm. Figure 8:1(c) and (d) show the deviation from the numerical solution for each of the approximate solutions in Fig. 8:1 (a) and (b).

Using Eqn. (8-7) for ϕ_{im} and assuming no work function difference or applied potential between the electrodes, the $\phi(x,s)$ graphs shown in Figure 8:2 were obtained. Notice the degradation of the barrier as the electrode spacing decreases below 1 nm. The presence of a bias alters the symmetrical shapes of these graphs and is included in the forthcoming calculations of the barrier.

8.1.2 Theoretical slope determinations for ln I(s) curves

By considering the effect of the image potential upon the electron barrier, it will be shown that decreasing values for the slopes of ln I(s) curves can be expected.

Simmons' work emphasizes the exponential term but disregards the transmission prefactor[4] for an electron incident on a tunneling barrier. Combining Simmons' I_o/s surface charge related current prefactor[5] with the transmission probability flux prefactor for a single electron of kinetic energy E_k, incident on a barrier of average energy V(s), yields the basic tunneling equation

$$I(s) = \frac{I_o}{s}\left[1 + \frac{\left[e^{-k_o B(s)} - e^{-k_o B(s)}\right]^2}{16\,\frac{E_k}{V(s)}\left(1 - \frac{E_k}{V(s)}\right)}\right]^{-1}, \qquad \textbf{(8-8)}$$

where $V(s) = E_k + \frac{1}{s}\int \phi(x,s)\cdot dx$, *and* $B(s) = \int \phi(x,s)^{½}\cdot dx$

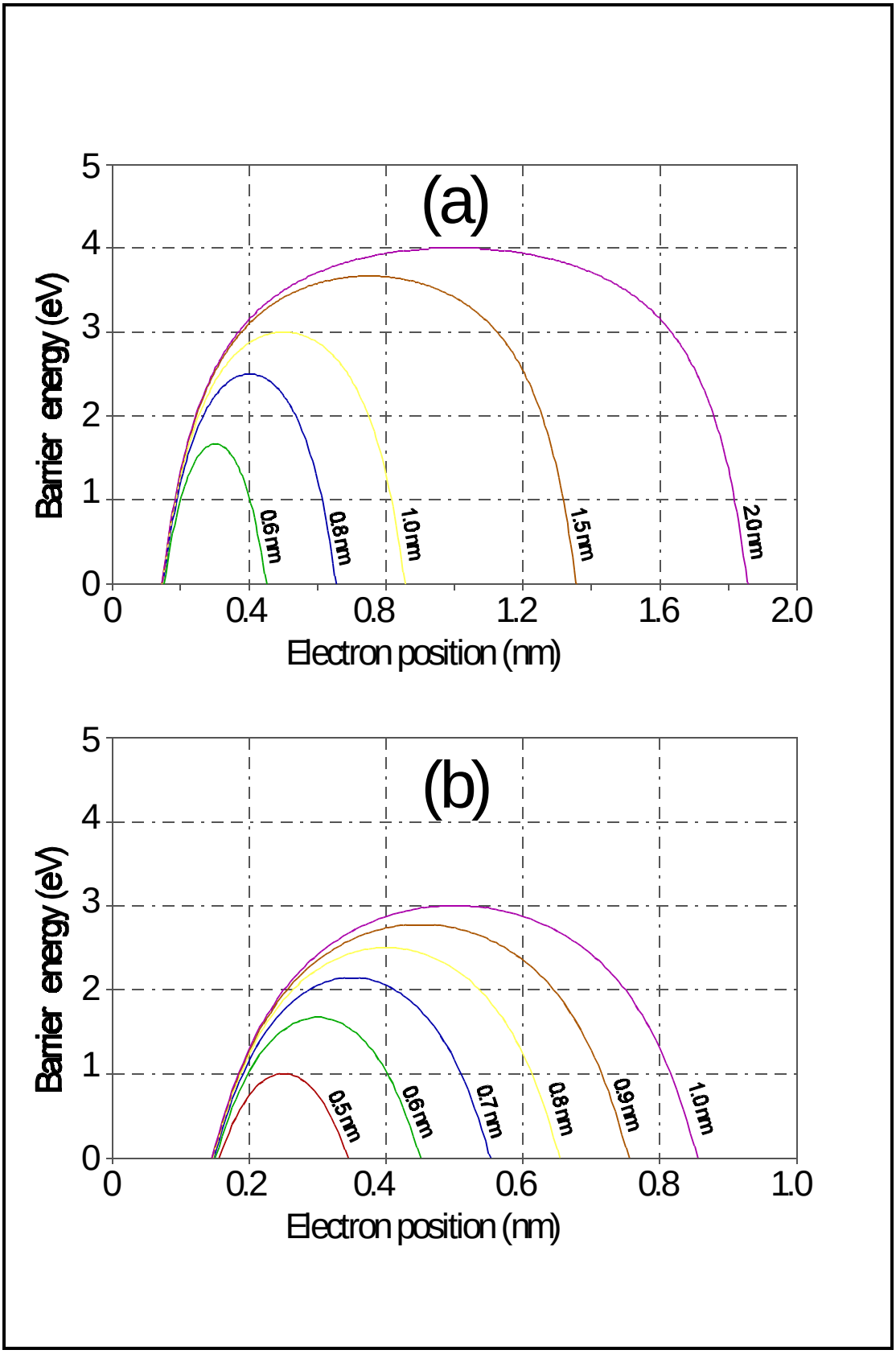

Figure 8:2. Electron barrier energy as a function of electron position between two HOPG planes of various spacing. (a) shows separations up to 2 nm and (b) shows separations below 1 nm.

k_o is equal to $(2m^*)½2\pi h^{-1}$, where m^* is the effective mass of the electron and h is Plancks constant. The function, B(s). is hereafter called the *barrier integrity*. It is derived from the WKB[6] approximation. The WKB approximation includes k_o in the term so that the transmission probability per unit time, D, of an electron is

$$D = e^{-2K},$$

$$\text{where } K = \int_{x_1(E_x)}^{x_2(E_x)} \left[\frac{2m^* \cdot 4\pi^2}{h^2} \left[V(x) - E_k \right] \right]^{\frac{1}{2}}. \qquad \textbf{(8-9)}$$

The term $V(x)-E_k$ is equal to $\phi(x,s)$, where V(x) is the potential barrier the electron sees and E_k is the kinetic energy of the electron. x_1 and x_2 are the edges of the barrier.

An approximation[4] of Eqn. (8-8) which reveals the additional transmission prefactor, T(s), is

$$I(s) \approx \frac{I_o}{s} T(s)\, e^{-2k_o B(s)} = \frac{I_o}{s} \left[16 \frac{E_k}{V(s)} \left(1 - \frac{E_k}{V(s)} \right) \right] e^{-2k_o B(s)}, \qquad \textbf{(8-10)}$$

The barrier integrity, B(s), was calculated for ±0.65 V potentials between the planes and is shown as square symbols in Figure 8:3(a). The ±0.65 V potentials correspond to a 0-1.3 V bias due to the 0.65 V work function difference between sample and tip. For comparison, the barrier integrity for a linear barrier (**not** including the image force) is shown with a dashed line. A empirically determined equation for B(s) using a linear-exponential sum was found to be

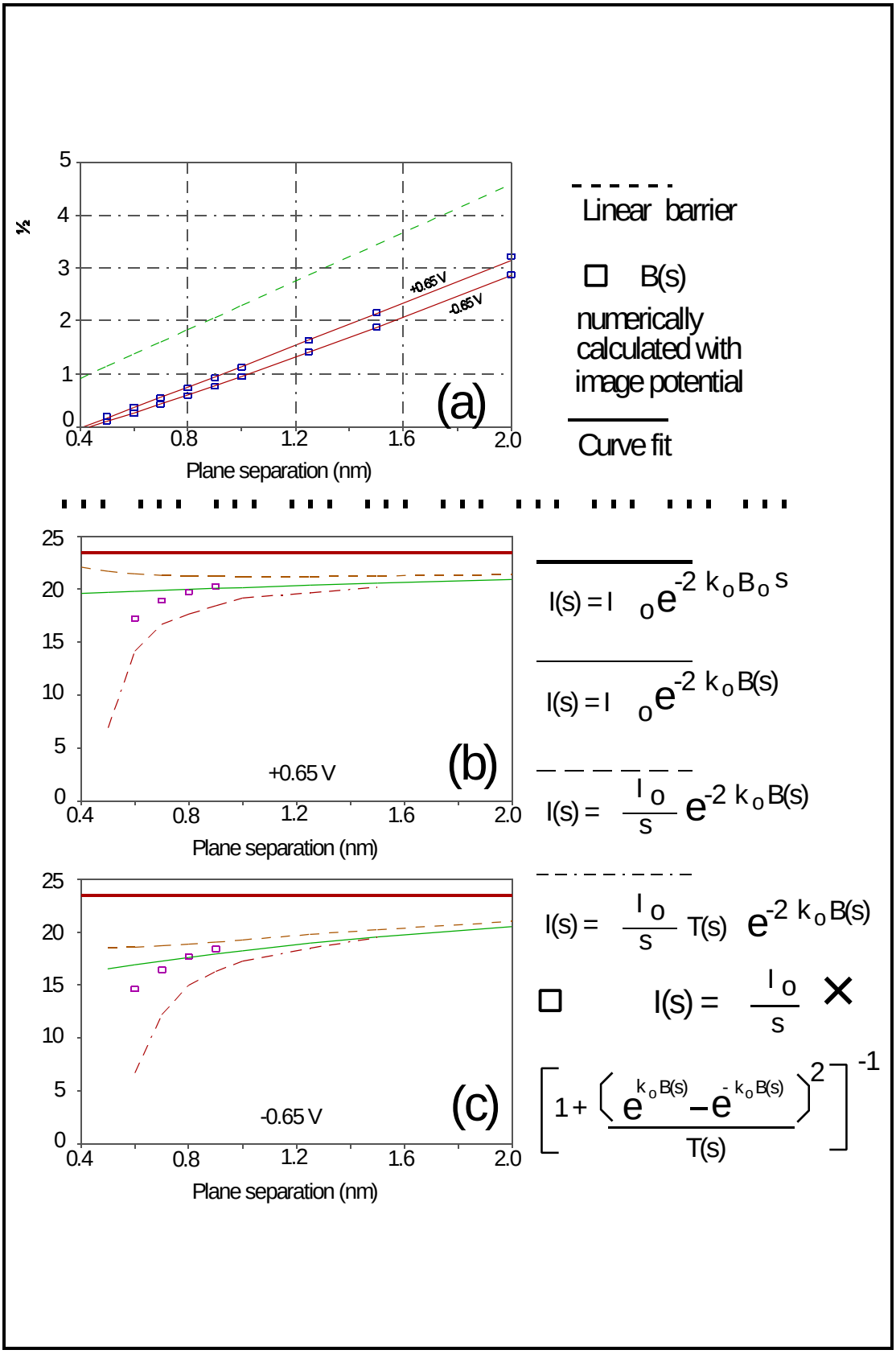

Figure 8:3. (a) Barrier integrity for a linear barrier and image potential barrier with applied voltages of ±0.65 V. (b) and (c) Resultant theoretical slopes of Ln I(s) curves at ±0.65 V for increasingly detailed I(s) equations.

$$B(s) = A_o + 2.29 \cdot s + 1.6e^{\left[\frac{-s}{s_o}\right]}, \qquad \textbf{(8-11)}$$

where s is in nanometers and B(s) is in $(eV)^{½}$nm. For a potential of 0.65 V, A_o=2.38 $(eV)^{½}$nm and s_o=3.8 nm. For a potential of -0.65 V, A_o=2.23 $(eV)^{½}$nm and s_o=1.75 nm. The empirical curve fits of Eqn. (8-11) for ±6.5 V potentials are shown graphed in Figure 8:3(a). Using Eqn. (8-11) and the correct constants for the barrier integrity, the expected slopes of ln I(s) curves were calculated for increasingly detailed current equations. These are shown in Figs. 8:3(b) and (c) for +0.65 V and -0.65 V respectively. As the I(s) equations become more detailed, the slopes are found to decrease a substantial amount as the electrode spacing decreases below 1 nm. This agrees with our experimental observation of decreasing slope values.

The prefactor I_o is a constant in Simmons equation, but actually depends on the barrier integrity which changes substantially for s < 1 nm. Although this would decrease the slope further, it was not included since this value may actually approach a limiting value[7] in more detailed theory. However, it has been shown that slopes of ln I(s) are predicted to decrease as two planar electrodes approach each other for separations less than 1 nm. Since real tips are conical and not planar, an accurate prediction of the rate of change of slopes is theoretically much more complicated. However, a similar trend is expected.

8.2 Surface potential corrugations

Another important result of including the image potential is that the barrier disappears when the planes are about 0.4 nm apart depending on the electrode potential difference. It is near this distance where the electronic corrugation of the surface becomes manifest when scanning atomically flat surfaces in the STM. These corrugations are thought to be due to the bonding of the solid, such that, the valence electrons do not have close spherical orbits around the positively charged atomic nuclei. The bonding of electrons forces them to be localized between the atomic cores.

Using a hexagonal single layer[8] of graphite, classical electrostatic potential calculations were made as a function of position, x, normal to the layer. The potentials were calculated by summing (superposition) a series of potentials due to point charges according to the classical equation

$$V(r) = \frac{q_n}{4 \pi \epsilon r(x)} \quad ,$$

where q_n is the charge at a given position in the graphite lattice and r is the distance between the charges and the point where the potential is being calculated.

Illustrated in Fig. 8:4, the static model potential calculations consisted of atomic cores ($+4e^+$) at hexagonal graphite lattice positions, 3 bonding electrons/atom spaced midway between the lattice positions

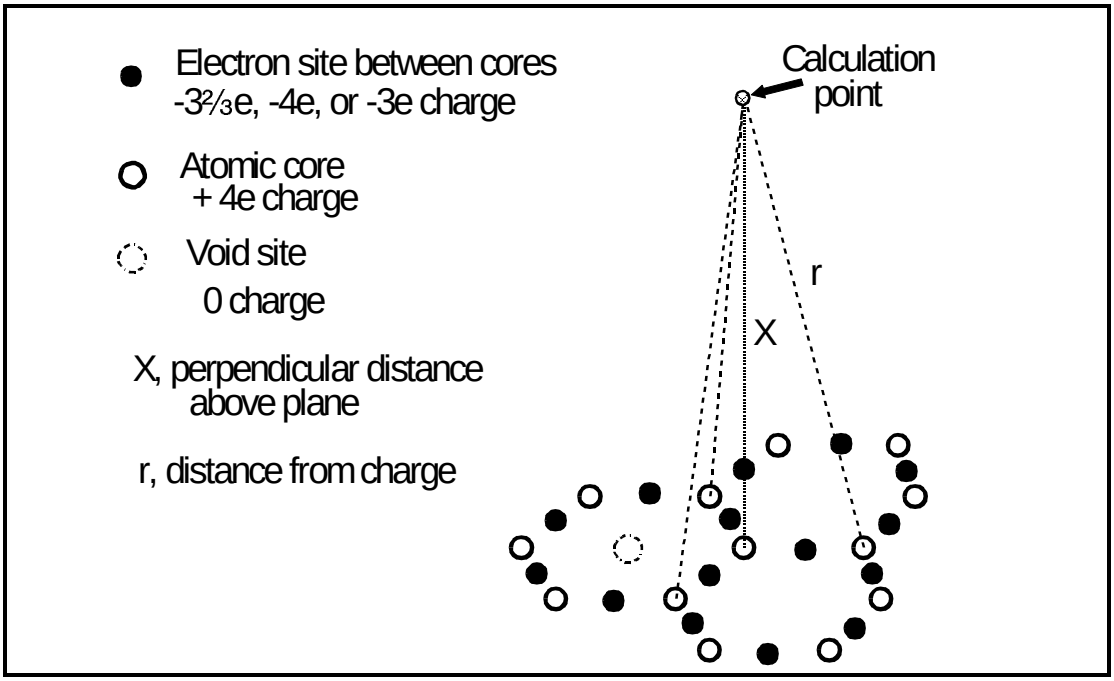

Figure 8:4. Illustration of the method used for calculation of potentials above a graphite sheet. Three lines illustrate the symmetry of calculations.

(atomic cores), and one free electron/atom also midway between atomic cores. Since the free electron resonates between the three bonding positions, a charge of $2e^+/3$ was placed at each of the positions of bonding electrons for initial calculations. The equation was of the form

$$V(x) = \sum_{1}^{n} V(q_n,r_n) \text{ where } \sum_{1}^{n} q_n = 0$$

or

$$V(x) = V(q_1,r_1) + V(q_2,r_2) + V(q_3,r_3) \ldots + V(q_n,r_n)$$

such that

$$q_1 + q_2 + q_3 \ldots + q_n = 0$$

To keep the charge neutrality of the finite plane, the superposition summation was required to have an equal number of positive and negative charges[9]. This required summing the potentials due to hundreds of atoms (over 1000 charges). In order to simplify the calculations by

symmetry, the potential was only calculated over the atom site, electron site, and void site. The summation was done from closest charges radially out from the calculation position.

The resulting calculated potentials at positions above the three sites are shown in Figure 8:5(a). Since the potentials are substantial to near 0.2 nm, they probably affect the tunneling barrier as it diminishes. Since an electron must be present in order to tunnel, the potential above the electron site is most relevant. By holding the free electron fixed at different positions, the potentials of Figure 8:5(b) were obtained. Although the potential above an electron site with a free electron absent appears to be substantial beyond 0.2 nm, the potential probably converges[10] as more atoms are included.

These calculations were carried out by constraining the electron in the plane. If Fig. 8:5 (a) and (b) were inverted (i. e. in eV units) they could be added directly to the barrier potentials for calculations. This was not done because they serve only as an estimation of how far the electronic corrugation extends for the graphite plane. In the real situation (dynamic not static), the free electrons are not planar but move in and out of the plane depending on the electrons' state[11]. The amount these electrons move in and out of the plane will affect the surface potential corrugation and influence the tunneling barrier (at 0.2 nm) as the plane separation approaches 0.4 nm. Since the electron can only exist in discrete states, this may be responsible for discrete values of ln I(s) slopes.

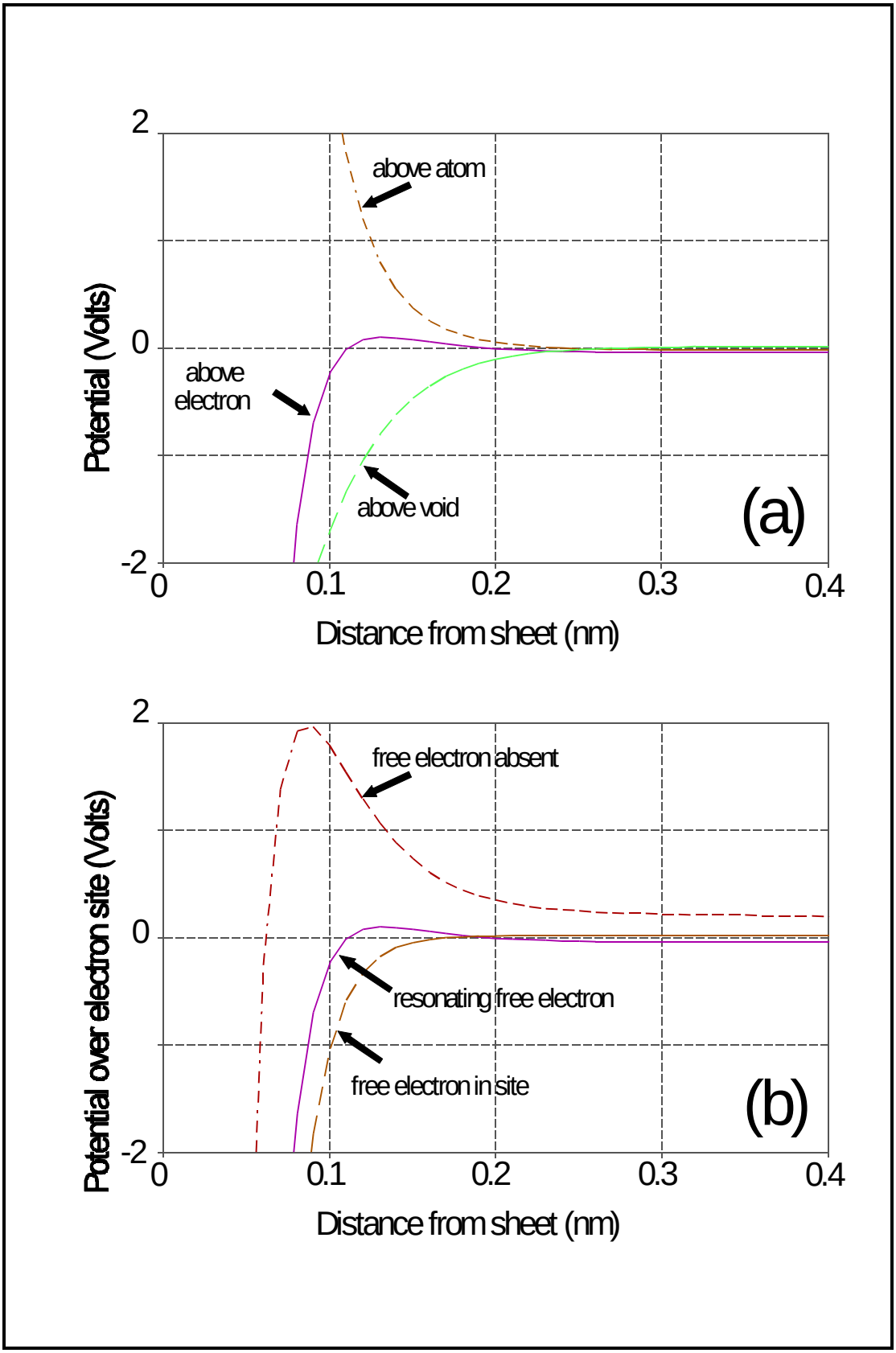

Figure 8:5. Static calculation of potentials above a graphite sheet. (a) Above atom, void, and resonating electron sites. (b) Above electron site for resonating and fixed position electrons.

8.3 Anomalous STM imaging of graphite

STM has produced a set of anomalous images of the surface of graphite. Previous attempts to explain these images include tip and second layer electronic effects. Representative images were produced with the same tip by using mechanical and electrical stimuli. Using a Pt-Ir tip[12], HOPG was imaged[13] in air over an extended period of time and the surfaces shown in Image 8:1 were obtained. The various images were induced by mechanical tapping of the STM or by electronically switching the bias between ±0.1 V. The effect of the tapping or bias switching was not predictable with the most attempts producing some apparent surface electronic alteration.

Image 8:1(a) is representative of a "normal" dual trigonal surface. Notice that the I-image contains current maxima (represented by the white areas), current minima (represented by the dark areas) and saddle points of intermediate current (represented by the grey areas). Image 8:1(b) shows an image of a hexagonal ring pattern and Image 8:1(c) shows an image of a row pattern. Image 8:1(d-f) reveals various step patterns observed.

Anomalous surface images have been explained using various models of tip electronic/geometric structure[14]. Some of these models consider the current flowing between the surface and multiple atoms on the tip with the atoms either separated or side by side at the tip apex. The electronic state of the outermost electron of the apex atom has been

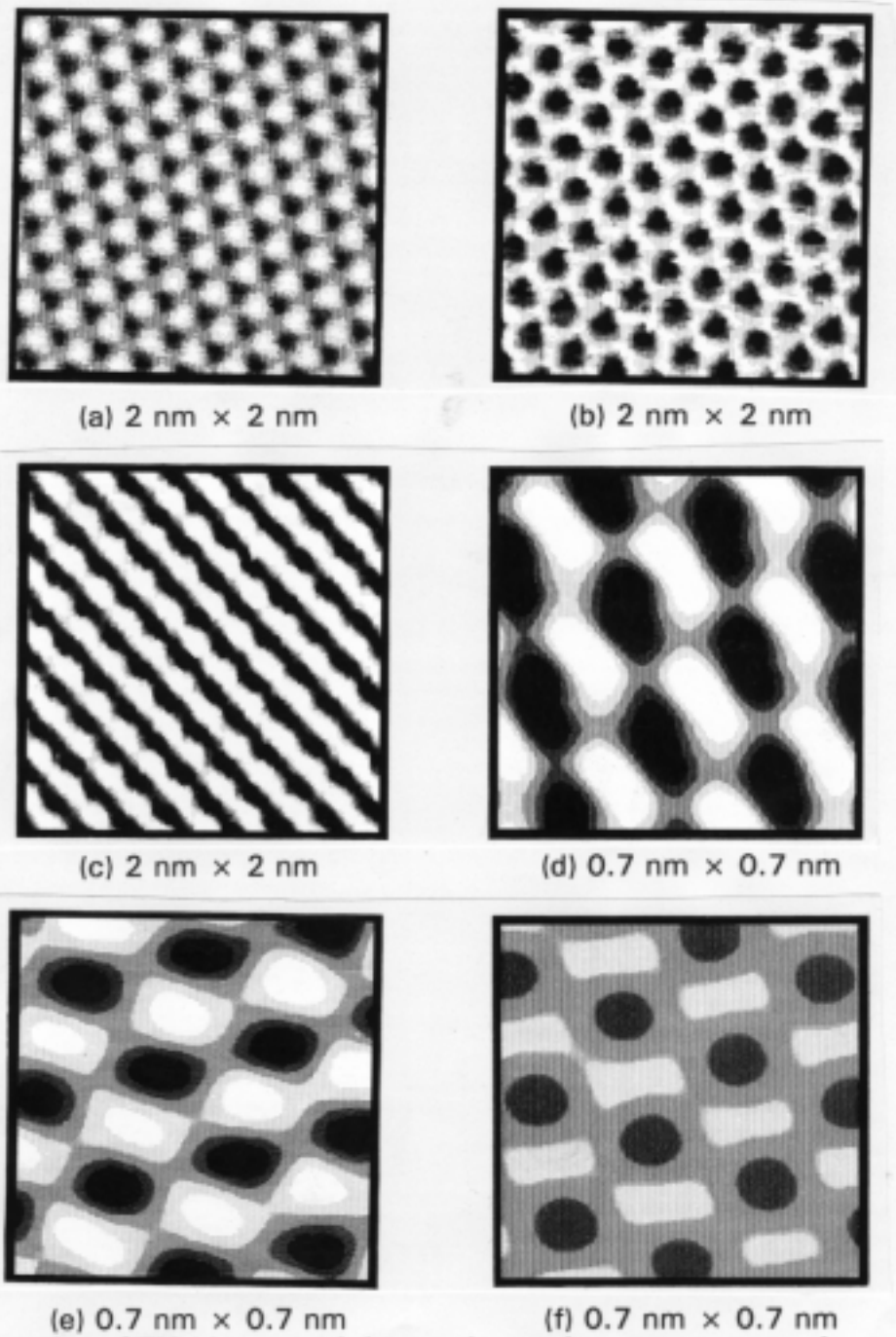

Image 8:1. *STM I-images of the varying surface appearance of HOPG. (a) normal image (usually observed) and (b-f) anomolic images (filtered to remove high frequency noise). Sizes are shown with each image.*

shown to significantly affect the resolution[15]. Surface states and bulk properties have both been theorized as the source of the normal dual trigonal surface structure. The theoretical potential calculations in the literature were carried out for semi-static conditions where there is no net current flow. Considering these facts and supposing that the electronic structure of the near surface atoms (and thus the STM image) could be altered with a transverse potential or current, a corroborating experiment was conceived.

8.4 Recoverable, transverse current induced HOPG appearance alteration

Carbon is capable of forming single or multiple bonds with itself and other elements enabling it to form over a million compounds. In graphite, carbon forms resonant[16] bond structures in which the true state of a the bond is a weighted linear combination of three different valence bond structures. The weights are equal under static conditions for graphite.

Measurement with an STM is a dynamic rather than static process. It requires a current to be conducted through the sample at the same time a measurement is being made. Calculations of the electronic structure of graphite, which assume that the p_z electrons are localized (p_z orbitals), that the structure is static, or that there is no net charge in the region, may therefore not be valid.

An experiment was designed to determine if a transverse surface current would change the weights of the resonant structure enough to

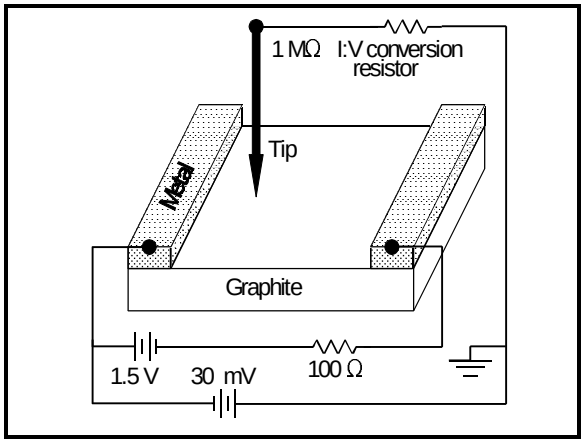

Figure 8:6. Experimental setup used to induce surface currents and image the resulting surface appearance.

alter the tunneling current and thus change the STM image. Using the experimental configuration of Figure 8:6, the surface appearances shown in Image 8:2 were obtained. By connecting and disconnecting the 1.5 V battery, the appearance of the surface was altered. With the battery disconnected, the normal dual trigonal appearance shown in Image 8:2(a) was observed. After connecting the battery, the row pattern seen in Image 8:2(b) was observed. Disconnecting the battery again, resulted in the surface appearance shown in Image 8:2(c) which eventually returned to the normal dual trigonal after 10 sec. The battery was reconnected again and the image began changing again. The change of the surface can be seen in Image 8:2(d) where the beginning (top) of the scan was dual trigonal and transformed into a row pattern over time. After complete transformation to a row pattern, Image 8:2(e) was obtained. After again disconnecting the battery, the dual trigonal pattern shown in Image 8:2(f) was obtained. There is a 20 s time differential between each of the images with a 10 s scan time. All of the images are shown with the same greyscale parameters.

With the battery connected, there was a 1.28 V drop across the 100 Ω resistor. That means in the worst possible case, the bias between

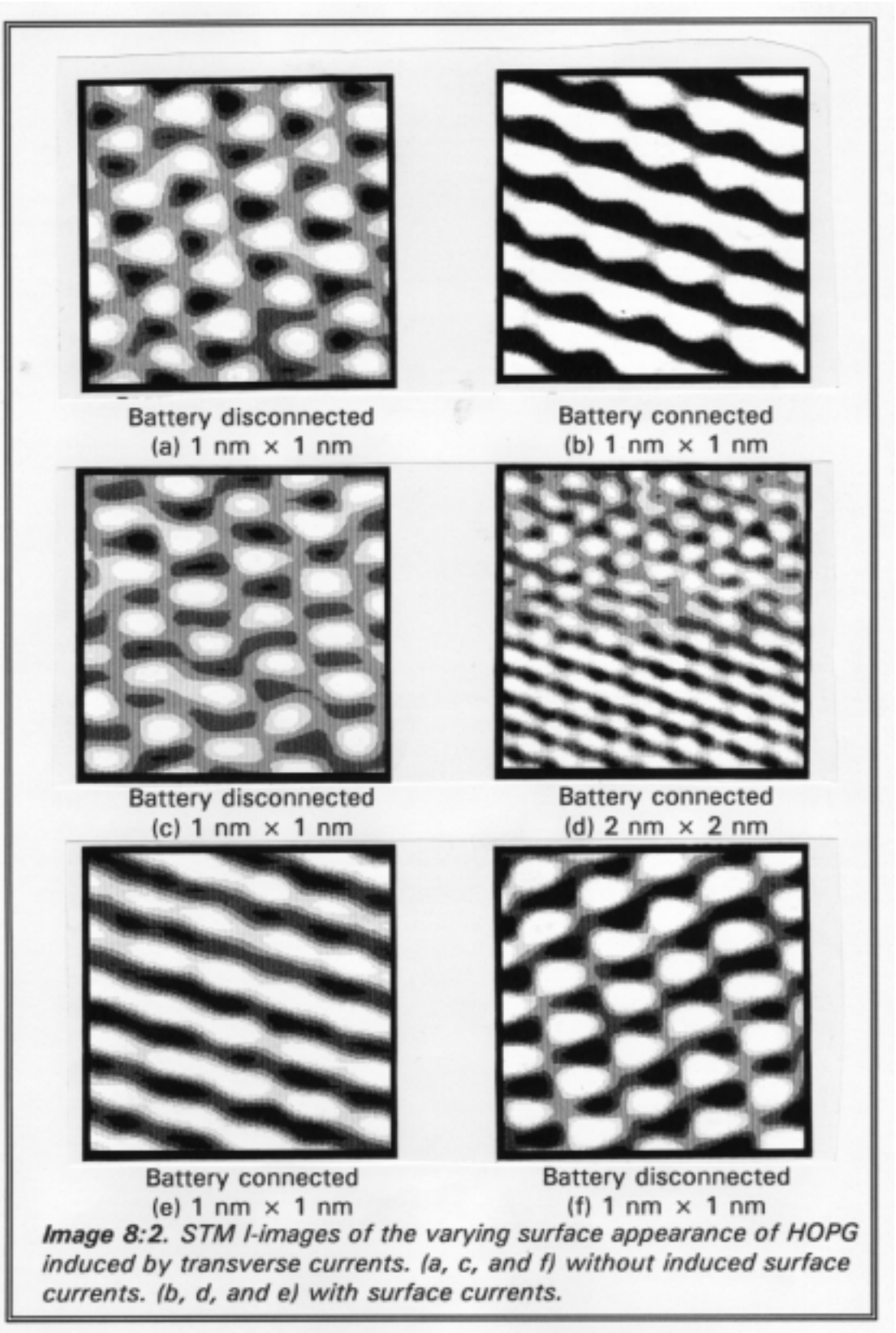

***Image 8:2**. STM I-images of the varying surface appearance of HOPG induced by transverse currents. (a, c, and f) without induced surface currents. (b, d, and e) with surface currents.*

the tip and sample could have changed to -0.3 V. But an increase in bias would result in a considerable decrease in resolution[17] which was not observed. From this it is concluded that the row patterns are produced by a change in the resonant structure of the graphite surface.

Notice that the dual trigonal pattern of Image 8:2(a) appears different from that shown in Image 8:2(f) with the exchanging of the current maxima and saddlepoints positions. Since this was the same area of graphite, it is concluded that the higher current position is not due to the presence of a underlying atom in the next graphite plane. However, a maximum or minimum current on the surface may be determined by the electronic state of the underlying atom instead of its presence.

Since it has been shown that the resonant structure may be altered by a transverse current, it is possible to theorize[18] that the weights of the resonant bonding may cause the various surface appearances shown in Image 8:1. The electronic configuration of the tip could also affect the resonant weights and induce change in the surface appearance. In either case these effects may result in unpredictable surface images.

8.5 Discussion

Considering the image potential and tunneling transmission prefactor, evidence has been given to rationalize the decrease in the slope of the ln I(s) plots as the STM tip moves toward the surface. It has also been shown that the image of HOPG can be altered by an induced transverse surface current. Bryant [1986] has shown that an intercalated

Au atom electronically affects the surface appearance of HOPG depending on the tip-sample separation. Since the tip also is capable of various electronic states depending on the surface fields, one can hypothesize that as the tip moves closer to the sample, the surface fields change the electronic structure of the tip giving rise to discrete values for the slopes of the ln I(s) plots. Further advances in modeling using molecular dynamics are required to verify this hypothesis. Initial investigations by researchers show that higher energy electron states for graphite appear as rows across the surface.[19]

In regard to the relevance for making a nanomemory, the tip-sample current interaction must be repeatably predictable in order for voltage pulses to consistently alter the surface. Presently there is incomplete knowledge of all variables which must be controlled for this to be the case. Additionally, if the electronic state of the tip or substrate changes, the ability to read a manufactured bit without error may be corrupted.

[1] The approximate equation is from Simmons [1961]. The full equation containing the hyperbolic sine term $\{e^{kx}-e^{-kx}\}$ was first introduced in Equation (4-5) and is also shown expanded to include a non-linear barrier in Equation (8-8).

[2] As reported in Chapter 4. The work function is the amount of energy necessary for an electron (at Fermi energy, E_F) to escape from the surface into a vacuum.

[3] It is not known whether or not this or any similar equation has been reported in the literature.

[4] Eisberg, Robert and Resnick, Robert, *Quantum physics of atoms, molecules, solids, nuclei, and particles,* (Wiley & Sons, New York, 1974) page 218 (includes the prefactor and the approximation). The prefactor is a constant for a square potential barrier.

[5] See Equation 4-6 for a more detailed equation by Simmons containing the components of I_o.

[6] Wolf, E. L., *Principles of electron tunneling spectroscopy*, (Oxford University Press, New York, 1985) page 2.

[7] Simmons approximated a $(2k\phi^{½}(s)+1)$ term to $2k\phi^{½.}$

[8] The calculations for a single layer show the potentials converging below 0.2 nm. Since the interlayer separation of graphite is 0.35 nm, considering more than one plane would add no additional information for our model. This convergence appears even before including the superposition of the potentials of all charges within a 2 nm radius.

Electronic calculations by other researchers shows a slight variation in the electronic structure and potential due to the second layer. See Batra *et al.*[1987], Selloni *et al.*[1985], Tománek *et al.*[1987], and Tartar and Rabbi [1982].

[9] This was nontrivial since there are only certain radii which contain zero net charge. Although the potential converges toward zero beyond about 0.2 nm at subsequent radii with zero net charge, the convergence is oscillatory. This oscillatory convergence requires continuing the summation through several zero charge radii to obtain a close approximation.

[10] The calculation was made for 174.5 atoms (1396 charges). This was the first radius that contained a zero charge density. It was necessary to include 291 atoms (11^{the} possible radius) to observe the convergence of the resonant electron case. The void site was calculated with 181 atoms and the atom site with 452 atoms. The calculation for the free electron in site was done with 173.75 atoms.

[11] By state, we mean the associated wave function, This wave function is affected by such things as the current flowing between the electrodes and the electrons' drift velocity.

[12] There was no need to do any in-situ cleaning of the tip because it produced excellent images from the first time it was moved into the tunneling regime until five days later when the tip crashed into the sample leaving a conical hole 10 nm wide and 10 nm deep in the surface of the graphite.

[13] V_b = ±100 mV, I_{set} = 2 nA, low feedback response.

[14] Mizes *et al.* [1987], Horie and Miyazaki [1987], Doyen *et al.* [1990], Tsukada *et al.* [1991], Tománek *et al.* [1987], and Colton *et al.* [1988].

[15] Chen, C. Julian, "Origin of atomic resolution on metal surfaces in scanning tunneling microscopy", Phys. Rev. Lett. **65(4)**, 448-51 (1990). Chen, C. Julian, "Role of tip material in scanning tunneling microscopy", Preprints, IBM Research Division, Thomas J. Watson Research Center, P. O. Box 218, Yorktown Heights, New York 10598.

[16] For more detail on the resonance nature of carbon and graphite see Appendix D.

[17] Binnig *et al.* [1986].

[18] For a more detailed account of how the resonance structure can be theorized to produce the images see Miller, J. A., and Hocken, R. J., "Dangling, double and resonance carbon bonds on highly oriented pyrolytic graphite imaged by scanning tunneling microscopy", UNCC Precision Engineering Laboratory Internal Report #jam.005 [1992].

[19] Arthur Edwards and John Pickard, University of North Carolina at Charlotte, Electrical Engineering Department, private communication, manuscript in preparation).

Chapter 9.

A Potpourri of Considerations

This chapter examines various STM related phenomena that should be taken into consideration for the design, manufacture, and operation of a nanomemory. Among these are surface considerations, tip geometry considerations, and thin film topography. Comments about these arise from observations over a period of two years.

9.1 Silicon surface degeneration

In order to make a nanomemory that is inexpensive, it would be advantageous to exploit existing technologies. The silicon-based microelectronics industry is already polishing Si wafers to flatness levels that may be sufficient for the proposed nanomemory.

Image 9:1(a) shows the 7×7 reconstructed surface of (111) silicon

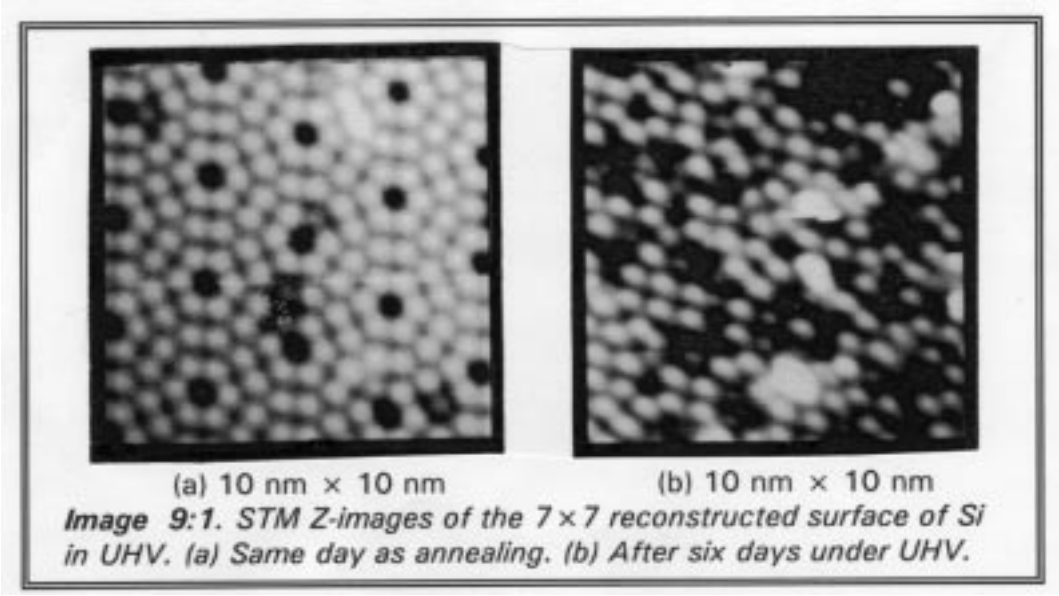

Image 9:1. *STM Z-images of the 7 × 7 reconstructed surface of Si in UHV. (a) Same day as annealing. (b) After six days under UHV.*

after it was annealed at 900^{o} C in a UHV environment. Initially the surface showed large flat reconstructed regions. The same sample was imaged over a period of several days. The surface became increasingly degraded each day. It was not possible to image the exact same area due to thermal drift and the withdrawal of the tip after each imaging session. Due to degradation of the tungsten tip, it was also necessary to clean the tip each day in situ by moving the tip to a remote area of the silicon and increasing the bias to several volts for several seconds. The process sometimes had to be repeated until atomic resolution was obtained. Then the tip was removed from the cleaning region to another area for imaging. Image 9:1(b) shows how the surface appearance is degraded after a period of six days. The degradation may be caused by the oxidation, hydration, or other contamination of the silicon surface. This reveals the commonly known reactive[1] nature of the Si surface which is thought to produce a nonconducting native oxide layer in an atmospheric environment. So the bare surface of silicon is unlikely for use in a nanomemory operating in air or UHV at room temperature.

This illustrates a problem which will be a factor in the operation of a nanomemory, that of contamination. Contamination results when the ambient gas or ambient impurity reacts with the surface producing a change in the electronic and tunneling characteristics. This contamination will subsequently change the parameters necessary for the alteration of a surface to produce a memory bit.

Another source of contamination is the actual processes used in

the production of the memory. For example, methanol along with H_2SO_4, H_2O_2, HF etc. are often used as cleaning[2] agents, not only for bare silicon, but also after other processing steps such as deposition and etching of thin films. The question arises as to whether a cleaning step could actually be the source of some nanometer scale contamination. A piece of Si wafer was allowed to soak in methanol for an extended[3] period of time. Then the surface was imaged by STM in air to see if there was any surface contamination. The result was a surface appearance like that shown in Image 9:2. The surface features may be due to a coagulation of hydrocarbons on the surface. Since practical cleaning steps take only a few minutes, only trace amounts of residue may be left which do not affect the operation of devices.

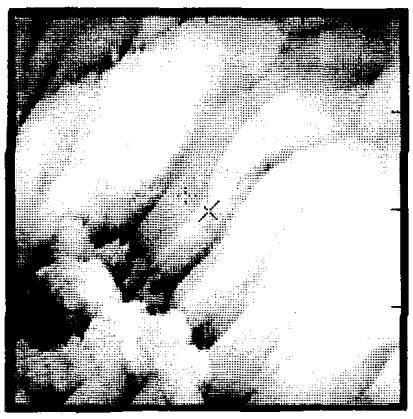

400 nm × 400 nm

Image 9:2*. STM Z-image of the surface of Si after an extended soak in methanol.*

9.2 Thin Films[4] on Silicon

Since silicon technology is highly advanced, but the highly reactive surface of Si forms a nonconducting oxide in air, thin films on Si could produce an inexpensive means of manufacturing the memory surface. However, thin film surfaces are not as flat as single crystal surfaces and must be carefully prepared to produce sub-nanometer scale roughness. The effect the processing has on the surface roughness is shown in

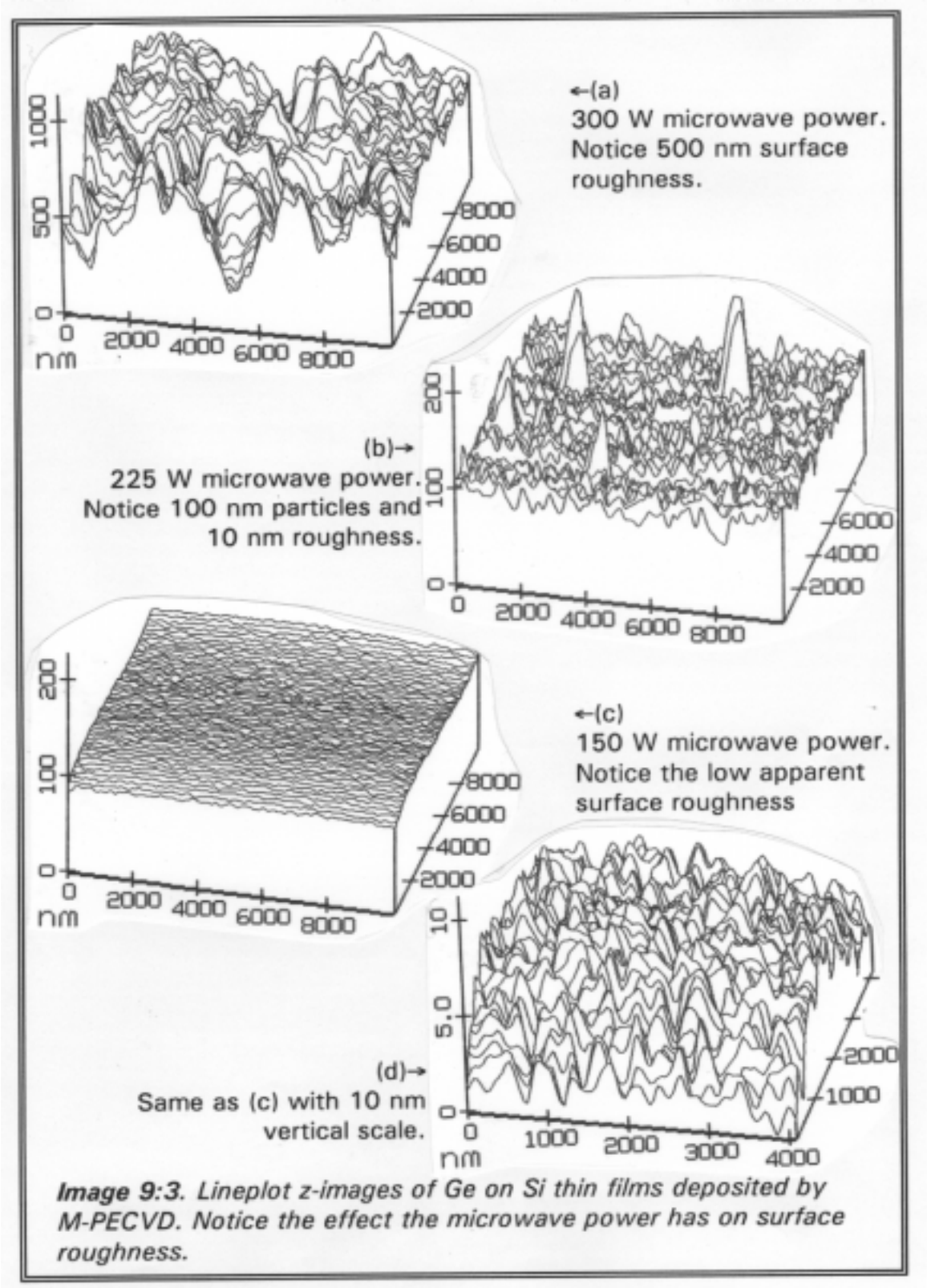

Image 9:3. *Lineplot z-images of Ge on Si thin films deposited by M-PECVD. Notice the effect the microwave power has on surface roughness.*

Image 9:3. The Ge films on Si shown in these STM images were deposited using microwave plasma enhanced chemical vapor deposition (M-PECVD)[5]. The largest surface roughness occurs with the highest microwave power. The films deposited with a 175 W microwave plasma may be smooth enough for surface alteration, if the bits produced are greater than 10 nm. However, the Ge films were difficult to image due to a GeO_2 monolayer on the surface which resulted in unstable tunneling currents, and so, surface alteration was not attempted.

Unstable tunneling currents resulting in intimate tip-surface contact can also cause the tip to change often reducing resolution in the STM image. STM images of the same area of a diamond on Si thin film showing the time degradation of image resolution are shown in Image 9:4. Since the diamond on Si thin films[6] were insulating, the circuit

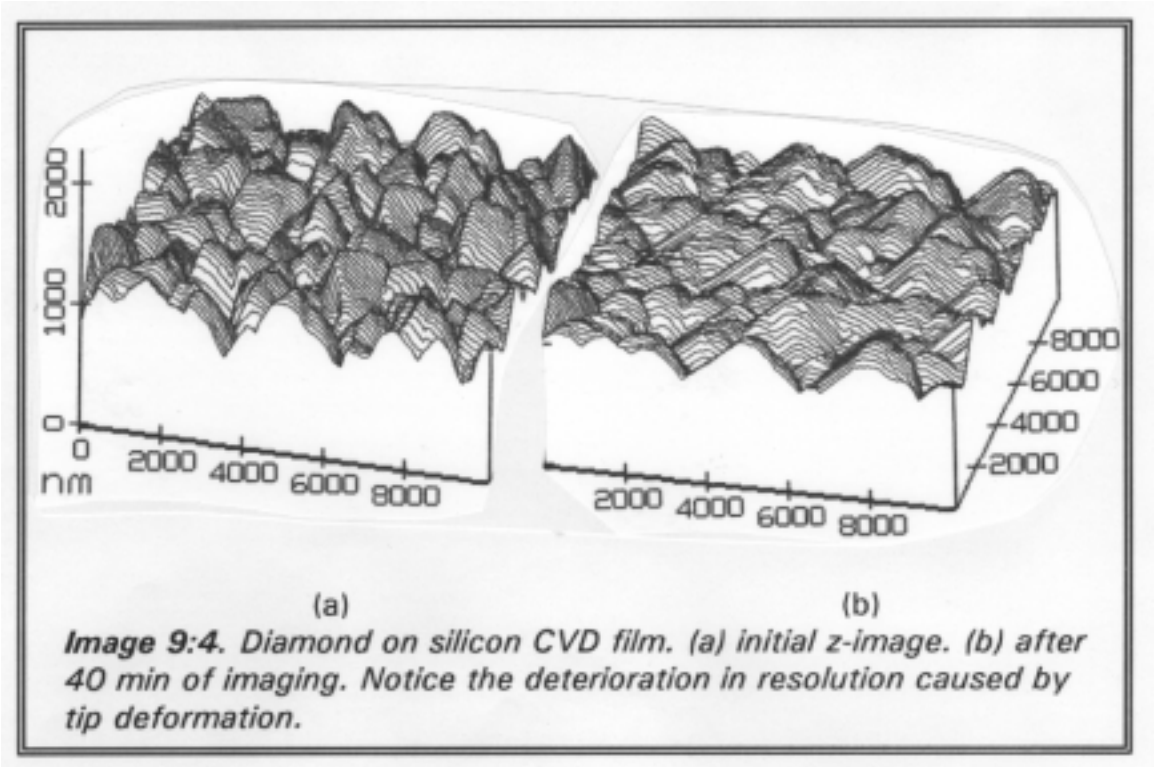

Image 9:4. *Diamond on silicon CVD film. (a) initial z-image. (b) after 40 min of imaging. Notice the deterioration in resolution caused by tip deformation.*

shown in Figure 9:1 was used to inject[7] electrons into the diamond for STM tunneling at the surface. The ac signal produces a depletion layer in the doped silicon. Electrons are accelerated across the depletion region to gain enough energy to overcome the barrier between the silicon and diamond and reach the conduction band of the diamond.

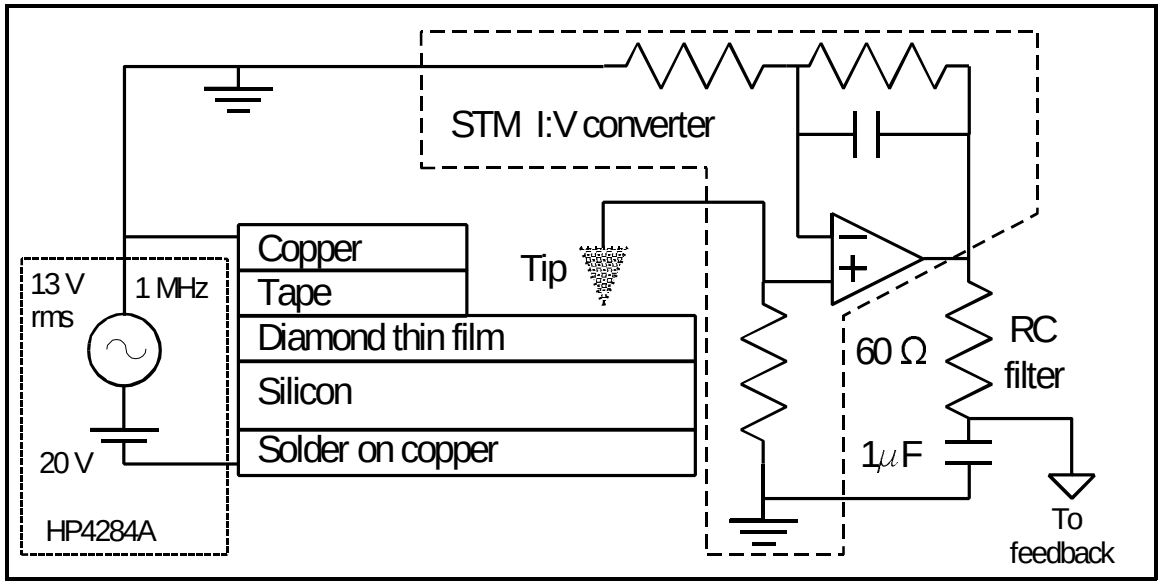

Figure 9:1. Circuit used to inject electrons into diamond thin film on Si. The injected electrons are the source of tunneling electrons at the surface.

9.3 More tip geometry effects

Decreasing tip resolution would cause manufactured bits in a nanomemory to *appear* to change lateral and vertical size. Image 9:5 illustrates this effect on the apparent surface topography of a Pd on Cu thin film on Si.[8] Image 9:5(a) was acquired with a sharp tip and Image 9:5(b) was acquired with a more blunt tip. Notice the apparent increase in feature diameter from 10 to 20 nm and apparent decrease in height from 10 to 5 nm.

The minimum apparent (imaged) width of a feature is always larger than the shape of the tip due to convolution. If surface feature widths are smaller than the tip, then the sample ends up imaging the tip and its shape will be seen repetitively in the STM image. This effect is shown in Image 9:6 (a) and (b), with (a) revealing a sharper tip.

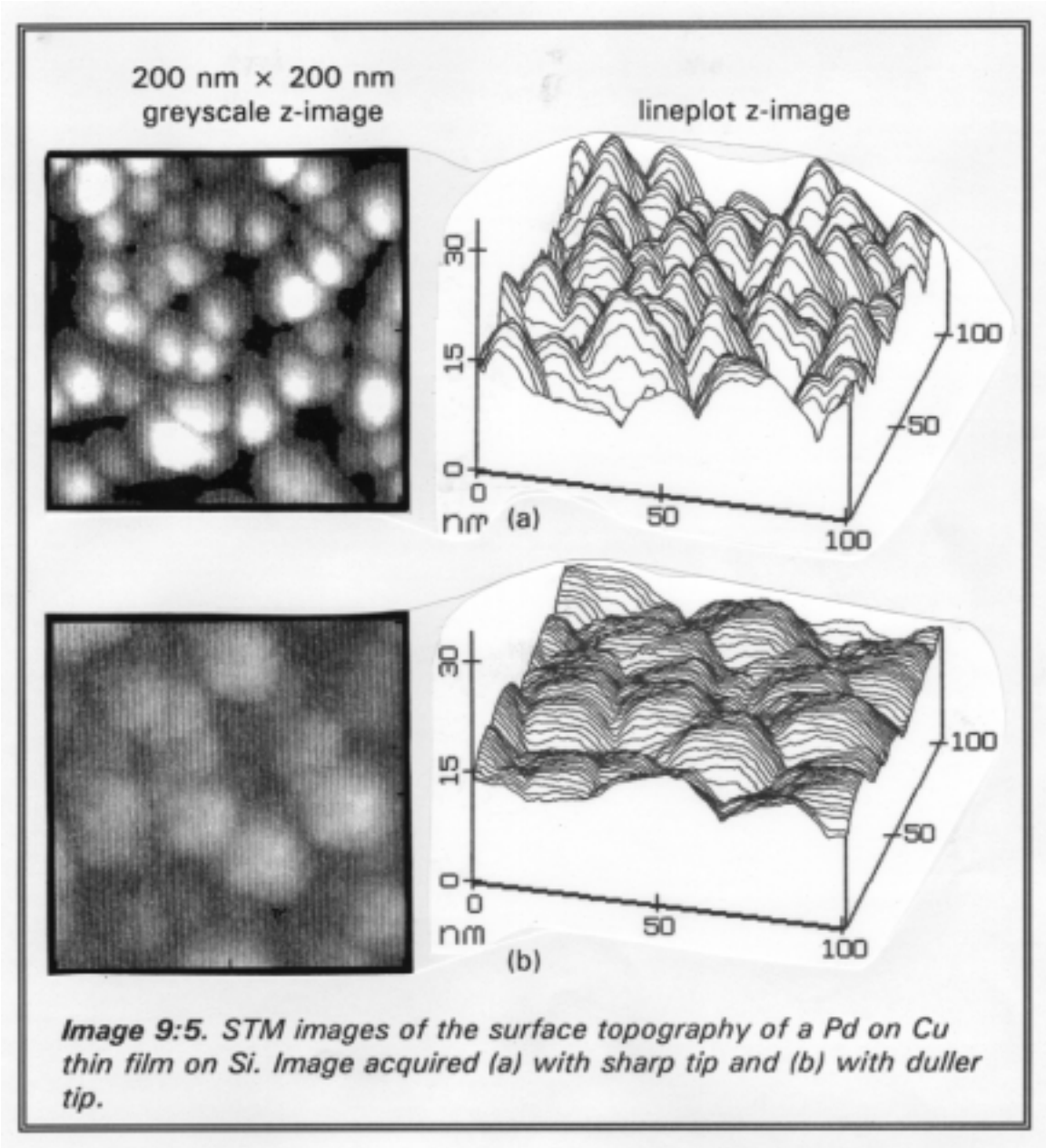

Image 9:5. *STM images of the surface topography of a Pd on Cu thin film on Si. Image acquired (a) with sharp tip and (b) with duller tip.*

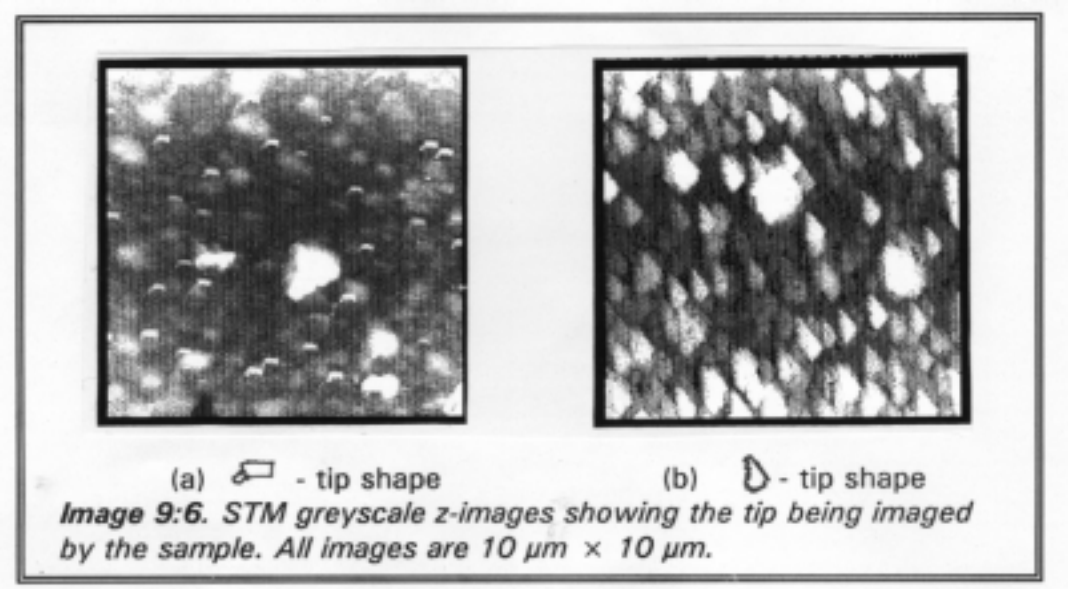

Image 9:6. *STM greyscale z-images showing the tip being imaged by the sample. All images are 10 µm × 10 µm.*

Another major problem would occur in the reading of memory bits when the tunneling probe has more than one tunneling asperity. This is illustrated in Image 9:7. A diffraction grating with a 1 μm spacing is shown imaged with a double tip in Image 9:7(a). Notice the doubling of the crest of the grating. Image 9:7(b) shows an altered area on the surface of graphite imaged with a double tip. Notice that one of the

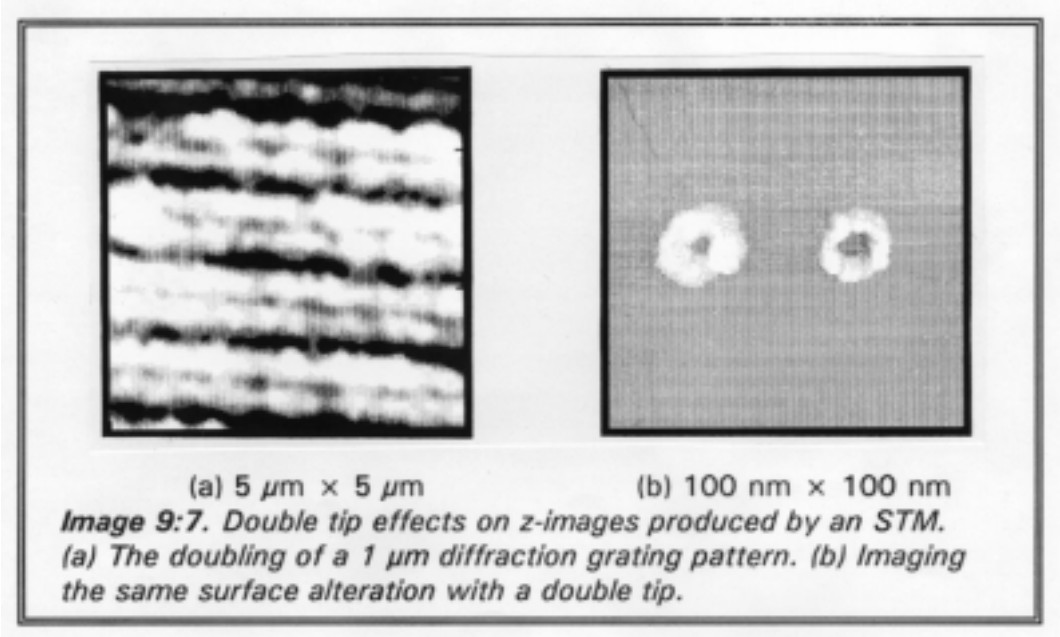

Image 9:7. *Double tip effects on z-images produced by an STM. (a) The doubling of a 1 µm diffraction grating pattern. (b) Imaging the same surface alteration with a double tip.*

circles appears slightly smaller than the other. This is due to asperities not being the same distance above the bulk surface.

9.4 Discussion and summary

It has been shown that surfaces can react with the surrounding ambient thus changing the surface appearance. So, a substrate used for a nanomemory should either be inert or have been made to react with the ambient to produce a stable surface. Some precious metals are inert in air. However, previous results for Au and Pt show that they exhibit diffusion of surface features. The inert surface of graphite was also eliminated as a nanomemory substrate due to surface diffusion. To prevent the degeneration of other reactive surfaces, they should be annealed in a passivating environment or air to accelerate the surface reaction so that further reactions are inhibited. Care should be taken in choosing such a surface that does not react to become insulating.

Thin film deposition was shown to have inherent topography depending on the processing. Thus, if thin films are used, the deposition should introduce minimum surface structure. The larger the deposited surface features, the larger the surface alteration required in order to be readable. Also, subsequent processing steps after the deposition should not be allowed to contaminate the thin film surface.

The shape of the tip was also shown to affect the apparent image of a surface. The tip radius should be at least as small as the anticipated surface alteration size in order to facilitate reading of the alteration as a

memory bit. The ability to mass produce tips of consistent radii will be critical in producing memories that will operate similarly enough to be predictable and exchangeable. The tip material should also be taken into consideration like the substrate surface. The tip used to observe the silicon degradation in UHV was made of tungsten. This tip had to be cleaned in situ every day to produce atomic resolution. This eliminates bare tungsten for a tip material due to its instability which even occurred in UHV. Tungsten and platinum compound (Pt-Ir, Pt-Re, etc.) tips are the most common for STM use. For production of a tunneling based nanomemory, a study would have to be undertaken into the development of a tip material which is durable enough to withstand the bit-manufacturing mechanism and also be stable enough not to affect the process.

[1] Nicollian, E. H., and Brews, J. R., *MOS (Metal Oxide Semiconductor) Physics and Technology*, (Wiley, New York, 1982). p. 650.

[2] Ghandi, Sorab K., *VLSI Fabrication Principles*, (Wiley, New York, 1983) page 519.

[3] The time period was on the order of two months. Although it is extensively longer than the time required for a production step, the surface alteration would probably occur on a smaller scale for a shorter time. Note that it is not the surface of Si that we are imaging, because the native oxide of Si prevents quality imaging in air.

[4] For techniques used for producing thin films on silicon see Ghandi, Sorab K., *VLSI Fabrication Principles*, (Wiley, New York, 1983).

[5] The samples were deposited at the University of Vermont and STM characterized at UNC-Charlotte. See Varhue, W. J., Carulli, J. M., Miller, J. A., and Peterson, G. G., "Surface morphology of epitaxial Ge on Si grown by plasma enhanced chemical vapor deposition", J. Vac. Sci. Technol. **B 9**, 2022 (1991).

[6] The films were prepared by Ron Rudder at the Research Triangle institute, Research Triangle Park, North Carolina. For a more detailed report on the diamond on Si thin film see Miller J. A. "Diamond thin films on silicon imaged by scanning tunneling microscopy", UNCC Precision Engineering Laboratory Internal Report #jam.009.

[7] Nicollian, E. H., and Brews, J. R., *MOS (Metal Oxide Semiconductor) Physics and Technology*, (Wiley, New York, 1982) p. 495.

[8] The film was e-beam deposited by Chin-An Chang of IBM T. J. Watson Research Center, Yorktown Heights, NY 10598. For description of process see Chang, Chin An, "Deposition of (100) Au, Ag, Pd, Pt, and Fe on (100) using different metal seed layers", J. Vac. Sci. Technol. **A** 9(1) Jan/Feb 1991 (p.98). For more detail of STM imaging see Miller, J. A., and Chaffin, J., "Cu, Pd/Cu, and Pt/Pd/Cu thin layered films on Silicon imaged by scanning tunneling microscopy", UNCC Precision Engineering Laboratory Internal Report #jam.010.

Chapter 10.

Summary and Conclusions

In Chapter 1, the possibility of transferring STM technology into memory technology in order to produce a **nanomemory** with an 10^5-10^6 increase in the areal bit density times was presented.

10.1 Historical developments

Historical developments of memory devices were discussed including: visual storage from the **camera obscura** to photographic chemical storage; audio storage including the mechanically based **phonograph, graphophone,** and **gramophone**; and electromagnetic storage developments of the 1800's resulting in the invention of the **telegraphone**. Examples of early numerical storage devices (**abacus** and **quipu)** have been given along with the development of mechanical calculating machines. Development of three generations of computers has also been discussed. Vacuum tube and capacitor memory were used in first generation developments with semiconductor transistors and core memory being typical of second generation advancements, while current third generation techniques use solid state technology and integrated circuits along with technically advanced magnetic memory. Also discussed was how memory is achieved with magnetic reversals within a material.

Development of the STM was recounted with mention of its

precursors: the optical and electron microscopes, stylus instruments, and the **topografiner**.

10.2 Nanomemory synthesis

Operation of magnetic memory and tunneling microscopy were compared to present the synthesis of the nanomemory concept. In Chapter 2, various schemes of changing the surface of a material with a tunneling probe were described. They include mechanical contact, field evaporation of surface atoms, field deposition onto a substrate from the tip or ambient, field induced surface chemical alteration, electrical charging, and magnetization.

10.3 Alteration experiments and results

State of the art literature involving experiments related to these surface alteration schemes have been reported in Chapter 3. Chapter 4 recounted personal experiments designed to investigate the areas which are necessary to implement a nanomemory. The areas considered were the ability to produce surface alterations along with their reproducibility, durability, and readability.

A review of basic tunneling theory, resulted in three initial parameters which affect the alteration. They were initial bias, tunneling current, and the spacing between the sample and tunneling probe. Setting any two of these determined the third. Since there was no way of accurately determining the spacing, initial bias and current were used as

the basis of experiments. HOPG and Pt thin films were used as surface materials, and Pt-Ir and tungsten as tunneling tips.

Because of the simplicity of application, voltage pulses were employed to increase the field between the tip and sample. This increased field served as the mechanism for surface alteration.

Alteration was found to be inconsistent with current. Keeping other parameters constant, a decrease in the initial current (which should increase the spacing and lower the field) sometimes resulted in greater areas of alteration. Other times the region of alteration decreased. This prevented a predictable trend in feature production dependent on initial current.

Varying the amplitude of the alteration pulse resulted in an apparent threshold for modification. This threshold was found to be tip dependent. Also, near the threshold, surface alteration was found to have poor repeatability, a property hostile to the operation of a memory.

A regular L-shaped 40 nm sized structure was produced using pulses. However, the pulse amplitude had to be increased to complete the formation. An I-shaped structure made of pulse produced holes has been also shown. The holes were made while keeping all modification parameters constant. However, the holes have been shown to vary substantially in size as the I-shape was completed. This also would be inconsistent with a reliable memory.

Although we found that it was possible to produce nanometer surface alteration, their durability was limited. Nanometer structures were

observed to move, change, and disappear. The tips were also found to alter during the modification process which would affect the readability and addressability of a memory.

10.4 Material considerations

In relation to alterability, reproducibility, durability, and readability, the types and mechanism of alteration along with ambient environment, bit size and writing time have been considered. Nanomemory propensity for the materials used along with those reported from the literature have been summarized and tabulated for quick reference in Chapter 5. No clear cut material was identified that readily lends itself for use as a nanomemory substrate. Problems such as bit diffusion, nonreproducible features and unpredictable feature types, minimum bit sizes too large, ambient not practical, unrealistic bit writing time, and inconsistent or deficient surface conductance were observed. Although many materials had positive aspects, each showed at least one basic problem which limits its use as a memory substrate.

10.5 STM design effects

In Chapter 6, investigations into the effect of mechanical and electrical STM design on the application of voltage pulses between the tip and substrate were reported. A theoretical electronic circuit model of the STM, including stray capacitances, was developed from equivalent parallel capacitance and resistance measurements. A theoretical

capacitance between a planar sample and conical tip was also calculated using Laplace's equation and Gauss's law.

From the theoretical circuit, potential degradation of high frequency pulses has been predicted. The response of the I-V converter has also been considered as a factor in the nanomemory writing time. The results led to four proposed design criteria for the construction of a tunneling probe and electronics for use in the proposed nanomemory. The criteria have been tabulated in Chapter 6.

10.6 I(s) anomalies

Noting the inconsistency in field induced surface alteration for graphite, investigations were made into the tunneling current characteristics as a function of relative tip-sample separation. These investigations have been detailed in Chapter 7. The construction of an x-ray calibrated tunneling probe resulted in the observation of I(s) and ln I(s) characteristics that varied slightly for each measurement from an individual tip and considerably from tip to tip. Results have been corroborated with a commercial instrument along with the applied bias having an affect on the characteristics.

Analyzing ln I(s) curves revealed a departure from theoretical slopes predicted by simple tunneling theory. STM images with subsequent I(s) measurements revealed that ln I(s) slopes that were closer to the predicted value (simple theory) were concurrent with images having diminished resolution.

Another investigation revealed a significant variation in I(s) curves for various ambient gases. These experiments exposed a lack of predictability for tip-sample separation. This unpredictable separation produces correspondingly unpredictable fields at the tip-surface interface, and is suspect in the reported erratic field induced surface alteration.

10.7 Theoretical results

In Chapter 8, increasingly detailed tunneling theory was examined to see if there was theoretical rational for a deviation of Ln I(s) slope values from simple tunneling theory. A more accurate equation for the image potential of an electron between two planes has been presented. The equation was deduced from observation and the application of boundary conditions. Also included in the tunneling detail was a prefactor that was dependent on the ratio of the potential barrier to the electron's kinetic energy. The results of the analysis showed that the slope of Ln I(s) curves should significantly decrease as two planes approach each other below a separation of 1 nm.

The analysis also implied that the barrier completely disappears when the electrodes are separated by about 0.4 nm. A static calculation of the potential corrugation due to core atoms and valence electrons has been presented. The results showed that the corrugation extends about 0.2 nm. It was concluded that the electronic corrugation should also affect the tunneling characteristics at separations less than a nanometer. This effect is in agreement with experiments involving lateral surface

currents on graphite. The currents were found to alter the appearance of STM images. The normal image was restored with the cessation of surface currents. Since all tips vary in electronic structure at the tip, the I(s) tunneling characteristics will be slightly different for each tip. Again, since I(s) characteristics cannot be predictable, neither can field induced surface alteration.

10.8 Other considerations

Due to their availability and low cost, the use of thin films on Si has been discussed. It is shown that surfaces may change due to reaction with the ambient. Reading and writing problems due to the topographic surface structure of thin films has also been deliberated along with surface contamination.

Tip durability, sharpness, and shape are all considered in relation to the ability to read a memory bit. The different problems resulting from tip geometric structure such as tip-surface convolution is also illustrated.

10.9 Nanomemory conclusions

10.9.1 Unfeasible methods

Mechanical indentation as a means of producing a surface alteration is thought to be unfeasible for two reasons. First, the time necessary to stop the tip and advance it toward the sample and then achieve tunneling again would be prohibitive. Second, contact between

the tip and sample would cause the tip to change resulting in corrupted addressing.

Field induced modification is deemed to be impractical due to the unpredictable I(s) characteristics. This type of modification has also been shown to alter the tip which would corrupt addressing.

Charging of materials would only be impractical if the charge diffuses or if the minimum bit size was too large. Magnetizing a homogeneous surface is thought to be impractical due to the known diffusion of magnetic domain walls.

10.9.2 Ambient considerations

Since we desire a memory that is practical, an inexpensive and readily achievable ambient should also be chosen. Any ambient that would cause expensive packaging problems and continual maintenance expense should be avoided. This need not be limited to air, since hermetically sealing the structures with a positive vapor pressure of an inert or appropriate gas may allow desired effects.

10.9.3 Materials selections

Materials should be selected which are inert in the chosen ambient. Any material which may react should be previously passivated and that passivation should be electrically conductive if it is to be a tunneling surface. This would eliminate most materials. The materials which have been investigated which are inert (Pt, Au, HOPG) have shown diffusion properties that are not conducive to a field induced nanomemory.

The tip should also be inert in the chosen ambient. A Pt or Au

coating could provide this, but the underlying material should be stiff to increase the structural integrity and resonance frequency of the memory.

10.9.3 A proposed memory stratagem for future investigation

Considering the previous recommendations, a proposed memory stratagem is shown in Figure 10:1. A magnetic thin film is deposited onto a flat silicon substrate. The magnetic thin film is then oxidized to produce a nonmagnetic oxide. Afterwards, a layer of nanometer scale particulates is

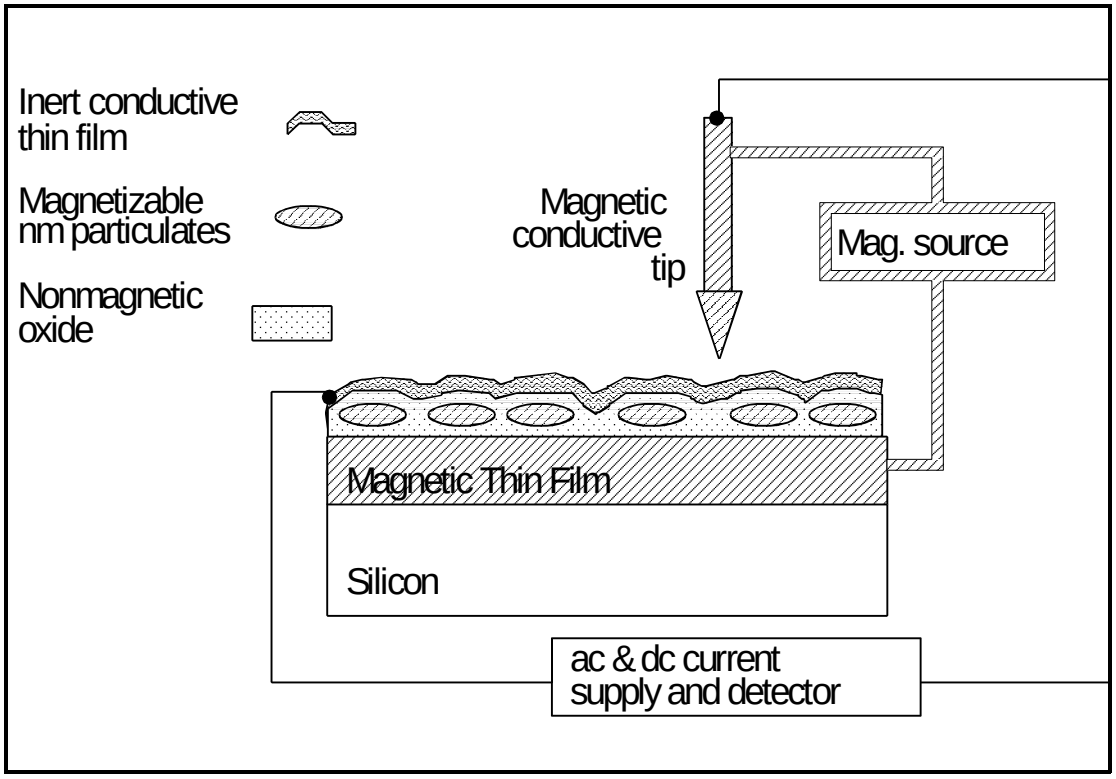

Figure 10:1. Proposed memory stratagem which embraces specified recommendations.

deposited (perhaps e-beam). The particulates are then oxidized forming a nonmagnetic barrier between the particulates. An inert thin film such as Pt or Au is subsequently deposited on the surface to prevent any further surface reaction. The particulates are used as the memory bits. The

magnetic source induces the magnetization of one or more of the particulates. The magnetized particulates effect a conductance change between the tip and inert film to produce a readable bit. The tip could be servoed to the surface by either STM of AFM means. The oxide between the particulates should prevent the magnetized particles from losing their magnetization.

10.10 General conclusions

Although the thrust of this thesis has been to determine the feasibility of producing a nanomemory using a tunneling probe, other important repercussions have been ascertained.

The tip-sample I(s) characteristics have been shown to be unpredictable. Also, an important result has been that simple tunneling theory cannot be used for accurate prediction of electrode spacings below 1 nm. In addition, transverse currents within the substrate have been shown to affect quantum mechanical electron tunneling. This demonstrates a highly intricate electronic effect due to the chemical, physical, geometric, and electronic interaction of the tip and sample.

These results suggest that using the tunneling probe for absolute Angstrom metrology is not possible with present technology. Also, other devices such as the patented magnetometer and tunneling microphone will demonstrate unpredictable transfer functions due to factors which also affect tunneling.

Appendix A

Computer Programs

A.1 Asyst program for electrical analysis of STM head

filename: STM.CIR

```
echo.off
forget.all
\ This is a program to calculate the ac impedance and current on
\ the nanoscope head
\
\
\
\
12 5 sci.format
dp.real dim[ 24 ] array omega   \  2 * pi * frequency
dp.real dim[ 24 ] array absimp  \ absolute value of the impedance
dp.real dim[ 24 ] array freq    \ frequency array
real dim[ 2 ] array px          \ max and min x scale values for plot
real dim[ 2 ] array py          \ max and min values for y axis scale
dp.real dim[ 24 ] array %vtip      \ % voltage from tip to sample
\ load frequency values for calculations
1   freq [ 1 ]  := 2   freq [ 2 ]  := 4 freq   [ 3 ]  :=
10  freq [ 4 ]  := 20  freq [ 5 ]  := 40 freq  [ 6 ]  :=
100 freq [ 7 ]  := 200 freq [ 8 ]  := 400 freq [ 9 ]  :=
1e3 freq [ 10 ] := 2e3 freq [ 11 ] := 4e3 freq [ 12 ] :=
1e4 freq [ 13 ] := 2e4 freq [ 14 ] := 4e4 freq [ 15 ] :=
1e5 freq [ 16 ] := 2e5 freq [ 17 ] := 4e5 freq [ 18 ] :=
1e6 freq [ 19 ] := 2e6 freq [ 20 ] := 4e6 freq [ 21 ] :=
1e7 freq [ 22 ] := 2e7 freq [ 23 ] := 4e7 freq [ 24 ] :=
freq pi * 2 * omega :=
: plot.axes cr \ plot axes with readable scales
logarithmic
." Input x-scale minimum : "
#input px [ 1 ] := cr
." Input x-scale maximum : "
#input px [ 2 ] := cr
." Input y-scale minimum : "
#input py [ 1 ] := cr
." Input y-scale maximum : "
#input py [ 2 ] := cr
"  " symbol
px py xy.auto.plot
.01 .01 .01 .01 " * " dashed&symbol
;

\ circuit components
dp.real scalar  r1
dp.real scalar  r2
dp.real scalar  r3
dp.real scalar  r4
```

```
dp.real scalar  c1
dp.real scalar  c2
dp.real scalar  c3
dp.real scalar  c4
dp.real scalar  c5
dp.real scalar  c6
dp.real scalar  c7
dp.real dim[ 24 ] array rp  \ equiv. parallel resistance array
dp.real dim[ 24 ] array cp  \ equiv. parallel capacitance array
complex dim[ 2 , 2 , 24 ] array coeffs
complex dim[ 24 ] array z1  \ impedance from body to ground not via tip
complex dim[ 24 ] array z2  \ impedance from tip to ground not via body
complex dim[ 24 ] array z3  \ impedance between tip and holder
complex dim[ 24 ] array z4  \ impedance across tip
complex dim[ 24 ] array z5  \ impedance of cap. from body to tip wire
dim[ 24 ] array rstore    \ storage array
dim[ 24 ] array vstore    \ storage array
real dim[ 24 ] array %v_unins \ % v tip drop, body connected to holder
real dim[ 24 ] array %v_gnd   \ % v tip drop, body grounded
real dim[ 24 ] array %v_ins   \ % v tip drop, body insulated from holder
complex dim[ 24 ] array zstore  \ storage array
dp.real dim[ 2 ] array ac 100 ac :=  \ ac ampl. to produce %v
complex dim[ 2 , 24 ] array %v
: circuit.diagram                              cr
."                                      "                    cr
."        ---------------------------- SAMPLE  "                    cr
."        |     |              |        "  ." R1= " r1 .        cr
."        R4     C7               C6        "  ." R2= " r2 .        cr
."        |     |              |        "  ." R3= " r3 .        cr
."   TIP   ----------- C5 ------------ BODY    "  ." R4= " r4 .        cr
."        |       |      |      |        "  ." C1= " c1 .        cr
."        C4       |      |      C1        "  ." C2= " c2 .        cr
."        ------    |      |      |        "  ." C3= " c3 .        cr
."        |   |   |      C2      |        "  ." C4= " c4 .        cr
."        R3   C3   R2      |      |        "  ." C5= " c5 .        cr
."        |   |   |      |      R1        "  ." C6= " c6 .        cr
."        |   |   |      |      |        "  ." C7= " c7 .        cr
."        ---------------------------- GROUND  " ." R's in ohms "      cr
."                                       " ." C's in Farads "    cr
;
: TBG.IMP
     r1 omega c1 * inv neg z=x+iy
     inv 0 omega c2 * z=x+iy + inv z1 :=
\    r1 inv c1 omega * z=x+iy inv 0 c2 omega * inv neg z=x+iy + z1 :=
\    r3 c4 omega * inv neg z=x+iy inv
\    r2 inv c3 omega * z=x+iy + inv z2 :=
     r3 inv c3 omega * z=x+iy inv 0 c4 omega * neg inv z=x+iy + inv
     r2 inv + inv  z2 :=
     0 c5 omega * neg inv z=x+iy z5 :=
     0 c6 omega * neg inv z=x+iy z3 :=
```

```
     r4 inv c7 omega * z=x+iy inv z4 :=
;
: get.values  cr circuit.diagram
." Enter R1 value in ohms : " #input  r1 := cr
." Enter R2 value in ohms : " #input  r2 := cr
." Enter R3 value in ohms : " #input  r3 := cr
." Enter R4 value in ohms : " #input  r4 := cr
." Enter C1 value in farads : " #input  c1 := cr
." Enter C2 value in farads : " #input  c2 := cr
." Enter C3 value in farads : " #input  c3 := cr
." Enter C4 value in farads : " #input  c4 := cr
." Enter C5 value in farads : " #input  c5 := cr
." Enter C6 value in farads : " #input  c6 := cr
." Enter C7 value in farads : " #input  c7 := cr
TBG.IMP
;
: fill.matrix
z2 inv z5 inv z4 inv + + z4 * coeffs xsect[ 1 , 1 , ! ] :=
z4 z5 / neg coeffs xsect[ 1 , 2 , ! ] :=
z3 z5 / neg coeffs xsect[ 2 , 1 , ! ] :=
z1 inv z5 inv z3 inv + + z3 * coeffs xsect[ 2 , 2 , ! ] :=
;
: solve.float
" load.overlay matfit.sov " "exec
25 1 do
  " coeffs xsect[ ! , ! , i ] ac solve.sim.eqs " "exec
  %v xsect[ ! , i ] :=
loop
100 %v xsect[ 1 , ! ] - z4 / 100 %v xsect[ 2 , ! ] - z3 / + inv 100 *
dup zmag absimp :=
inv zre&im omega / cp := inv rp :=
%v xsect[ 1 , ! ] zmag neg 100 + %vtip :=
;

: TB.CAL
    z1 z2 + inv z5 inv + zre&im omega / cp := inv rp :=
;
: TG.CAL
    z1 z5 + inv z2 inv + zre&im omega / cp := inv rp :=
;
: BG.CAL
     z2 z5 + inv z1 inv + zre&im omega / cp := inv rp :=
;
: T_BG.CAL z2 inv z5 inv + zre&im omega / cp := inv rp := ;

: G_TB.CAL z1 inv z2 inv + zre&im omega / cp := inv rp := ;

: B_TG.CAL z1 inv z5 inv + zre&im omega / cp := inv rp := ;

: TB.CMEAS.PLOT   \ plot the measured tip to body values in pF
```

```
    100 18.5 position " TB " label
    1e3 17.6 position " TB " label
    1e4 11.1 position " TB " label
    1e5 9.7  position " TB " label
    1e6 9.6  position " TB " label
;
: TB.RMEAS.PLOT \ plot th log of measured tip to body res. vals. in ohms
    1e3 77e6  log position " TB " label
    1e4 5.3e6 log position " TB " label
    1e5 3.7e6 log position " TB " label
    1e6 988e3 log position " TB " label
;
: TG.CMEAS.PLOT \ plot measured tip to ground wire cap vals
    1e2 20.0  position " TG " label
    1e3 19.9  position " TG " label
    1e4 19.86 position " TG " label
    1e5 19.8  position " TG " label
    1e6 19.7  position " TG " label
;
: TG.RMEAS.PLOT  \ measured tip to ground parallel resitance
    1e2 996e3 log position " TG " label
    1e3 995e3 log position " TG " label
    1e4 994e3 log position " TG " label
    1e5 933e3 log position " TG " label
    6e5 510e3 log position " TG " label
    1e6 291e3 log position " TG " label
;
: BG.CMEAS.PLOT \ plots measured body to ground par. capacitances
    1e2 19.8 position " BG " label
    1e3 19.5 position " BG " label
    1e4 19.1 position " BG " label
    1e5 18.7 position " BG " label
    1e6 18.0 position " BG " label
;
: BG.RMEAS.PLOT  \ plotd meas'd body to ground par. res. meas's
    1e4 60e6  log position " BG " label
    1e5 4.7e6 log position " BG " label
    1e6 110e3 log position " BG " label
;
 : freq.lab
    11 color
    1 -1 position " O " label
    1e1 -1 position " 1 " label
    1e2 -1 position " 2 " label
    1e3 -1 position " 3 " label
    1e4 -1 position " 4 " label
    1e5 -1 position " 5 " label
    1e6 -1 position " 6 " label
    1e7 -1 position " 7 " label
    1e8 -1 position " 8 " label
```

```
    0.5 -1.5 position " 1O " label
    5e0 -1.5 position " 1O " label
    5e1 -1.5 position " 1O " label
    5e2 -1.5 position " 1O " label
    5e3 -1.5 position " 1O " label
    5e4 -1.5 position " 1O " label
    5e5 -1.5 position " 1O " label
    5e6 -1.5 position " 1O " label
    5e7 -1.5 position " 1O " label
    5e3 -2.5 position " FREQUENCY " label
;
: cap.lab
    .4 0 position " O " label
    .4 2 position " 2 " label
    .4 4 position " 4 " label
    .4 6 position " 6 " label
    .4 8 position " 8 " label
    .4 10 position " 1O " label
    .4 12 position " 12 " label
    .4 14 position " 14 " label
    .4 16 position " 16 " label
    .4 18 position " 18 " label
    .4 20 position " 2O " label
    1 21 position " PARALLEL CAPACITANCE (pF) " label
;
: STANDARD.GRAPH
    16 label.color
    1 0 axis.point logarithmic
    0 py [ 1 ] := 20 py [ 2 ] := px  1 px [ 1 ] := 1e8 px [ 2 ] :=
    "  " symbol
    px py xy.auto.plot 11 label.color
    freq.lab cap.lab
;

: CAL.MEAS.PLOT
    standard.graph freq.lab cap.lab
    2 5 position " log PARALLEL RESISTANCE (ohms) " label
    10 4 position " TG - TIP TO GROUND " label
    10 3 position " TB - TIP TO BODY " label
    10 2 position " BG - GROUND TO BODY " label
    5e4 14 position " LINES - CALCULATED VALUES " label
    5e4 12 position " SYMBOL - MEASURED VALUES " label
    10 color solid
    tb.cal  freq cp 1e12 * xy.data.plot freq rp log xy.data.plot
    TB.CMEAS.PLOT
    TB.RMEAS.PLOT
    11 color .01 .01 .01 .01 dashed
    tg.cal freq cp 1e12 * xy.data.plot freq rp log xy.data.plot
    TG.CMEAS.PLOT
    TG.RMEAS.PLOT
```

```
    12 color  .02 .02 .02 .02 dashed
    bg.cal freq cp 1e12 * xy.data.plot freq rp log xy.data.plot
    BG.CMEAS.PLOT
    BG.RMEAS.PLOT
    10 label.color
;
: default.cir
    1.74e5 r1 := 1e6 r2 := 1e2 r3 := 1e9 r4 :=
    1.7e-12 c1 := 15.0e-12 c2 := .1e-12 c3 := 18.3e-12 c4 :=
    1.8e-12 c5 := 90e-12 c6 := 1e-15 c7 :=
    TBG.IMP
;

: tip.cal
fill.matrix
solve.float
;
: default.plot
    default.cir cal.meas.plot
;
: %plot
    0 py [ 1 ] := 100 py [ 2 ] := px  1 px [ 1 ] := 1e8 px [ 2 ] :=
    "  " symbol
    px py 16 label.color xy.auto.plot solid
    14 color solid TIP.CAL freq %vtip xy.data.plot  %vtip %v_ins :=
    11 color
    .5 00 position " O " label
    .4 10 position " 1O " label
    .4 20 position " 2O " label
    .4 30 position " 3O " label
    .4 40 position " 4O " label
    .4 50 position " 5O  " label
    .4 60 position " 6O " label
    .4 70 position " 7O " label
    .4 80 position " 8O " label
    .4 90 position " 9O " label
    .3 100 position " 1OO " label
    1 -5 position " O " label
    1e1 -5  position " 1 " label
    1e2 -5  position " 2 " label
    1e3 -5  position " 3 " label
    1e4 -5  position " 4 " label
    1e5 -5  position " 5 " label
    1e6 -5  position " 6 " label
    1e7 -5  position " 7 " label
    1e8 -5  position " 8 " label
    0.5 -9  position " 1O " label
    5e0 -9  position " 1O " label
    5e1 -9  position " 1O " label
    5e2 -9  position " 1O " label
```

```
    5e3 -9  position " 1O " label
    5e4 -9  position " 1O " label
    5e5 -9  position " 1O " label
    5e6 -9  position " 1O " label
    5e7 -9  position " 1O " label
    5e3 -15 position " FREQUENCY " label
    z3 zstore := 1 z3 := tip.cal freq %vtip
    .01 .01 .01 .01 dashed 12 color xy.data.plot %vtip %v_unins :=
    zstore z3 := z1 zstore :=  1 z1 := tip.cal freq %vtip %vtip %v_gnd :=
    .02 .02 .02 .02 dashed 10 color xy.data.plot zstore z1 := tip.cal
    11 color
    1 105 position " % VOLTAGE DROP FROM TIP TO SAMPLE " label
    5 85 position " SOLID - HEAD/HOLDER INSULATED " label
    5 70 position " SMALL DASHES - HEAD/HOLDER UNINSULATED " label
    5 55 position " LARGE DASHES - HEAD GROUNDED " label
;
: IMP.PLOT \ plots measured & calculated circuit impedance
    standard.graph
    freq.lab cap.lab 1 21 position 16 color " PARALLEL CAPACITANCE (pF) " label
    10 color
    100 9e6 log position " ^ " label
    1e3 1.06e6 log position " ^ " label
    1e4 1.17e5 log position " ^ " label
    1e5 1.3e4 log position " ^ " label
    1e6 1.5e3 log position " ^ " label
    11 color
    100 8.22e6 log position " v " label
    1e3 950e3 log position " v " label
    1e4 106e3 log position " v " label
    1e5 11.7e3 log position " v " label
    1e6 1.39e3 log position " v " label
    5 19 position " log IMPEDANCE VS FREQUENCY " label
    8 18 position " ^ - BIAS TO GROUND THROUGH CABLE (NO HEAD) "
    label
    8 16 position " v - BIAS TO GROUND THROUGH CABLE (HEAD CONNECTED) "
    label
    8 14 position " SOLID LINE - CALCULATED SAMPLE - GROUND IMPEDANCE " label
    14 color solid freq absimp log xy.data.plot
;
: circuit.menu cr
." plot.axes to create specific axes "  cr
." circuit.menu to get menu list " cr
." circuit.diagram to view circuit " cr
." get.values to input new r's & c's  " cr
." default.plot plot head A caps & res's from default values " cr
." cal.meas.plot to plot calculated and measured data " cr
." tip.cal to calculate circuit equivalence and % volt across tip " cr
." %plot to plot % voltage drop across tip " cr
; circuit.menu
```

A.2 Asyst program for D/A pulse and sample hold

filename: WAVE.

```
echo.off
normal.display
forget.all
\ This is a program to create a one shot pulse
\ The user will enter initial, pulse step, and final voltages
\   and also ramp and pulse durations


\ Create variables
real scalar initial.val    \ initial dc voltage in volts
real scalar initial.dur    \ time at initial value in msec.
real scalar ramptime.ini   \ present to initial ramp duration in msec.
real scalar pulse.stp      \ delta value oulse step in volts
real scalar pulse.dur      \ time the pulse stays constant in msec.
real scalar final.val      \ the final voltage of the waveform in volts.
real scalar ramptime.fin   \ the time desired from pulse to final dc voltages
integer scalar present.val \ the present digital value of the dc output
integer dim[ 100 ] array ramp.pi \ declare array for ramp to initial value
real scalar c.d1    \ conversion delay for wave1
real scalar c.d2    \ conversion delay for wave2
real scalar c.d3   .5 c.d3 := \ final delay for sample hold
integer dim[ 3 ] array bits \ array for digital pulses
0 0 10 40 window win.top \ create text window top half screen
11 0 24 79 window win.bot \ create text window bottom half screen
0 41 10 79 window win.ur \ create upper right window
0 bits [ 1 ] := 1 bits [ 2 ] := 256 bits [ 3 ] :=

: values.get              \ input values for waveform variables
cr
." Enter initial output value in volts :  "
   #input initial.val :=
cr
." Enter initial output duration in seconds :  "
   #input 1000 * initial.dur :=
cr
." Enter present to initial ramp duration ( 1 msec min ) : "
   #input ramptime.ini :=
cr
." Enter pulse step value in volts :  "
   #input pulse.stp :=
cr
." Enter pulse duration (0.01 < x < 10 msec) :  "
   #input pulse.dur :=
cr
." Enter final output value in volts :  "
   #input final.val :=
```

```
cr
." Enter pulse to final ramp duration (milliseconds)  "   cr
." (If > 5 * " pulse.dur "." "type ." use multiples) : "
   #input ramptime.fin :=
cr
win.ur 12 foreground 0 background screen.clear  cr cr
."    initial.val  (volts) = " initial.val . cr
."    initial.dur  (msecs) = " initial.dur . cr
."    ramptime.ini (msecs) = " ramptime.ini . cr
."    pulse.stp    (volts) = " pulse.stp . cr
."    pulse.dur    (msecs) = " pulse.dur . cr
."    final.val    (volts) = " final.val . cr
."    ramptime.fin (msecs) = " ramptime.fin . cr
win.bot
7 foreground 1 background
;


: r/d  \ scale real values to digital for output
-10.000000 10.000000 d/a.scale ;


dt2820                    \ initialize the type of board to be used
0 0 a/d.template pres.val  \ create an analog to digital template
0 0 d/a.template wave1 \ create a digital to analog template
0 0 d/a.template wave2 \ create a digital to analog template
0 0 d/a.template fixdc \ create a d\a template for setting present voltage
3 digital.template dig \ create digital template, sample-hold control
dig digital.init 256 digital.out
\ Subroutine to set output voltage
: volt.out   cr
." Enter desired output voltage  : " #input cr
r/d fixdc d/a.init d/a.out
;

: present.get        \ read the analog signal on ch0 from analog out ch0
.05 conversion.delay
pres.val a/d.init a/d.in present.val :=
;


: wave.create   \ create arrays for the voltage pulse
values.get
present.get
present.val initial.val r/d ramp.pi []fill
ramptime.fin 5 pulse.dur * <
  if
    " integer dim[ 100 pulse.dur * ] array pulse.constant " "exec
    " pulse.stp initial.val + r/d " "exec
    " pulse.constant := " "exec
```

```
    " integer dim[ 100 ramptime.fin * 2 + ] array ramp.pf " "exec
    " initial.val pulse.stp + r/d final.val r/d " "exec
    " ramp.pf []fill " "exec
    " pulse.constant ramp.pf sub[ 2 ] catenate " "exec
    " integer dim[ []size ] array wave wave := " "exec
  else
    " integer dim[ 1 ] array pulse.constant "  "exec
    " integer dim[ ramptime.fin pulse.dur / ] array wave " "exec
    " initial.val pulse.stp + r/d final.val r/d " "exec
    " wave []fill " "exec
  then
" wave.set " "exec
;
: ramp.set   \ Initialize d/a templates and associate buffers
wave1
reset.das.device clear.template.buffers
" ramp.pi []size template.repeat ramp.pi " "exec
" double.template.buffers cyclic " "exec
ramptime.ini 100 / dup c.d1 := conversion.delay
das.init wave1
;


: condel     \ Calculate conversion delay for pulse and ramp down
ramptime.fin pulse.dur 5 * <
     if  .01
     else pulse.dur
     then
    dup c.d2 := conversion.delay
;


: pulse.set  \ Join buffers to pulse template & set time delay
wave2
reset.das.device
"  clear.template.buffers wave []size template.repeat " "exec
" wave double.template.buffers cyclic " "exec
condel
das.init wave2
;


: wave.set  \ Initialize d/a.templates
ramp.set
pulse.set
;


: repeat.wav   \ form a continuous wave
 cr  ." Type any key to stop "
```

```
begin
    c.d1 conversion.delay das.init wave1
    array>d/a.out
    initial.dur msec.delay c.d2 conversion.delay
    dig digital.init 0 digital.out
    das.init wave2
    array>d/a.out
    dig digital.init 256 digital.out
  ?key
  until
;

: recreate  \ create new waveform
wave1
clear.template.buffers
wave2
clear.template.buffers
 " forget pulse.constant " "exec
screen.clear
 " wave.create " "exec
 " wave.set " "exec
;
: oneshot   \ a one shot output
    c.d1 conversion.delay das.init wave1
    array>d/a.out
    initial.dur msec.delay
    dig digital.init 0 digital.out
    c.d2 conversion.delay das.init wave2
    array>d/a.out
    c.d3 msec.delay
    dig digital.init 256 digital.out
;
: dig.out
    dig digital.init
    0 digital.out c.d1 msec.delay
    1 digital.out c.d2 msec.delay 256 digital.out
;
\ repeat digital outputs
: repeat.dig
    ." Hit any key to stop " cr   dig digital.init
    begin 0 digital.out 1 digital.out c.d2 msec.delay 256 digital.out
    ?key until
;
: trigger
    dig digital.init
    257 digital.out 256 digital.out
;
: menu
win.top   2 foreground 0 background screen.clear
." Type 'wave.create' to create 1st wave "   cr
```

```
." Type 'recreate' to create new wave "  cr
." Type 'repeat.wav' to repeat continuously " cr
." Type 'oneshot' to output only one pulse " cr
." Type 'volt.out' to reset voltage output " cr
." Type 'dig.out' to output digital pulse " cr
." Type 'repeat.dig' to repeat digital pulse" cr
." Type 'trigger' to toggle one digital line" cr
win.bot

;

echo.on cr screen.clear
menu
```

Appendix B

Data Tables

Table b-1. Measured equivalent parallel capacitances (C_p) and resistances (R_p) for various frequencies. Measurements are taken between two of three designated points on Nanoscope II head 'A'.

a. Measurements between tip and ground wire:

freq. (Hz)	C_p (pF)	R_p (ohms)
100	20.0	996k
1k	19.9	995k
10k	19.86	994k
100k	19.8	933k
200k	19.76	851k
400k	19.72	678k
500k	19.71	590k
600k	19.72	510k
800k	19.72	382k
1M	19.71	291k

b. Measurements between body and ground wire:

f (Hz)	C_p (pF)	R_p (ohms)
100	19.8	-----
1k	19.5	-----
10k	19.06	61M
100k	18.75	4.7M
1M	17.98	110k

c. Measurements between tip and body:

f (Hz)	C_p (pF)	R_p (ohms)
100	18.5	-----
1k	17.6	77M
10k	11.1	5.3M
100k	9.7	3.7M
1M	9.6	988k

Table b-2. The measured ac parallel capacitances (C_p) and resistances (R_p) as a function of frequency between one point of Nanoscope II head 'A' to the connected other two points.

a. Measurements from tip to connected ground and body:

f (Hz)	C_p (pF)	R_p (ohms)
100	18.2	996k
1k	20.2	995k
10k	20.3	994k
100k	20.2	943k
1M	20.1	318k

b. Measurements from body to connected tip and ground:

f (Hz)	C_p (pF)	R_p (ohms)
100	18.6	-----
1k	18.4	-----
10k	18	>100M
100k	17.7	9.9M
1M	17.4	174k

c. Measurements from ground to connected tip and body:

f (Hz)	C_p (pF)	R_p (ohms)
100	35	996k
1k	35	994k
10k	34.6	977k
100k	34.2	830k
1M	33.97	139k

Appendix C

Additional Graphs of Data

C.1 Power spectrum plots while tunneling

The figures in this section show additional I(s) and ln[I(s)] characteristics and power density during tunneling for various tips. The sample was HOPG. The tip materials are as follows:

Figure c:1 - Palladium

Figure c:2 - Palladium

Figure c:3 - Platinum

Figure c:4 - Platinum

Figure c:5 - Silver

Notice that some of the spectrums have peaks while others do not. Figure c:2 has peaks at multiples of 25 Hz, which could be due to a power line variation or a low frequency vibration in the isolation system. Figure c:3 has a sharp peak at 300 Hz and Figure c:4 shows several broad peaks near 200 Hz and 400 Hz The source of the peaks is undetermined. Since tip sample separation changes on the order of 1 nanometer can change the current by more than 50%, small vibrations can alter the data significantly. Figure c:5 shows a power spectrum has no visible peaks, which suggests that there is no inherent vibration of the translation stage.

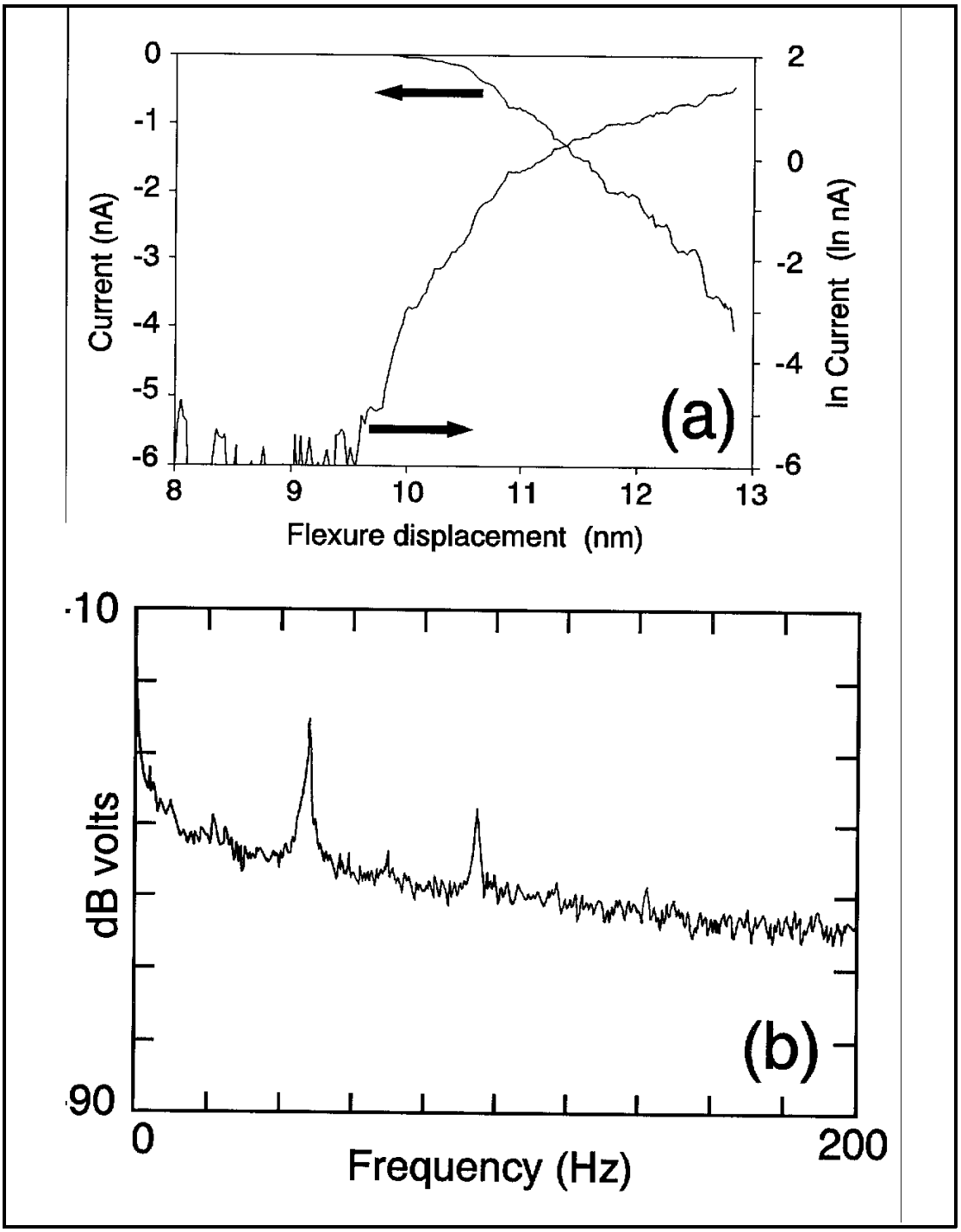

Figure c:1. (a) Current and it's natural log versus flexure displacement for a Pd-HOPG system. (b) The power spectrum from the I:V converter for the maximum current in (a).

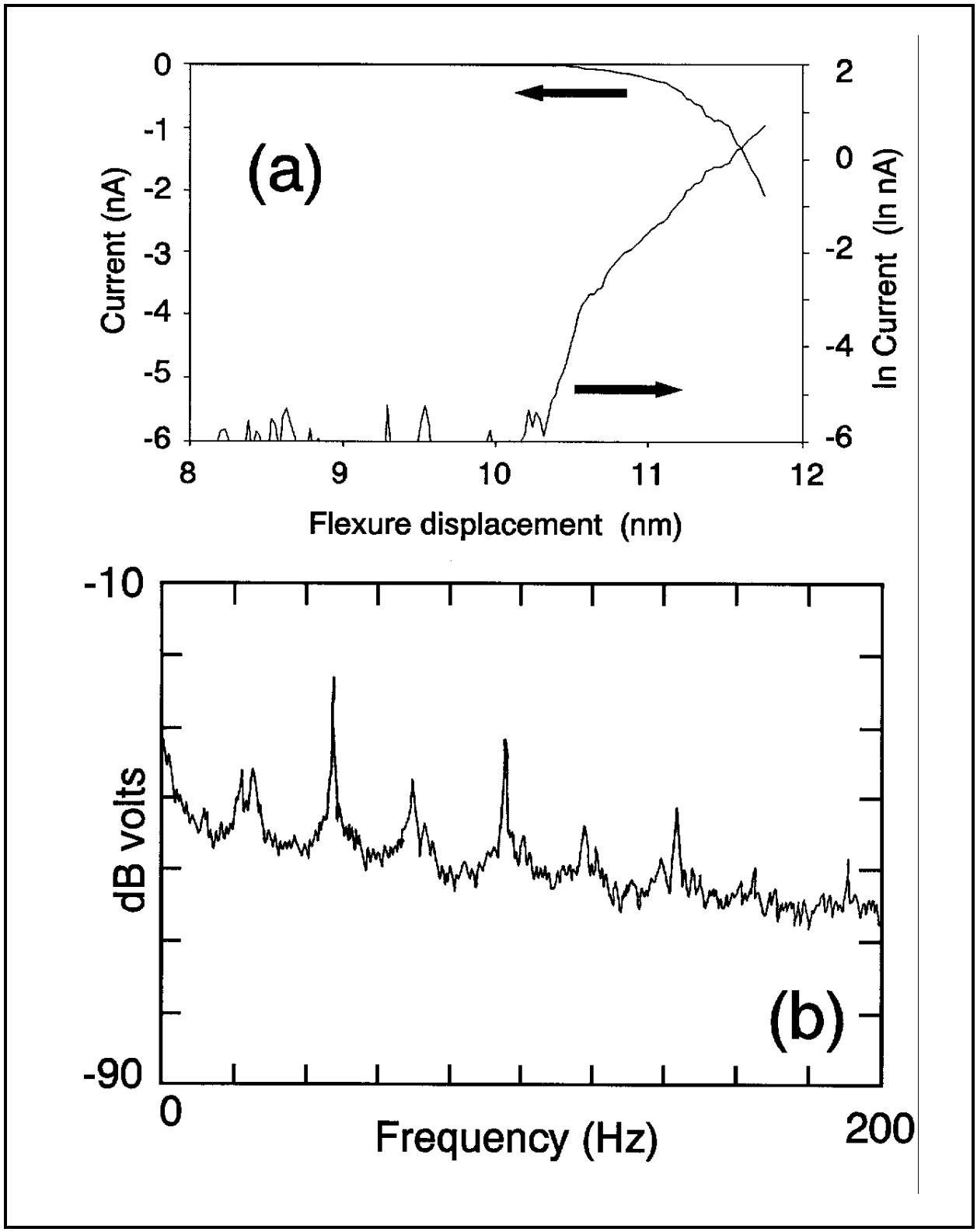

Figure c:2. (a) Current and it's natural log versus flexure displacement for a Pd-HOPG system. (b) The power spectrum from the I:V converter for the maximum current in (a).

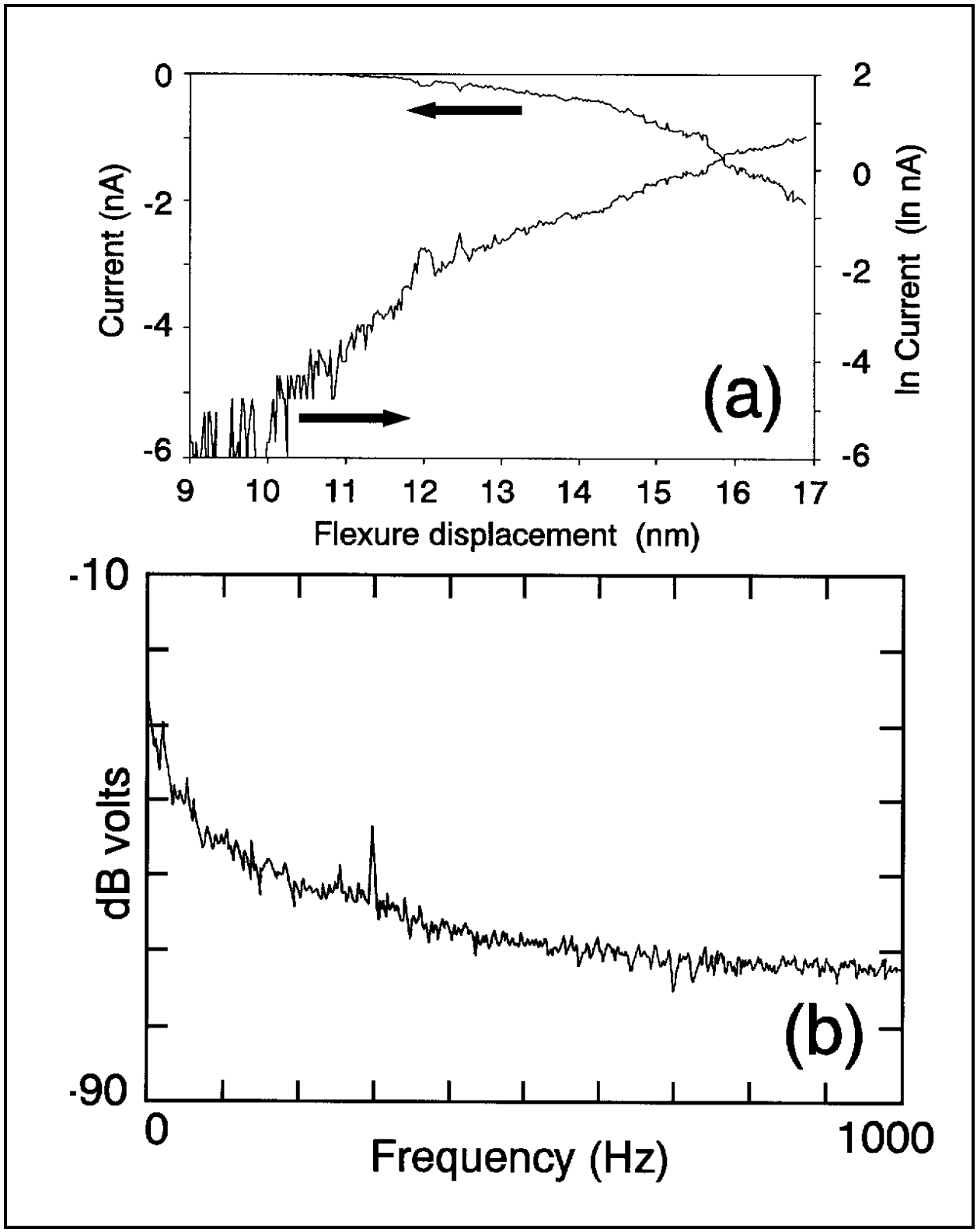

Figure c:3. (a) Current and it's natural log versus flexure displacement for a Pt-HOPG system. (b) The power spectrum from the I:V converter for the maximum current in (a).

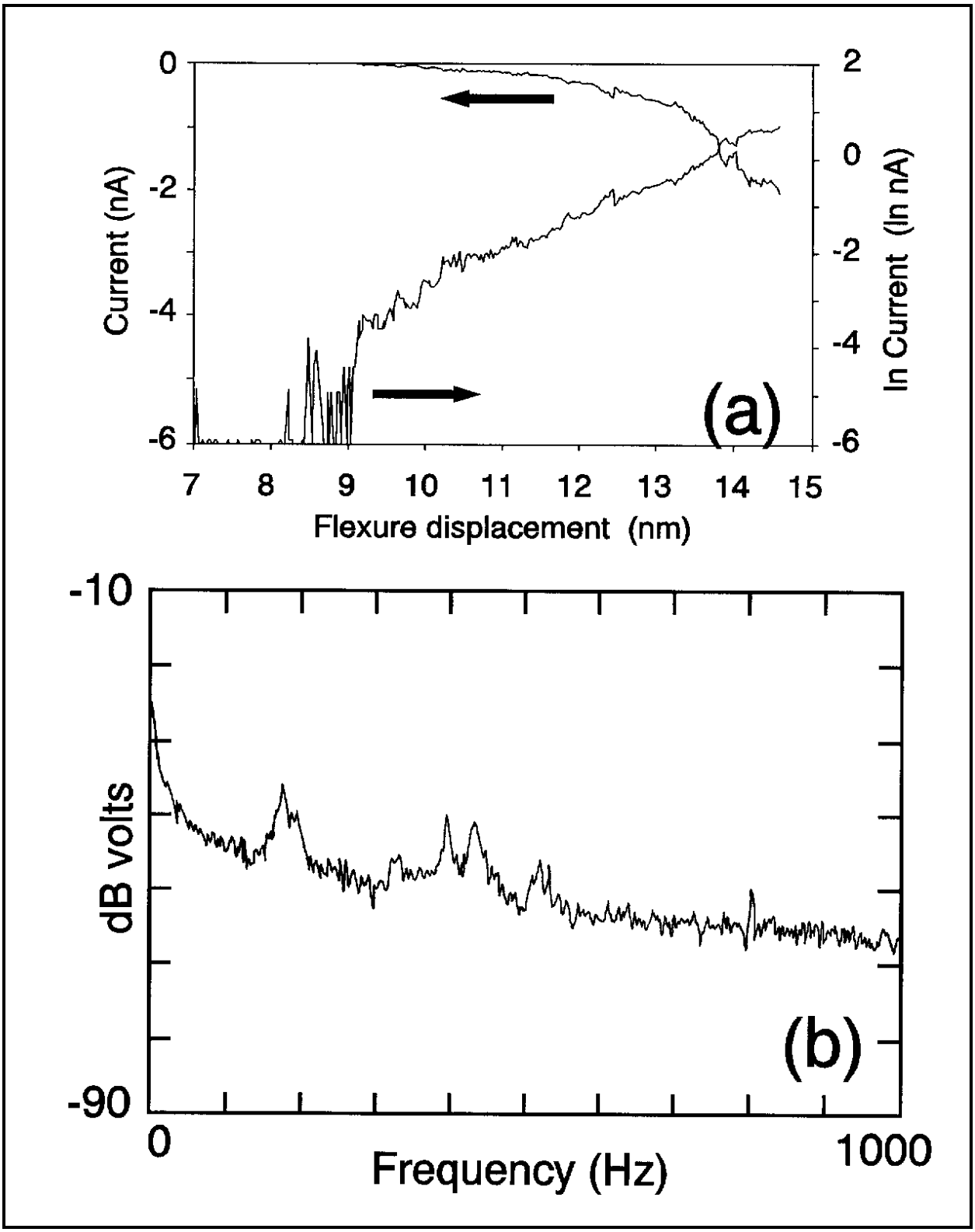

Figure c:4. (a) Current and it's natural log versus flexure displacement for a Pt-HOPG system. (b) The power spectrum from the I:V converter for the maximum current in (a).

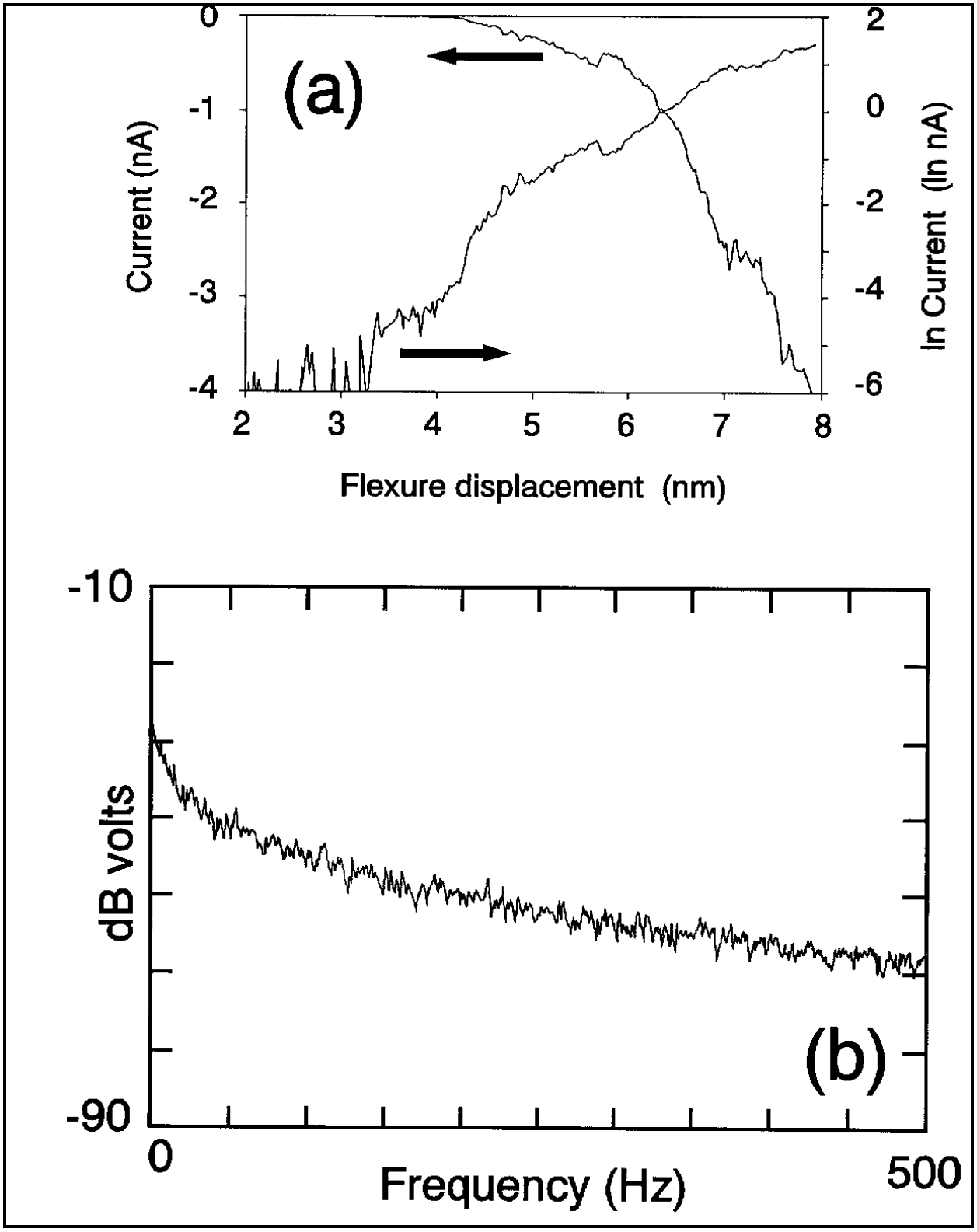

Figure c:5. (a) Current and it's natural log versus flexure displacement for a Ag-HOPG system. (b) The power spectrum from the I:V converter for the maximum current in (a).

C.2 Additional I(s) data from x-ray calibrated tunneling apparatus

This section contains over 50 data sets taken with the x-ray calibrated tunneling apparatus described in the main body. All data used a piece of HOPG for the sample. Data sets 1-33 are with several Pt-Ir tips. Data sets 36-42 are with a Pd tip. Data sets 46-56 are wit an Ag tip. All of the data was taken under room ambient conditions. Noisy data as well as 'good' data are included to show that a given tip can produce varied I(s) curves. Attempts to use a Cu tip did not produce good tunneling. Each graph contains it's I(s) data along with the natural log of the current versus flexure displacement. The Ln data also has lines fitted to the data. All of the line fits were done by the least squares regression in Quattro Pro unless they have a nc suffix. Where the slopes have a nc suffix, the best 'eye' fit has been made. The tunneling biases are included on each graph.

A compilation of the slopes for all of the data sets is given in Figure c:13. The slopes are marked directly above the data set numbers. The symbols have been chosen to reveal a possible propensity for certain slope values.

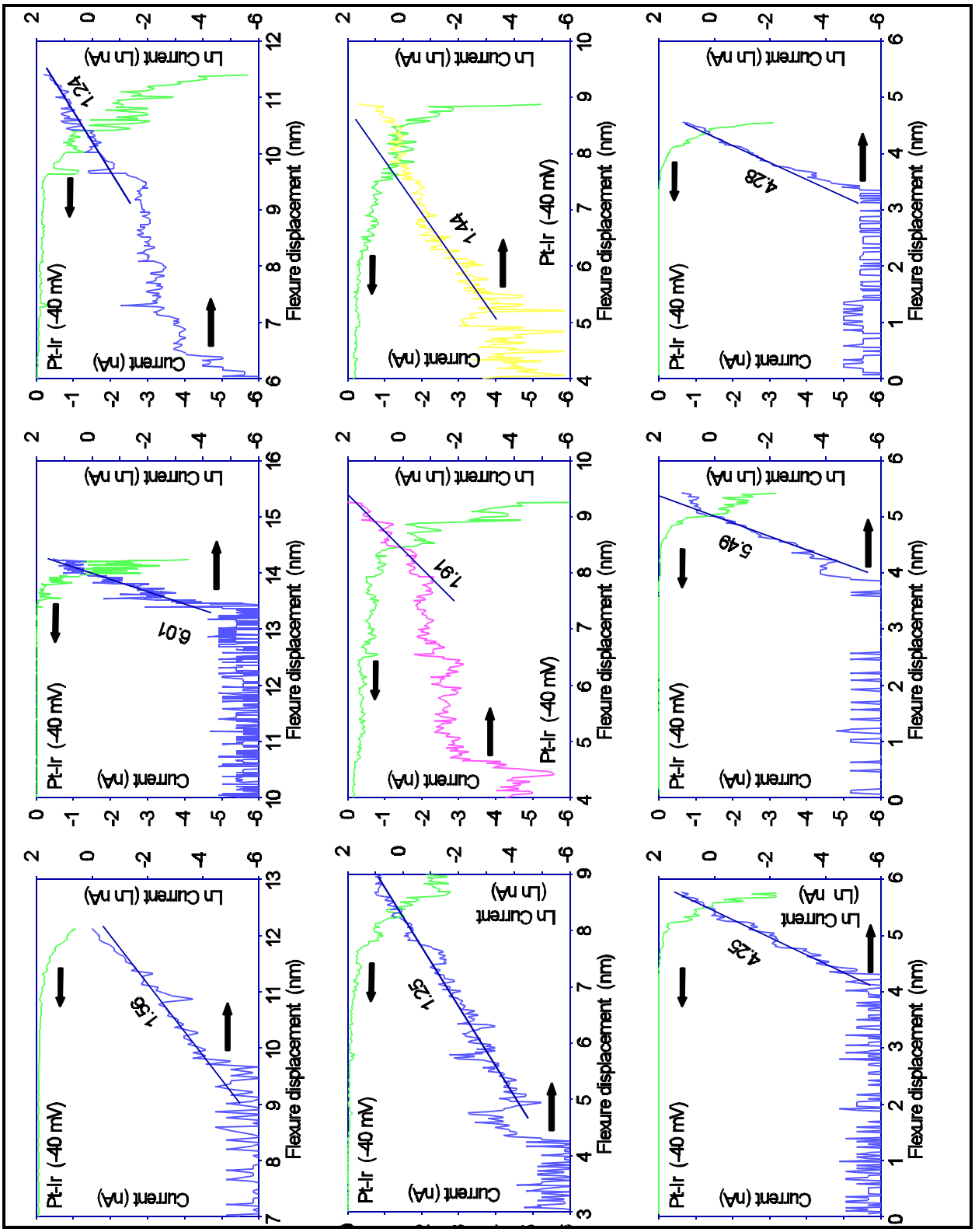

Figure c:6. I(s) and the natural log of I(s) curves. Data sets 1-9. The slopes to least squares fits to the Ln I(s) curves are in nm^{-1}.

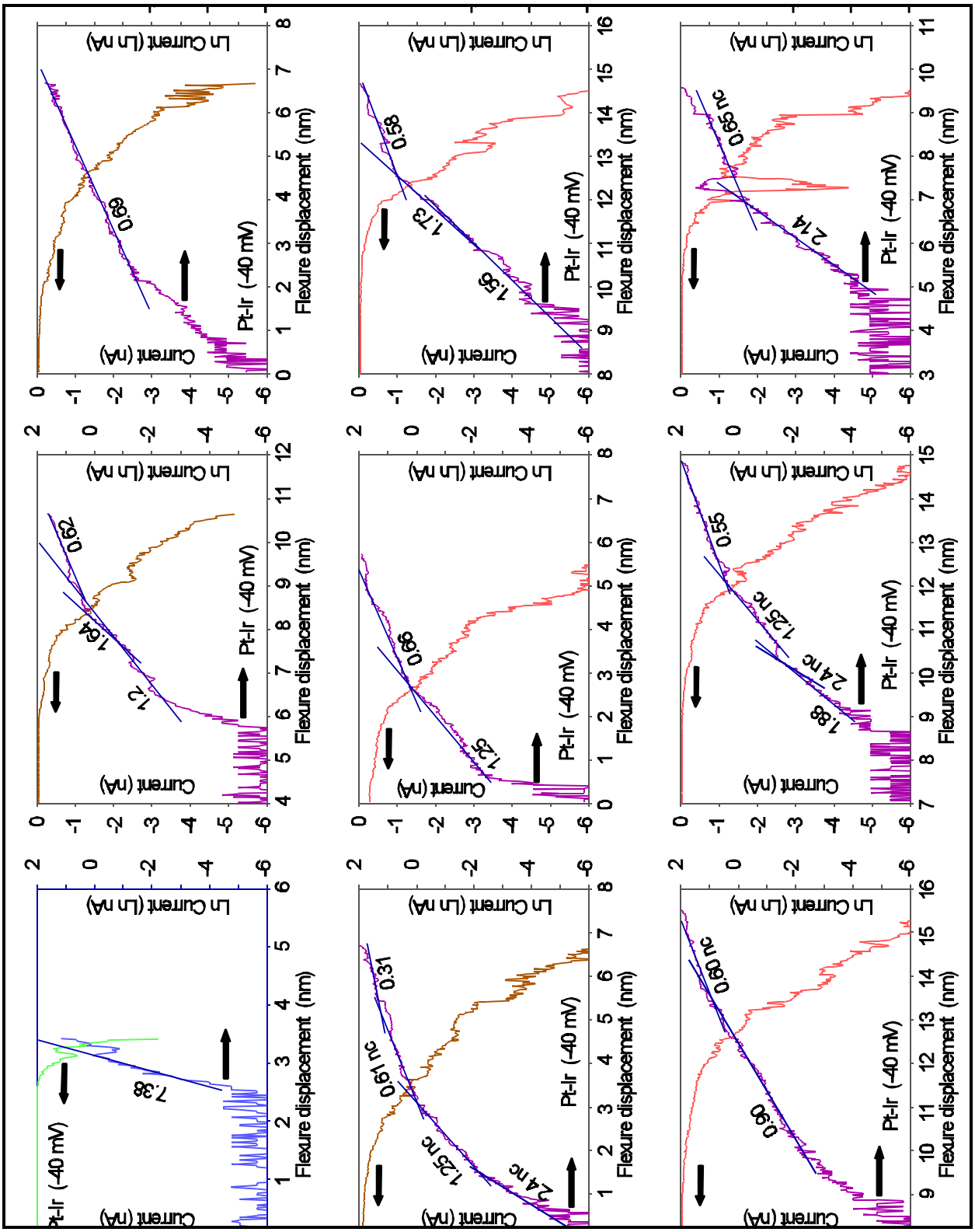

Figure c:7. I(s) and Ln I(s) of data sets 10-18. The slopes are in nm^{-1}. All slopes were calculated with a least squares regression unless followed by the suffix nc.

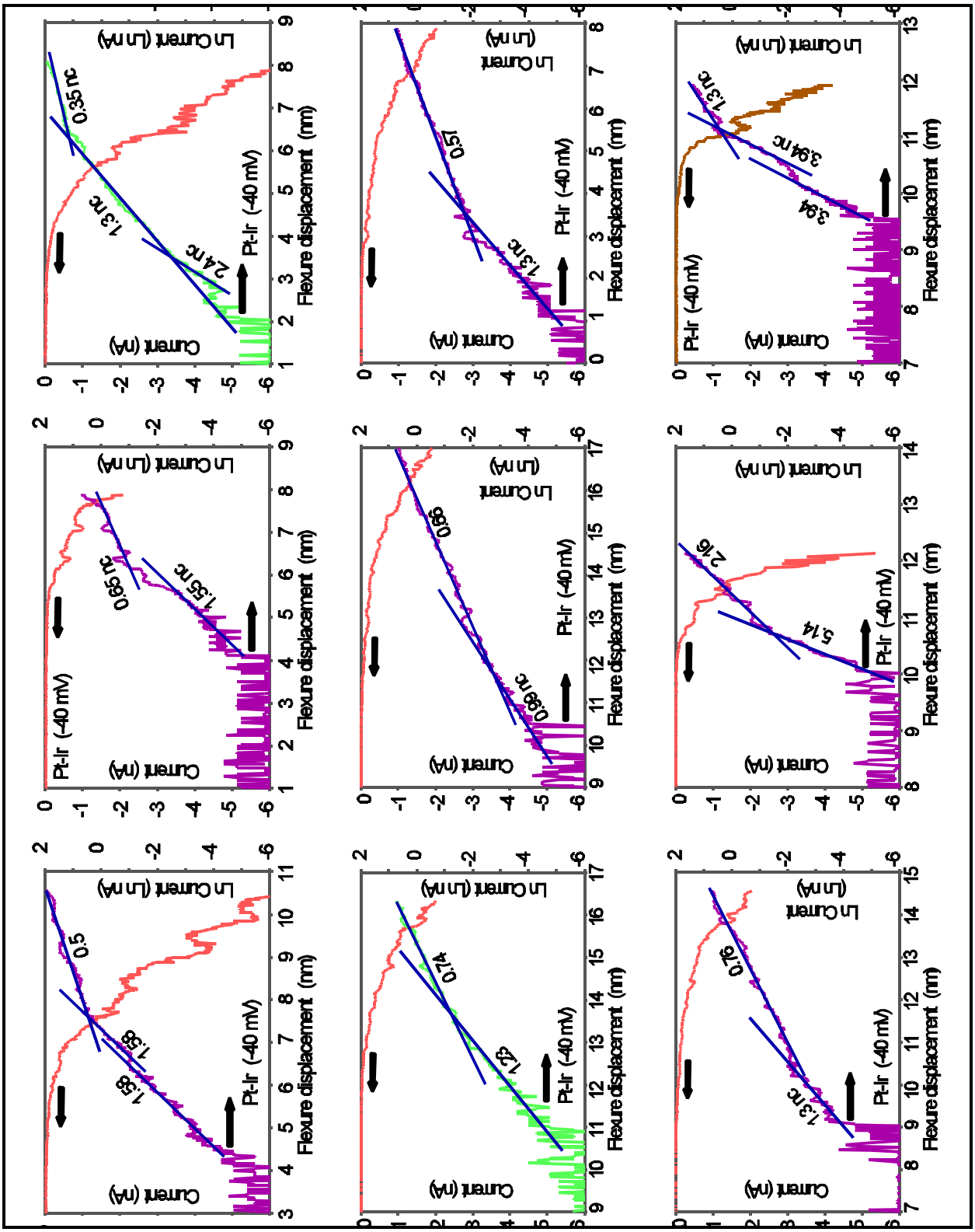

Figure c:8. I(s) and Ln I(s) of data sets 19-27. The slopes are in nm^{-1}. All slopes were calculated with a least squares regression unless followed by the suffix nc.

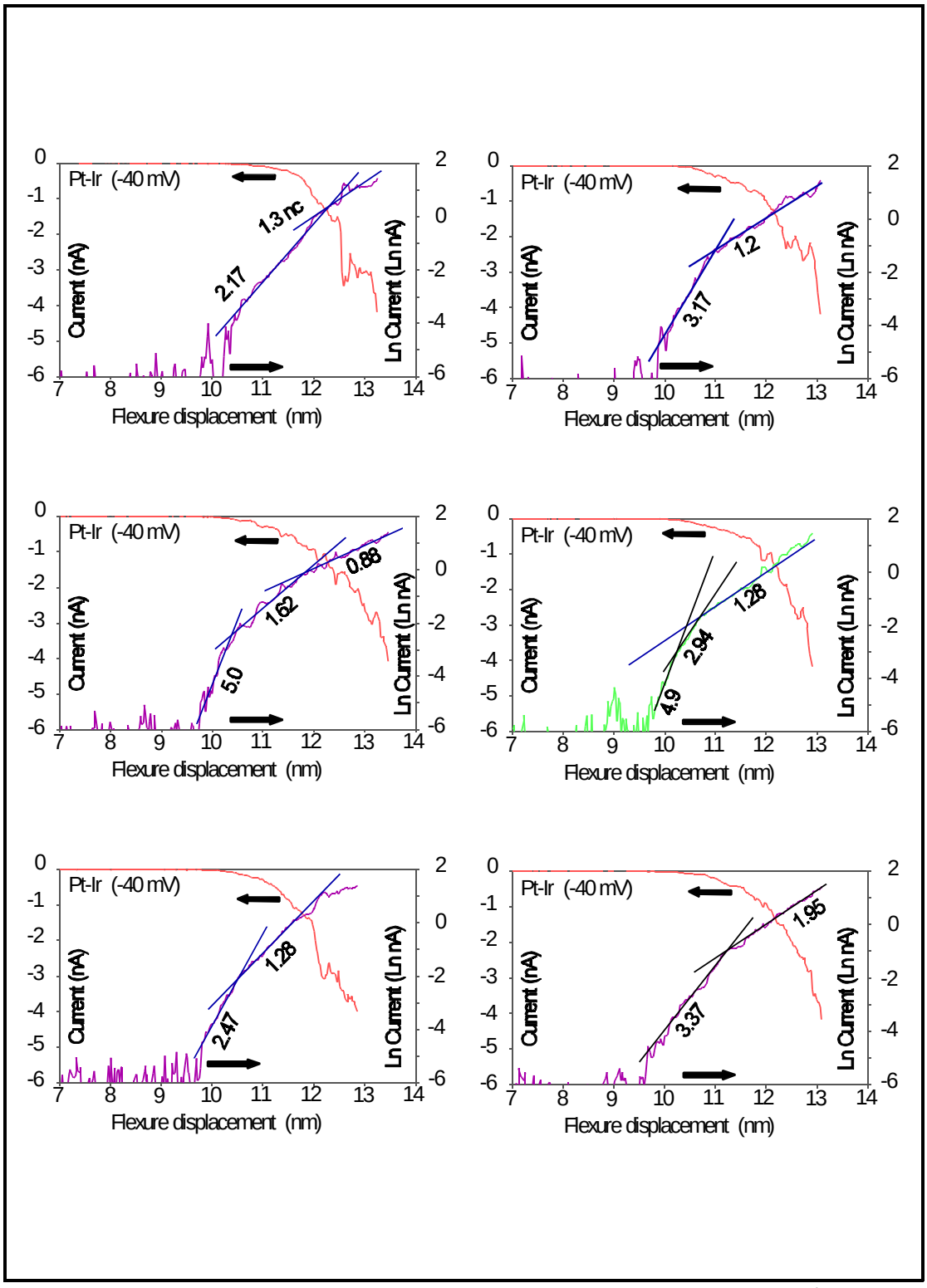

Figure c:9. I(s) and Ln I(s) of data sets 28-33. The slopes are in nm^{-1}. All slopes were calculated with a least squares regression unless followed by the suffix nc.

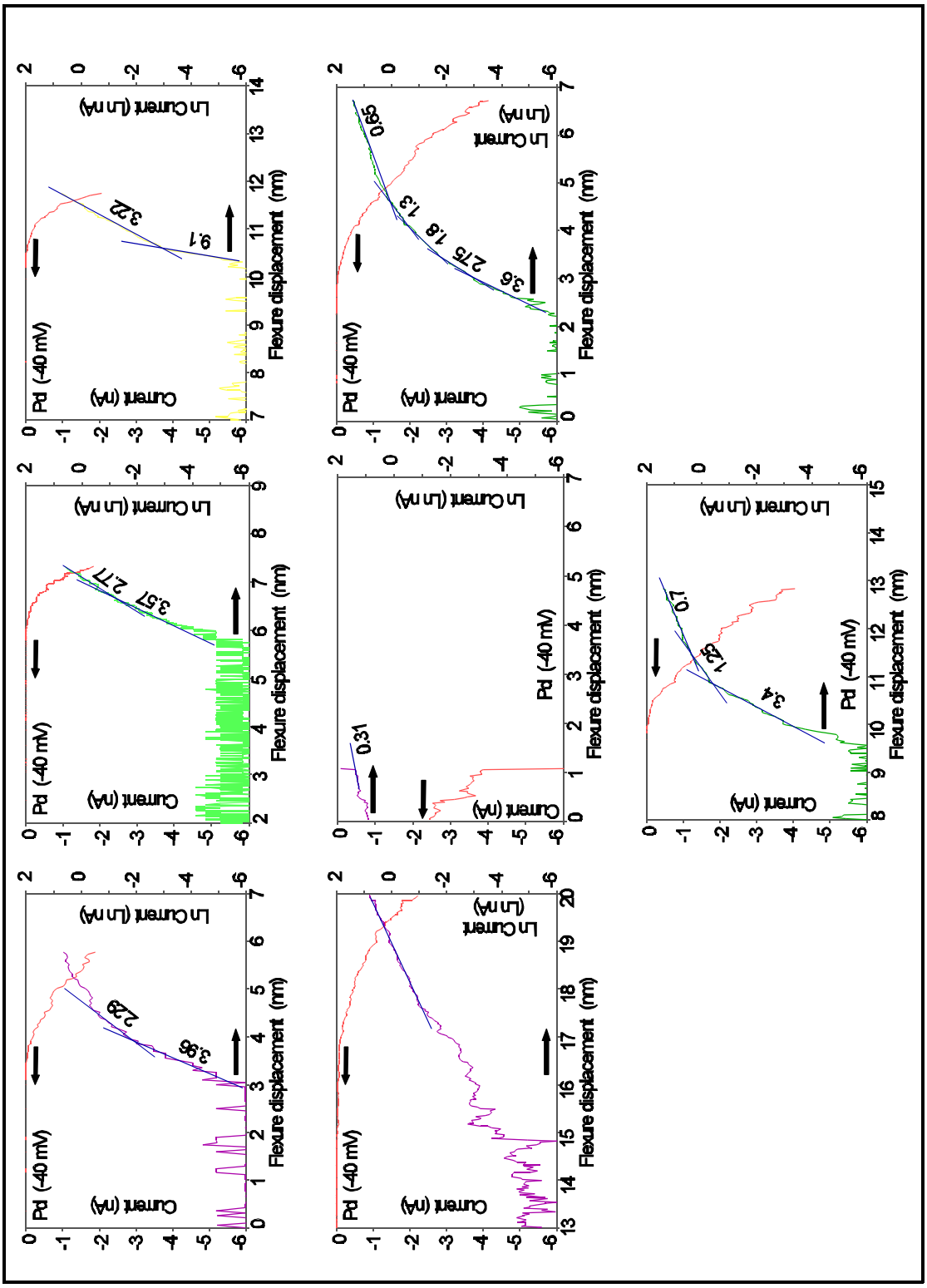

Figure c:10. I(s) and Ln I(s) of data sets 36-42. The slopes are in nm^{-1}. All slopes were calculated with a least squares regression unless followed by the suffix nc.

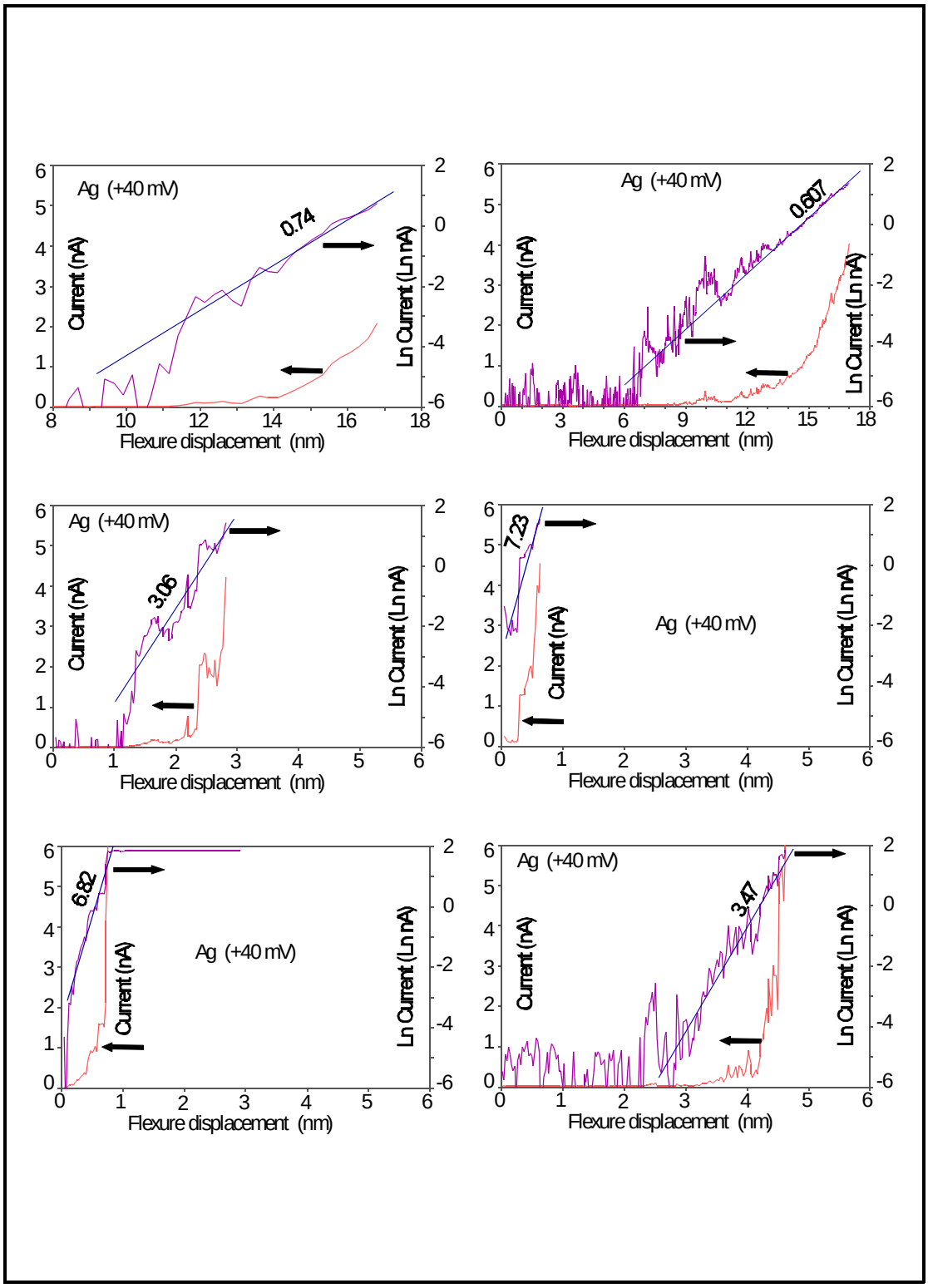

Figure c:11. I(s) and Ln I(s) of data sets 46-51. The slopes are in nm^{-1}. All slopes were calculated with a least squares regression unless followed by the suffix nc.

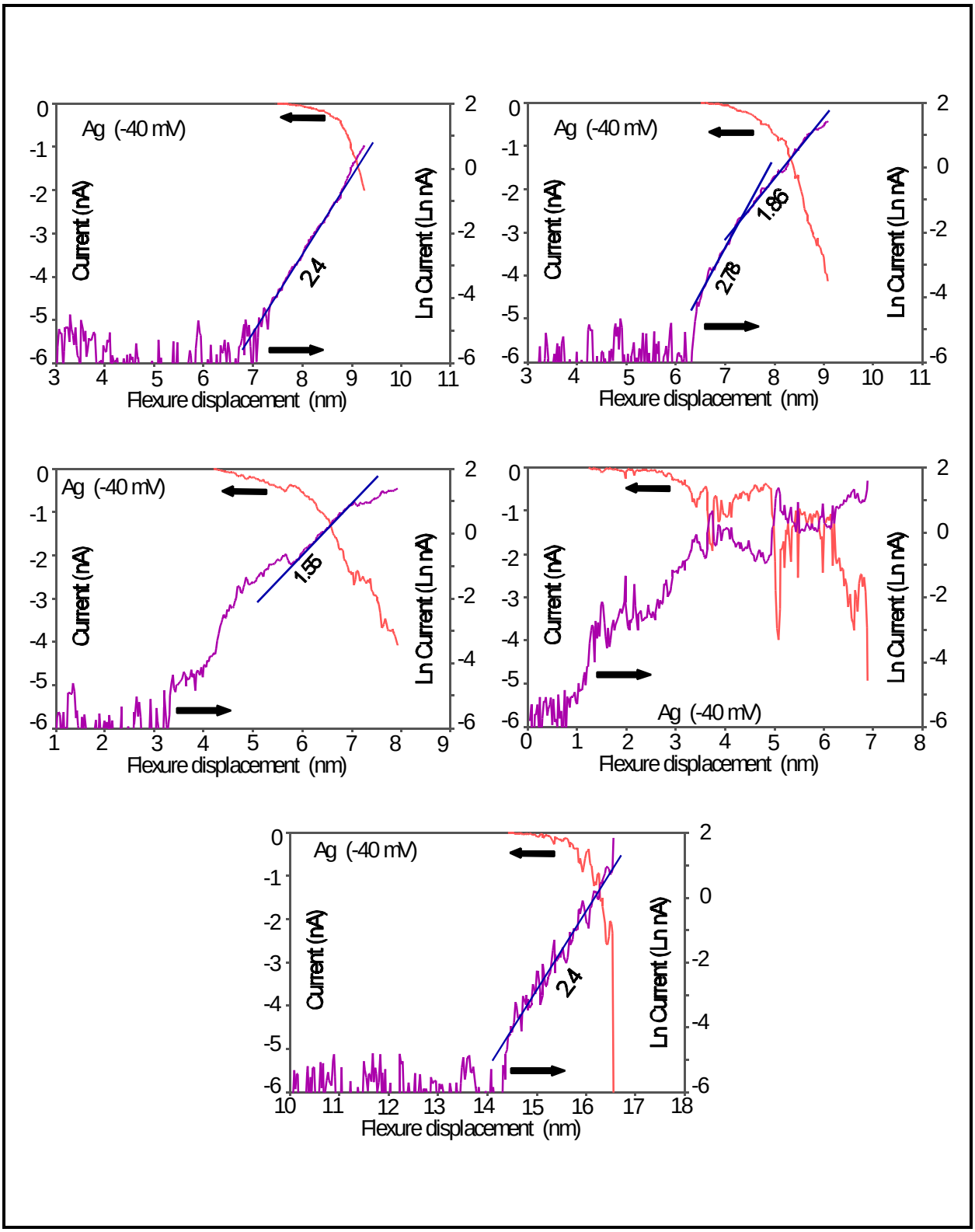

Figure c:12. I(s) and Ln I(s) of data sets 52-56. The slopes are in nm^{-1}. All slopes were calculated with a least squares regression unless followed by the suffix nc.

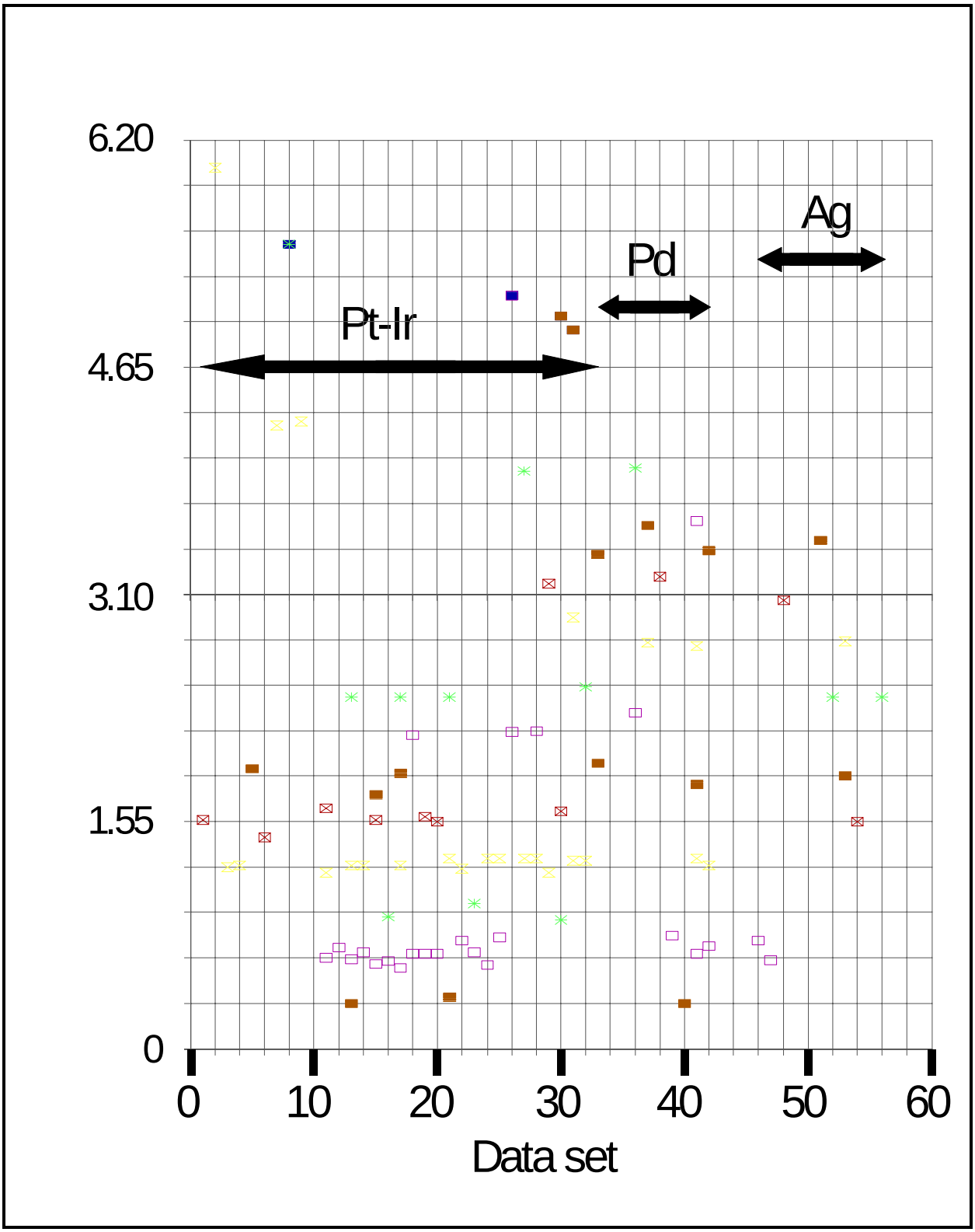

Figure c:13. Slopes from the natural log of I(s) curves the previous data sets taken with Pt-Ir, Pd, and Ag tips.

C.3 Additional I(s) data from Nanoscope II

The next four figures demonstrate the effect of bias and voltage pulsing on I(s) curves. Each of the figures contains at least two curves for 0.2 nA, 0.5 nA, and 2 nA currents. Figure appendix c-17 shows curves taken for a -50 mV sample bias and Figure c:15 shows curves taken for a -500 mV bias. After a extended voltage pulse, the data of Figures c:16 and c:17 were taken for -50 mV and -500 mV, respectively.

The data shows the -500 mV curves to be steeper than -50 mV curves at a given time, but if the tip is altered by something such as the voltage pulse the I(s) curves can change dramatically. In this case the curves became steeper after the application of an extended several volt pulse.

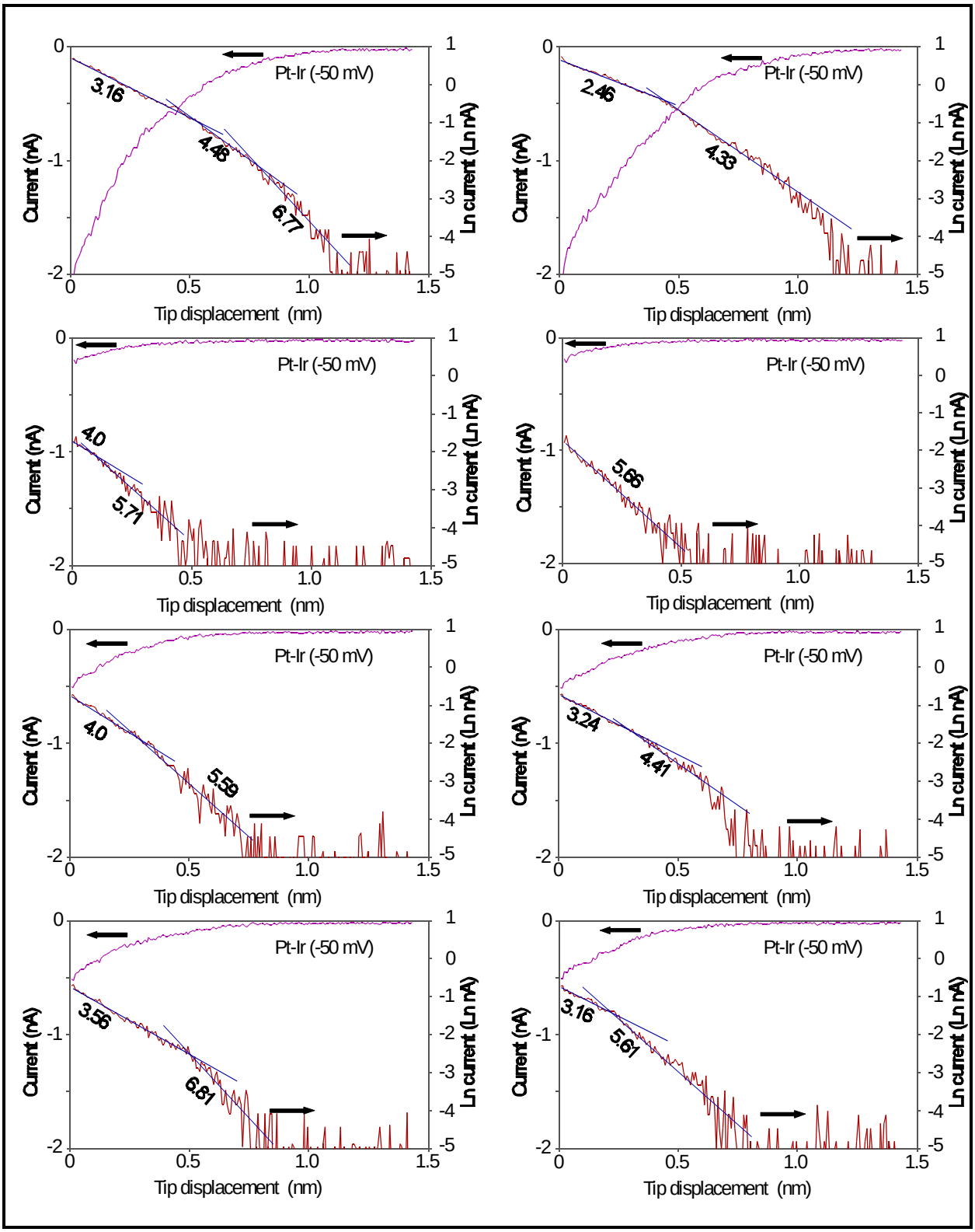

Figure c:14. I(s) curves taken with a -50 mV bias starting at currents of 0.2 nA, 0.5 nA, and 2.0 nA. Slopes of the Ln I(s) data are shown in nm^{-1}.

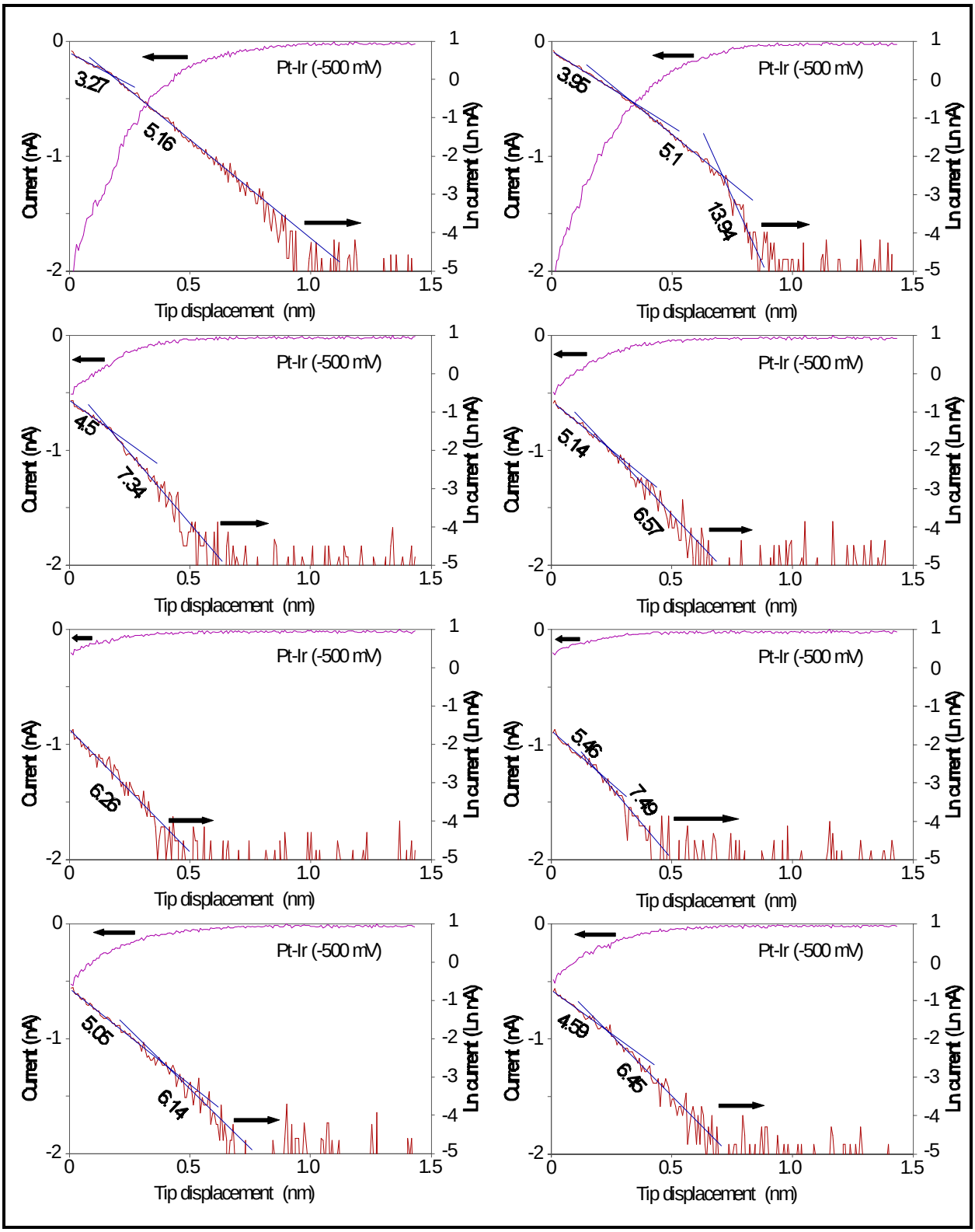

Figure c:15. I(s) curves taken with a -500 mV sample bias for currents of 0.2 nA, 0.5 nA, and 2 nA. Slopes are shown on the Ln I(s) data in nm^{-1}.

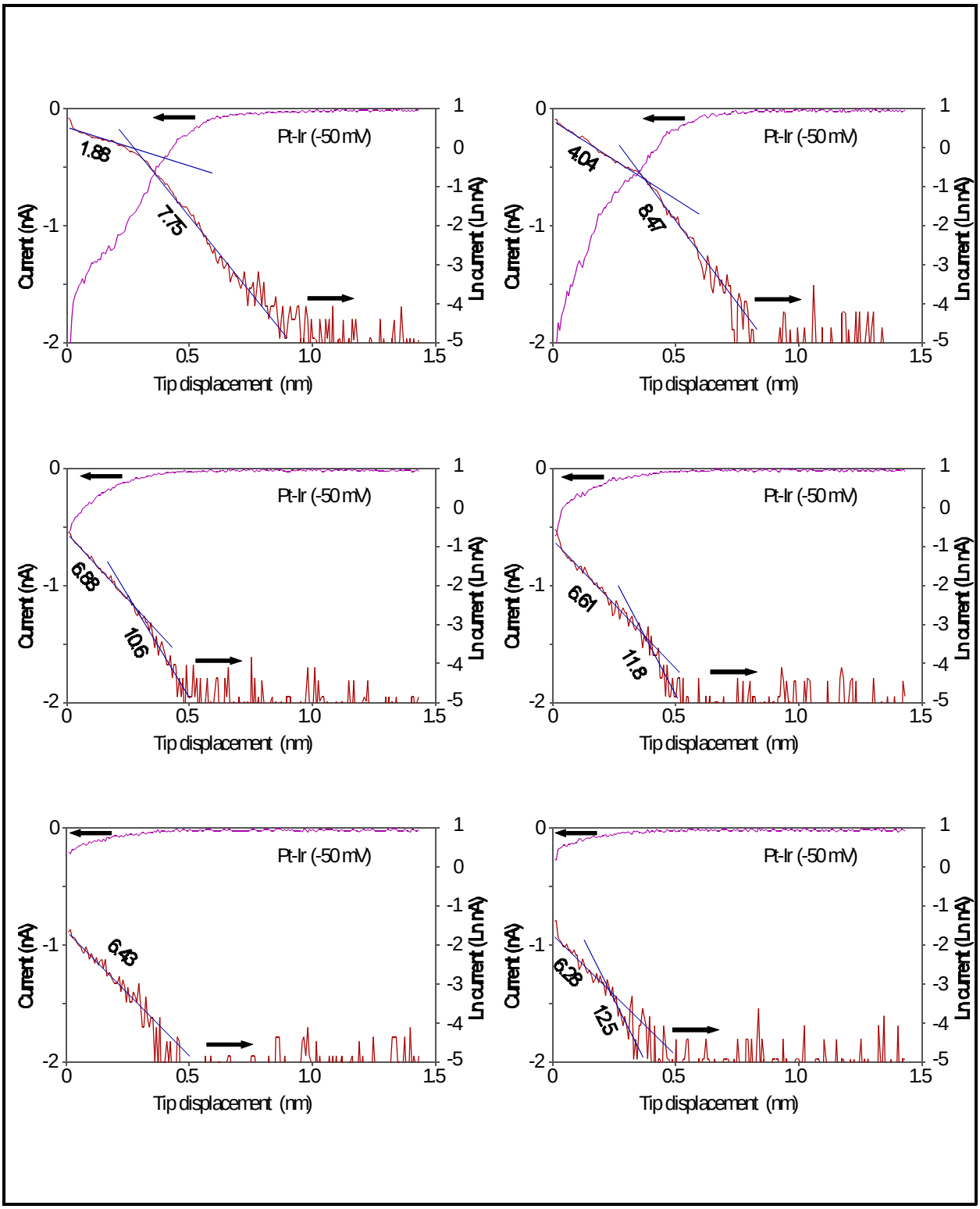

Figure c:16. I(s) curves taken after a several volt extended bias. Taken with a -50 mV sample bias for currents of 0.2 nA, 0.5 nA, and 2 nA. Slopes are shown on the Ln I(s) data in nm^{-1}.

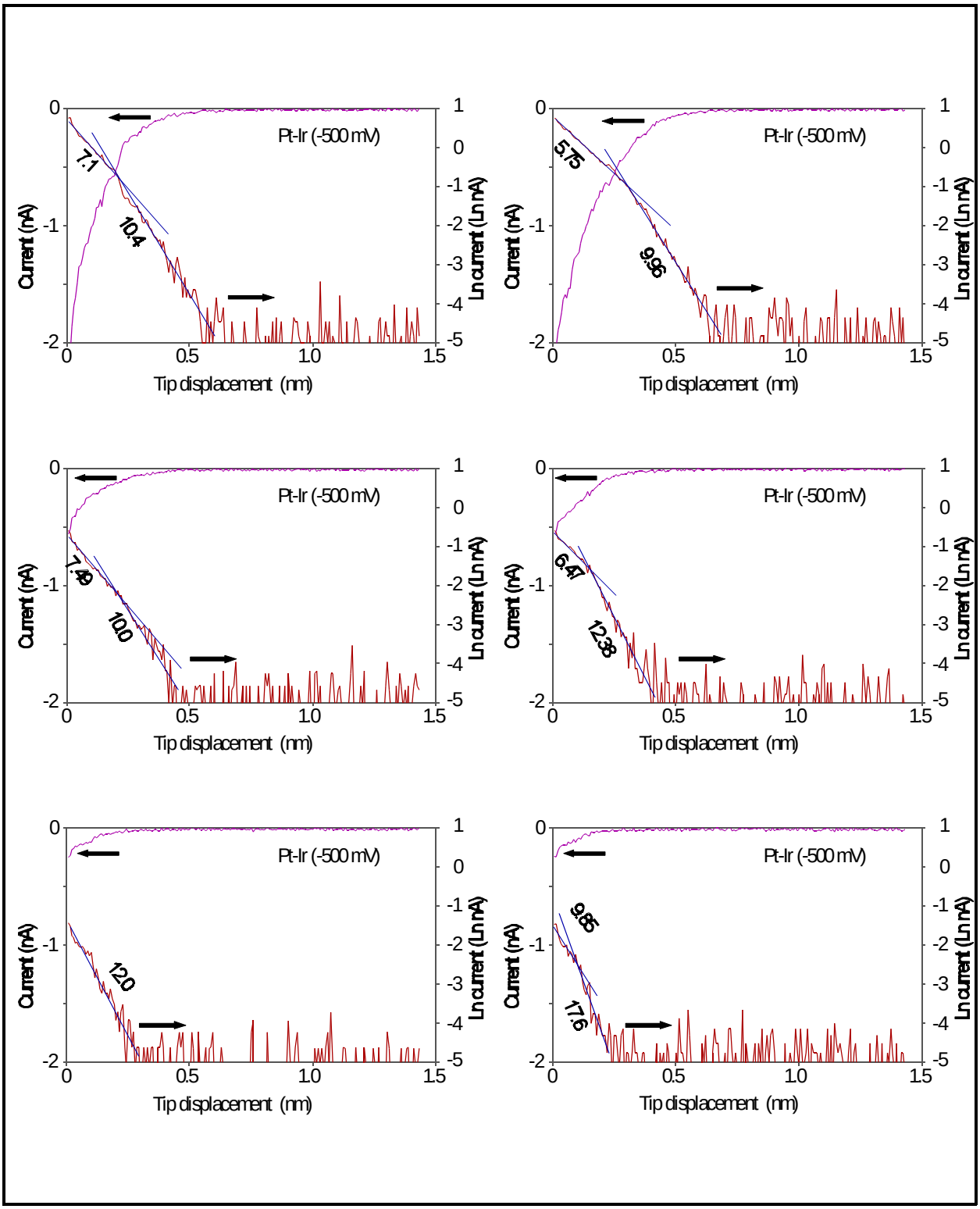

Figure c:17. I(s) curves taken after a several volt extended bias. Taken with a -500 mV sample bias for currents of 0.2 nA, 0.5 nA, and 2 nA. Slopes are shown on the Ln I(s) data in nm^{-1}.

Appendix D

Carbon Resonance Discussion

Carbon is capable of forming single or multiple bonds with itself and other elements enabling it to form over a million compounds. Diamond is the hardest carbon structure with all four valence electrons forming sp^3 hybridized bonds. Carbon is also capable of forming resonance[1] hybrid structures in which the true state of a molecule is intermediate between two or more different valence bond structures.

Quantum mechanically, resonance structure can be described as a weighted linear combination of possible molecular wave functions with the weights chosen to minimize the energy. Benzene (C_6H_6), pyridine, and pyrazine are examples of simple molecules in which resonance occurs. Properties of benzene can not be accounted for by simply assigning a valence bond structure with three carbon double bonds (C=C) and three carbon single bonds (C-C). The benzene bond lengths can only be accounted for by a resonance structure in which the six CC bonds have a 50 per cent double bond character. The four free p_z electrons of butadiene are capable of forming four different bond structures ($H_2C=CH-CH=CH_2$ for example), two of which dominate the resonance characteristics. Graphite is a sp^2 hybridized allotrope of carbon in which three of the four carbon valence electrons form trigonal covalent bonds (σ bonds) with 120^o angles separating them. The fourth valence electron, p_z type, has been described as forming hexagonal shaped resonance hybrid bonds, with each CC bond having a 1/3 double bond character[2]. Observed bond lengths of 1.415 Å confirm the resonance nature for graphite since CC single and double bonds would have lengths[2] of 1.54 Å and 1.34 Å, respectively. The interlayer bonding of graphite is thought by many to be caused by London forces (dipole interaction) although others consider it metallic or weakly covalent[2]. Graphite's resonance nature allows the p_z electrons to move easily within any layer causing it to appear metallic in a direction parallel to the layers. The conductance of graphite within a layer can be as much as 10^4-10^5 times as great as the conductance between layers for a natural, highly perfect, single crystal.[2] Defects between layers may explain any bulk conductance perpendicular to the layers. The conductance within the layer is considered to be caused

entirely by the π bands (which lie in the level of the chemical potential) with the σ orbitals not contributing to the conductivity.[2]

[1] Pauling, L., *The Nature of the Chemical Bond, 3rd ed.*, (Cornell, Ithica, 1960) pp. 10, 222, 224, and 228.

[2]Wheland, G. W., *Resonance in Organic Chemistry* (Wiley, New York, 1955).

Bibliography

Abraham, David W., Mamin, H. Jonathon, Ganz, Eric, Clarke, John, "Surface modification with the scanning tunneling microscope", IBM J. Res. Dev. **30**, 492 (1986).

Akari, S., Möller, R., and Dransfeld, K., "Triangular structures on tungsten diselenide induced and observed by scanning tunneling microscopy", Appl. Phys. Lett. **59,** 243 (1991).

Albrecht, T. R., Dovek, M. M., Lang, C. A., Grütter, Lang P., Quate, C. F., Kuan, S. W. J., Frank, C. W., and Pease R. F. W., "Imaging and modification of polymers by scanning tunneling and atomic force microscopy", J. Appl. Phys. **64,** 1178 (1988).

Albrecht, T. R., Dovek, M. M., Kirk, M. D., Lang, C. A., Quate, C. F., and Smith, D. P. E., "Nanometer-scale hole formation on graphite using a scanning tunneling microscope", Appl. Phys. Lett. **55,** 1727 (1989).

Awad, Elias M., *Businesss Data Processing*, (1980, Prentice Hall, Englewood Cliffs).

Barniol, N., Perez-Murano, F., and Aymerich, X., " Modification of HF-treated silicon (100) surfaces by scanning tunneling microscopy in air under imaging conditions", Appl. Phys. Lett. **61(4)**, 462 (1992).

Barrett, R. C., and Quate, C. F., "Charge storage in a nitride-oxide-silicon medium by scanning capacitance microscopy", J. Appl. Phys. **70,** 2725 (1991).

Batra, Inder P., Garcia, N., Rohrer, H., Salemink, H., Stoll, E., and Ciraci, S., "A study of graphite surface with STM and electronic structure calculations", Surf. Sci. **181**, 126 (1987).

Batra, Inder P., and Ciraci, S., " Theoretical scanning tunneling microscopy and atomic force microscopy study of graphite including tip-surface interaction",
J. Vac. Sci. Technol. **A(6),** 313-8 (1988).

Bearden, Alan, O'Neill, Michael, P., Osborne, Leslie C., and Wong, Terrence L., "Imaging and vibrational analysis with laser feedback interferometry", Optics Letters **18(3),** 238-40 (1993).

Becker, R. S., Golovchenko, J. A., and Schwartzentruber, B. S., "Atomic-scale surface modifications using a scanning tunneling microscope", Nat. **325**, 419 (1987).

Bernhardt, R. H., McGonigal, G. C., Schneider, R., and Thomsom, D. J., "Mechanisms for the deposition of nanometer-sized structures from organic fluids using the scanning tunneling microscope", J. Vac. Sci. Technol. **A 8,** 667 (1990).

Binnig, G., Rohrer, H., Gerber, Ch., and Weibel, E., "Surface studies by scanning tunneling microscopy", Phys. Rev. Lett. **49**, 57 (1982).

Binnig, G., and Rorher, H., "Scanning tunneling microscopy, and atomic probe", Scanning Electron Microscopy/1983/III 1079 (1983).

Binnig G., Fuchs, H., Gerber, Ch., Rohrer, H., Stoll, E., and Tosatti, E., "Energy-dependent state-density corrugation of a graphite surface as seen by scanning tunneling microscopy", Europhys. Lett. **1**, 36 (1986a).

Binnig, G., Garcia, N., Rohrer, H., Soler, J. M., and Flores, F., "Electron-metal-surface interaction with vacuum tunneling: observation of the image force", Phys. Rev. **B 30(8)**, 4816 (1984).

Binnig, G., and Rohrer, H., "Scanning tunneling microscopy", IBM J. Res. Dev. **30**, 355 (1986b).

Bocko, Mark F., Stephenson, Kendall A., and Koch, Roger H., "Vacuum Tunneling Probe: A Reduced-Back-Action Transducer", Phys. Rev. Lett. **61**, 726 (1988).

Bocko, Mark F., "The scanning tunneling microscope as a high gain, low noise displacement sensor", Rev. Sci. Instrum. **61**, 3763 (1990).

Bryant, A., Smith D. P. E., Binnig G., Harrison, W. A., and Quate C. F., "Anomalous distance dependance in scanning tunneling microscopy", Appl. Phys. Lett. **49**, 936 (1986).

Bugg, C. D., and King, P. J., "Scanning capacitance microscopy", J. Phys. E: Sci. Instrum. **21** 147 (1988).

Camras, Marvin, *Magnetic Recording Handbook*, (Rienhold, New York, 1988).

Casillas, Norberto, Snyder, Shelly R., and White, Henry S., "STM Fabrication of Platinum Disks of Nanometer Dimensions", J. Electrochem. Soc. **138**, 641 (1991).

Chen, C. Julian, "Origin of atomic resolution on metal surfaces in scanning tunneling microscopy", Phys. Rev. Lett. **65(4)**, 448-51 (1990).

Chen, C. Julian, "Role of tip material in scanning tunneling microscopy", Preprints, IBM Research Division, Thomas J. Watson Research Center, P. O. Box 218, Yorktown Heights, New York 10598.

Chen, Wei, and Ahmed, Haroon, " Fabrication of high aspect ratio silicon pillars of <10 nm diameter", Appl. Phys. Lett. **63(8)**, 23 (1993).

Chetwynd, D. G., Cockerton, S. C., Smith, S. T., and Fung, W. W., "The design and operation of monolithic x-ray interferometers for super-precision metrology", Nanotechnology **2**, 1 (1991).

Chetwynd, Derek G., and Smith, Stuart T., "High precision surface profilometry: from stylus to STM", in *From Instrumentation to Nanotechnology*, Gardner, J. W., and Hingle, H. T. eds. (Gordon and Breach, Philadelphia 1991).

Colton, R. J., Baker, S. M., Driscoll, R. J., Youngquist, M. G., Baldeschwieler, J. D., Kaiser, W. J., "Imaging graphite in air by scanning tunneling microscopy: Role of the tip", J. Vac. Sci. Technol. **A 6**, 349 (1988).

Coombs, J. H., and Pethica J. B., "Properties of vacuum tunneling currents: anomalous barrier heights", IBM J. Res. Dev. **30(5)**, 455 (1986).

Craston, Derek H., Lin, Charles W., and Bard, Allen J., "High Resolution Deposition of Silver in Nafion Films with the scanning tunneling microscope", J. Electrochem. Soc. 785 (Mar 1988).

Dagata, J. A., Schneir, J., Harary, H. H., Evans C. J., Postek, M. T. and Bennet, J., "Modification of hydrogen-passivated silicon by a scanning tunneling microscope operated in air", Appl. Phys. Lett. **56,** 2001 (1990a).

Dagata, J. A., Schneir, J., Harary, H. H., Bennet, J., and Tseng, W., "Pattern generation on semiconductor surfaces by a scanning tunneling microscope operating in air", J. Vac. Sci. Technol. **B 9**, 1384 (1991a).

Dagata, J. A., Tseng, W., Bennet, J., Evans C. J., Schneir, J., and Harary, H. H., "Selective-area epitaxial growth of gallium arsenide on silicon substrates patterned using a scanning tunneling microscope operating in air", Appl. Phys. Lett. **57,** 2437 (1990b).

Dagata, J. A., Tseng, W., Bennet, J. Schneir, J., and Harary, H. H., "Nanolithography on III-V semiconductor surfaces using a scanning tunneling microscope operating in air", J. Appl. Phys. **70,** 3661 (1991b).

Dagata, J. A., Tseng, W., Bennett, J., Dobisz, E. A., Schneir, J., and Harary, H. H., "Integration of scanning tunneling microscope nanolithography and electronics device processing", J. Vac. Sci. Technol. **A 10(4)** 2105-13 (1992).

Day, H. C., Allee, D. R., George, R., and Burrows, V. A., "Nanometer scale patterning of a monolayer Langmuir-Blodgett film with a scanning tunneling microscope in air", Appl. Phys. Lett. **62(14)**, 1629 (1993a).

Day, H. C., and Allee, D. R., " Selective area oxidation of silicon with a scanning force microscope", Appl. Phys. Lett. **62(21)**, 2691 (1993b).

Doyen, G., Koetter, E., Vigneron, J. P., and Scheffler, M., "Theory of scanning tunneling microscopy", Appl. Phys. **A 51**, 281 (1990).

Drexler, K. Eric, *Engines of Creation*, (Doubleday. New York, 1986).

Dujardin, G., Walkup, R. E., Avouris, P., "Dissociation of Individual Molecules with Electrons from the Tip of a Scanning Tunneling Microscope", Science **255**, 1232 (1992).

Ehrichs, E. E., and de Lozanne, A. L., "Etching of silicon (111) with the scanning tunneling microscope", J. Vac. Sci. Technol. **A 8**, 571 (1990).

Ehrichs, E. E., Yoon, S., and de Lozanne, A. L., "Direct writing of 10 nm features with the scanning tunneling microscope", Appl. Phys. Lett. **53**, 1187 (1988).

Eigler, D. M., Lutz, C. P., and Rudge, W. E., "An atomic switch realized with the scanning tunneling microscope", Nature **352**, 600 (1991).

Eigler, D. M., and Schweizer, E. K., "Positioning single atoms with a scanning tunneling microscope", Nature **344**, 524 (1990).

Eisberg, Robert and Resnick, Robert, *Quantum physics of atoms, molecules, solids, nuclei, and particles,* (Wiley & Sons, New York, 1974).

Emch, R., Nogami, J., Dovek, M. M., Lang, C. A., and Quate, C. F., "Characterization of gold surfaces for use as substrates in scanning tunneling microscopy studies", J. Appl. Phys. **65,** 79 (1989).

Feynman, Richard P., "There's plenty of room at the bottom" in *Miniaturization*, Horace D. Gilbert, ed., (Reinhold Publishing, New York, 1961).

Foster, J. S., Frommer, J. E., and Arnett, P. C., "Molecular manipulation using a tunnelling microscope", Nature **331**, 324 (1988).
Gane, M., and Cox, J. M., "The microhardness of metals at very low loads", Phil. Mag. 881-891 (1970a).

Gane, N., "Measurement of the strength of materials on a sub-micrometre scale", Proc. Roy. Soc. London **A317**, 367 (1970b).

Garcia, Richard, "Nanometer scale modification of biological membranes by field emmission scanning tunneling microscopy", Appl. Phys. Lett. **64(9)**, 1162 (1994).

Garfunkel, E., Rudd, G., Novak, D., Wang, S., Ebert, G., Greenblatt, M., Gustafsson, T., and Garofalini, S. H., "Scanning Tunneling Microscopy and Nanolithography on a conducting Oxide, $Rb_{0.3}MoO_3$", Science **246**, 99 (1989).

Ghandi, Sorab K., *VLSI Fabrication Principles*, (Wiley, New York, 1983).

Gimzewski, J. K., and Möller, R., "Transition from the tunneling regime to point contact studied using scanning tunneling microscopy", Physical Review B **36,** 1284 (1987).

Hansma, Paul K., and Tersoff, Jerry T., "Scanning tunneling microscopy", J. Appl. Phys. **61**, R1 (1987).

Harmer, Mark A., Fincher, Curtis R., and Parkinson, Bruce A., "Scanning tunneling microscopy of the surface topography and surface etching of nanoscale structures on the high-temperature superconductors", J. Appl. Phys. **70,** 2760 (1991).

Heinzelmann, H., Anselmetti, D., Weisendanger, R., Güntherodt, H.-J., Kadis, E., and Wisard, A., "Topography and local modification of the $HoBa_2Cu_3O_{7-x}$ (001) surface using scanning tunneling microscopy", Appl. Phys. Lett. **53**, 2447 (1988).

Heyvaert, I., Osquiguil, E., Van Heserdonck, C., and Bruynseraede, Y., "Etching of screw dislocations in $YBa_2Cu_3O_7$ films with a scanning tunneling microscope", Appl. Phys. Lett. **61(1)**, 111 (1992).

Hoffman-Millack, Britta, Roberts, Clive J., and Steer, William S., "Surface modification and atomic resolution on a vacuum-annealed gold foil in air by scanning tunneling microscopy", J. Appl. Phys. **67,** 1749 (1990).

Horie, Chuji, and Miyazaki, Hiroshi, "STM images of graphite dependent on the size of the tip", Jap. J. Appl. Phys. **26**, L995 (1987).

Hosaki, Shigeyuki, Hosaka, Sumio, and Hasegawa, Tsuyoshi, "Surface modification of MoS_2 using an STM", Appl. Surf. Sci. **60/61**, 643-7 (1992).

Huang, Jin-Lin, Sung, Yung-Eun, and Lieber, Charles M., "Field-induced surface modification on the atomic scale by scanning tunneling microscopy", Appl. Phys. Lett. **61(13)**, 1528-30 (1992).

Huskey, Harry D., and Korn, Granino A., *Computer Handbook*, (1962, McGraw Hill, New York).

Hüsser, O. E., Cranston, D. H., and Bard, A. J., "Scanning Electrochemical Microscopy High-Resolution Deposition and Etching of metals", J. Electrochem. Soc. **136**, 3222 (1989).

Jahanmir, J., West, P. E., Hsieh, S., and Rhodin, T. N., "Surface modification of a-Si:H with a scanning tunneling microscope operated in air" J. Appl. Phys. **65,** 2064 (1989).

Jahanmir, J., West, P.E., and Colter, P. C., "Local modification of thin SiO_2 films in a scanning tunneling microscope", J. Appl. Phys. **67,** 7144 (1990).

Jaklevik, R. C., and Elie, L., "Scanning-Tunneling-Microscope Observation of Surface Diffusion on an Atomic Scale", Phys. Rev. Lett. **60**, 120 (1988).

Kim, Yun, Huang, Jin-Lin, and Lieber, Charles M., "Characterization of nanometer scale wear and oxidation of transition metal dichalcogenide lubricants by atomic force microscopy", Appl. Phys. Lett. **59**, 3404 (1991).

Landman, Uzi, Luedtke, W. D., Burnham, Nancy J., and Colton, Richard J., "Atomistic Mechanisms and Dynamics of Adhesion, Nanoindentation, and Fracture", Science **248**, 454 (1990).

Lang, N. D., "Apparent barrier height in scanning tunneling microscopy", Phys. Rev. **B 37(17)** 10395 (1988).

Leung, On Man, and Goh, Cynthia, J., "Orientational Ordering of Polymers by Atomic Force Microscope Tip-Surface Interaction", Science **255**, 64 (1992).

Li, Wenjie, Virtanen, Joma A., Penner, Reginald, M., "Nanometer-scale electrochemical deposition of silver on graphite using a scanning tunneling microscope", Appl. Phys. Lett. **60,** 1181 (1992).

Li, Y. Z., Vazquez, L., Piner, R., Andres, R. P., and Reifenberger, R., "Writing nanometer-scale symbols in gold using the scanning tunneling microscope", Appl. Phys. Lett. **54,** 1424 (1989).

Lin, Charles, W., Fan, Fu-Ren F., and Bard, Allen J., "High Resolution Photoelectrochemical Etching of n-GaAs with the Scanning Electrochemical and Tunneling Microscope", J. Electrochem. Soc. **134**, 1038 (1987).

Lyo, In-Whan, and Avouris, Phaedon, "Field-Induced Nanometer- to Atomic-Scale Manipulation of Silicon Surfaces with the STM", Science **253**, 174 (1991).

Mamin, Jonathon H., Ganz, Eric, Abraham, David W., Thomson, Ruth Ellen, and Clarke, John, "Contamination-mediated deformation of graphite by the scanning tunneling microscope", Phys. Rev. **B 34**, 9015 (1986).

Mamin, H.-J., Geunthner, P. H., and Rugar, D., "Atomic Emission from a Gold Scanning-Tunneling-Microscope Tip", Phys. Rev. Lett. **65**, 2418 (1990).

Mamin, H.J., Chiang, S., Birk, H., Geunthner, P.H., and Rugar, D., "Gold deposition from a scanning tunneling microscope tip", J. Vac. Sci. Technol. **B 9,** 1398, (1991).

Mamin, H. J., Birk, H., Wimmer, P., and Ruger, D., "High speed STM: principles and applications", J. Appl. Phys. **75(1)**, 167 (1994).

Marchon, B., Salmeron, M., and Siekhaus, W., "Surface modification of a passivated Re(0001) surface by scanning tunneling microscopy", Surface and Coatings Technology, **36**, 319 (1988).

Marella, Paul F., and Pease, R. Fabian, 'Comment on "Writing nanometer-scale symbols in gold using the scanning tunneling microscope" ', J. Appl. Phys. **55**, 2366 (1989).

Marrian, C. R. K., and Colton, "R. J., Low-voltage electron beam lithography with a scanning tunneling microscope", Appl. Phys. Lett. **56,** 755 (1990).

Marrian, C. R. K., Dobisz, E. A., and Colton, R. J., "Investigations of undeveloped *e*-beam resist with a scanning tunneling microscope", J. Vac. Sci. Technol. **B 9,** 1367 (1991a).

Marrian, Christie R. K., Dobisz, Elizabeth A., and Peckerar, Martin C., "Nanostructure Patterning" Proc. IEEE **79,** 1149 (1991b).

Matey, J. R., and Blanc, J., "Scanning capacitance microscopy", J. Appl. Phys. **57** 1437 (1985).

McBride, S.E., and Wetsel Jr., G. C., "Nanometer-scale features produced by electric-field emission", Appl. Phys. Lett. **59**, 3056 (1991).

McCord, M. A., and Pease, R. F. W., "Lithography with the scanning tunneling microscope", J. Vac. Sci. Technol. **B 4,** 86 (1986).

McCord, M. A., and Pease, R. F. W., "Scanning tunneling microscope as a micromechanical tool", Appl. Phys. Lett. **50**, 569 (1987).

McCord, M. A., and Pease, R. F. W., "Lift-off metalization using poly(methylmethacrylate) exposed with a scanning tunneling microscope" J. Vac. Sci. Technol. **B 6,** 293 (1988).

Mee, C. Dennis, Daniel D., eds. *Magnetic Recording Volume I: Technology* (McGraw-Hill, New York, 1987).

Miller, Jimmie A., and Hocken, Robert J., "Scanning tunneling microscopy bit making on highly oriented pyrolytic graphite: Initial results", J. Appl. Phys. **68**, 905 (1990).

Mizes, H. A., Park, Sang-il, and Harrison, W. A., Multiple-tip interpretation of anomalous scanning-tunneling-microscopy images of layered materials", Phys. Rev. **B 36**, 4491 (1987).

Mizutani, Wataru, Inukai, Junji, and Ono, Masatoshi, "Making a Monolayer Hole in a Graphite Surface by Means of a Scanning Tunneling Microscope", Jap. J. Appl. Phys. **29**, L815 (May 1990).

Moreland, John, and Rice, Paul, "High-resolution, tunneling stabilized magnetic imaging and recording", Appl. Phys. Lett. **57,** 310 (1990).

Nagahara, L. A., Thundat, T., and Lindsay, S. M., "Nanolithography on semiconductor surfaces under and etching solution", Appl. Phys. Lett. **57,** 270 (1990).

Nicollian, E. H., and Brews, J. R., *MOS (Metal Oxide Semiconductor) Physics and Technology*, (Wiley, New York, 1982).

Ohmori, Takashi, Hashimoto, Kazuhito, and Fujishima, Akira, "Morphological Transformation of Palladium Caused by Measurement of a Scanning Tunneling Microscope", Jap. J. Appl. Phys. **30,** 1826 (1991).

Ostrom, R. M., Tamenbaun, D. M., and Gallager, Allen, " Construction of silicon nanocolumns with the scanning tunneling microscope", Appl. Phys. Lett. **61(8)**, 925 (1992).

Pan, X., Allee, D. R., Broers, A. N., Tang, Y. S., and Wilkinson C. W., "Nanometer scale pattern replication using electron beam direct patterned SiO_2 as the etching mask", Appl. Phys. Lett. **59,** 3157 (1991).

Parkinson, Bruce, "Layer by Layer Nanometer Scale Etching of Two-Dimensional Substrates Using the Scanning Tunneling Microscope", J. Am. Chem. Soc. **112,** 7498 (1990).

Penner, Reginald M., Heben, Michael J., Lewis, Nathan S., and Quate, Calvin F., "Mechanistic investigations of nanometer-scale lithography at liquid covered graphite surfaces", Appl. Phys. Lett. **58,** 1389 (1991).

Pethica, J. B., Hutchings, R., and Oliver, W. C., "Hardness measurement at penetration depths as small as 20 nm", Phil. Mag. **48** 593 (1983).

Phillips, H. M., Callahan, D. L., Sauerbrey, R., Szabo, G., and Bor, Z., "Sub-100 nm lines produced by direct laser ablation in polyimide", Appl. Phys.Lett. **58,** 2761 (1991).

Quate, Calvin F., "Method and means for data storage using tunnel current data readout", U. S. Patent # US4575822, Mar. 11, 1986.

Rabe, Jürgen P., Buchholz, Stefan, and Ritcey, Anna M., "Reactive graphite etch and the structure of an adsorbed monolayer - a scanning tunneling microscope study", J. Vac. Sci. Technol. **A 8,** 679 (1990).

Rabe, Jürgen P., and Buchholz, Stefan, "Fast nanoscale modification of Ag(111) using a scanning tunneling microscope", Appl. Phys. Lett. **58,** 702 (1991).

Ringger, M., Corb, B. W., Hidber, H.R., Schlögl, R., Wiesendanger, R., Stemmer, A., Rosenthaler, L., Brunner, A. J., Oelhafen, P., Günthrodt, H.-J., "STM activity at the University of Basil", IBM J. Res. Dev. **30**, 500 (1986).

Ringger, H. R., M. Hidber, H.R., Schlögl, R., Stemmer, A., Rosenthaler, L., Brunner, A. J., Oelhafen, P. C., Günthrodt, H.-J., "Nanometer Lithography with the scanning tunneling microscope", Appl. Phys. Lett. **46**, 832 (1985).

Roberts, Clive, Hoffman-Millack, Britta, and Steer, William S., "Surface microfabrication of a gold surface in argon using scanning tunneling microscopy" Surf. Sci. **254**, L448 (1991).

Roberts, C. J., Davies, M. C., Jackson, D. E., Tendler, S. J. B., and Williams, P. M., Controlled nanometer-scale line and symbol formation on graphite in air using a scanning tunneling microscope, J. Phys.: Condens. Matter **3**, 7213, (1991).

Ross, Claudia B., Sun, Li, and Crooks, Richard M., "Scanning probe lithography. 1. scanning tunneling microscope induced lithography of self-assembled *n*-alkanethiol monolayer resists", Langmuir **9,** 632-6 (1993).

Sarid, Dror, *Scanning Force Microscopy*, (Oxford University Press, New York, 1991).

Saulys, D., Rudd, G. and Garfunkel, E., "Scanning tunneling microscopy assisted oxide surface etching", J. Appl. Phys. **69,** 1707 (1991).

Schimmel, Th., Fuchs, H., Akari, S., and Dransfeld, K., "Nanometer-size surface modifications with preserved atomic order generated by voltage pulsing", Appl. Phys. Lett. **58** 1039 (1991)

Schneir, J., Hansma, P.K., Elings, V., Gurley, John, Wickramasinghe, K., and Sonnenfeld, R., "Creating and observing surface features with a Scanning Tunneling Microscope", SPIE Vol. 897 *Scanning Microscopy Technologies and Applications,* 16 (1988a).

Schneir, J., Sonnenfeld, R., Marti, O., Hansma, P.K., Demuth, J. E., and Hamers, R. J., "Tunneling microscopy, lithography, and surface diffusion on an easily prepared, atomically flat gold surface", J. Appl. Phys. **63**, 717 (1988b).

Scott, James F., and Paz de Araujo, "Ferroelectric Memories", Science **246**, 1400 (1989).

Selloni, A., Carnevali, P., Tosatti, E., and Chen, C. D., "Voltage-dependent scanning-tunneling microscopy of a crystal surface: Graphite", Phys. Rev. **B 31**, 2602 (1985); Erratum: Phys Rev B **34(10)** 7406 (1986).

Shedd, Gordon M., Russell, Phillp E., "STM Studies of Clusters and Nanomodifications", Nanotechnology **1** 67 (1990).

Shen, T. C., Brockenbrough, R. T., Hubacek, J. S., Tucker, J. R., Lyding, L. W., "Ion irradiation effects on graphite with the scanning tunneling microscope", J. Vac. Sci. Technol. **B 9**, 1376 (1991).

Shimizu, Kazuhiro, Nakakita, Hideaki, and Oda, Shunri., "Nanometer Patterning by Electron Beam Lithography Using an Amorphous Film as an Intermediate Layer", Jap. J. Appl. Phys. **30,** 890 (1991).

Shtokman, M. I., "Possibility of laser nanomodification of surfaces by means of a scanning tunneling microscope" in *Optoelectronics, instrumentation, and data processing*, vol. 3 27-37 (1989).

Silva, L. A., Laitenberger, P., and Palmer, R. E., "Nanofabrication of metal structures in gold films deposited on mica", J. Vac. Sci. Technol. **B 11(6)**, 1992 (1993).

Silver, R. M., Ehrichs, E. E., and de Lozanne, A. L., "Direct writing of submicron metallic features with a scanning tunneling microscope", Appl. Phys. Lett. **51**, 247 (1987).

Simmons, John G., "Generalized Formula for the Electric Tunnel Effect between Similar Electrodes Separated by a Thin Insulating Film", J. Appl. Phys. **34**, 1793 (1963).

Smith S. T., and Chetwynd, D. G., "An optimised magnet-coil force actuator and its application to linear spring mechanisms", Proc. Inst. Mech. Eng. **204(C4)**, 243 (1990).

Sommerfeld, David A., Cambron, R. Thomas, Beebe Jr., Thomas P., "Topographic and Diffusion Measurements of Gold and Platinum Surfaces by Scanning Tunneling Microscopy", J. Phys. Chem. **94,** (1990).

Staufer, U., Scandella, L., Rudin, H., Günthrodt, H.-J., and Garcia, N., "Tailoring nanostructures with a scanning tunneling microscope", J. Vac. Sci. Technol. **B 9** 1389 (1991).

Staufer, U., Wiesendanger, R., Eng, L., Rosenthaler, L., Hidber, H. and Güntherodt, H.-J., "Nanometer scale structure fabrication with the scanning tunneling microscope", Appl. Phys. Lett., **51,** 244 (1987).

Stern, J. E., Terris, B. D., Mamin, H. J., and Rugar D., "Deposition and imaging of localized charge on insulator surfaces using a force microscope", Appl. Phys. Lett. **53,** 2717 (1988).

Stockman, L., Neuttiens, G., Van Hansendonck, C., and Bruynseeraede, V., "Submicron lithographic patterning of thin gold films with a scanning tunneling microscope", Appl. Phys. Lett. **62(23)**, 2935 (1993).1

Stroscio, Joseph A., and Eigler, D. M., "Atomic and Molecular Manipulation with the Scanning Tunneling Microscope" Science **254**, 1319 (1991).

Sugimura, Hiroyuki, Uchida, Tatsuya, Kitamura, Noboru, and Masahara, Hiorshi, "Tip induced anodization of titanium surface by scanning tunneling microscopy: a humidity affect on nanolithography", Appl. Phys. Lett. **63(9)**, 1288 (1993).

Sze, S. M., *Semiconductor Devices, physics and technology, (Wiley & Sons, New York, 1985).*

Tartar, R. C., and Rabii, S., "Electronic properties of graphite: a unified theoretical study", Phys. Rev. **B 25**, 4126 (1982).

Taylor, Geoffrey, "Disentigration of water drops in an electric field", Proc. R. Soc. A **280**, 383 (1964).

Tendler, J. B., Roberts, Clive J., Davies, Martyn C., and Jackson, David E, "The observation of a deuterium effect in controlled line and symbol formation on graphite using a scanning tunneling microscope", J. Phys. Condens. Matter **4**, L331-L334 (1992).

Terashima, Kazuo, Kondoh, Minoru, Takamura, Yuzuru, and Komaki, Hisashi, "Surface modification of Ba-Sr-Ca-Cu-O films deposited *in situ* by radio frequency plasma flash evaporation with a scanning tunneling microscope", Appl. Phys. Lett. **59**, 644 (1991).

Terashima, Kazuo, Kondoh, Minoru, and Yoshida, Toyonobu, " Fabrication of nucleation sites for nanometer size selective deposition by scanning tunneling microscope" J. Vac. Sci. Technol. **A 8,** 581 (1990).

Terris, B. D., Stern, J. E., Rugar, D., and Mamin, H.-J., "Localized charge force microscopy", J. Vac. Sci. Technol. **A 8,** 374 (1990).

Thibaudan, F., Roche, J. R., and Salvan, F., "Nanometer scale lithography on Si surfaces by decomposition of ferrocene molecules using a scanning tunneling microscope", Appl. Phys. Lett. **64(4)**, 523 (1994).

Thundat, T., Nagahara, L. A., and Lindsay, S. M., "Scanning tunneling microscopy studies of semiconductor electrochemistry", J. Vac. Sci. Technol. **A 8,** 539 (1990).

Tománek, David, Louie, Stephen G., Mamim, H. Jonathon, Abraham, David W., Thomson, Ruth Ellen, Ganz, Eric, and Clarke, John, "Theory and observation of highly asymmetric atomic structure in scanning-tunneling microscopy images of graphite", Phys. Rev. **B 35**, 7790 (1987).

Tsukada, Masaru; Kobayashi, Katsuyoshi; and Ishiki, Nobuyuki, " Effect of tip atomic structure on scanning tunneling microscopy/spectroscopy", Surface Science **242**, 12 (1991).

Utsugi, Yasushi, "Nanometre-scale chemical modification using a scanning tunneling microscope", Nat. **327**, 747 (1990).

Umbach, C. P., Broers, A. N., Koch, R. H., Wilson, C. G., and Laiowitz, R. B., "Nanolithography with a high resolution STEM", IBM J. Res. Develop. **32**, 454 (1988).

van Loenen, E. J., Dijkkamp, D., Hoeven, A. J., Lenssinck, J. M., and Dieleman, J., "Direct writing in Si with a scanning tunneling microscope", Appl. Phys. Lett. **55** 1312 (1989); "Nanometer scale structuring of silicon by direct indentation", J. Vac. Sci. Technol. **A 8**, 574 (1990).

Varhue, W. J., Carulli, J. M., Miller, J. A., and Peterson, G. G., "Surface morphology of epitaxial Ge on Si grown by plasma enhanced chemical vapor deposition", J. Vac. Sci. Technol. **B 9**, 2022 (1991).

Virtanen, J.A., Suketu, P., and Huth, G. C., "Fabrication of nanometer flat areas onto $YBa_2Cu_3O_{7-x}$ thin film surfaces by scanning tunneling microscope", J. Appl. Phys. **70**, 3376 (1991).

Wandass, Joseph H., Colton, Richard J., and Murday, James S., "Magnetic field sensor and device for determining the magnetostriction of a material based on a tunneling tip detector and methods of using same", U. S. Patent #US5103174

Wang, Chen, Giambattista, B., Slough, C. G., Coleman, R. V., and Subramanian, M. A., "Energy gaps measured by scanning tunneling microscopy", Phys. Rev. **B 43(14)**, 8890 (1990).

Wang, Zhouhang, and Moskovits, Martin, "Scanning tunneling microscope promoted growth of nanometer-scale uniform gold stripes on reconstructed Au(111) surfaces", J. Appl. Phys. **71(11)**, 5401 (1992).

Wang, Hong, Jing, Jing, Chu, H. T., and Henriksen, P. N., "Rearrangement of Au(111) surface as a result of scanning with scanning tunneling/atomic force microscopes", J. Vac. Sci. Technol. **B 11(6)**, 2000 (1993).

Weisenhorn, A. L., MacDougall, J. E., Gould, S. A. C., Cox, S. D., Wise, W. S., Massie, J., Maivald, P., Elings, V. B., Stucky, G. D., and Hansma, P. K., "Imaging and Manipulating Molecules on a Zeolite Surface with an Atomic Force Microscope", Science **247**, 1330 (1990).

Whitman, L. J., Stroscio, Joseph, A., Dragoset, R. A., and Celotta, R. J., "Manipulation of Adsorbed Atoms and Creation of New Structures on Room-Temperature Surfaces with Scanning Tunneling Microscope", Science **251**, 1206 (1991).

Wolf, E. L., *Principles of electron tunneling spectroscopy*, (Oxford University Press, New York, 1985).

Wuu, Yee-Min, Fan, Fu-Ren F., and Bard, Allen J., "High Resolution Deposition of Poly aniline on Pt with the Scanning Electrochemical Microscope", J. Electrochem. Soc. **136,** 885 (1989).

Yau, S.-T., Saltz, D., Wriekat, A., Nayfeh, M. H., "Nanofabrication with a scanning tunneling microscope", J. Appl. Phys. **69**, 2970 (1991a).

Yau, S.-T., Saltz, D., and Nayfeh, M. H., "Scanning tunneling microscope-laser fabrication of nanostructures", J. Vac. Sci. Technol. **B 9,** 1371 (1991b).

Yau, S.-T., Zheng, X., and Nayfeh, M. H., "Nanolithography of chemically prepared Si with a scanning tunneling microscope", Appl. Phys. Lett. **59,** 2457 (1991c).

Yokohata, Toru, Kato, Koji, and Ohmura, Kenji, "Nanometer-scale roughness study and indentation test with a scanning tunneling microscope", J. Vac. Sci. Technol. **A 8**, 585 (1990).

Young, Russell D., "Surface microtopography", Physics Today, **Nov** 43 (1971).

Young, Russell, Ward, John, and Scire, Frederic, "The topografiner: An instrument for measuring surface microtopography", Rev. Sci. Instrum. **43**, 999 (1972).

Zhang, H., Hordon, L. S., Kuan, S. W. J., Maccagno, P., and Pease, R. F. W., "Exposure of ultra-thin polymer resists with the scanning tunneling microscope", J. Vac. Sci. Technol. **B 7,** 1717, (1989).